ISSN 2233-9485 (Print)
ISSN 2233-9574 (Online)

International Symposium on Magnetism and Magnetic Materials 2018

ABSTRACTS

Date November 21- 23(Wed.-Fri.), 2018

Place Hotel Nongshim, Busan, Korea

Organized by The Korean Magnetics Society

Sponsored by The Korean Federation of Science and Technology Societies(KOFST)

Digests of the International Symposium on Magnetism and Magnetic Materials 2018
The Korean Magnetics Society

International Symposium on Magnetism and Magnetic Materials 2018

ABSTRACTS

Date November 21- 23(Wed.-Fri.), 2018

Place Hotel Nongshim, Busan, Korea

Organized by The Korean Magnetics Society

Sponsored by The Korean Federation of Science and Technology Societies(KOFST)

"This work was supported by the Korean Federation of Science and Technology Societies(KOFST) Grant funded by the Korean Government."

Notice

1. Presenters should follow the below guidelines.

1) The size of the board is 100cm(width) by 180cm(height).
2) The scheduled posters should be displayed from 13:30 to 18:00 on the day of their session.
Poster Discussion will take place in the poster session room(Emerald, 2nd Floor) from 17:20 to 18:00 and poster presenters must be present at their poster during this time.

2. Program at a Glance

Nov. 21(Wed.)	13:00~	Registration				
	14:30~16:30	Blind Wine Tasting Challenge (Crystal, 2nd Floor)				
	16:30~18:00	Welcome Reception and Talk Concert (Crystal, 2nd Floor)				
Nov. 22(Thu.)	08:30~	Registration				
	09:00~10:20	Ⓔ Special Session I (Daecheong A, 2nd Floor)	Oral Session I (Crystal, 2nd Floor)	Oral Session II (Sapphire, 2nd Floor)	Special Session II (Emerald, 2nd Floor)	
	10:20~10:40	Coffee Break				
	10:40~12:20	Ⓔ Special Session I (Daecheong A, 2nd Floor)	Special Session III (Crystal, 2nd Floor)	Oral Session II (Sapphire, 2nd Floor)	10:40~11:20	Special Session II (Emerald, 2nd Floor)
	12:20~13:30	Lunch				
	13:30~15:00	Special Session IV (Daecheong A, 2nd Floor)	Ⓔ Special Session V (Crystal, 2nd Floor)	Oral Session III (Sapphire, 2nd Floor)	Poster Session (Emerald, 2nd Floor)	
	15:00~15:20	Coffee Break				
	15:20~17:20	Special Session IV (Daecheong A, 2nd Floor)	Ⓔ Special Session V (Crystal, 2nd Floor)	Oral Session III (Sapphire, 2nd Floor)		
	17:20~18:00	Poster Discussion (Emerald, 2nd Floor)				
	18:00~18:30	KMS Regular General Meeting & KMS Awards (Daecheong A, 2nd Floor)				
	18:30~20:00	Banquet (Daecheong B, 2nd Floor)				
Nov. 23(Fri.)	08:30~	Registration				
	09:00~12:00	Special Session VI (Crystal, 2nd Floor)	Ⓔ Special Session VII (Sapphire, 2nd Floor)			
	12:00~13:30	Lunch				
	13:30~15:00	Special Session VI (Crystal, 2nd Floor)	Special Session VIII (Sapphire, 2nd Floor)			
	15:00~16:00	Poster Awards & Closing Ceremony (Crystal, 2nd Floor)				

3. The Poster Awards Ceremony will take place in the main room (Crystal, 2nd Floor) from 15:00 to 16:00 on November 23.
(If the winner (presenter) does not attend the ceremony, the awards will be cancelled.)

KMS

Nov. 21 (Wed.)

Time	PROGRAM
13:00 ~	**Registration**
14:30 ~ 16:30	**Blind Wine Tasting Challenge (Crystal, 2nd Floor)**
16:30 ~ 18:00	**Welcome Reception and Talk Concert (Crystal, 2nd Floor)** **'Magnetics for future vehicle'** Chair : Pan Kyu Choi(Travel Planner) Speakers : Jung Pyo Hong(Hanyang Univ.), In-Soung Jung(KETI), Young Wook Son(KATI)

Nov. 22 (Thu.)

Time	PROGRAM							
08:30 ~	**Registration**							
09:00 ~ 10:20		**Ⓔ Special Session I (Daecheong A, 2nd Floor) 'Hard Magnetic Materials'** Chair : Chul Jin Choi (KIMS)		**Oral Session I (Crystal, 2nd Floor) 'Soft Magnetic Materials'** Chair : Chang Uk Jung (Hankuk Univ. of Foreign Studies)		**Oral Session II (Sapphire, 2nd Floor) 'Magnetization dynamics and Spin orbit coupling phenomena'** Chair : Gyungchoon Go (Korea Univ.)		**Special Session II (Emerald, 2nd Floor) 'Magnetics for Defence'** Chair : Dong Young Kim (Andong Nat'l Univ.)
	09:00 ~ 09:20	(Invited)S-I-1. Current Status and Research Trend of Rare-earth Permanent Magnet for Environment-friendly Automobiles Wooyoung Lee (Yonsei Univ.)	09:00 ~ 09:20	O-I-1. The role of strain on magnetism and orbital anisotropy in $La_{0.88}Sr_{0.12}MnO_3$ epitaxial thin film Sangkyun Ryu (Pusan Nat'l Univ.)	09:00 ~ 09:20	O-II-1. Experiment for maximum speed of projectile using 2 stage coil gun Se Jong Kim (Yeongnam Univ.)	09:00 ~ 09:20	(Invited)S-II-1. A Magnetic Treatment Technique for Magnetic Field Reduction of a Naval Ship without Degaussing Coil Hyun-Ju Chung (ADD)
	09:20 ~ 09:40	(Invited)S-I-2. Suppression of eddy-current-caused-temperature-rise in Nd-Fe-B-type magnet with high electrical resistivity H. W. Kwon (Pukyong Nat'l Univ.)	09:20 ~ 09:40	O-I-2. Magnetic oxide nanomaterials as high efficient magnetically recyclable visible light photocatalysts Chunli Liu (Hankuk Univ. of Foreign Studies)	09:20 ~ 09:40	O-II-2. Magnetization switching via electric field in FePt/MgO(001) film Qurat-ul-ain (Univ. of Ulsan)	09:20 ~ 09:40	(Invited)S-II-2. A Study on the Effect of Multiple Materials on Demagnetization Sang Hyeon Im (Pusan Nat'l Univ.)
	09:40 ~ 10:00	(Invited)S-I-3. Research Trends and Future Prospects of La-Ce rare earth magnet Donghwan Kim (Star Group)	09:40 ~ 10:00	O-I-3. Magnetism of wetted brownmillerite $SrFe_{0.5}Co_{0.5}O_{2.5}$ oxygen sponges Joonhyuk Lee (Pusan Nat'l Univ.)	09:40 ~ 10:00	O-II-3. Magnetic Facet domains and Spin Torques Kyoung-Woong Moon (KRISS)	09:40 ~ 10:00	(Invited)S-II-3. Construction of 3-axis Flux-gate Magnetometer for Harbor Surveillance System Jin-Suk Cho (LIGNex1 Co.)
	10:00 ~ 10:20	(Invited)S-I-4. Coercivity Mechanism for Nd-Fe-B Sintered Magnets and Ferrite Magnets Derived from the Relation Between the Alignment Dependence of Coercivity and the Angular Dependence of Coercivity Yutaka Matsuura (Reserach Institute for Applied Sciences)	10:00 ~ 10:20	O-I-4. Magnetically Soft FeCoTiZrB Alloys with High Saturation Magnetization Sumin Kim (Sookmyung Women's Univ.)	10:00 ~ 10:20	O-II-4. Compatibility between interfacial Dzyaloshinskii-Moriya interaction measurement schemes Dae-Yun Kim (Seoul Nat'l Univ.)	10:00 ~ 10:20	(Invited)S-II-4. A Degaussing Technique of a Naval Ship Considering the Linearity of Induced Magnetic Field under the Earth Magnetic Field Hyun-Ju Chung (ADD)

Nov. 22 (Thu.)

Time	PROGRAM							
10:20 ~ 10:40	**coffee break**							
10:40 ~ 12:20	10:40 ~ 11:00	**Ⓔ Special Session I (Daecheong A, 2nd Floor) 'Hard Magnetic Materials'** Chair : Pan Kyu Choi (Travel Planner) (Invited)S-I-5. Fabrication and characterization of Mn-Al based new magnetic materials — Jihoon Park (KIMS)	10:40 ~ 11:00	**Special Session III (Crystal, 2nd Floor) 'Soft Magnetic Materials'** Chair : Haein Yim (Sookmyung Women's Univ.) (Invited)S-III-1. Magnetic properties of insulator-coated soft magnetic composites — Sang-Im Yoo (Seoul Nat'l Univ.)	10:40 ~ 11:00	O-II-5. Interfacial Dzyaloshinskii-Moriya interactions in W/CoFeB/MgO film systems — Gyu Won Kim (Korea Univ.)	10:40 ~ 11:00	(Invited)S-II-5. Orthogonality corrected 3-axis Flux-gate Magnetometer for Total Magnetic Field Measurements — Derac Son (Sensorpia Co.)
	11:00 ~ 11:20	(Invited)S-I-6. First-Principles Prediction of Giant Uniaxial Magnetic Anisotropy in Tetragonal FeCo — D. Odkhuu (Incheon Nat'l Univ.)	11:00 ~ 11:20	(Invited)S-III-2. Analysis of high frequency behaviors of Fe-Co Micro Hollow Fiber Composites — Jongryoul Kim (Hanyang Univ.)	11:00 ~ 11:20	O-II-6. Experimental observation of the correlation between the interfacial Dzyaloshinskii–Moriya interaction and work function in metallic magnetic trilayers — Yong-Keun Park (Seoul Nat'l Univ.)	11:00 ~ 11:20	(Invited)S-II-6. Inductive displacement sensor for automobile application — Kwang-Ho Shin (Kyungsung Univ.)
	11:20 ~ 11:40	(Invited)S-I-7. Iron Based Non-Rare Earth Permanent Magnets — Youn-Kyoung Baek (KIMS)	11:20 ~ 11:40	(Invited)S-III-3. Effect of Additives on Soft Magnetic Properties of Fe-based Nanocrystalline alloys — Hwijun Kim (KIIT)	11:20 ~ 11:40	O-II-7. Highly efficient magneto-ionic control of interfacial magnetism using YSZ (Yttria-Stabilized Zirconia) gate oxide — Sujin Jo (KIST)		
	11:40 ~ 12:00	(Invited)S-I-8. How to search a new permanent magnet by using first-principles calculations — S. C. Hong (Univ. of Ulsan)	11:40 ~ 12:00	(Invited)S-III-4. Magnetic Shielding Materials for Wireless Power Transfer: Ferrites to Fe-based nanocrystalline ribbons — Jung Young Cho (KICET)	11:40 ~ 12:00	O-II-8. Deterministic writing and deleting of single skyrmion observed by time-resolved X-ray imaging — Kyung Mee Song (KIST)		
	12:00 ~ 12:20	(Invited)S-I-9. A Preliminary Study on Beam Modulation of Build-Up Regions of Photon Beam for Radiotherapy Using Low Strength Magnetic Field — Woo Sang Ahn (Univ. of Ulsan)			12:00 ~ 12:20	O-II-9. Vanishing skyrmion Hall effect at the angular momentum compensation temperature of a ferrimagnet — Duck-Ho Kim (Kyoto Univ.)		
12:20 ~ 13:30	**Lunch**							

KMS

Nov. 22 (Thu.)

Time	PROGRAM						
		Special Session IV (Daecheong A, 2nd Floor) 'Electric Machines and Magnetic Materials' Chair : Jang-Young Choi (Chungnam Nat'l Univ.)		**Ⓔ Special Session V (Crystal, 2nd Floor) 'Spintronics I'** Chair : Kyung-Jin Lee (Korea Univ.)		**Oral Session III (Sapphire, 2nd Floor) 'Hard Magnetic Materials'** Chair : Hyo Jun Kim (Jahwa Electronics)	**Poster Session (Emerald, 2nd Floor)** Session BM [Biomedical Magnetics] Session HM [Hard-magnetic Materials] Session MO [Magnetic Oxides and Multiferroics] Session MT [Magnetic theory and calculations] Session MD [Magnetization dynamics] Session NM [Nanoscale Magnetism] Session NS [Nano-structured materials] Session OT [Others] Session SS [Semiconductor spintronics] Session SA [Sensor and Applications] Session SM [Soft-magnetic Materials] Session SO [Spin orbit coupling and related phenomena] Session ST [Spin transfer torque for magnetic memory] Session JR [Junior Session]
13:30 ~ 15:00	13:30 ~ 14:00	(Invited)S-IV-1. Comparison of EV Traction Motor performance according to magnetic materials — Yun-Sung Jo (Hanyang Univ.)	13:30 ~ 14:00	(Invited)S-V-1. Spin Hall effect from the interplay between spin and orbital — Hyun-Woo Lee (POSTECH)	13:30 ~ 13:50	O-III-1. A Facile Synthesis of Peapod-like α''-$Fe_{16}N_2$ Magnetic Particles in Silica Shell — Youn-Kyoung Baek (KIMS)	
	14:00 ~ 14:30	(Invited)S-IV-2. Core Loss Analysis in Laminated Core of Electric Motor according to Welding Conditions — Min-Bok Cho (Hanyang Univ.)	14:00 ~ 14:30	(Invited)S-V-2. Charge-Spin Conversion in a Rashba Channel — Hyun Cheol Koo (KIST)	13:50 ~ 14:10	O-III-2. The effects of composition on microstructure and magnetic properties of MnBi alloys — Yang Yang (KIMS)	
					14:10 ~ 14:30	O-III-3. Preparation and Characterization of Fe-rich compound for permanent magnetic materials — Jung Tae Lim (KIMS)	
	14:30 ~ 15:00	(Invited)S-IV-3. Design and Verification of High Speed Permanent Magnet Synchronous Motor for Centrifugal Pumps Considering the Mechanical Stability — Gang-Hyeon Jang (Chungnam Nat'l Univ.)	14:30 ~ 15:00	(Invited)S-V-3. Magnetic memristor driven by spin-orbit torque — Byoung-Chul Min (KIST)	14:30 ~ 14:50	O-III-4. Structure and magnetic properties of Fe-rich permanent magnetic materials prepared by melt spinning — Hui-Dong Qian (KIMS)	
15:00 ~ 15:20	**coffee break**						
15:20 ~ 17:20	15:20 ~ 15:50	(Invited)S-IV-4. Torque Calculations and Measurements of Synchronous Magnetic Coupling/Gear Based on Analytical Method — Jang-Young Choi (Chungnam Nat'l Univ.)	15:20 ~ 15:50	(Invited)S-V-4. Spin currents and spin-orbit torques in ferromagnetic trilayers — Gyungchoon Go (Korea Univ.)	15:20 ~ 15:40	O-III-5. The influence of Sm-Fe-Cu-Al eutectic binder on the magnetic properties and microstructure of $Sm_2Fe_{17}N_3$ sintered magnets — Hee-Ryoung Cha (KIMS)	
	15:50 ~ 16:20	(Invited)S-IV-5. Development of Dy Free Bonded Magnet IPM Type Synchronous Motor for ISG — Salman Khaliq (KETI)	15:50 ~ 16:20	(Invited)S-V-5. Writing and deleting magnetic skyrmions by electric currents examined by full-field soft X-ray microscopy — Soong-Geun Je (LBL)	15:40 ~ 16:00	O-III-6. A comparison of the magnetic properties and hot-deformation behavior of Nd-Fe-B magnets made from melt-spun and HDDR powder — Jae-Gyeong Yoo (KIMS)	

Nov. 22 (Thu.)

<table>
<tr><th>Time</th><th colspan="6">PROGRAM</th></tr>
<tr><td rowspan="2">15:20
~
17:20</td><td>16:20
~
16:50</td><td>(Invited)S-IV-6.
Improved Characteristic of IPMSM for High Speed Drive Using High Tensile Strength Steel
Ki-O Kim
(Hanyang Univ.)</td><td rowspan="2">16:20
~
17:10</td><td rowspan="2">Half plenary

(Invited)HP-I-1.
An investigation of magnetic nanostructures using synchrotron x-rays
Z. Q. Qiu
(UC-Berkeley)</td><td>16:00
~
16:20</td><td>O-III-7.
Effect of iron content of rare earth-substituted Sr M-type hexagonal ferrites synthesized by solid-state reaction
Kang-Hyuk Lee
(Seoul Nat'l Univ.)</td></tr>
<tr><td>16:50
~
17:20</td><td>(Invited)S-IV-7.
Preliminary Design of 10-MW Class Actively Shielded Superconducting Generator
Han-Wook Cho
(Chungnam Nat'l Univ.)</td><td>16:20
~
16:40</td><td>O-III-8.
Study of Magnetic properties and MCA Strain effected $Fe_{13}Co_3$
Jin Sik Park
(Univ. of Ulsan)</td></tr>
<tr><td>17:20
~
18:00</td><td colspan="6">Poster Discussion (Emerald, 2nd Floor)
Chairs : Man-Seok Han(Kangwon Nat'l Univ.) / Ki-Suk Lee(UNIST)</td></tr>
<tr><td>18:00
~
18:30</td><td colspan="6">KMS Regular General Meeting & KMS Awards (Daecheong A, 2nd Floor)</td></tr>
<tr><td>18:30
~
20:00</td><td colspan="6">Banquet (Daecheong B, 2nd Floor)</td></tr>
</table>

Nov. 23(Fri.)

Time	PROGRAM			
08:30 ~	**Registration**			
09:00 ~ 12:00	**Special Session VI (Crystal, 2nd Floor) 'Spin Magnetism for Bioconvergence'** Chair : J. D. Lee (DGIST)			**Ⓔ Special Session VII (Sapphire, 2nd Floor) 'Spintronics with quantum materials'** Chairs : Sonny H. Rhim and Sanghoon Kim (Univ. of Ulsan)
	09:00 ~ 09:30	(Invited)S-VI-1. Magnetic bead signal measurement by using PHR sensors — Dong Young Kim (Andong Nat'l Univ.)	09:00 ~ 09:30	(Invited)S-VII-1. Effective gauge field theory of spintronics — Gen Tatara (RIKEN)
	09:30 ~ 10:00	(Invited)S-VI-2. Micromagnets for synchronous separation of multiple bio-functionalized particles and cells — CheolGi Kim (DGIST)	09:30 ~ 10:00	(Invited)S-VII-2. Topological and ferromagnetic properties of iron-based van der Waals metals — Jun Sung Kim (POSTECH)
	10:00 ~ 10:30	(Invited)S-VI-3. Complementary spin logic operation based on electric-field controlled spin-orbit torques — Byong-Guk Park (KAIST)	10:00 ~ 10:30	(Invited)S-VII-3. Theoretical Proposals for New Edelstein effects — Shuichi Murakami (Tokyo Institute of Technology)
	10:30 ~ 11:00	(Invited)S-VI-4. Manipulation of Magnetic Skyrmions Motion in Confined Geometries for Potential Neuromorphic Applications — Ki-Suk Lee (UNIST)	10:30 ~ 11:00	(Invited)S-VII-4. Chiral anomaly effect in electrical transport of $Bi_{0.96}Sb_{0.04}$ — Heon-Jung Kim (Daegu Univ.)
	11:00 ~ 11:15	**coffee break**		
	11:15 ~ 11:30	(Invited)S-VI-5. Magnetic hyperthermia for removal of leukemia cells in circulatory system and thymus of mice — Eunjoo Kim (DGIST)		
	11:30 ~ 11:45	(Invited)S-VI-6. Multi-level anomalous Hall resistance changes due to DW motion in a single Hall cross for the application of neuromorphic device — Yoonui Kim (DGIST)		
	11:45 ~ 12:00	(Invited)S-VI-7. Controlling the configuration and creationof magnetic skyrmionsby various manipulation techniques studied based on full-field soft X-ray microscopy — Mi-Young Im (LBL)		
12:00 ~ 13:30	**Lunch**			

Nov. 23 (Fri.)

Time	PROGRAM			
	Special Session VI **(Crystal, 2nd Floor)** **'Spin Magnetism for Bioconvergence'** Chair : J. D. Lee (DGIST)		**Special Session VIII** **(Sapphire, 2nd Floor)** **'Medical Science Research'** Chair : Man-Seok Han (Kangwon Nat'l Univ.)	
13:30 ~ 15:00	13:30 ~ 14:00	(Invited)S-VI-8. Creation of valley magnetic domain and manipulation J. D. Lee (DGIST)	13:30 ~ 13:50	(Invited)S-VIII-1. Development of phantom for IMRT delivery quality assurance in Tomotherapy Jae-Uk Jang (Chungnam Nat'l Univ. Hospital)
	14:00 ~ 14:30	(Invited)S-VI-9. Longitudinal Monitoring of Cytokines in Mouse Tumor Models Using Magnetic Biosensors Jung-Rok Lee (Ewha Womans Univ.)	13:50 ~ 14:10	(Invited)S-VIII-2. Development of sensitivity enhancement detector using pixelization of block scintillator with 3D laser engraving Jong Hun Won (Kangwon Nat'l Univ.)
	14:30 ~ 14:45	(Invited)S-VI-10. Fabrication of Large-area Plasmonic Substrate for Magneto-optical Sensing Platform Jong-Ryul Jeong (Chungnam Nat'l Univ.)	14:10 ~ 14:30	(Invited)S-VIII-3. A Study on the Image Distortion and Signal Intensity Change due to the Correlation between Segment and GRAPPA in RESOLVE DWI when using Gd Contrast Agent Yong Soo Han (Dongguk Univ. Ilsan Medical Center)
	14:45 ~ 15:00	(Invited)S-VI-11. Control of Exchange Anisotropy inFM/AFM Bilayers by Piezoelectric Strains Jung-Il Hong (DGIST)	14:30 ~ 14:50	(Invited)S-VIII-4. Study about Correction of Error in Patients Positioning System of Medical LINAC using Low-energy Electromagnetic Radiation Jeong Ho Kim (Kon Yang Univ. Hospital)
15:00 ~ 16:00	**Poster Awards & Closing Ceremony (Crystal, 2nd Floor)**			

CONTENTS

Nov. 21(Wed.), 16:30~18:00
Session : 'Magnetics for future vehicle'

Crystal, 2nd Floor

Chair : Pan Kyu Choi (Travel Planner)

Nov. 22(Thu.), 09:00~12:20
Ⓔ Special Session I 'Hard Magnetic Materials'

Daecheong A, 2nd Floor

Chairs : Chul Jin Choi (KIMS) / Pan Kyu Choi (Travel Planner)

Nov. 22(Thu.), 09:00~10:20
Oral Session I 'Soft Magnentic Materials'

Crystal, 2nd Floor

Chair : Chang Uk Jung (Hankuk Univ. of Foreign Studies)

Nov. 22(Thu.), 09:00~12:20
Oral Session II 'Magnetization dynamics and Spin orbit coupling phenomena'

Sapphire, 2nd Floor

Chair : Gyungchoon Go (Korea Univ.)

Nov. 22(Thu.), 09:00~11:20
Special Session II 'Magnetics for Defence'

Emerald, 2nd Floor

Chair : Dong Young Kim (Andong Nat'l Univ.)

Nov. 22(Thu.), 10:40~12:00
Special Session III 'Soft Magnetic Materials'

Crystal, 2nd Floor

❀ Chair : Haein Yim (Sookmyung Women's Univ.)

Nov. 22(Thu.), 13:30~17:20
Special Session IV 'Electric Machines and Magnetic Materials'

Daecheong A, 2nd Floor

❀ Chair : Jang-Young Choi (Chungnam Nat'l Univ.)

Nov. 22(Thu.), 13:30~17:10
Ⓔ Special Session V 'Spintronics I'

Crystal, 2nd Floor

Chair : Kyung-Jin Lee (Korea Univ.)

Nov. 22(Thu.), 13:30~16:40
Oral Session III 'Hard Magnentic Materials'

Sapphire, 2nd Floor

Chair : Hyo Jun Kim (Jahwa Electronics)

Nov. 22(Thu.), 13:30~18:00
Poster Session

Emerald, 2nd Floor

Chairs : Man-Seok Han (Kangwon Nat'l Univ), Ki-Suk Lee (UNIST)

○ Session BM[Biomedical Magnetics]

○ Session HM[Hard-magnetic Materials]

○ Session SM[Soft-magnetic Materials]

○ Session SO[Spin orbit coupling and related phenomena]

○ Session ST[Spin transfer torque for magnetic memory]

○ Session JR[Junior Session]

Nov. 23(Fri.), 09:00~15:00
Special Session VI 'Spin Magnetism for Bioconvergence'

Crystal, 2nd Floor

Chair : J. D. Lee (DGIST)

Nov. 23(Fri.), 09:00~11:00
Ⓔ Special Session VII 'Spintronics with quantum materials'
Sapphire, 2nd Floor

Chairs : Sonny H. Rhim and Sanghoon Kim (Univ. of Ulsan)

Nov. 23(Fri.), 13:30~14:50
Special Session VIII 'Medical Science Research'
Sapphire, 2nd Floor

Chair : Man-Seok Han (Kangwon Nat'l Univ.)

International Symposium on Magnetism and
Magnetic Materials 2018

Talk Concert

'Magnetics for future vehicle'

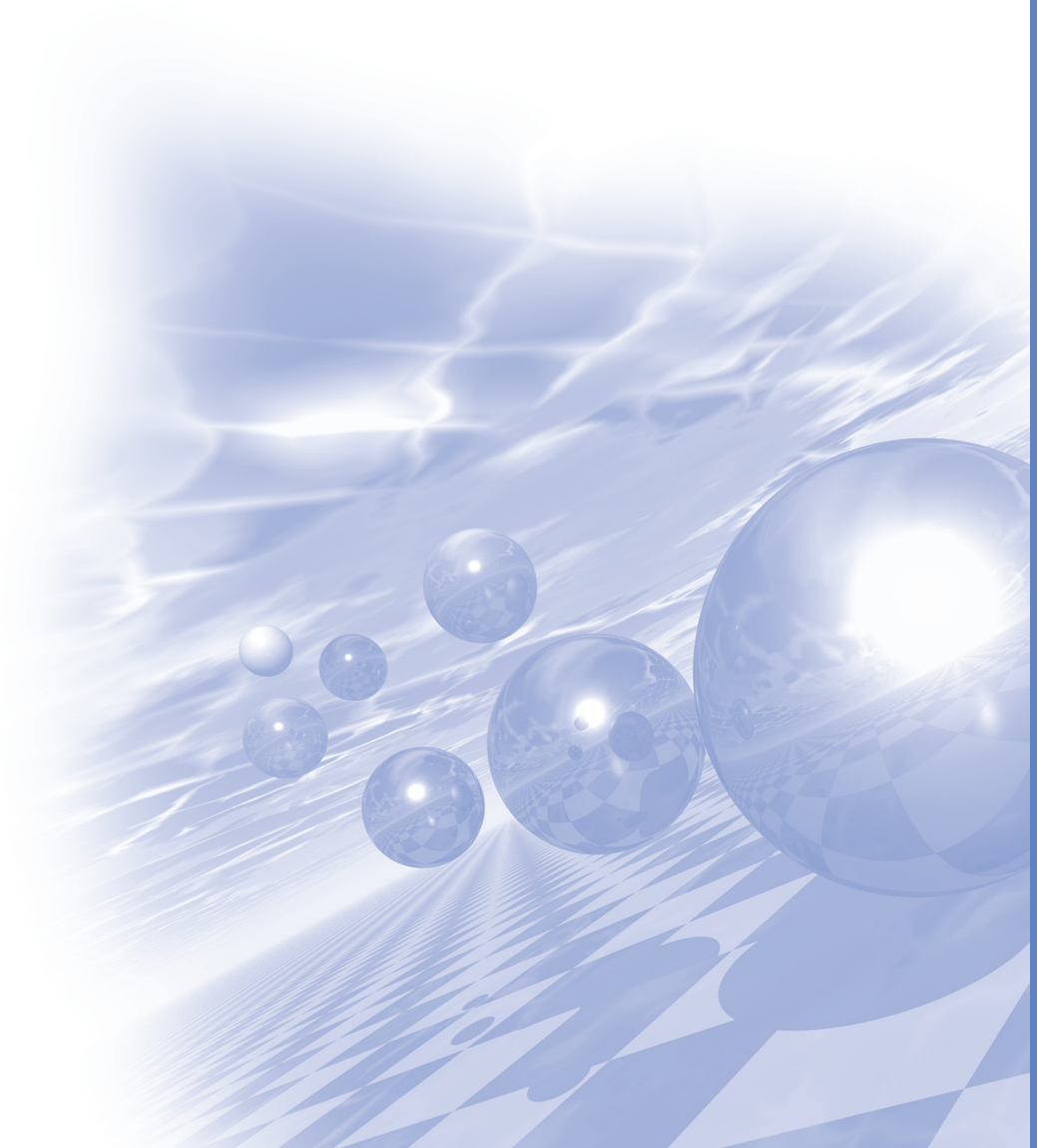

Rare-earth Free Motor Design using Bi-state Magnetic Material Core

Young-Hoon Jung, Jung-Pyo Hong*
Department of Automobile Engineering Hanyang University

The rare-earth permanent magnet motors can achieve high power density. However, the rare-earth materials are mostly out of control, and there is a problem in that the prices and the supply is unstable according to the international situation. In order to overcome this problem, researches on the rare-earth-free motors such as an induction motor, a wound field synchronous motor, and a motor using a non-rare-earth permanent magnet became main interest. Since ferrite permanent magnets, which are representative non-rare-earth permanent magnets, have a residual induction of 1/3 of the rare-earth permanent magnets, the induced electromotive force and the magnetic torque are reduced. One of the solutions is to arrange permanent magnets with several layers to increase reluctance torque by increasing the difference of d-q axis inductance. This kind of motor is called multi-layer IPMSM. However, multi-layer IPMSM requires ribs and bridges to support mechanical structure of the motor. When using conventional electric steel sheets, ribs and bridges can cause leakage flux and this leakage flux causes the motor to increase in size. On the other hand, the Bi-state magnetic material (BSMM) has low permeability and saturation magnetic flux density as compared with conventional electric steel sheet, but when the heat treatment is performed on a specific part, the part has non-magnetic properties. By using this BSMM in the rotor, it is possible to reduce leakage flux in ribs and bridges, and to reduce size.

In this presentation, we study the effectiveness of rare-earth-free motors using BSMM rotor comparing with rare-earth permanent magnet motors.

Current Status of Domestic EV & Charging Infrastructure based on Individual EV Driving Experiences

In-Soung Jung*
Regional President, Gwangju Regional Branch, Korea Electronics Technology Institute

Globally, electric vehicles have been increased since 2010, and currently they are exceeding 1% of new car sales. In Korea, electric vehicles have been distributed in public since 2014, and the distribution numbers has been doubling every year. In 2015, I actually bought an electric vehicle named Soul-EV and started using it. And, recently, I purchased an additional long-distance electric vehicle named Niro-EV that can run 400km with one charging. I present the experience of actual use of electric car for three years, including the lack of initial charging infrastructure and the experience of electric vehicle performance limitations. I will present the advantages and disadvantages of electric vehicles, and the status of charging infrastructure. In addition, I would like to present development trends and prospect of electric vehicles and charging infrastructure.

The Status and Policy of Domestic Electric Vehicle Supply

Young Wook Son*
Korea Automotive Technology Institute, Cheonan-si 31214, Korea

Eco-friendly vehicles (EVs, PHEVs, FCEVs) account for 3% of global auto sales in 2020, 8% in 2025, and 24% in 2030, which is expected to increase sharply from the previous forecasts. By region, sales of eco-friendly cars will increase mainly through China, US, Germany, Britain, and France until 2035, but after that, sales of other countries are expected to increase significantly. And China is expected to maintain its position as the world's largest eco-friendly car market. In the first half of 2018, according to the statistics of automobile registration the number of domestic electric vehicles is 25,593. In addition, the current state of charging infrastructure for electric vehicles has been built for public use, with a total of 6,115 units, consisting of 2,551 rapid chargers and 3,564 slow chargers. Looking at the domestic exports of electric vehicles in the first half of 2018, a total of 11,430 units were exported, including 4,833 units of Kia SOUL EV, 5,441 units of Hyundai IONIQ EV, and 1,156 units of Hyundai KONA EV. However domestic EVs accounted for 3.9% of the global EV market in 2017, falling short of the global market share of 8.5% in the domestic automobile industry in 2016. Therefore, Strong government policy support is needed to expand domestic eco-friendly cars and market share.

Looking at the current status of EV technology, EVs with a charge mileage of about 400km are being competitively released to overcome short mileage in each country. In Korea, Hyundai Kia Motors has released Kona EV and Niro EV, which can run over 400km with a battery of 64kWh in this year. Although domestic EV shows high technology, core parts (especially, material) technology is insufficient, except for battery technology. The reality is that the development gap of EVs is still far behind advanced countries due to limited mileage, expensive car prices, and dependence on core materials and parts. In order to improve performance and price competitiveness compared to advanced countries in overseas markets, development of technologies for EV platform and open platform / component sharing have not been attempted, and there are limitations in realizing excellent vehicle performance and price reduction of EVs. In order to solve this problem, the government needs to expand R&D support and it is time to raise government policy to strengthen R&D of small and medium-sized enterprises by inducing R&D investment from large enterprises.

Table 1. 2017 EV World Sales Ranking

순위	그룹	판매대수
1	BAIC (BAIC, Changhe, BAIC BJEV)	109,122
2	Tesla	101,357
3	Renault-Nissan Alliance (Renault, Nissan, Mitsubishi, Dongfeng Sokon)	95,688
4	Geely Holding Group(Geely Emgrand, Zoyte Zhidou, KANDI)	85,521
5	BYD Auto	42,715
6	GM Group (Chevrolet, Shanghai GM Wuling)	39,469
7	Zoyte Holding Group (Zoyte)	36,979
8	Chery Automobile (Chery)	34,058
9	BMW Group	31,641
10	Jiangling Motors Co. Group (JMC)	30,015
13	**Hyundai Kia Automotive Group (Hyundai, Kia, Beijing Hyundai)**	**26,504**

International Symposium on Magnetism and
Magnetic Materials 2018

Special Session I

'Hard Magnetic Materials'

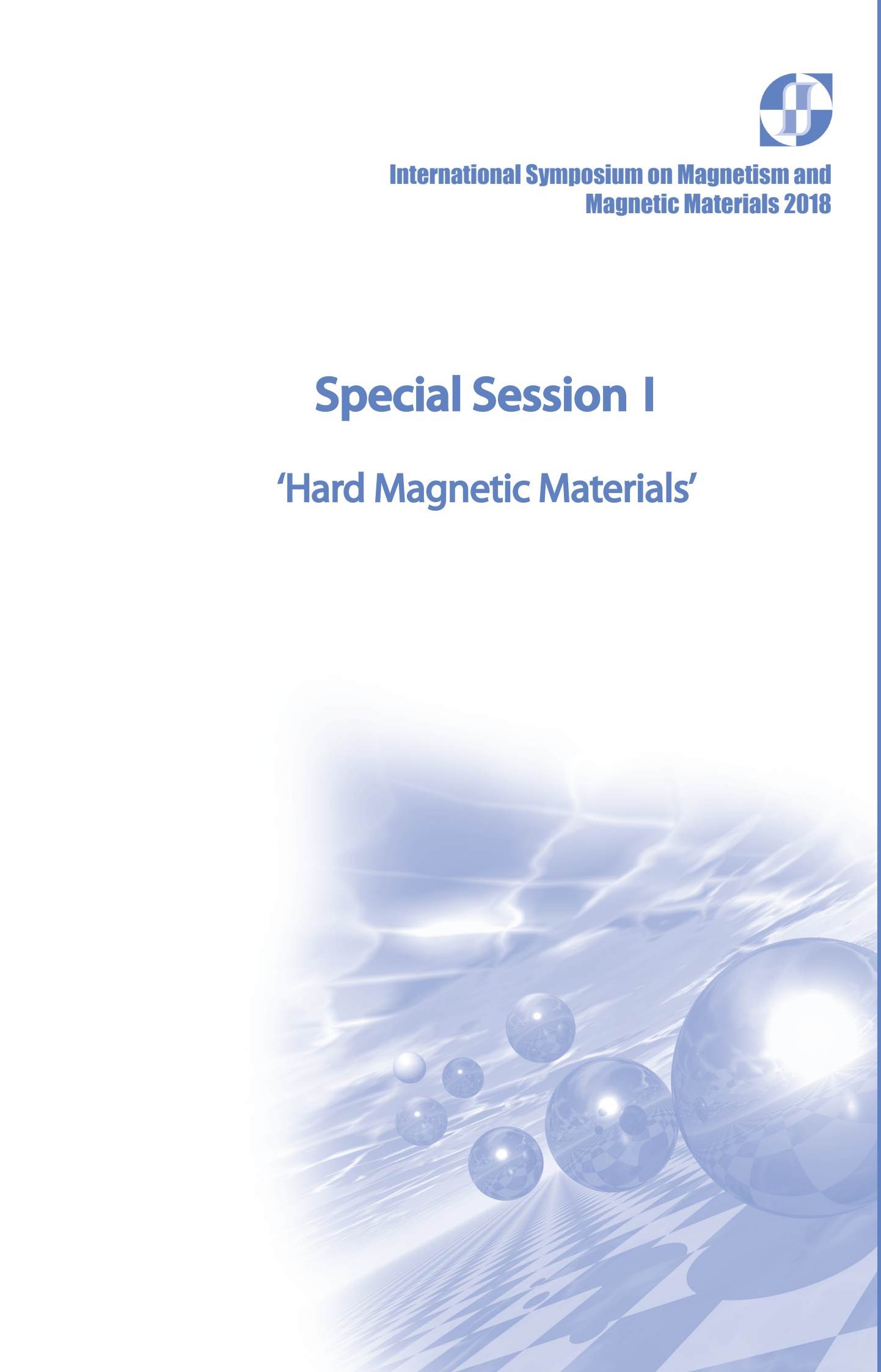

Current Status and Research Trend of Rare-earth Permanent Magnet for Environment-friendly Automobiles

Wooyoung Lee*
Department of Materials Science and Engineering, Yonsei University, Seoul 03722, Republic of Korea

A compelling need for high magnetic properties led to active consideration of rare-earth permanent magnets, which have been used in various applications such as communication, memory, and audio equipment. Since their discovery in 1984, high-coercivity sintered Nd-Fe-B magnets have found numerous practical and industrial applications, e.g., as components of actuators, motors, generators, robots, and wind power plants due to the rise of the fourth industrial revolution and problematic issues of air pollution and fine dust generation. In particular, demand for high-performance permanent magnets is rapidly increasing to meet the ever growing interest in the industry of environment-friendly automobiles (hybrid / electric vehicles). However, since the rare-earth magnets are expensive and have limitation in high-temperature applications such as an automobile motor, it is essential to develop a permanent magnet with reduced rare-earth concentration that can bear high temperatures. Consequently, several major corporations have established a high-performance permanent magnet research team and are pursuing new businesses. At this point of view, the present article reviews a summary of the history and the R & D trends of rare-earth permanent magnets that have been developed in the past.

Suppression of eddy-current-caused-temperature-rise in Nd-Fe-B-type magnet with high electrical resistivity

H. W. Kwon[1*], K. M. Kim[1], M. S. Kang[1], J. G. Lee[2], J. H. Yu[2], and K. H. Shin[3]
[1]Pukyong National University, Busan, Republic of Korea
[2]Korea Institute of Materials Science, Changwon, Republic of Korea
[3]Kyungsung University, Republic of Korea

Nd-Fe-B-type magnet is exclusively used as rotor magnet in traction motor of hybrid electric vehicle (HEV) and electric vehicle (EV) by virtue of its high performance. As Curie temperature of the magnet is comparatively low and worse still, operating temperature of the magnet in traction motor is overly high (>150 °C), its poor thermal stability, in particular high temperature coefficient of coercivity (β) has been worrisome to be solved. Current standard approach around the problem is enhancing coercivity of the magnet. Overly high operating temperature of the magnet in traction motor is due largely to eddy current caused in the magnet by varying magnetic field from slots of stator. Enhancing electrical resistivity in the magnet can, therefore, have especially positive effect on suppressing over-rise of operating temperature of the magnet, and it would create added synergy when combined with coercivity enhancement. In the present study, isotropic and anisotropic Nd-Fe-B-type magnets with high electrical resistivity were fabricated by hot-pressing or die-upsetting the mixture of Nd-Fe-B-type magnetic particles (melt-spun flakes, HDDR powder) and dielectrics (Dy salt, oxide). Fabrication of Nd-Fe-B-type magnet with high electrical resistivity was feasible by consolidating the magnetic powder using the dielectric materials. Measurable suppression of temperature-rise due to eddy current generated under varying magnetic field was verified in the Nd-Fe-B-type magnet with high electrical resistivity.

Research Trends and Future Prospects of La-Ce rare earth magnet

Donghwan Kim*, Kun-seung Kong
Star Group, 8 Horim-dong, Dalseo-gu, Daegu

The largest rare earth mine located in Podu of China has mixed rare earth components which contains 77% of La-Ce, 15% of Pr and 3% of other rare earth metals. In order to produce Pr-Nd, main component of the permanent magnet, a large quantity of La-Ce is produced as a by-product. Since, only a small amount of these metals are used in products such as abrasives, the price dropped to as low as 1/10th of Pr-Nd metal and available stocks increased.

In order to solve the unbalanced use of resources and to concurrently cope with the anticipated increase in demand for rare earth magnet, the Chinese government strived to diversify the use of La-Ce for rare earth magnets and reinforced R&D. In 2017, approximately 15% of the rare earth magnets produced in China are La-Ce magnets.

In fact, studies on the basic properties of La-Ce-Fe-B rare earth magnets have been carried out a long time ago. The problem is that when Nd is substituted with La-Ce, the saturated magnetic flux density and curie temperature dramatically decreases which ultimately leads to substandard performance and hence usage is limited to toys, stationaries and low-performance speakers. However, technological progress has been made in various fields such as particle refinement, magnetic field orientation and grain boundary diffusion to simultaneously improve the residual magnetic flux density and coercivity of rare earth magnets. Utilizing the technologies on La-Ce magnets, facilitating widespread application may be possible as far as to some motors.

In this study, we review recent research trends of La-Ce magnets and results, and propose technical issues and methods for developing rare earth magnets with high performance which uses La-Ce.

References

[1] Jiaying Jin, Yujing Zhang, Tianyu Ma, and Mi Yan, IEEE TRANSACTIONS ON MAGNETICS, VOL. 52, NO. 7, JULY 2016

[2] Le-le Zhang, Zhu-bai Li a, Qiang Maa, Yong-feng, Qian Zhao, Xue-feng Zhang, Journal of Magnetism and Magnetic Materials 435 (2017) 96-99

Coercivity Mechanism for Nd-Fe-B Sintered Magnets and Ferrite Magnets Derived from the Relation Between the Alignment Dependence of Coercivity and the Angular Dependence of Coercivity

Yutaka Matsuura*
Research Institute for Applied Sciences 49 Tanaka Ohi-cho, Sakyo-ku, Kyoto 606-9202, Japan

When the world record for maximum energy product BH_{max}=474 kJ/m^3 of a magnet was achieved by our group in 2005, it was found that the coercivity (H_{cJ}) decreased with improved alignment [1]. It was verified that these phenomena occur not only in Nd-Fe-B sintered magnets but also in ferrite magnets, as shown in Fig. 1. We showed that the coherent rotation of magnetization as represented by the standard and modified Stoner-Wohlfarth models, where the latter includes secondary anisotropy energy (K_2), do not explain these experimental results, while the magnet domain wall motion (D-W) model could qualitatively explain the results [2]. We also undertook calculating the alignment dependence of coercivity (ALDC) using the alignment distribution (AD) of $Nd_2Fe_{14}B$ grains, where it was postulated that every grain independently follows the D-W, and compared these with experimental results. The alignment (α) agrees well with the calculated results, but the coercivity change ratio (β) exhibits large discrepancies with the calculated results. This discrepancy signifies that every grain does not independently reverse by D-W, but instead, for aligned magnets, a number of grains simultaneously reverse at coercivity [3]. From our previous study, it was found that the ALDC of these magnets correlates with the angular dependence of coercivity (ANDC) [4]. The angles of the magnetization reversal area (AMRA) obtained from experimental results and the calculated AMRA were compared and it was found that the AMRA of aligned magnets expands from the calculated AMRA with the same alignment, while the AMRA in aligned magnets is the same as that of low alignment in the calculated results. This result suggests that magnetic domain walls are pinned at tilted grains, and when de-pinned they jump through several grains. When the ANDC with the same AMRA of the calculated results was used, the ANDC could be calculated and compared with the

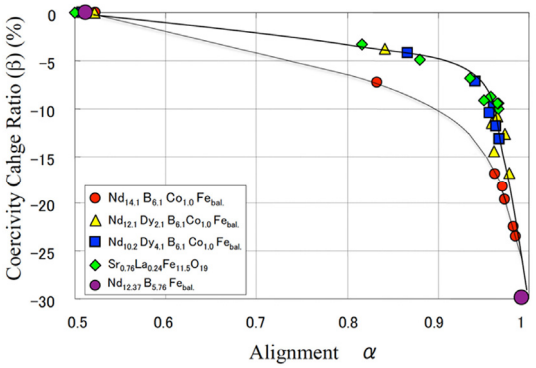

Fig. 1. Alignment dependence of coercivity for various magnets

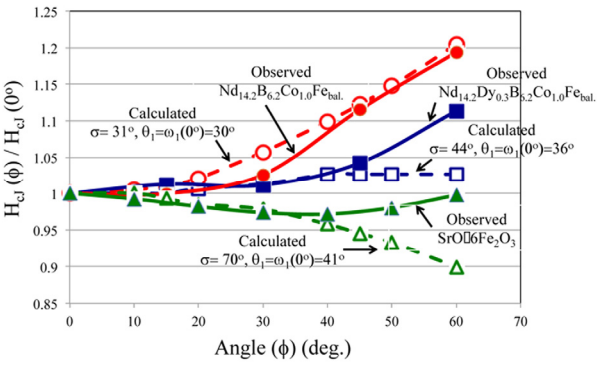

Fig. 2. Experimental and calculated angular dependence of coercivity for various magnets

experimental results. Figure 2 shows the calculated and experimental results of the ANDC for various magnets [5], where the calculated results can qualitatively explain the experimental results. It is predicted from the ALDC that, in isotropically aligned magnets, every grain independently reverses by D-W. It was found that the calculated and experimental results of ANDC in isotropically aligned Nd-Fe-B magnets and ferrite magnets agree well until 60^{o} without any postulation.

References

[1] Daisuke Harimoto, Yutaka Matsuura, Hitachi Metals Technical Review Vol. **23** (2007) 69

[2] Yutaka Matsuura et al., J. Magn. Magn., Mater. **336** (2013) 88.

[3] Yutaka Matsuura et al., J. Magn. Magn., Mater. **346** (2013) 113.

[4] Yutaka Matsuura et al., J. Magn. Magn. Mater. **398** (2016) 246.

[5] Yutaka Matsuura et al., AIP Adv. **8**, 1 (2018) 015226.

Fabrication and characterization of Mn-Al based new magnetic materials

Jihoon Park[1*], Hui-Dong Qian[1,2], Yang Yang[1,2], Yongho Shin[1], Jung Tae Lim[1], Ping-Zhan Si[1,3], Jong-Woo Kim[1], Kook Chae Chung[1], Chul-Jin Choi[1]

[1]Powder & Ceramic Division, Korea Institute of Materials Science, Changwon, Gyeongnam, 51508, R. Korea

[2]School of Materials Science and Engineering, Pusan National University, Busan, Korea

[3]College of Materials Science and Engineering, China Jiliang University, Hangzhou, 310018, China

Theoretically, Mn has the highest magnetic moment among all the 3*d* transition metals according to Hund's rule. Therefore, there have been intensive studies on Mn-based magnetic materials to achieve outstanding magnetic properties, such as high magnetization and coercivity [1,2]. The magnetic properties of the Mn-based magnetic materials are superior to ferrite magnets [3], but still inadequate for industrial application because the manufacturing cost is much more expensive than the ferrite and the magnetic properties are not high enough to compensate the cost. In efforts to improve the magnetic properties and make the Mn-based magnetic materials industrially usable as permanent magnets, we have optimized fabrication methods, deformation conditions, and doping elements, and studied phase transformation mechanism, exchange coupling effects, etc. for Mn-Al based magnetic materials. The produced Mn-Al exhibits highest recorded coercivity. The details of the fabrication methods and characterization results of the Mn-Al based magnetic materials will be discussed.

References

[1] T. Kubo, T. Ohtani, S. Kojima, N. Kato, K. Kojima, Y. Sakamoto, I. Konno, and M. Tsukahara, U.S. Patent US3,976,519, 24 August 1976.

[2] Q. Zeng, I. Baker, J.B. Cui, and Z.C. Yan, J. Magn. Magn. Mat. **308**, 214 (2007).

[3] J. M. D. Coey, J. Phys: Condens. Matter. **26**, 064211 (2014).

First-Principles Prediction of Giant Uniaxial Magnetic Anisotropy in Tetragonal FeCo

D. Odkhuu[1*], T. Tsevelmaa[2], and S. C. Hong[2]
[1]Department of Physics, Incheon National University, Incheon 22012, South Korea
[2]Department of Physics and EHSRC, University of Ulsan, Ulsan, South Korea

Pushing uniaxial magnetic anisotropy energy (K_u) up to an order of meV per atom in bulk structures composed of only 3*d* magnetic elements with large spontaneous magnetization and Curie temperature has been a long-term goal of the permanent magnet and spintronics studies. Herein, using *ab initio* calculations we predict an unexpectedly large K_u of up to 1/2 meV/atom in B2-ordered FeCo, which is even comparable or more than those for the known permanent magnetic materials with 5*d* and 4*f* orbitals. This giant K_u is associated with an interplay mechanism of the large tetragonal distortion induced by doping with an interstitial 2p-electron element, herein N and P as examples, and the strong orbital hybridization between 3*d* and 2*p* states. Our findings demonstrate the feasibility of significant enhancement in magnetic anisotropy through the interstitial doping with 2*p*-electron nonmetals, which could also be generalized to other pnictogen to halogen dopants.

This research was supported by Future Materials Discovery Program through the National Research Foundation of Korea (NRF) funded by the Ministry of Science and ICT (2016M3D1A1027831).

Iron Based Non-Rare Earth Permanent Magnets

Youn-Kyoung Baek* and Jung-Goo Lee
Powder&Ceramic Division, Korea Institute of Materials Science, Korea
e-mail: ykbaek@kims.re.kr

Rare earth magnets are the strongest type of permanent magnets made and are integral to the high tech industry, particularly in clean energies, such as electric vehicle motors and wind turbine generators. The high price of rare earth materials and the imbalance in supply and demand are expected to continue to be a stumbling block to the utilization of rare earth permanent magnet in related industries. Recently, studies on non-rare earth magnet materials have been increasing to solve these problems, and government-led research projects are being carried out in the world. However, the cost of both raw material and fabrication process should be considered in the beginning of development for the industrial utilization of non-rare earth magnets.

From this point of view, our research team is developing a non-rare-earth permanent magnet based on common and low cost iron material. In particular, iron-based materials have a high magnetization value but a low coercive force, which limits their applications, and thus an attempt to improve coercivity is essential. The control of the size and shape of the magnetic particles would be effective to enhance coercivity, which can be realized by combining bottom-up and top-down fabrication process. In this presentation, we will discuss the whole development trend of Fe-based non-rare earth permanent magnet materials.

This work was supported by Fundamental Research Program (PNK 5550) of Korea Institute of Materials Science (KIMS) and National Research Council of Science & Technology(NST) grant by the Korea government (MSIP) (No. CPS-18-05-KAERI).

How to search a new permanent magnet by using first-principles calculations

S. C. Hong[1*] and D. Odkhuu[2]
[1]Department of Physics and EHSRC, University of Ulsan, Ulsan 44610, South Korea
[2]Department of Physics, Incheon National University, Incheon 22012, South Korea

A good permanent magnet must have large magnetization, high coercivity, thermal stability, and high Curie temperature. Furthermore, reducing the cost to produce the materials is also required. Optimization of the properties is so difficult that a new high performance permanent magnet is not realized yet since discovery of Nd-Fe-B magnets even though some materials such as R_2Fe_{17}, $R(Fe, M)_{12}$, $L1_0$ Mn-based alloys etc. Here R stands for rare-earth elements and M does for transition metals.

In this talk, first we will present what physical properties we should calculate by reviewing magnetic properties of a permanent magnet. Next, we will discuss our recent calculational results of $Sm(FeCo)_{12}$, FeCo, FeNi, FePt, and FePd alloys, and some Mn-based alloys. Finally, we hope to suggest the way how to have a new optimal permanent magnet using first-principles calculation

Supported by Future Materials Discovery Program (2016M3D1A1027831) through NRF funded by the Korea government (MSIT).

A Preliminary Study on Beam Modulation of Build-Up Regions of Photon Beam for Radiotherapy Using Low Strength Magnetic Field

Woo Sang Ahn[1*], Wonsik Choi[1], Jungwon Kwak[2], In-Hye Jung[1], Seong Soo Shin[1]

[1]Department of Radiation Oncology, Gangneung Asan Hospital, University of Ulsan College of Medicine, Gangneung 25440, Korea

[2]Department of Radiation Oncology, Asan Medical Center, University of Ulsan College of Medicine, Seoul 05505, Korea

Traditionally, low-energy photon beams (4 MV or ^{60}Co) were used to deliver sufficient dose to the target volume adjacent to the skin such as the glottic cancer. Recently, as the use of photon beams over 6 MV has increased, insufficient doses are delivered in the build-up region of photon beams due to the lack of electron equilibrium. In this study, the feasibility of the use of beam spoiler on dose enhancement in build-up region of 6 MV photon beam using the magnetic field with a low strength of 0.5 T was experimentally evaluated.

A homemade magnet device which can apply a transverse magnetic field to photon beam was manufactured. The effect of dose enhancement in build-up region was investigated by the beam spoiler-to-magnet distance (BMD), the magnet-to-magnet distance (MMD), and the magnet-to-surface distance (MSD). Build-up regions of 6 MV photon beam with and without the magnetic field were measured for the field size to 5 × 5 cm^2.

The skin dose was reduced by about 5% compared with skin dose of 4 MV photon beam without the magnetic field. Especially, the dose distribution in build-up region was about 2% higher than the build-up of 6 MV without the magnetic field.

The use of a beam spoiler in the magnet device designed in this study is expected to be an option of radiation therapy which could provide sufficient dose to skin surface due to the sufficient production of secondary electron.

International Symposium on Magnetism and
Magnetic Materials 2018

Oral Session I

'Soft Magnetic Materials'

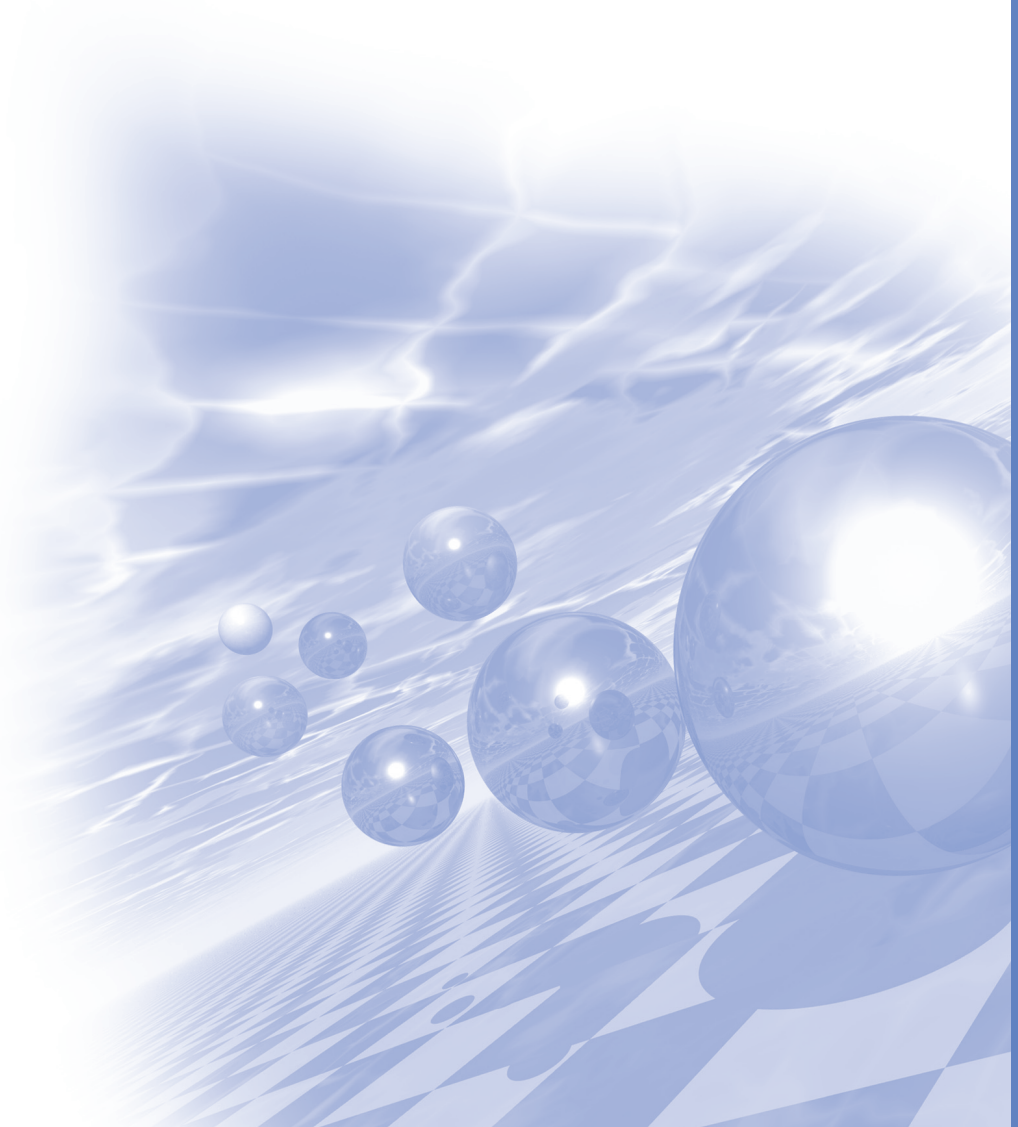

The role of strain on magnetism and orbital anisotropy in $La_{0.88}Sr_{0.12}MnO_3$ epitaxial thin film

Sangkyun Ryu[1*], Jinhyung Cho[2], Younghak Kim[3], Ryan Need[4], Brian Kirby[4], Hyoungjeen Jeen[1†]

[1]Department of Physics, Pusan National University, Busan, 46241, Korea
[2]Department of Physics Education, Pusan National University, Busan, 46241, Korea
[3]Pohang Accelerator Laboratory, Pohang University of Science and Technology, Pohang, 37673, Korea
[4]NIST Center for Neutron Research, Gaithersburg, Maryland, 20899, USA

Hole doped maganites have many different ground states like ferromagnetic insulating phase (FMI), paramagnetic insulating phase, etc. These ground states affect by competing internal degrees of freedom and external stimuli like temperature, magnetic field, electric field, and stress. Among these ground states, we`re interested in FMI phase in $La_{0.88}Sr_{0.12}MnO_3$. About this phase the relation between external stimuli and physical properties has not been established. In this work, we attempted to change magnetic properties of LSMO thin films by epitaxial strain. (110) NGO was used as a substrate. Interestingly, (110) NGO has different in-plane lattice constants. (7.73 Å along [1-10] NGO and 7.71 Å along [001] NGO). Thus, it is expected the higher compressive strain along [001] NGO. The result form high-resolution x-ray diffraction, epitaxial LSMO films were stabilized. Temperature dependent transport data show anisotropic resistivities by anisotropic strain. Furthermore, we confirmed magnetic anisotropy by x-ray magnetic circular dichroism (XMCD) study. This work was supported by the Basic Science Research Program through the National Research Foundation of Korea (NRF) funded by the Ministry of Education (NRF-2015R1D1A1A02062175).

Magnetic oxide nanomaterials as high efficient magnetically recyclable visible light photocatalysts

Yuefa Jia and Chunli Liu*
Department of Physics and Oxide Research Center, Hankuk University of Foreign Studies, Yongin, 17035

Perovskite $BiFeO_3$ (BFO) is currently of great research interest for data storage, sensors, and spintronics devices applications. Magnetic BFO can also function as a catalyst for water splitting and the degradation of organic pollutants due to its narrow bandgap (Eg=2.2 eV), excellent chemical stability, and low cost. In the present work [1], N doped $BiFeO_3$ (N-BFO) nanoparticles have been synthesized via a sol-gel rapid calcination technique using melamine ($C_3H_6N_6$) as the N precursor. It is found that N-doping could effectively narrow the band gap of BFO, which obviously enhanced the visible light adsorption capability. Meanwhile, N-doping could lead to significant increase in the magnetization of BFO. Particularly, the saturation magnetization (M_s) was increased up to 0.35 emu/g (as compared to that of pure BFO: 0.07 emu/g) when 12.5 mmol N doping precursor was used (12.5N-BFO). The catalytic performance of N-BFO nanoparticles was evaluated through the degradation of bisphenol A (BPA) under visible light irradiation. 12.5N-BFO was found to be an efficient catalyst of BPA, and the addition of H_2O_2 (10 mmol/L) or H_2O_2 (10 mmol/L)/L-cysteine (0.25 mmol/L) can further enhance the degradation efficiency up to 60% and 94% within 120 min, respectively. The 12.5N-BFO nanoparticles were very stable during photocatalytic processes and their photo-Fenton catalytic activity can be retained even after three recycling processes.

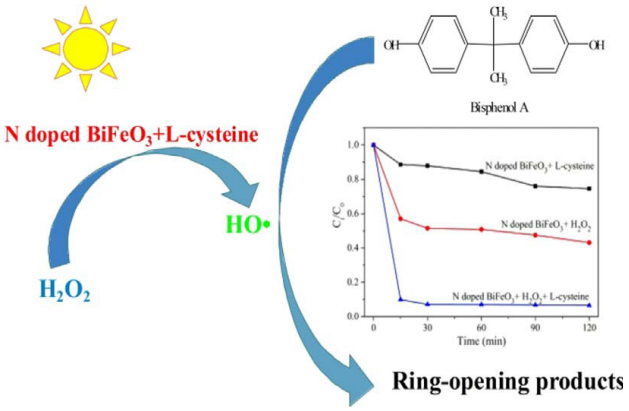

Reference

[1] Y. Jia, C. Liu, etc. Chemical Engineering Journal 337 (2018) 709-721.

Magnetism of wetted brownmillerite $SrFe_{0.5}Co_{0.5}O_{2.5}$ oxygen sponges

Joonhyuk Lee[1*], Younghak Kim[2], Hiromichi Ohta[3], Jinhyung Cho[4], and Hyoungjeen Jeen[1†]

[1]Department of Physics, Pusan National University, Busan, 46241, Korea

[2]Pohang Accelerator Laboratory, Pohang University of science and Technology, Pohang, 37673

[3]Research Institute for Electronic Science, Hokkaido University, N20W10, Kita, Sapporo, 001-0020, Japan

[4]Department of Physics Education, Pusan National University, Busan 46241

Topotactic "oxygen sponge" materials have received considerable attention due to the reversible transformation of their structure and physical properties by simple oxygen exchanges. In this work, we have tuned properties of brownmillerite $SrFe_{0.5}Co_{0.5}O_{2.5}$ (BM-SFCO) by interfacing with various oxides. By making a heterogeneous oxide interface, we could possibly transmit oxygens. We call this process "wetting" and studied changes in structure, valence state and magnetism using high resolution x-ray diffraction, x-ray absorption spectroscopy and x-ray magnetic circular dichroism. This work is valuable asset for designing interfacial structures like artificial superlattices.

This work was supported by the Basic Science Research Program through the National Research Foundation of Korea (NFR) funded by the Ministry of Education (NFR-2015R1D1A1A02062175).

Magnetically Soft FeCoTiZrB Alloys with High Saturation Magnetization

Sumin Kim[1*], Bo-Kyeong Han[1], Jin-Yoo Suh[2], Seon-Dae Kim[3], Dong-Hyun Kim[3], Young Keun Kim[4], Haein Choi-Yim[1]

[1]Department of Physics, Sookmyung Women's University, Korea

[2]High Temperature Energy Materials Research Center, Korea Institute of Science and Technology, Korea

[3]Department of Physics, Chungbuk National University, Korea

[4]Department of Materials Science and Engineering, Korea University, Korea

Soft magnetic materials are ubiquitously utilized in various applications such as motors, actuators, sensors, and so forth. The requirements for efficient cores in electric power transmission devices include low core loss and high saturation magnetization. Here we report the magnetic properties of Fe-based soft magnetic alloys with the compositions $Fe_{67-x}Co_{20}Ti_7Zr_6B_x$ (x = 0, 2, 4, and 6 at.%) produced by melt-spinning. The highest saturation magnetization achieved is 190 emu g−1 (1.79 T) for the $Fe_{67}Co_{20}Ti_7Zr_6$ system. This performance is attributed to the uniform distribution of nanometer-sized α-Fe nanocrystals. In addition, the experimentally measured magnetic properties are reproduced well by micromagnetic simulations.

International Symposium on Magnetism and
Magnetic Materials 2018

Oral Session II

'Magnetization dynamics and Spin orbit coupling phenomena'

Experiment for maximum speed of projectile using 2 stage coil gun

Kim Se Jong*, Kim Jin Ho†
Division of Mechanical Engineering, Yeongnam University

This study deals with the design and experiment of the coil gun of the projectile in the electromagnetic launch device. When a current is applied to a coil of a solenoid type, the coil gun is driven by a method of accelerating the projectile by converting it into mechanical kinetic energy through electromagnetic force generated by Fleming's right-hand rule. In order to increase the speed of the projectile, a multi stage solenoid is essential and a solenoid is designed in a 2-stage manner. In operation, when a current is applied to the first coil, the projectile is subjected to a force toward the coil, and when the first coil passes, the current is cut off and a current is applied to the second coil. The projectile receives the force in the direction of the second coil again, and when it reaches the second coil, it cuts off the current and it is fired at the maximum speed.

In this study, the number of turns of the solenoid, the position of the initial projectile and the size of projectile were selected as design variables. The speed of the launch vehicle of the 2-stage coil gun was designed using the MAXWELL electromagnetic program. Based on the data on the speed according to the change of the design variables, the optimal design was performed through the PIANO, a commercial PIDO tool, and design variables to obtain the maximum speed of the 2 stage coil gun were derived.

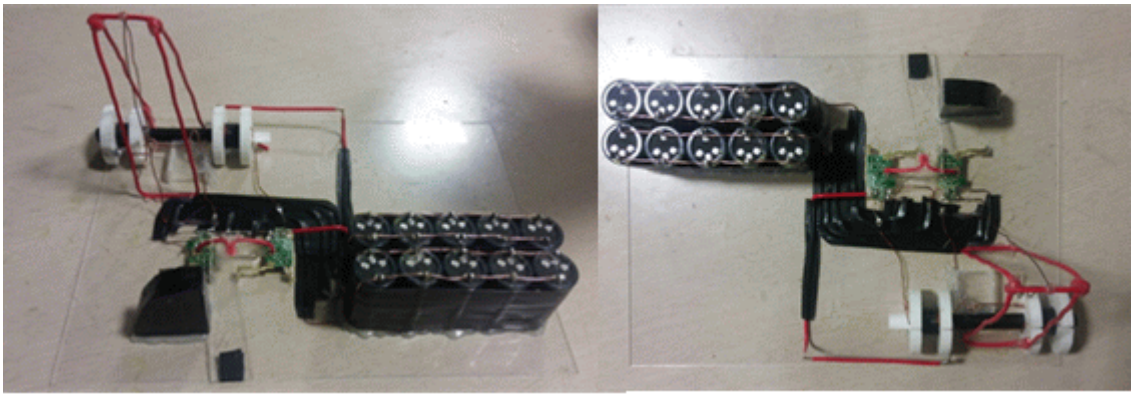

Fig. 1. Prototype of 2stage coil gun

O-II-2

Magnetization switching via electric field in FePt/MgO(001) film

Qurat-ul-ain[1*], D. Odkhuu[2], S. H. Rhim[1†], and S. C. Hong[1]

[1]Department of Physics and Energy Harvest-storage Research Center, University of Ulsan, Ulsan, Republic of Korea

[2]Department of Physics, Incheon National University, Incheon, Republic of Korea

Gaining control of magnetic properties by an external electric field can be a potential candidate to overcome the high-power consumption limitation for non-volatile magnetoelectric random access memory (MeRAM). Here using first principles calculations, we report a potential hetrostructure of FePt/MgO with a huge voltage control magnetic anisotropy (VCMA) coefficient »1.77 (-1.36) pJ/(V.m) for Fe- (Pt) interface. Fe-interface FePt/MgO film exhibits strain-induced magnetization reorientation instigated through second order magnetoelastic coupling. We predict a significant effect of external field on the induced electric dipole that can be understood in terms of charge accumulation or depletion at the metal/dielectric interface. Finally we demonstrate that VCMA behavior is extremely sensitive to the applied strain due to induced orbital reconstruction. These results are a step forward to achieve a full potential of MeRAM with write voltage below 1 V and switching bit energy below 1 fJ.

Magnetic Facet domains and Spin Torques

Kyoung-Woong Moon[1*], Changsoo Kim[1], Jungbum Yoon[1], Jun Woo Choi[2], Dong-Ok Kim[2,3], Kyung Mee Song[2,4], Dongseuk Kim[1], Byong Sun Chun[1], Chanyong Hwang[1]

[1]Spin Convergence Research Team, Korea Research Institute of Standards and Science, Daejeon 34113, Republic of Korea

[2]Center for Spintronics, Korea Institute of Science and Technology, Seoul 02792, Republic of Korea

[3]Department of Physics, Soongsil University, Seoul 06978, Republic of Korea

[4]Department of Physics, Sookmyung Women's University, Seoul 04130, Republic of Korea

An electric current can generate spin torques that act as prominent driving mechanism of magnetic domain wall motions because the spin torques push multiple domain walls to a certain direction that conserves the magnetization state. There are two distinct mechanisms for spin torques. One describes the domain wall motions by the current in the magnet. When the current in the magnet feels the magnetization change, the current exerts a torque on the local magnetization. The other type spin torque comes from a current flow in attached heavy metals to the magnet. The spin Hall effect splits the spin direction of the current in the heavy metal and a certain spins are pumped into the magnet that generates the spin torque. These two kinds of spin torques are not mutually exclusive thus separation of these two effect is an challenging problem. Here, we show a new method for measuring and separating two spin torques. This method observes nontrivial magnetic domain that is the "facet domain." The facet domain has straight domain walls that represent compensation of several driving mechanisms including an external field and the two spin torques. Studies on the domain wall angles as a function of external fields reveal a way to separate two kinds of spin torques.

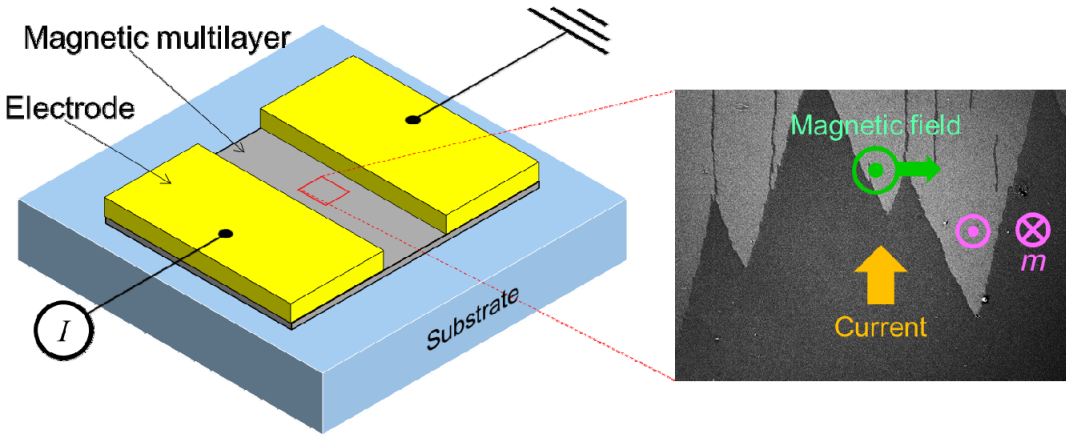

Fig. 1. A schematics of sample structure and an example of facet domain.

Compatibility between interfacial Dzyaloshinskii-Moriya interaction measurement schemes

Dae-Yun Kim[1*], Nam-Hui Kim[2], Yong-Keun Park[1,3], Byoung-Chul Min[3], Sug-Bong Choe[1], and Chun-Yeol You[2]

[1]Seoul National University, Korea

[2]Daegu Gyeongbuk Institute of Science and Technology

[3]Korea Institute of Science and Technology

The magnetic exchange interaction is the one of the key factors governing the basic characteristics of magnetic systems. Unlike the symmetric nature of the Heisenberg exchange interaction, the interfacial Dzyaloshinskii-Moriya interaction (DMI) generates an antisymmetric exchange interaction which offers challenging opportunities in spintronics with intriguing antisymmetric phenomena. The role of the DMI, however, is still being debated, largely because distinct strengths of DMI have been measured for different magnetic objects, particularly chiral magnetic domain walls (DWs) and non-reciprocal spin waves (SWs). In this paper, we show that, after careful data analysis, both the DWs and SWs experience the same strength of DMI. This was confirmed by spin-torque efficiency measurement for the DWs, and Brillouin light scattering measurement for the SWs. This observation, therefore, indicates the unique role of the DMI on the magnetic DW and SW dynamics and also guarantees the compatibility of several DMI-measurement schemes recently proposed.

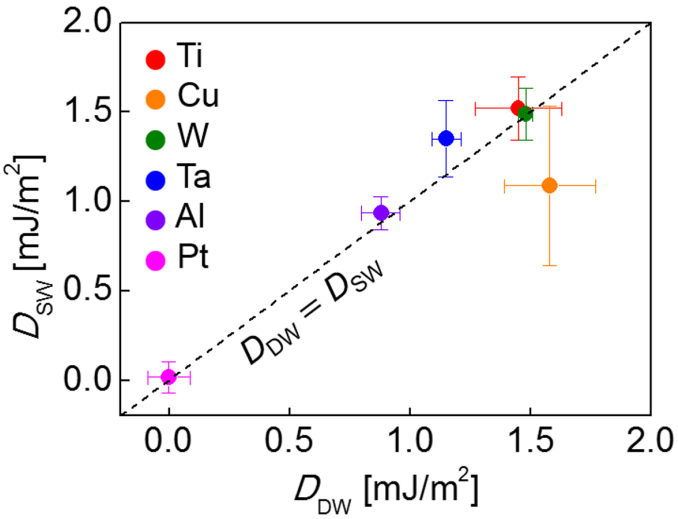

Fig. 1. Comparison of DMI constants determined by domain-wall- and spin-wave-based measurement schemes

Interfacial Dzyaloshinskii-Moriya interactions in W/CoFeB/MgO film systems

Gyu Won Kim[1*], Alexander S. Samardak[2,5,6], Yong Jin Kim[1], In Ho Cha[1], Alexey Ognev[2], Alexandr V. Sadovnikov[3,4], Sergey A. Nikitov[3,4], and Young Keun Kim[1,3†]

[1]Department of Materials Science and Engineering, Korea University, Seoul 02841, Korea
[2]School of Natural Sciences, Far Eastern Federal University, Vladivostok 690950, Russia
[3]Laboratory "Metamaterials", Saratov State University, Saratov 410012, Russia
[4]Kotel'nikov Institute of Radioengineering and Electronics, Russian Academy of Sciences, Moscow 125009, Russia
[5]Center for Spin-Orbitronic Materials, Korea University, Seoul 02841, Korea
[6]National Research South Ural State University, Chelyabinsk 454080, Russia

For the development of next-generation magnetic memory or logic devices, understanding microscopic origins of interfacial magnetic properties such as perpendicular magnetic anisotropy (PMA) and interfacial Dzyaloshinskii-Moriya interaction (iDMI) are important. In particular, the iDMI has drawn considerable attention because it can generate additional exchange energy term and manipulate intra-atomic magnetization dynamics. The iDMI appears when a thin ferromagnetic (FM) layer is in contact with a heavy metal (HM) [1].

In this study, we investigated the iDMI energy density and surface PMA energy in W/CoFeB/MgO trilayers with different phases of W layer. To induce phase transition we varied the thickness of W layer from 1 nm to 15 nm and used different annealing temperatures.

Since it is known as that iDMI and PMA have the same interface originated magnetic properties, we calculated surface contribution of PMA energy and found that it showed similar oscillatory behavior to the iDMI energy with different W thicknesses and phases. Both these two physical properties showed two maximum values at amorphous and alpha-W phases, while minimum value at beta-W phase. We think that their variation occurs because of the changing in the lattice parameter of W when it underwent the phase transformation. Also, we could confirm interatomic distance between W and CoFeB is important factor that determine the strength of iDMI energy.

Reference

[1] A. Fert et al., Nat. Nanotech. 8, 152 (2013)

Experimental observation of the correlation between the interfacial Dzyaloshinskii-Moriya interaction and work function in metallic magnetic trilayers

Yong-Keun Park[1,2*], Dae-Yun Kim[1], Joo-Sung Kim[1], Yune-Seok Nam[1], Min-Ho Park[1], Hyeok-Cheol Choi[1], Byoung-Chul Min[2], and Sug-Bong Choe[1]

[1]Department of Physics and Astronomy, Seoul National University, Seoul 08826, Republic of Korea

[2]Center for Spintronics, Korea Institute of Science & Technology, Seoul 02792, Republic of Korea

The Dzyaloshinskii-Moriya interaction (DMI) generates intriguing chiral magnetic objects, such as magnetic skyrmions and chiral domain walls, that can be used as building blocks in emerging magnetic nanodevices. Because of the academic interest and technological importance, better understanding and precise control of the DMI strength is one of the key issues for achieving better stability and functionality of these chiral objects. However, detailed relation between the DMI strength and the nature of the interface remains elusive. Our motivation is to find dominant parameter that related to the DMI to provide a guideline for DMI engineering. We report that in magnetic trilayer films, the DMI strength exhibits a noticeable correlation with the work functions of the nonmagnetic layers interfaced to the magnetic layer [1].

For this examination, we fabricate a series Pt/Co/X (X=Pt, Pd, Au, Ru, Al, Ta, W, Ti, and Cu) films. The films basically have the same structure except the upper layer material X. Figure 1 plots measured D with respect to ΔW, where ΔW is difference between measured work function of X and Co. The figure shows a noticeable correlation between D with respect to ΔW. Though the exact value of D in real films may depend on many other parameter and condition of the interface, the present observation provides a good guideline to design the film structure for optimal DMI.

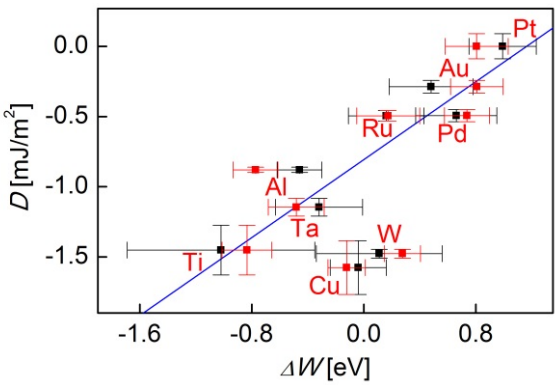

Fig. 1. Plot of the with respect to the, for Pt/Co/X films with various materials X as denoted in the figure.

Reference

[1] Y.-K. Park et al. NPG Asia Materials, accepted.

Highly efficient magneto-ionic control of interfacial magnetism using YSZ (Yttria-Stabilized Zirconia) gate oxide

Sujin Jo[1*], Jung-Hoon Park[2], Aik Jun Tan[3], Ho-Il Ji[2], Ji-Won Son[2], Geoffrey S. D. Beach[3], Seonghoon Woo[1†]

[1]Center for Spintronics, Korea Institute of Science and Technology, Seoul 02792, South Korea

[2]High Temperature Energy Materials Research Center, Korea Institute of Science and Technology, Seoul 02792, South Korea

[3]Department of Materials Science and Engineering, Massachusetts Institute of Technology, Cambridge 02139, USA

Voltage control of magnetism has been a remarkable subject of spintronics research for many years, mainly due to their possibility for the realization of memory devices with ultra-low power consumption[1,2]. Among few suggested methods, the magneto-ionic control of magnetism that utilizes the reversible oxidation/reduction of buried ferromagnet have demonstrated significant modulation of magnetic anisotropy on the order of ~ 1 erg cm^{-2}, which is much larger than any other voltage-induced effect[3,4]. However, the early works utilized voltage-induced oxygen migration, which inevitably suffers from i) irreversible oxidation damage resulting in poor cyclability[5] and ii) high operation temperature required for the fast switching on the order of ~100 ms[4]. Recently, it has been demonstrated that, unlike oxygen-based devices, hydrogen-based magneto-ionic devices where interfacial magnetism is controlled by hydrogen loading/unloading could offer largely enhanced device characteristics, exhibiting high reliability (>2000 cycles) and fast switching (~100 ms) at room temperature.[6] However, the switching speed may still need to be improved significantly, for the application to nanosecond-switching memory devices.

In this presentation, we show that the performance of hydrogen-based magneto-ionic devices can be significantly improved using an yttria-stabilized zirconia (YSZ) gate oxide, which is a well-known proton conductive oxide due to its relatively open lattice space and the high concentration of oxygen vacancy sites. We utilized the ferromagnetic heterostructure of Pd/Co/Pd/YSZ/Pt, where YSZ and Pt served as a proton-migrating layer and a water-splitting top electrode, respectively. Figure 1 summarizes device structure and the experimentally measured device characteristics. When positive gating voltage of +6 V is applied, protons generated from the top electrode migrate across YSZ and eventually are accumulated at Pd layers, due to their significantly larger proton solubility compared to that of Co. Protons accumulated at Pd then modulates spin-orbit coupling (SOC) at the Pd/Co & Co/Pd interfaces, eventually switching the magnetic anisotropy of the trilayer from perpendicular magnetic anisotropy (PMA) to in-plane anisotropy, as shown in Fig. 1(b). When the opposite voltage polarity is applied, V = -6 V, accumulated protons are pulled out of the structure, recovering PMA. We then performed the cyclic voltage application between V = ±6 V at the voltage reversal frequency of f = 0.5 Hz, and measured the magnetic states as a function of time. Surprisingly, as shown in Fig. 1(c), we achieved the fast switching speed (<1 ms) and the high stability (> 10^3 cycles). In particular, the magnetic anisotropy switching speed is measured to be 10^3 times faster than the state-of-the-art magneto-ionic devices reported to date. We believe that further material/interface engineering based on YSZ gate oxide could reduce the switching speed, down to 10 ~ 100 times the nanoseconds, highly suitable for the realization of ultra-low-power spintronic memory devices.

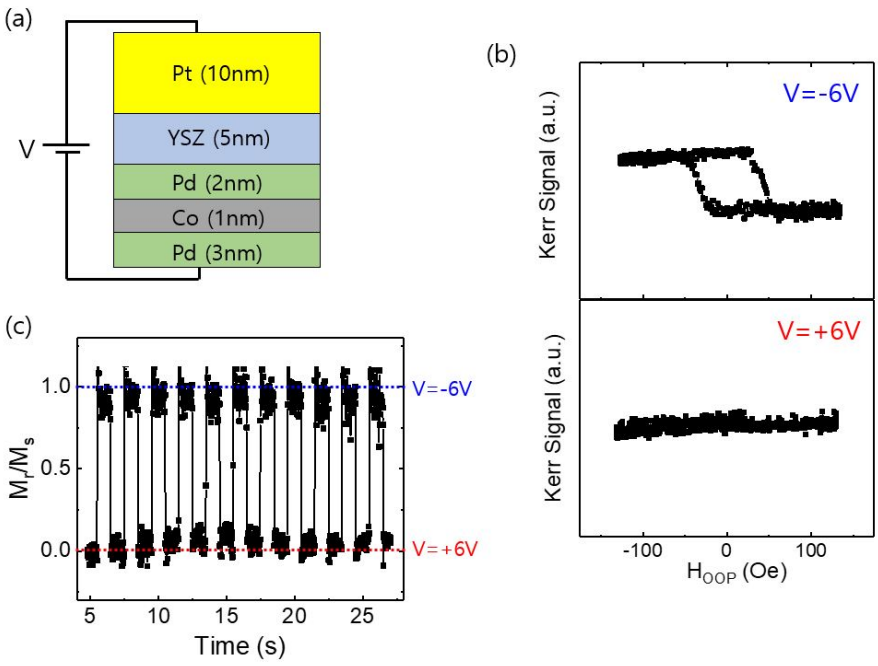

Fig. 1. (a) Device structure. (b) Voltage-controlled modulation of remnant magnetization (M_r/M_s) at zero magnetic field under cyclic voltage application (V=6V & V=-6V at f_{cycle} = 0.5Hz). (c) Hysteresis loops at V=6V and V=-6V.

References

[1] Matsukura, F. et al. Nat. Nanotechnol. **10,** 209-220 (2015).

[2] Song, C. et al. Prog. Mater. Sci. **87,** 33-82 (2017).

[3] Bauer, U. et al. Nat. Mater. **14,** 174-181 (2015).

[4] Bi, C. et al. Phys. Rev. Lett. **113,** 267202 (2014).

[5] Gilbert, D. A. et al. Nat. Commun. **7,** 12264 (2016).

[6] Tan, A. J. et al. submitted (2018); Proc. of 2018 Int. Conf. on Magn.

Deterministic writing and deleting of single skyrmion observed by time-resolved X-ray imaging

Kyung Mee Song[1,2*], Xichao Zhang[3], Motohiko Ezawa[4], Yan Zhou[3], Xiaoxi Liu[5], Markus Weigand[6], S. Finizio[7], J. Raabe[7], Min-Chul Park[8], Seonghoon Woo[1]

[1]Center for Spintronics, Korea Institute of Science and Technology, Seoul 02792, Korea

[2]Department of Physics, Sookmyung Women's University, Seoul 04130, Korea

[3]School of Science and Engineering, Chinese University of Hong Kong, Shenzhen, Guandong 518172, China

[4]Department of Applied Physics, University of Tokyo, 7-3-1 Hongo, Tokyo 113-8656, Japan

[5]Department of Electrical and Computer Engineering, Shinshu University, 4-17-1 Wakasato, Nagano 380-8553, Japan

[6]Max-Planck-Institut für Intelligente Systeme, 70569 Stuttgart, Germany

[7]Swiss Light Source, Paul Scherrer Institut, 5232 Villigen, Switzerland

[8]Center for Opto-Electronic Materials and Devices, Korea Institute of Science and Technology, Seoul 02792, Korea

Magnetic skyrmionic devices are one of the most promising candidate for the next-generation memory application due to their nanometer-size, topological stability and efficient current-driven dynamic motion. Recently, interfacial Dzyaloshinskii-Moriya interaction (DMI) leads stabilization of magnetic skyrmions in heavy metal/ferromagnetic hetrostructure at room-temperature. While efficient modulation of current-driven displacement of magnetic skyrmions have been demonstrated [1]-[2], still many challenges remain to utilize of fully functional skyrmionic devices. In particular, the experimental observation of controllable creation and annihilation of a single skyrmion at room-temperature have been elusive so far, even though it may be an indispensable part to operate future skyrmionic devices.

In this work, for the first time, we demonstrate the electrical creation and deletion of a single ferrimagnetic skyrmion at room-temperature in practical device scheme [3]. The stroboscopic pump-probe X-ray measurement is performed to reveal the deterministic and reproducible nature of this process. $[Pt/GdFeCo/MgO]_{20}$ multilayer structures with perpendicular magnetic anisotropy (PMA) are chosen (Fig. 1(a)), due to their ferrimagnetic nature exhibiting the enhanced current-driven skyrmion behaviors such as the suppression of skyrmion Hall angle [4]. We first experimentally show that unbalanced bipolar current pulses can efficiently create and annihilate a single skyrmion in ferrimagnetic materials, GdFeCo, in nanosecond time scale as shown in Fig. 1 (c)-(f). Micromagnetic simulations reveal the microscopic origin behind the observed topological fluctuation with qualitative and quantitative agreement. We believe that our findings offer a distinct electrical manipulation method for the skyrmion writing/deleting process which is important feature for the all-electrically operated skyrmionic devices.

References

[1] W. Jiang et al., Science, 349 (6245), 283-286, (2015)

[2] S. Woo et al., Nature Materials, 15 (5), 501-506, (2016)

[3] S. Woo et al., Nature Electronics, 1(5), 288-296, (2018)

[4] S. Woo et al., Nature Communications, 9 (1), 959 (2018)

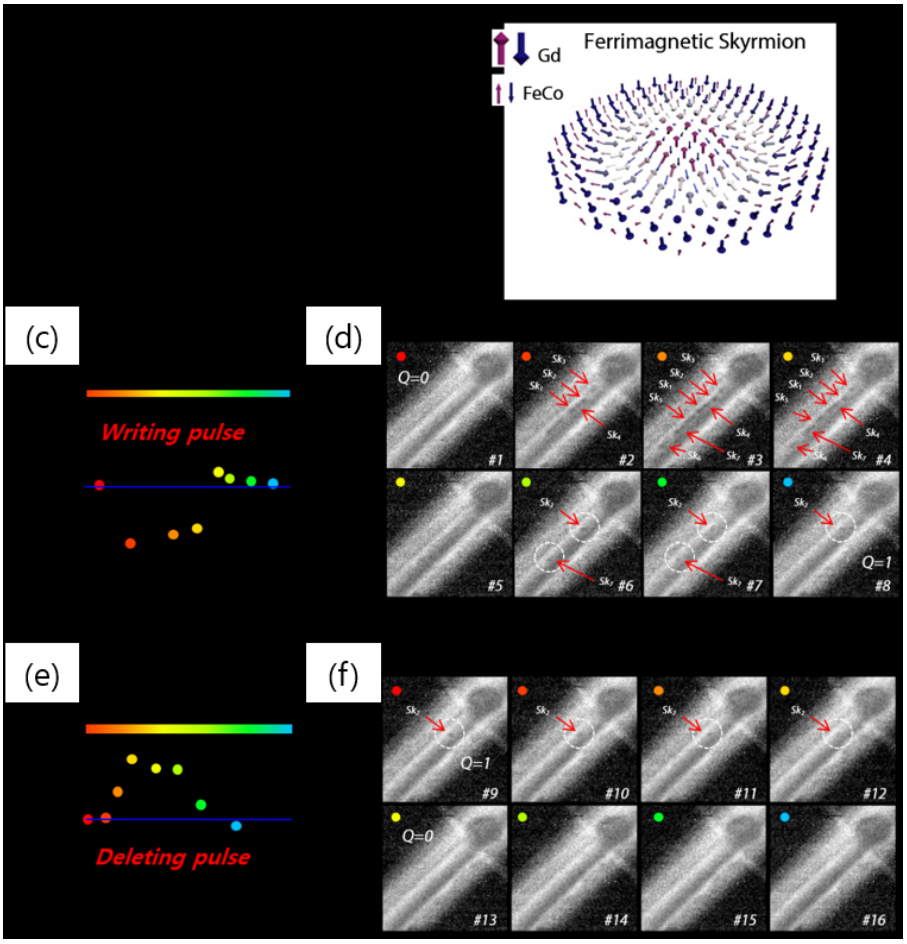

Fig. 1. Hysteresis loops of ferrimagnetic multilayer structure and field-driven domain evolution within in device. (a) Out-of-plane hysteresis loop for $[Pt/GdFeCo/MgO]_{20}$ multilayers measured by vibrating sample magnetometer (VSM). (b) is the schematics of ferrimagnetic skyrmions. Fig. 1 (c) ~ (f) show the time-resolved pump-probe X-ray microscopy measurement. (c) The pulse profiles used for skyrmion writing and (d) creation configuration of magnetic skyrmion at different time delays. (e) The pulse profile used for skyrmion deleting and (f) its deleting process observed by time-resolved STXM.

Vanishing skyrmion Hall effect at the angular momentum compensation temperature of a ferrimagnet

Duck-Ho Kim[1*], Yuushou Hirata[1], Se Kwon Kim[2], Dong-Kyu Lee[3], Se-Hyeok Oh[4], Dae-Yun Kim[5], Tomoe Nishimura[1], Takaya Okuno[1], Yasuhiro Futakawa[6], Hiroki Yoshikawa[6], Arata Tsukamoto[6], Yaroslav Tserkovnyak[2], Yoichi Shiota[1], Takahiro Moriyama[1], Sug-Bong Choe[5], Kyung-Jin Lee[3,4,7], and Teruo Ono[1,8]

[1]Institute for Chemical Research, Kyoto University, Uji, Kyoto 611-0011, Japan
[2]Department of Physics and Astronomy, University of California Los Angeles, California 90095, USA
[3]Department of Materials Science & Engineering, Korea University, Seoul 02841, Republic of Korea
[4]Department of Nano-Semiconductor and Engineering, Korea University, Seoul 02841, Republic of Korea
[5]Department of Physics and Institute of Applied Physics, Seoul National University, Seoul 08826, Republic of Korea
[6]College of Science and Technology, Nihon University, Funabashi, Chiba 274-8501, Japan
[7]KU-KIST Graduate School of Converging Science and Technology, Korea University, Seoul 02841, Republic of Korea
[8]Center for Spintronics Research Network (CSRN), Graduate School of Engineering Science, Osaka University, Osaka 560-8531, Japan

Charged particles exhibit the Hall effect in the presence of magnetic fields. Analogously, ferromagnetic skyrmions with non-zero topological charges and finite fictitious magnetic fields exhibit the skyrmion Hall effect, which is detrimental for applications. The skyrmion Hall effect has been theoretically predicted to vanish for antiferromagnetic skyrmions because the fictitious magnetic field, proportional to net spin density, is zero. We experimentally confirm this prediction by observing current-driven transverse elongation of pinned ferrimagnetic bubbles. Remarkably, the skyrmion Hall effect, estimated with the angle between the current and bubble elongation directions, vanishes at the angular momentum compensation temperature where the net spin density vanishes. This study establishes a direct connection between the fictitious magnetic field and spin density, offering a pathway towards the realization of skyrmionic devices.

International Symposium on Magnetism and Magnetic Materials 2018

Special Session II

'Magnetics for Defence'

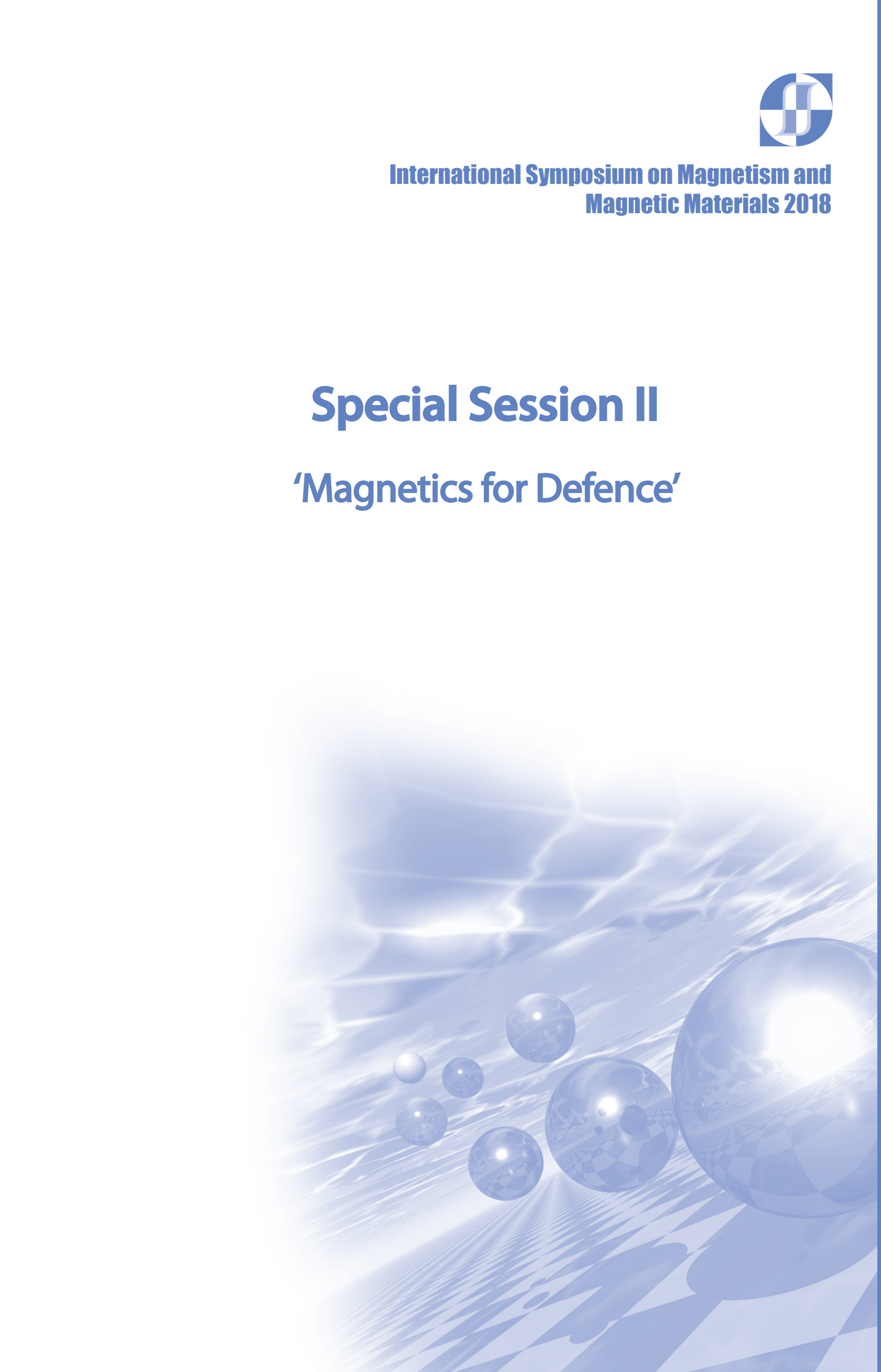

Magnetic Treatment Techniques for Magnetic Field Reduction of a Naval Ship without Degaussing Coil

Hyun-Ju Chung*, Ki-Woong Bae, Chang-Seob Yang and Woo-Jin Jung
Naval Systems R&D Institute, Agency for Defense Development, Changwon 51678, South Korea

The magnetic field generated from the ferromagnetic hull of a ship can be classified into the field by permanent magnetization (PM) and the one by induced magnetization (IM). PM field can be reduced by demagnetization process such as ship deperming. On the other hand IM field can be only reduced by a ship's degaussing coil. Thus the ships without degaussing coil are vulnerable to the threat of underwater weapon system which detect magnetic field from target in the underwater. However, it is not easy to install degaussing system inside a small naval ship or submarine because of the limitation such as heavy weight, installation space and electric power consumption of the degaussing system.

As a best way to reduce magnetic field for a naval ship without a degaussing system, it is widely used an anhysteretic deperm or a flash-D deperm method as conventional demagnetization method. Basically these methods are to reduce magnetic fields from a ship as obtained the reverse permanent vertical magnetization (PVM) that counteracts the induced vertical magnetization (IVM) in the target ship due to the earth's magnetic field as shown in Fig. 1. An anhysteretic demagnetization method is a little simple, but the long term stability for keeping the reverse PVM is not so good. On the other hand, a flash-D demagnetization method has a good long term stability of reverse PVM compared the anhysteretic deperm. However, the process is a little complex to use in a real ship because it involves three stages. Therefore, In previous paper, we has proposed two-stage demagnetization protocol for enhancing the bad stability on the keeping reverse PVM of anhysteretic deperm and the difficulty in a practice of the flash-D deperm.

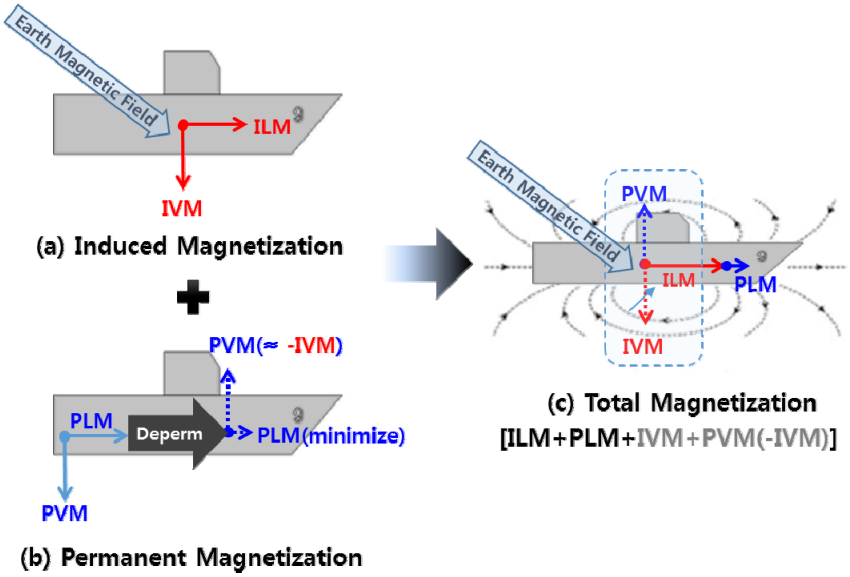

Fig. 1. A basic concept for reducing ship's magnetic field by obtaining the reverse PVM that counteracts the IVM

Fig. 2 shows proposed two-stage demagnetization protocol. In the first stage, we obtain a very strong PVM. In the second stage, we gain the wanted PVM for compensating the IVM with minimization of a permanent longitudinal magnetization as adjusting the value of a horizontal start field and the total applied field number of the second stage. Therefore this method is very simple compared to the flash-D method and the long term stability on the keeping reverse PVM is better compared to the anhysteretic method. In previous paper, we already applied the two-stage demagnetization to a scaled model ship and verified the effectiveness on the keeping the stability of a reverse PVM.

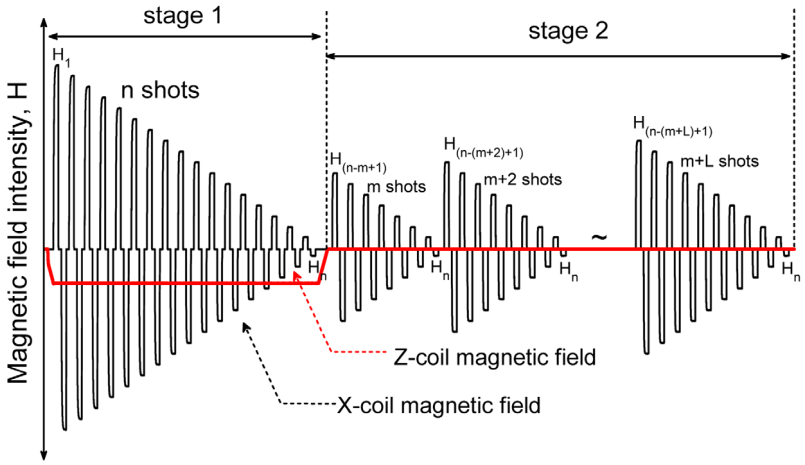

Fig. 2. The proposed two-stage demagnetization protocol

Fig. 3 shows the magnetic field from a real ship after anhysteretic(x year) deperm or two-stage demagnetization (x+3 year) process. Three years after anhysteretic demagnetization to the real ship, we can know that the ship's magnetic field was returned to its original state again. It means that the long term stability of anhysteretic deperm is not so good. Thus in this paper, we applied two-stage demagnetization process to real ship as applied to the scaled model ship instead anhysteretic deperm. As a result of that, we could determine successfully the protocol which can remove VM of the real ship. And the maximum absolute magnetic field could be reduced to 50% of the original magnetic field. We will continue to observe the performance of the long term stability on the two-stage demagnetization in the future.

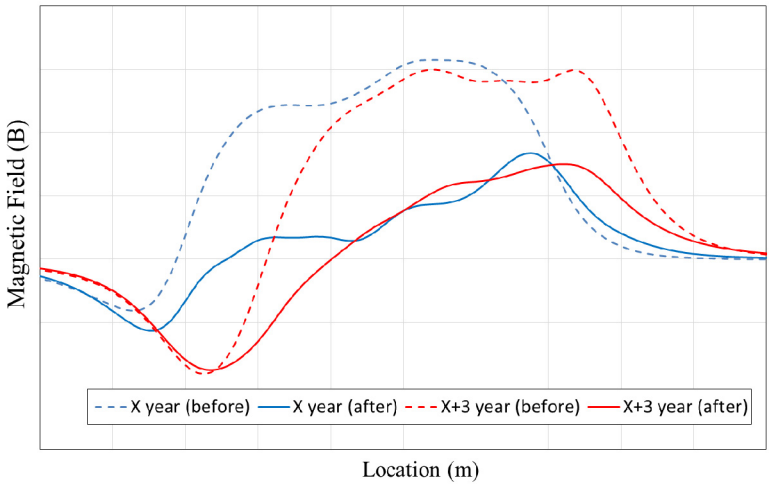

Fig. 3. The ship's magnetic field after anhysteretic(x year) deperm and two-stage demagnetization(x+3 year) process

A Study on the Effect of Multiple Materials on Demagnetization

Sang Hyeon Im*, Ho Yeong Lee, Gwan Soo Park
ADepartment of Electrical and computer Engineering, Pusan National University, Korea

Demagnetization is to reduce the residual magnetization in magnetic materials and to remove the magnetic field signal from the outside. It is very important in the national defense to prevent damages caused by magnetic mines on the sea.

The studies on the demagnetization of the warship have been studied continuously from the past [2][3]. Most of them have been studied for a deperming protocol, assuming that the warship was made of one magnetic material. However, it consists of various materials which makes it impossible to represent a single material. If a protocol was applied for one material, a large magnetic signal will be generated from other materials. Therefore, it is necessary to study the magnetic interactions of various materials on the demagnetization and propose optimal protocol for submarine.

In this paper, the effects of magnetic interaction in the warship during deperming were analyzed by using Preisach model. Hollow cylinders that made of different materials were used as equivalent models of a warship. The hysteresis characteristics of each materials were represented by Preisach model. After the deperming protocols for the each parts of that were applied respectively, the internal magnetization was analyzed and the magnetic field at the sensor were measured by using Preisach model. According to this, the influences of the interaction of multiple materials on the demagnetization were analyzed and the experiment was conducted to validate in a scaled-down MTF test room.

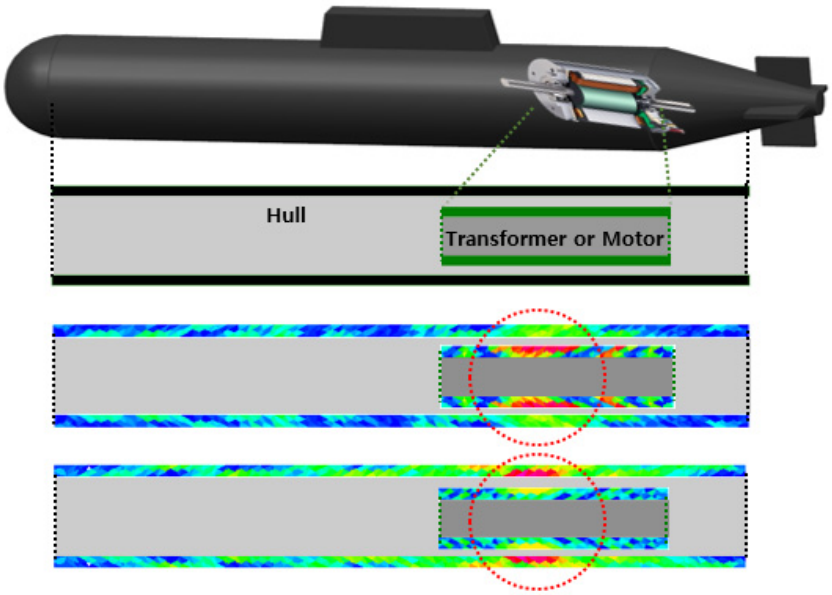

Fig. 1. The warship equivalent model and magnetization distribution after deperming protocols for each parts

This study assumed that the warship consists of two parts, hull, transformer or motor with different magnetic properties. Fig. 1 shows the equivalent and analytical model. The interaction effects that occurred during demagnetization were analyzed by a program combining Preisach modelling and Finite Element Method. As shown in Fig. 1, when the protocol for removing magnetization of each hull, transformer and motor was applied, it can be seen that the magnetization in the target is greatly reduced, but a large magnetization remains in the other part. According to this, the magnitude of the magnetic flux density measure by the sensor becomes very large, which increases the risk of the magnetic mines. Therefore, a deperming protocol considering interaction of each material is required.

Construction of 3-axis Flux-gate Magnetometer for Harbor Surveillance System

Eunhae Kim[1], Derac Son[1], Jin-Suk Cho[2*], Hyun-Ju Chung[3]
[1]Sensorpia Co., Yuseong-daero 1596-64, 34054, Rep. of Korea
[2]LIGNex1 Co., 333, Pangyo-ro, Bundang-gu, Seongnam-si, Gyeonggi-do, Rep. of Korea
[3]Naval Systems R&D Institute, Agency for Defense Development, Changwon 51678, Rep. of Korea

To surveil unidentified objects which are moving in harbor, passive and active sonar, and magnetic field detection technologies have been used. Magnetic field detection technology becomes more important due to higher detection probability. To detect magnetic field generated by unidentified objects, we must distinguish magnetic field signal from object and earth magnetic field. In ideal case, all magnetometers should be laid underground of sea water with the same magnetic field measuring axis i.e. south-north, east-west, and vertical direction. But it is impossible to achieve and actually we cannot know attitude of the magnetometers which are laid. Due to this problems, total of magnetic field measurement have been used to observe magnetic objects. In this case, the same scale factor of the 3-axis and orthogonality between 3-axis are very important.

In this work we developed 3-axis flux-gate magnetometer which has high orthogonality using special algorithm and high linearity using compensation of magnetic field to be measured. Fig. 1 shows schematics of the developed magnetometer which consists of analogue PCB for sensor core magnetization and feedback system for magnetic field compensation, digital PCB for 24 bit ADC RS422 interface. Fig. 2 shows 3-axis Helmholtz coil system for magnetometer calibration and measured linearity of magnetometer better than 10^{-4}.

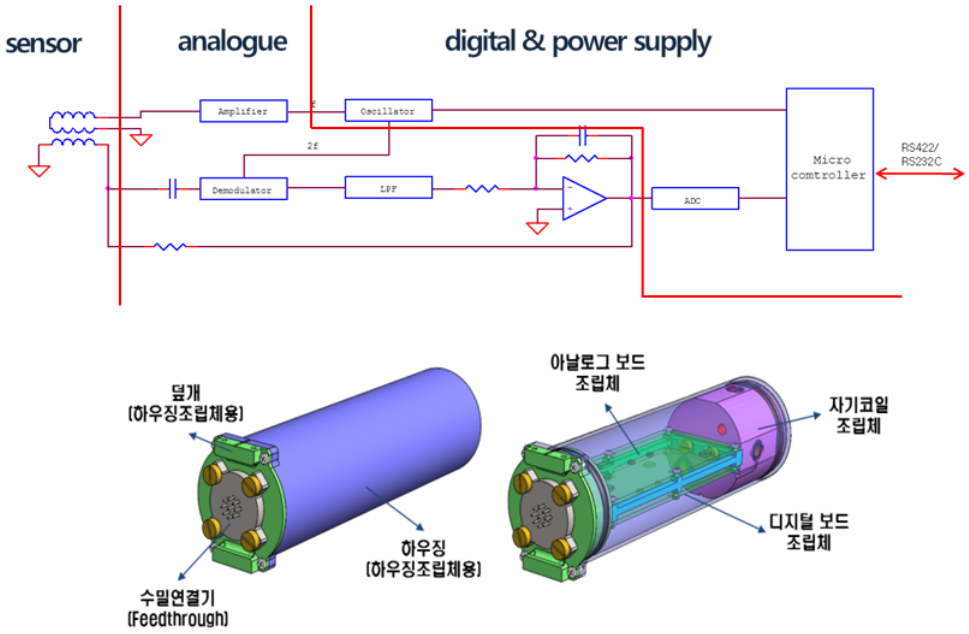

Fig. 1. Structure of the 3-axis flux-gate magnetometer.

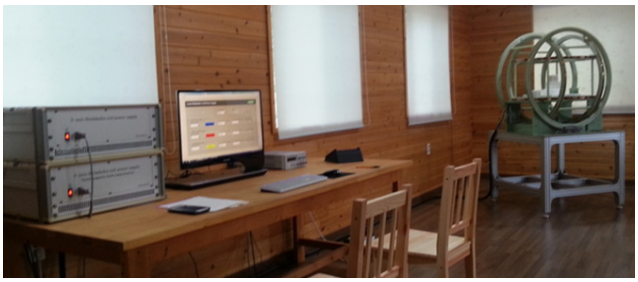

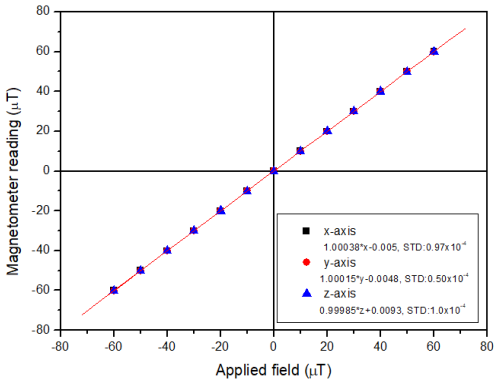

Fig. 2. Calibration system for the magnetometer and linearity of the developed magnetometer.

Fig. 3 shows frequency bandwidth measuring equipment and measured results. Frequency bandwidth was about 4Hz.

Fig. 4 shows long term stability measurement of the developed magnetometer put into the magnetic shield chamber which has 4-shielding can and shielding factor of 80dB. Fig. 5 shows photograph of the assembled magnetometers before tubing for underwater laying.

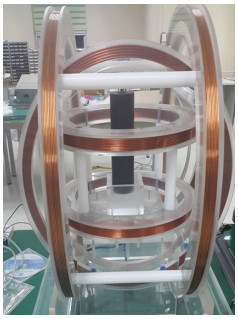

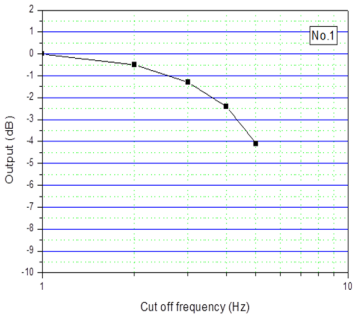

Fig. 3. Frequency bandwidth measurement of the magnetometer.

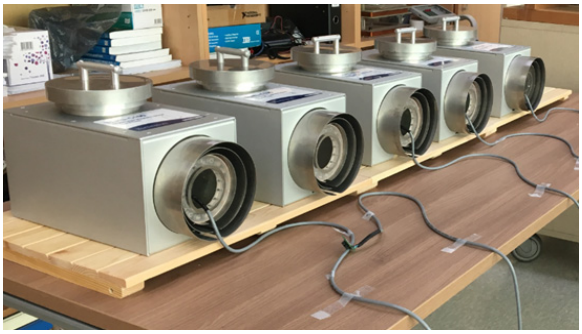

Fig. 4. Long term drift measurement of the magnetometer.

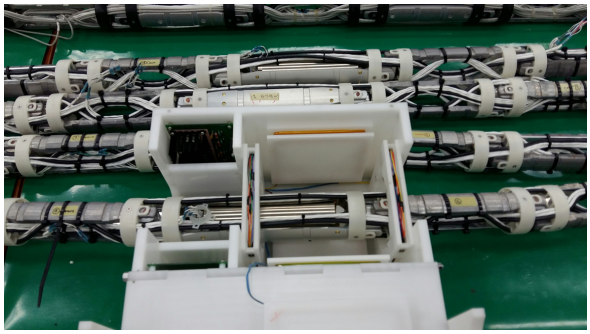

Fig. 5. Assembled magnetometers before tubing for underwater laying.

A Degaussing Technique of a Naval Ship Considering the Linearity of Induced Magnetic Field under the Earth Magnetic Field

Hyun-Ju Chung*, Ki-Woong Bae, Chang-Seob Yang and Woo-Jin Jung
Naval Systems R&D Institute, Agency for Defense Development, Changwon 51678, South Korea

Under the earth's magnetic field, the ferromagnetic hull of a naval ship is magnetized and accordingly it induces underwater magnetic field around the ship. Underwater surveillance system and maritime patrol aircraft with magnetic sensor can easily detect the presence of a ship. Furthermore, the field can be a trigger source for actuating underwater influence mine with magnetic sensor. Therefore reducing the magnetic field from a naval ship is very important to decrease the probability of being detected from various threats, which is influenced to the magnetic field.

The magnetic field generated from the ferromagnetic hull of a ship can be classified into the field by permanent magnetization (PM) and the one by induced magnetization (IM). PM field can be reduced by demagnetization process such as ship deperming. The residual permanent magnetic field after deperming and IM field can be controlled by a ship degaussing process. The principle of the ship degaussing is to generate degaussing coil magnetic field of which the magnitude is similar to that of the field due to the hull, but the polarity of two fields (i.e. ship magnetic field and coil magnetic field) are opposite to each other.

For a ship degaussing, a degaussing equipment consisting of degaussing coils, power supplies for degaussing coil, magnetic sensor probe and control unit is installed inside a ship. The degaussing coils also consist of longitudinal (L), athwartship (A) and vertical (V) coils (refer to Fig. 1). In order to minimize the magnetic field from a naval ship, the currents applied to individual degaussing coil are elaborately calibrated during a degaussing process at the ship's magnetic field measurement station (degaussing range).

In this paper, we describe the ship's degaussing technique carried out with a scaled model ship in the non-magnetic facility. For that, we made up a scaled model ship, small degaussing equipment for the scaled model ship and magnetic sensor probe as shown in Fig. 1.

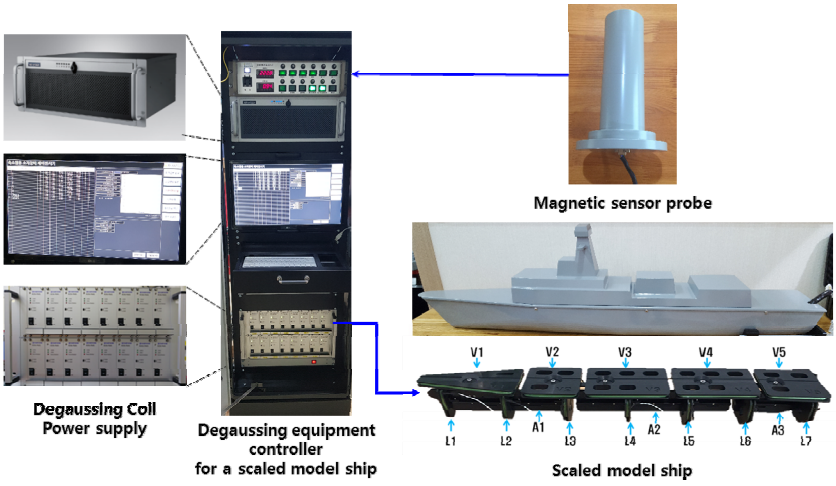

Fig. 1. A degaussing equipment for a scaled model ship

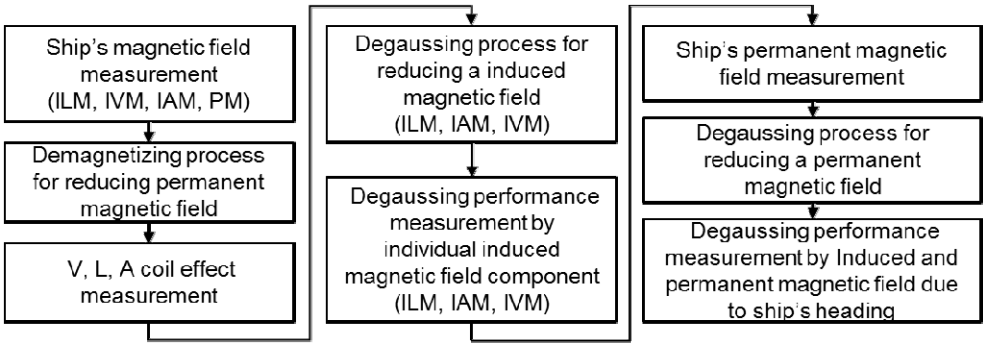

Fig. 2. A degaussing process for reducing the ship's magnetic field.

Fig. 2 shows the procedure for reducing the ship's magnetic field through degaussing process. Through a ship deperming process, ship's permanent magnetization can be reduced. However ship's induced magnetization can be only controlled by degaussing process because IM field only depends on the present earth magnetic field. Thus when ship's bow direction is the northward or the southward, ILM (induced longitudinal magnetization) and IVM (induced vertical magnetization) are induced on the ship's hull. On the other hand, in the bow direction of the eastward or the southward, IAM (induced athwartship magnetization) and IVM are induced on the ship's hull. ILM field is controlled by L degaussing coils, IAM field is controlled by A coil and IVM field is controlled by V coils.

The degaussing coil currents on the ILM, IAM and IVM field are calculated individually at the degaussing range and the IM fields can be reduced by below 90% of its original magnetic field through degaussing process. The IM field increases and decreased almost linearly according to the magnitude of earth magnetic field. Therefore the coil currents in other regions, where degaussing process is executed, are adjusted linearly in proportion to the magnitude of each earth magnetic fields (Bx, By, Bz) measured by magnetic sensor probe equipped on the ship mast.

Generally, the IVM field is almost constant regardless of ship's bow direction under the similar earth magnetic field. However horizontal IM field is affected by ship's bow direction. The horizontal IM field according to ship's bow direction such as northeast or southwest can be calculated simply as shown Fig. 3. Fig. 4 and Fig. 5 show the ILM and IAM fields before and after degaussing. The field after degaussing reduced by below 90% of its original magnetic field. Fig. 6 shows the horizontal IM field at the bow direction of the southwestward before and after degaussing. L and A coil current can be controlled by the equation of the Fig. 3 from L and A coil current used for ILM and IAM field compensation in the Fig. 3 and Fig. 4. As a result of that, the horizontal IM field can be also reduced by below 90% of its original magnetic field at the ship direction of the southwestward.

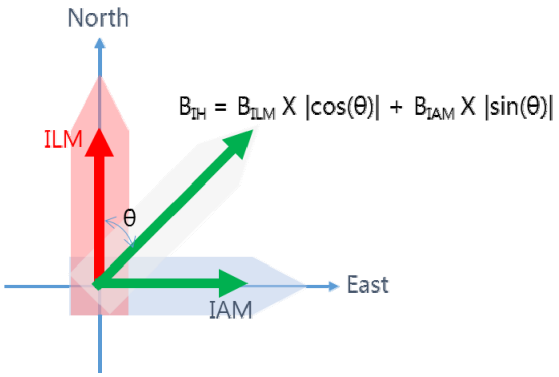

Fig. 3. Horizontal IM field according to bow direction

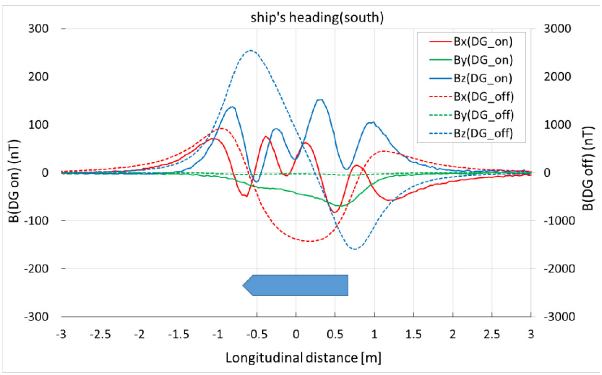

Fig. 4. IM field at the southward ship heading

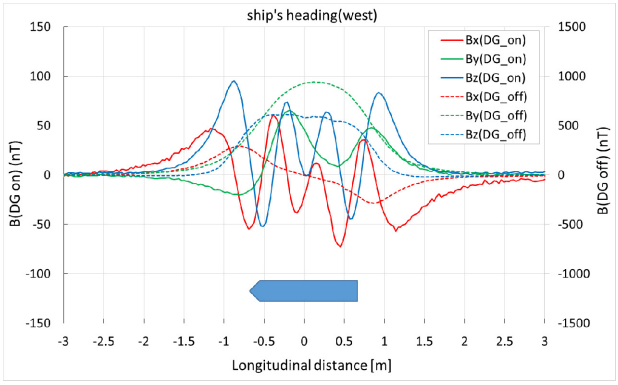

Fig. 5. IM field at the westward ship heading

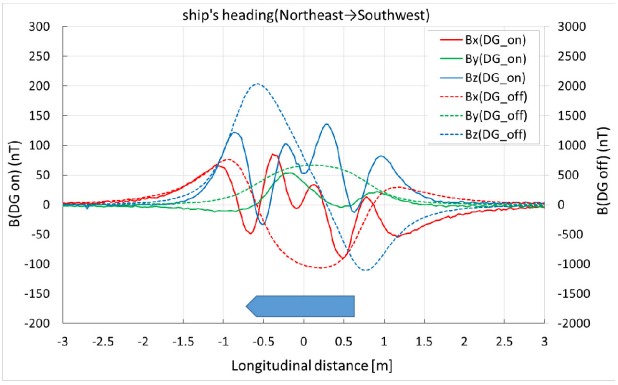

Fig. 6. IM field at the southwestward ship heading

In conclusion, we can reduce the ship magnetic field by less than 90% of its original magnetic field at all ship's direction by using degaussing technique considering the linearity of IM field under the earth magnetic field.

Orthogonality corrected 3-axis Flux-gate Magnetometer for Total Magnetic Field Measurements

Derac Son*
Sensorpia Co., Yuseong-daero 1596-64, 34054, Rep. of Korea

To measure magnetic field of the earth magnetic field and generated from objects, we need 3-axis magnetic field components and total magnetic field. But one magnetometer has not been used for this purpose because conventional 3-axis magnetometers have not measure magnetic field components ideally, i.e. angles between axes are not orthogonal and scale factor between 3-axis are same.

In this work, we tried 3-axis magnetometer which measure not only 3-axis magnetic field components but also total magnetic field. When we calculate total magnetic field using measured values from 3-axis magnetometer is not total magnetic field as follows due to the angles between 3-axis are not orthogonal and scale factor between 3-axis are same.

$$B_m^t \neq \sqrt{B_{mx}^2 + B_{my}^2 + B_{mz}^2} \qquad (1)$$

If we correct scale factor and after that rotate axes of the magnetometer using following equation(2) using microprocessor in smart sensor, we can get total magnetic field using equation(3).

$$\begin{pmatrix} B_{cx} \\ B_{cy} \\ B_{cz} \end{pmatrix} = \begin{pmatrix} T_{11} & T_{12} & T_{13} \\ T_{21} & T_{22} & T_{23} \\ T_{31} & T_{32} & T_{33} \end{pmatrix} \cdot \begin{pmatrix} B_{mx} \\ B_{my} \\ B_{mz} \end{pmatrix} \qquad (2)$$

$$B_m^t \neq \sqrt{B_{cx}^2 + B_{cy}^2 + B_{cz}^2} \qquad (3)$$

Fig. 1 shows schematic diagram of the 3-axis flux-gate magnetometer used in this work. For the correction of scale factor and rotation of sensor axis, we used 24 bit δ-σ ADC and Atmega 8-bit microcontroller.

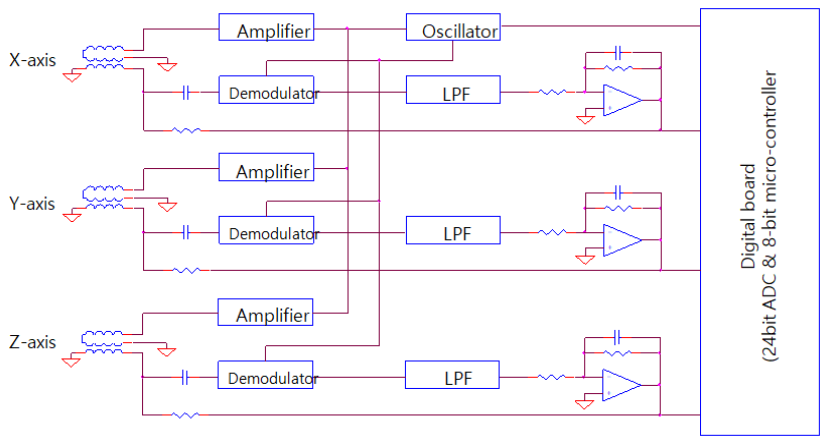

Fig. 1. Schematics of the 3-axis flux-gate magnetometer.

Fig. 2 shows constructed precise 3-axis Helmholtz coil system for the scale factor calibration and angle between axes of the magnetometer to calculated coordinate rotation matrix of equation. Scale factor difference between 3-axis was smaller than $5x10^{-4}$, and linearity was better than $1x10^{-4}$.

Fig. 2. Calibration system for the magnetometer and linearity of the developed magnetometer.

Table 1 shows magnetometer output before rotation of magnetometer axes and Table 2 shows magnetometer output after rotation of magnetometer axes. We can see that constructed precise 3-axis Helmholtz coil system for the scale factor calibration and angle between axes of the magnetometer to calculated coordinate rotation matrix of equation. Scale factors difference between 3-axis were smaller than $5x10^{-4}$, and linearity was better than $1x10^{-4}$. Table 3 shows total magnetic field measured values when magnetic field of 60 μT simultaneously applied to 2 axis of the magnetometer using Helmholtz coil. Relative uncertainty was smaller than 0.015 degree.

Table 1. Angle error between 3-axis of the flux-gate magnetometer.

Applied field(μT)	x-reading	y-reading	z-reading
60 at x-axis	60.005	-0.048	-1.198
60 at y-axis	0.852	60.008	-0.210
60 at z-axis	0.095	0.592	60.002

Table 2. Angle error between 3-axis of the flux-gate magnetometer after magnetometer axes rotation.

Applied field(μT)	x-reading	y-reading	z-reading	Uncertainty(Degree)
60 at x-axis	60.007	0.009	0.004	0.010
60 at y-axis	-0.010	60.005	0.015	0.015
60 at z-axis	-0.003	-0.016	60.003	- 0.015

Table 3. Total magnetic field measured after rotation of magnetometer axis angle, magnetic fields were applied 60 μT to 2 axis of Helmholtz simultaneously.

Applied field(μT)	x-reading	y-reading	z-reading	Total field	uncertainty
60 at x,y-axis	59.998	59.992	0.001	84.846	-8.3E-5
60 at x,z-axis	60.001	-0.009	59.995	84.850	-3.3E-5
60 at y,z-axis	-0.008	59.982	60.018	84.853	9.4E-8

Inductive displacement sensor for automobile application

Kyeong-Won Kim, Kwang-Ho Shin*
Kyungsung University, Korea

Recently, as automobiles are advanced with high performance options, demand for highly accurate and reliable sensors is increasing. Particularly, when electronic parts including sensors used in automobiles malfunction, they can be life-threatening, so more strict reliability standards are being applied for development and production of them. Moreover, automobile sensors must be guaranteed to be operated in a harsh environment; eg, high temperature, Abrupt temperature change, Polluted atmosphere and Serious vibration. In this study, we proposed a displacement sensor of which inductance was changed by displacement of object. Because we used a differential measurement method with two identical coils to detect changes in displacement, we were able to make the sensor operate reliably over a wide temperature range from -40℃ to 150℃. Another advantage of differential measurement is increased resolution for displacement measurement. Fig. 1(a) shows the magnetic flux density around two sensor coils. When the metal object approaches, the distribution of magnetic flux density is changed. This leads to a change in inductance. Fig. 1(b) represents the displacement dependence of inductance change.

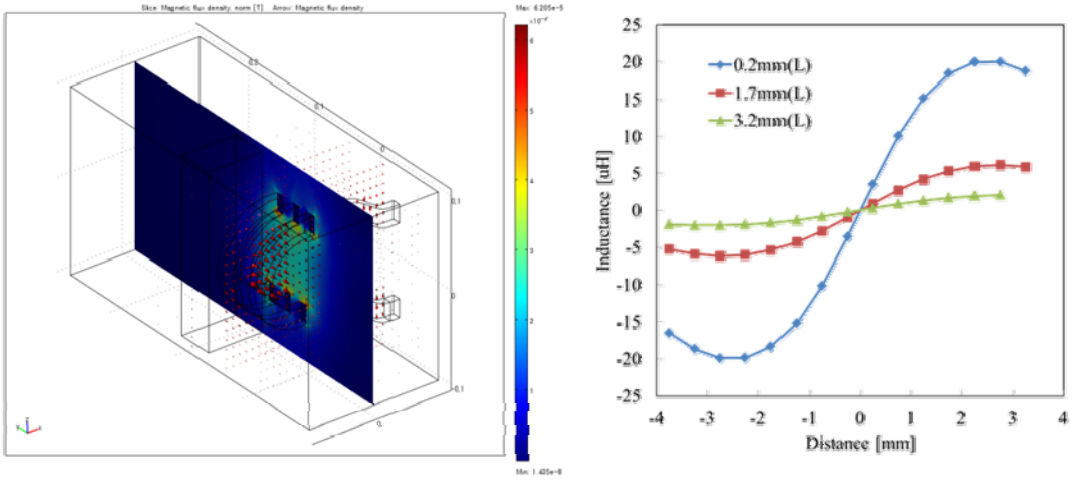

(a) (b)

Fig. 1. Magnetic flux density around sensor coils (a) and displacement dependence of inductance change according to the vertical distance (b).

International Symposium on Magnetism and
Magnetic Materials 2018

Special Session III

'Soft Magnetic Materials'

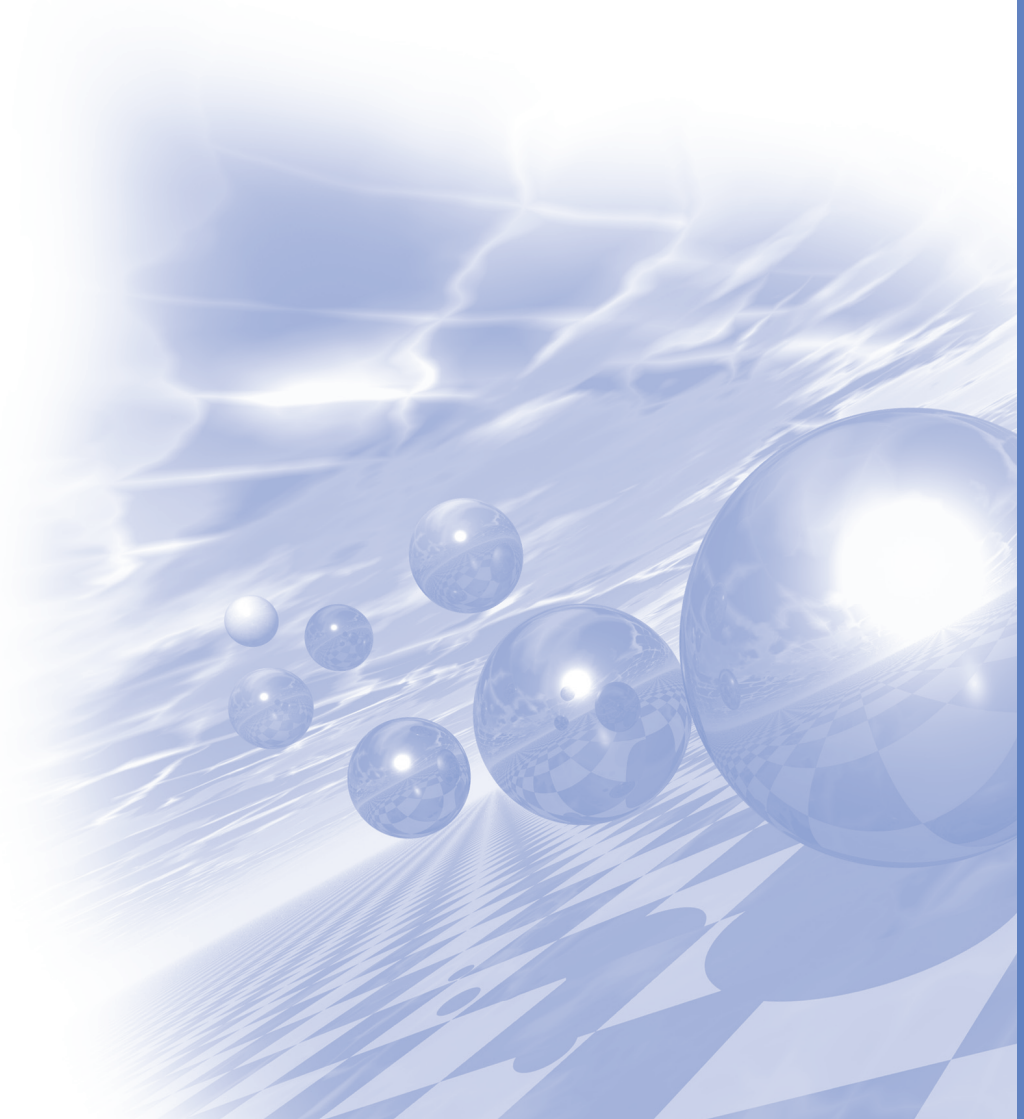

Magnetic properties of insulator-coated soft magnetic composites

Sang-Im Yoo*, Sungjoon Choi, and Sunwoo Lee
Department of Materials Science and Engineering, Research Institute of Advanced Materials (RIAM), Seoul National University, Seoul 151-744, Republic of Korea

In order to reduce a serious eddy current loss in soft magnetic composites (SMCs) composed of magnetic metal powders like Fe, insulation coating on their surface has been utilized. For the same purpose, our group has developed the sol-gel coating technology on Fe powders for the insulating layers, including iron phosphate, TiO_2, Al_2O_3, and SiO_2 and also characterized their effects on high-frequency ac losses of SMC samples. All these insulating layers could be successfully coated on the surfaces of Fe particles to form a Fe core-insulator shell structure, which was confirmed by field emission scanning electron microscopy (FE-SEM) and transmission electron microscopy (TEM), and also by element-mapping with an energy dispersive spectrometer (EDS). The eddy current loss of SMCs could be significantly reduced especially at high frequency in accordance with our expectation. For instance, from *a*-Al_2O_3-coated Fe SMC sample in comparison with uncoated Fe SMC sample, although the magnetic permeability was slightly decreased from 33.8 to 32 at 100 kHz, the eddy current loss was considerably decreased from 128 mW/cm^3 to 94 mW/cm^3 at 100 kHz with the amplitude of 50 mT. In this talk, I will present the processing-property relationship in insulator-coated SMC samples.

Analysis of high frequency behaviors of Fe-Co Micro Hollow Fiber Composites

Moosung Choi , Jongryoul Kim*
Department of Material Engineering, Hanyang University, Ansan 15588, Republic of Korea

In recent years, the electromagnetic (EM) wave absorbing techniques have been considered as a critical issue for the development of wireless/mobile electronic devices. Especially, it is required to develop new absorbing sheets containing magnetic materials for the next generation mobile electrics that work in the gigahertz range with wide broadband frequency. In order to use them as high frequency absorbers, magnetic materials should have high saturation magnetization (M_S) as well as high anisotropy field (H_a). Fe-Co hollow fibers with a high aspect ratio (AR) can be one of excellent candidates as a magnetic material for high frequency absorbers. In addition, the absorption behaviors of magnetic composites are known to be strongly dependent on their microstructures, such as the volume fraction, distribution and shape of magnetic materials. Up to now, the frequency-dependent permeability behaviors of composites with extra high-volume fraction of magnetic powders with complex shapes have not been deeply investigated. This strongly indicates that the model for the permeability behaviors of magnetic fibers and plates should be developed to predict the absorption behaviors. Thus, we aim to develop a simulation method for the magnetic permeability of composites and to confirm the validity of the simulation method. In this study, Fe-Co hollow fibers were fabricated using electroless deposition on micro polymer fibers and then were incorporated into composite sheets with different concentrations and AR values. The magnetic and high frequency behaviors of the sheets were measured and analyzed.

Figure 1 shows fabricated Fe-Co hollow fibers and their composite sheet. As shown in the figure, the average inner radius, outer radius, and length of the fabricated fibers measured 0.4, 1.5, and 200 μm, respectively. The M_S of the fibers was 203 $A \cdot m^2/kg$ and the electric conductivity was estimated to be a 6.3×10^6 S/m using Fe-Co fibers, which were compacted into a disk shape. These hollow fibers were mixed with EPDM resin and their weight concentrations were controlled to 60, 70, and 80 wt%. The M_S of these sheets were 121.5, 143.5, and 166 $A \cdot m^2/kg$, respectively. These values indicate that the sheets were manufactured to have the intended fractions.

Using the measured values of Fe-Co fibers and sheets, a simulation of the frequency-dependent permeability behaviors of Fe-Co hollow fiber composite sheets was carried out using the Landau-Lifshitz-Gilbert equation and the effective medium theory. In this simulation, the effects of the eddy current losses of isolated fibers and magnetostatic correction in high volume fractions were considered. In addition, the clustering effect on changes in the eddy current loss of the composites, which should be a critical factor on the high frequency behaviors, was involved. Figure 2 shows the simulated and the measured results of the composite sheets. As can be seen in the figure, the simulated results are in good accordance with the measured results. These results confirm that the proposed simulation method can explain the changes in the ferromagnetic resonance and eddy losses of these composites as a function of the powder concentration and shape. Therefore, the proposed simulation method can provide an effective tool for determining the frequency-dependent magnetic properties of composite sheets which include clustered particles.

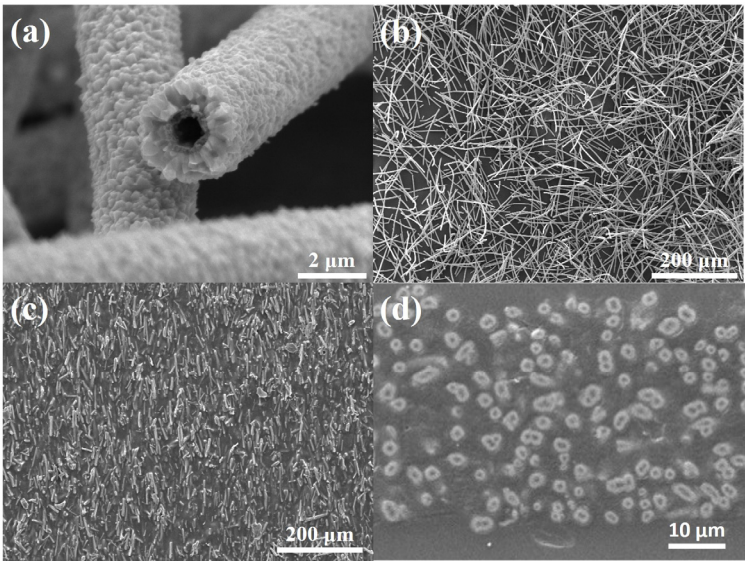

Fig. 1. SEM images of (a), (b) Fe-Co hollow fibers and (c), (d) their composite sheet; (c) surface and (d) cross sectional image of the sheet

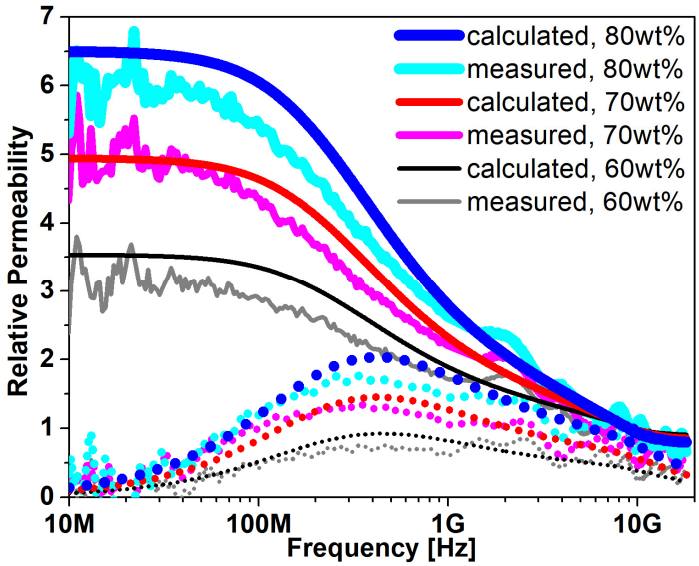

Fig. 2. Permeability behaviors of composites as function of fiber content (line: real permeability, dot: imaginary permeability)

Effect of Additives on Soft Magnetic Properties of Fe-based Nanocrystalline alloys

Hwijun Kim*, Sunyoung Ki
Korea Institute of Industrial Technology, Korea

Due to the characterization of low coercivity and high permeability, soft magnetic amorphous alloys have been used in various industrial fields such as high frequency inductor core, transformer core, sensor, and electromagnetic wave shielding sheets. Especially, because of low cost, many studies of Fe-based alloys with nanocrystalline phases have been proceeded briskly. To enhance both glass forming ability and soft magnetic properties alloy design of Fe-based soft magnetic alloy has been performed by adding transition metal alloying elements which have larger atomic radius. As contents of transition metal elements increase, saturated magnetic flux density is deteriorated. To increase improve saturated magnetic flux density with keeping coercivity low, nanocrystalline alloys have been studied by many researchers.

Thus, in this study, we focused on investigating the effect of additive transition metal on glass forming ability and soft magnetic properties of $Fe_{[87.2-x]}Tm_X[SiPBC]_{12.8}$ (Tm= Ni, Ti, Mo, W, x=0,1,2,3) alloys. Their ribbons were fabricated by melt spinning process by which rapid solidified ribbons could be obtained. Thermal analysis was conducted by DSC analysis and it was indicated that crystallization temperature of $Fe_{[87.2-x]}Tm_X[SiPBC]_{12.8}$ alloys was raised with increasing the content of transition metal with high melting temperature.

Heat treatment for nanocrystalline was conducted at just below crystallization temperature within 10 mins. Soft magnetic properties with the variation of crystalline volume fraction were measured by VSM. Furthermore, morphology and phase of nanocrystallines were analyzed by SEM and TEM. It was found that nanocrystallines exhibited α-Fe phases with the size of 20 ~ 90 nm containing metalloid elements such as B, C, P and Si. As the fraction of nanocrystalline in amorphous matrix was raised by increasing the time of heat treatment, saturated magnetic flux density was continuously raised but coercivity was rapidly deteriorated upward more than 30 % in nanocrystalline fraction.

Magnetic Shielding Materials for Wireless Power Transfer: Ferrites to Fe-based nanocrystalline ribbons

Jung Young Cho*
Principal Researcher, Energy Efficient Materials Center, Energy & Environment Division,
Korea Institute of Ceramic Engineering & Technology
E-mail: jycho93@kicet.re.kr

Since Nicola Tesla realized his idea for wireless power transfer (WPT) in 1890s, it has been struggled to be applied in practical use for more than 100 years. However, nowadays, wireless charging of electronic devices became one of the most emerging technologies. WPT offer human being usability by eliminating the use of conventional copper cables and current carrying wires when charging the various electronic devices. The inductive coupling technique is widely used due to its easiest applicability of wireless power transfer with high efficiency and large amount of the energy transferred compared to the resonant coupling technique. The biggest challenge that WPT is currently facing to expand its application area is finding appropriate shielding materials to protect electronic devices as well as human from harmful electromagnetic field when it is operating. In addition, searching for right shielding materials is a critical key to increase the transferring power. In this talk I will briefly present the role of magnetic shielding materials for wireless power transfer and then show the history of development for the magnetic shielding materials especially in the mobile phone application. Finally, I will discuss about which way we should look for to improve applicability of WPT based on magnetic shielding materials.

International Symposium on Magnetism and Magnetic Materials 2018

Special Session IV

'Electric Machines and Magnetic Materials'

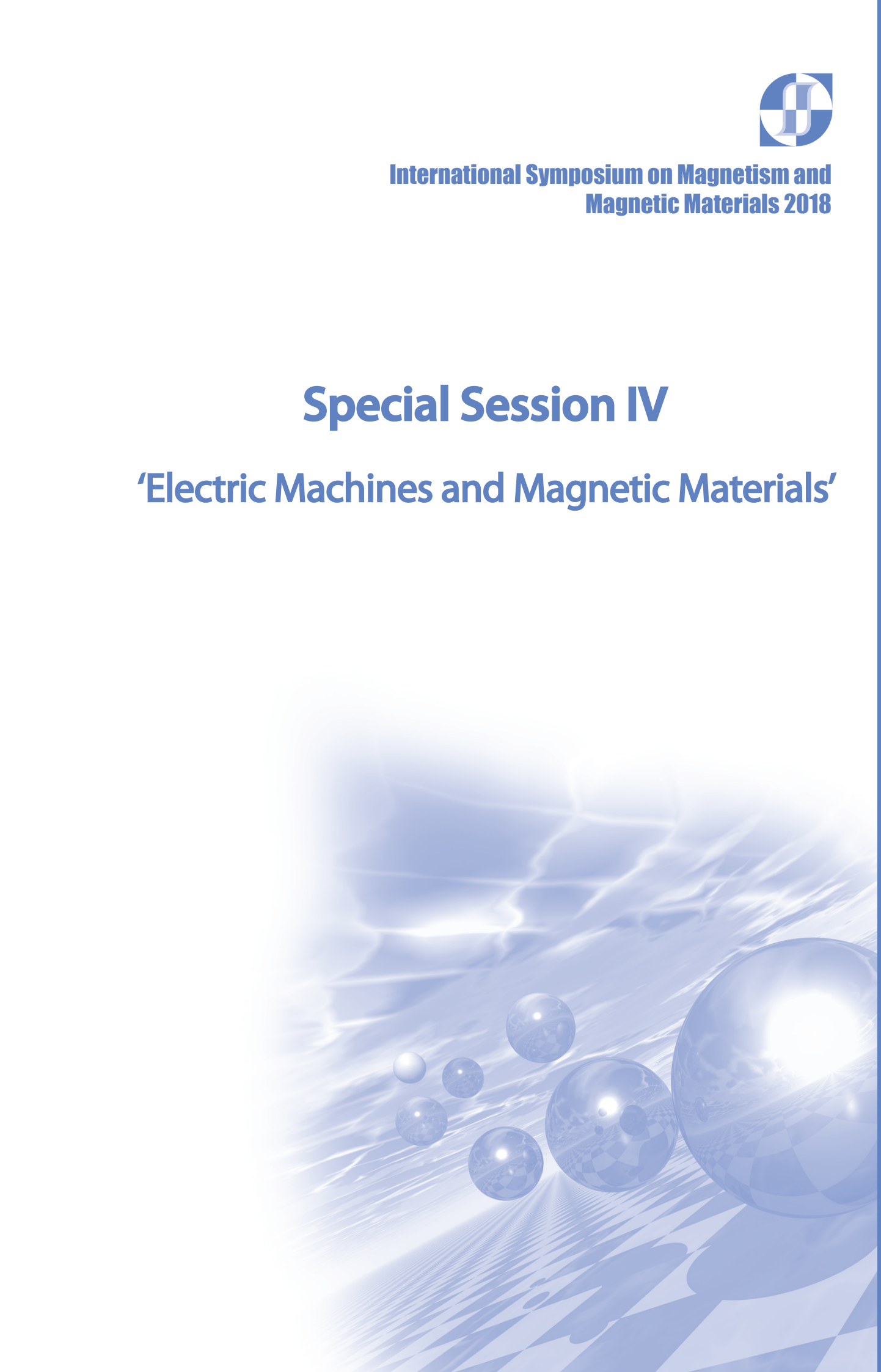

Comparison of EV Traction Motor performance according to magnetic materials

Yun-Sung Jo*, Dong-Min Kim, Hyeon-Jin Park, Jung-Pyo Hong†
Department of Automotive Engineering, Hanyang University, Korea

Recently, air pollution policies have been actively implemented Internationally. The regulations for carbon-producing products are gradually being strengthened with the aim of creating a low-carbon green village. Moreover, to reduce carbon emissions from automobiles, an eco-friendly vehicle such as electric vehicles (EVs), hybrid electric vehicles (HEVs), and fuel cell electric vehicles (FCEVs) are recommended. In particular, for EV structure, the electric motor is the most important part since it acts as a combustion engine of the conventional vehicle. Thus, the energy efficiency improvement of the electric motor will be one of the biggest concern increasing the mileage of the EV.

In this paper, the effect of the magnetic materials was analyzed in the aspect of energy efficiency of the EV traction motor. First of all, the concept model for EV vehicle was adopted and depicted in Fig.1. The type of this motor is the interior permanent magnet synchronous motor (IPMSM) with 8 poles and 48 slots. The shape of the permanent magnet inserted in the rotor is 1-layer U-shape. The permanent magnet and the electrical steel sheet used for this model are N39UH and 50PN470 respectively.

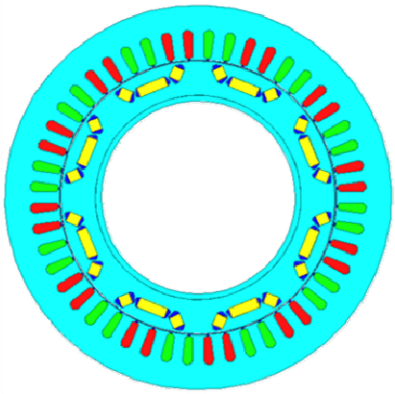

Fig. 1. Cross-sectional view of traction motor

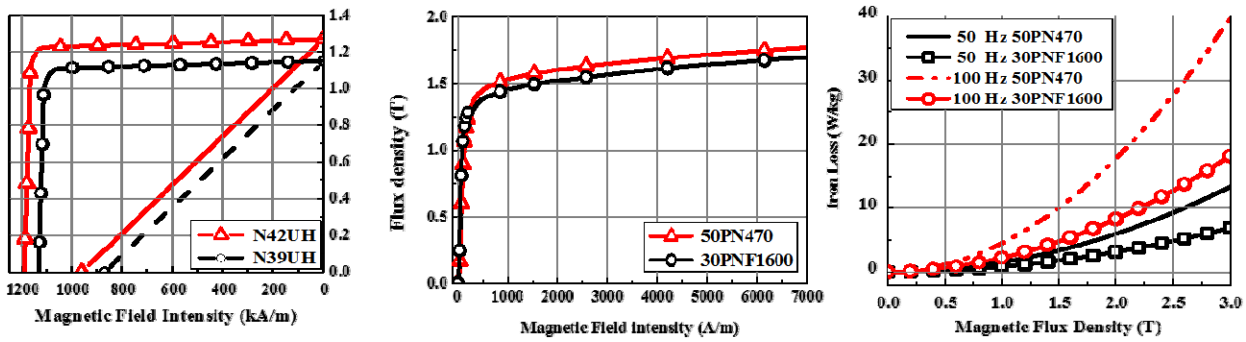

(a) Demagnetization Curve (b) B-H Curve (c) Iron Loss

Fig. 2. Magnetic material characteristics

After that, the loss calculation procedure of the copper loss and the iron loss were introduced. However, the mechanical loss was excluded for observing the change of the electric motor characteristics due to the changing of magnetic materials. Based on magnetic material characteristics as shown in Fig 2, efficiency variation was researched depending on using different magnetic materials in permanent magnet and steel sheet. To compare with concept model, the permanent magnet and the electrical steel sheet were replaced by N42UH and 30PNF1600.

When residual induction value is increased by the change of the permanent magnet, the magnetic torque increases and current will be decreased. This result is advantageous in that the copper loss can reduce in the low speed-high torque section. Also, iron loss is proportional to the square of the frequency, so the iron loss will be rapidly increased when the vehicle speed increases. In order to overcome these disadvantages, it is possible to reduce iron loss at a high speed-low torque section by using low iron loss steel sheet.

The efficiency results of magnet material changing are shown in Fig 3. As a result, the efficiency of most driving sections was increased, especially in a high-speed section. However, the efficiency was not increased in the low-speed section below 500 RPM because the B-H curve characteristic of 30PNF1600 is relatively bad. Therefore, the input current increased, and it caused copper loss increased. But, this section is not the main driving section, so there is no influence on energy efficiency.

Target vehicle specifications were shown in Table 1. and operating areas by using the Artemis driving cycle are marked in Fig 3(a). The points indicate each driving area such as urban, rural, motorway.

In future work, vehicle simulation will be conducted by using a concept model and improved model efficiency map. For this simulation, urban, rural, and motorway driving condition will be considered. It will show that how much magnetic material affects the energy efficiency in each driving conditions.

Table 1. Target vehicle specifications

Width (m)	1.3
Height (m)	1
Wheel radius (m)	0.3
Curb weight (kg)	900
Air density (kg/m^3)	1.275
Gear ratio	8.5 : 1
Drag coefficient	0.24
Rolling resistance coefficient	0.01

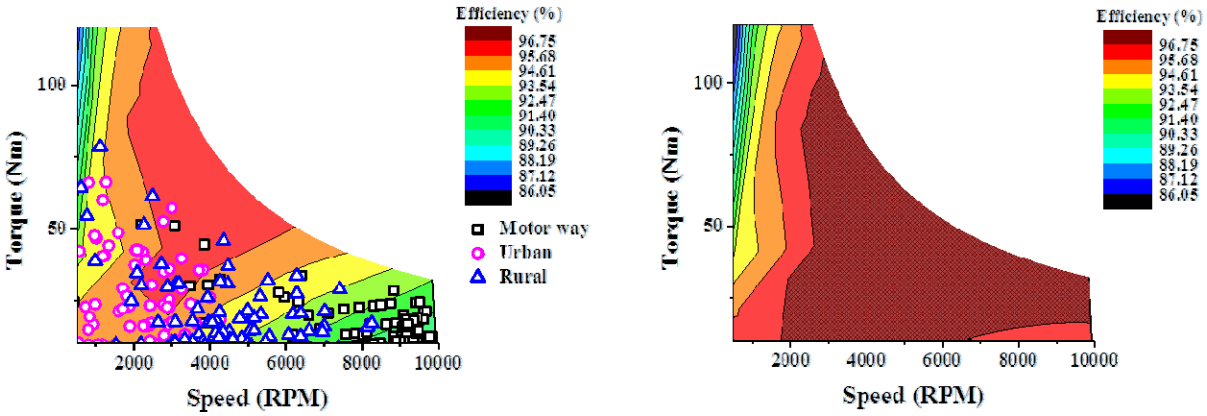

(a) Concept Model (b) Improved Model

Fig. 3. Efficiency map

Core Loss Analysis in Laminated Core of Electric Motor according to Welding Conditions

Min-Bok Cho*, Kyung-Tae Jung, Dae-Kee Kim, Dong-Kyun Son, Jung-Pyo Hong†
Department of Automotive Engineering, Hanyang University, Korea

To reduce the core loss of the electric motor, a laminated core made by stacking thin electric steel plates is used. Usually welding, riveting, or interlocking are used in laminated core to prevent each plate from falling off. Among these methods, when the welding is used, the welding bead can make a closed-loop in the laminated core. By Faraday's law, current is induced in the closed-loop making additional core loss. In this paper, the core loss of the electric motor is analyzed according to the position and the number of welding on laminated stator core.

To analyze the effect of welding condition on core loss, wires are used to make the closed-loop at each position of the stator instead of welding. The closed-loop made by the welding bead is replaced by the closed-loop made by the wire. When the wires are wound on the stator, the time-varying magnetic flux induce a current in the wires making additional copper loss. By analyzing this copper loss, the additional core loss caused by the welding can be predicted.

The wires are wound on stator teeth and yoke, respectively, as shown in Fig. 1, to analyze the effect of welding position on the core loss. As can be seen in Fig. 2, the additional loss is greater when the wires are wound on the teeth than on the yoke. Also, it can be confirmed that the additional loss is proportional to the number of welding.

As a result, the additional copper loss is larger when the wires are wound on the teeth than on the yoke. The additional core loss caused by the welding in laminated core may have same tendency. This is because the time-varying magnetic flux flowing through the closed-loop becomes smaller in that order.

The result of FEA will be added in the future to verify the test result. Also, additional analysis which cannot be obtained in the test like welding from teeth to yoke will be added by using FEA.

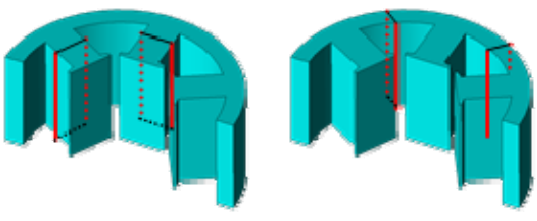

(a) Welding on teeth (b) Welding on yoke

Fig. 1. Welding Position

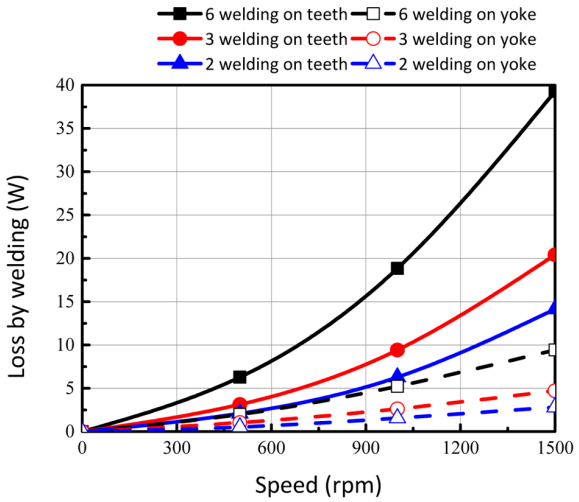

Fig. 2. Loss by welding on the teeth and yoke

Design and Verification of High Speed Permanent Magnet Synchronous Motor for Centrifugal Pumps Considering the Mechanical Stability

Gang-Hyeon Jang, Sung-Won Seo, Kyung-Hun Shin, Chang-Woo Kim, and Jang-Young Choi*
Dept. of Electrical Engineering, Chungnam National University, 99 Daehak-ro, Yuseong-gu, Daejeon 34134, Korea

High-speed permanent magnet synchronous motors(PMSMs) are attracting attention in many industries based on high efficiency and reliability. In particular, efficiency and power density can be improved by removing a speed-increasing gear and using a high-speed permanent magnet motor in a high-speed system using a conventional induction machine and a speed increasing gear. Also, the maintenance and repair cost due to the absence of the speed increasing gear can be reduced. In this paper, the design and characterization of a permanent magnet motor for the development of a high-speed and high head centrifugal pump with a permanent magnet motor were discussed. High-speed motors should be designed not only for electromagnetic performance, but also for mechanical and structural stability during high-speed operation unlike general motors. Stress analysis and dynamics analysis are essential for high speed operation. Structural analysis such as electromagnetic excitation analysis, vibration mode shape, and natural frequency analysis are also essential. In addition to the design of the stator and rotor, the design of bearings and mechanisms for high-speed rotation must also be made. Therefore, the design of a high-speed system using a high-speed permanent magnet motor should be performed to satisfy electromagnetic performance in consideration of mechanical stability. Figure 1 (a) shows the structure and shape of a high-speed permanent magnet motor designed with mechanical stability. It has a structure of 2 poles and 24 slots. Figure 1 (b) shows the experimental setup for verifying the performance of the permanent magnet motor. The motor and the pump are directly connected to each other using a torque meter to measure the performance of the motor. In this study, the design of 12500rpm, 110HP permanent magnet motor considering mechanical stability was discussed and the validity of the design technique was verified by fabricating the motor and confirming its performance.

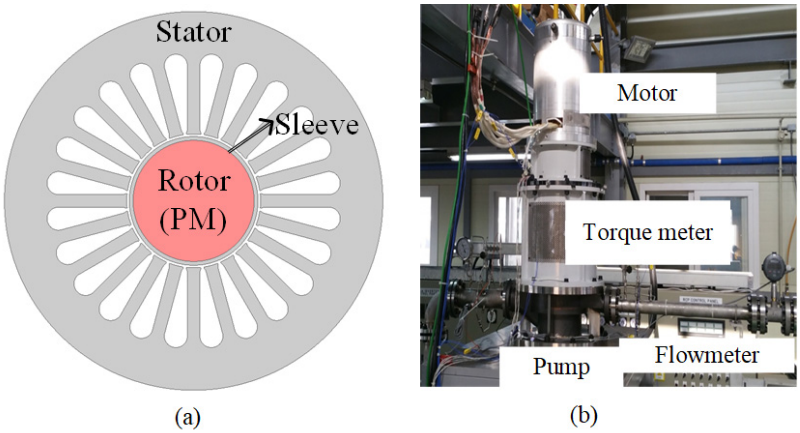

Fig. 1. Designed model and experimental set: (a)Structure of high-speed PMSM and (b) experimental set for verification design method.

Torque Calculations and Measurements of Synchronous Magnetic Coupling/Gear Based on Analytical Method

Jang-Young Choi[1*], Kyung-Hun Shin[1] and Han-Wook Cho[2]

[1]Dept. of Electrical Engineering, Chungnam National University, 99 Daehak-ro, Yuseong-gu, Daejeon 34134, Korea

[2]Dept. of Electric, Electronic and Comm. Eng. Edu., Chungnam National University, 99 Daehak-ro, Yuseong-gu, Daejeon 34134, Korea

In the case of mechanical gears and couplings that transmit power through mechanical contact, problems such as environmental, maintenance, noise, and system failures are caused by dust due to contact, abrasion due to friction, driving noise, and breakage due to overload. To solve this problem, a magnetic device in which a power transmission unit is physically separated has attracted attention as an effective alternative. Typical magnetic devices include magnetic couplings (MCs) and magnetic gears (MGs). MC and MG are used to transmit a torque between two rotating parts without mechanical contact. They are widely used in industrial applications and especially well-suited for hazardous or corrosive environments. However, as compared with a mechanical power transmission device, magnetic devices have a low torque density per unit volume, and thus there is a continuing need for a method for increasing the power density. It is essential to design techniques that can clarify the relationship between design variables and performance based on understanding of electromagnetic field as well as development of manufacturing technology and processing technology such as permanent magnet and electrical steel. Therefore, as shown in Fig. 1, the analytical solutions of MC and MG, which are representative non-contact magnetic devices, are derived, and the torque characteristics of each device are analyzed and tested. Based on the magnetic vector potential and two-dimensional (2D) polar coordinate system, we derived the analytical solutions for the magnetic fields produced by interaction between the inner and outer PMs. Then, the magnetic torque was calculated using the magnetic field solutions and Maxwell stress tensor. All analytical results were validated with nonlinear two-dimensional finite element analysis and experiments.

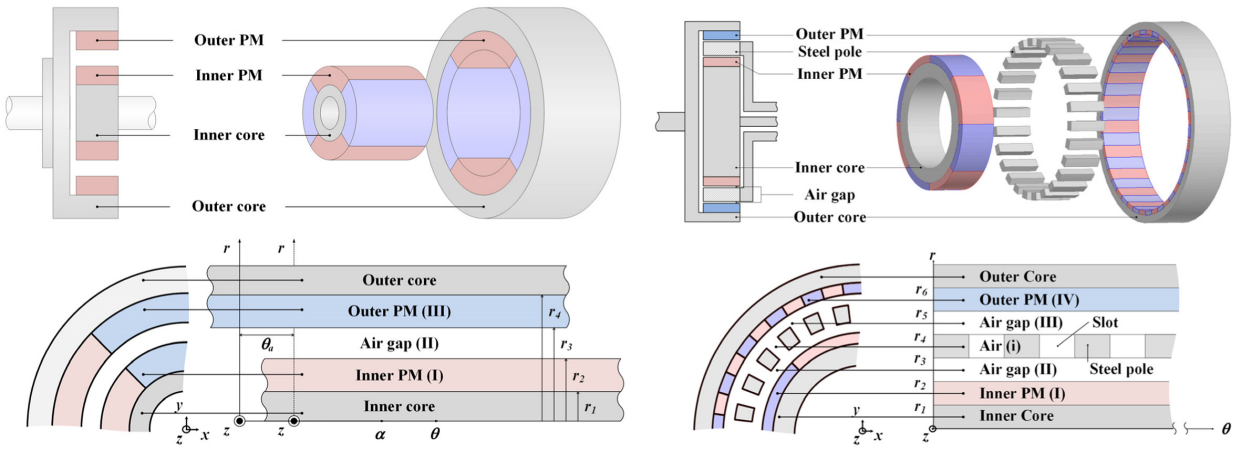

(a) (b)

Fig. 1. Structure and analysis model: (a) magnetic coupling and (b) magnetic gear

Development of Dy Free Bonded Magnet IPM Type Synchronous Motor for ISG

Salman Khaliq*, Se-Hyun Rhyu, Jeong-Jong Lee and Ki- Deok Lee
Intelligent Mechatronics Research Center, Korea Electronics Technology Institute, South Korea

In the recent decades, usage of permanent magnets (PM) has been increased in the electric motors in various home appliances and electric vehicle (EV) applications due to the advantages of compact and brushless structure and high efficiency. Among these PM motors, Interior PM synchronous motors (IPMSM) showed higher torque density and considered suitable for EV applications due to the presence of a reluctance torque component in the output. However, these PMs in the motors contain rare earth materials like Dysprosium (Dy) which are expensive and also, there is a concern regarding the consistent and stable supply of such materials. Therefore, research has been focused recently on to develop electrical machines which use Dy free PM materials, also referred to in this paper as anisotropic bonded PM motors. However, without the use of rare earth elements like Dy, PM remanence (Br) and coercive force (Hc) reduces, which in turn reduces the magnetic torque produced by the motor and decreases the power density of the machine. Therefore, there is a need to develop a rotor geometry which can compensate for the reduced magnetic torque within the same sized structure. Synchronous Reluctance motors (SynRMs) have been researched intensively over the past few decades and generates higher reluctance torque with a suitable flux barrier design. However, SynRMs do not use PMs, and therefore its torque density and power factor are lower than the PM motors. Therefore, to improve the torque density and power factor, PM assisted SynRMs are used in which PM material is installed in the flux barrier of SynRM. Therefore, when using bonded PM instead of sintered PM, SynRM structure can compensate for the reduced magnetic torque with the reluctance torque.

In this paper, we designed an IPM rotor with bonded PM material, aiming to generate similar output torque compared to sintered spoke type IPM rotor. Both machines stator and winding designs were kept the same. Rotor design in the developed model was changed to the SynRm structure to compensate for the magnetic torque with the generated reluctance torque due to the inherent structure. Rotor flux barriers were made half circular shape and filled with the radially magnetized bonded PM. Two layered structure of flux barriers was selected as the final design after various considerations of PM and rib width, and number of layers. Br value of the sintered Nd is about 1.2T, and that of bonded PM is 0.68T, which is almost half. Therefore, a more significant amount of PM material is utilized in the bonded PM motor compared to sintered PM model within the same rotor size. As the bonded PM is cheaper due to the absence of rare earth material, therefore the material cost is lower, and the high volume usage does not increase the cost of the rotor. The sintered PM model utilized about 120 cm3 while the bonded PM model employed 247 cm3, generating a 1.58 Nm/cm3 and 0.78 Nm/cm3 of torque to PM volume density, respectively. Due to the higher remanence of the sintered PM, the magnetic torque produced by the sintered PM model was almost 21% higher than the bonded PM model. As both models, i.e. sintered Nd and bonded PM had different dq inductance due to the rotor structure, therefore the applied load current angle was advanced to increase torque output. Sintered Nd model produced maximum torque at a current angle of 20o, while the developed bonded PM model produced maximum torque at 30o, which also shows higher saliency ratio

and reluctance torque component in the developed model with the same size rotor. The torque ripple at the rated condition for the developed model was almost double (32%) than the sintered Nd model (18%). There were two reasons mainly for this phenomenon: (1) the SynRM has inherently higher torque ripple than the PM machines due to the development of reluctance torque (2) and the rib structure between the layers tend to saturate at the rated torque condition which increased the torque ripple in the developed model. Therefore, rotor outer diameter structure was modified to reduce torque ripple and made sinusoidal with an unequal airgap between rotor and stator surfaces. This reduced the torque ripple to about 20% in the developed model which was more reasonable and close to the sintered PM model. Furthermore, the reluctance torque component produced by the sintered Nd model was 7.4% of the total torque, which was increased to 18.3% with the SynRM structure in the developed bonded PM model. Furthermore, the bonded PM material does not experience eddy current losses like sintered PM due to its inherent structure; therefore, it will be more suitable and show higher efficiency at higher speed.

In this work, we demonstrated that the similar torque density can be produced with the rare earth free anisotropic bonded PM motor compared with the costly sintered PM motor intended for integrated starter generator (ISG) application. SynRM rotor shaped structure was developed for the rare earth free bonded PM motor within the same size as sintered PM spoke type structure, and the performance is compared. It is shown that the loss of magnetic torque in the developed model was compensated with the SynRM reluctance structure. Such models can reduce the dependency on the expensive rare earth sintered PM motors.

Improved Characteristic of IPMSM for High Speed Drive Using High Tensile Strength Steel

Ki-O Kim*, Soo-Gyung Lee, Young-Hoon Jung, Hyeon-Jin Park, Jung-Pyo Hong†
Department of Automotive Engineering, Hanyang University, Korea

Recently, many studies have focused on motors capable of high output and high speed drive. Due to rotor saliency, an Interior Permanent Magnet Synchronous Motor (IPMSM) is suitable for an application requiring a high power density and a wide speed range. However, excessive mechanical stress is applied to the rotor while IPMSM is working at a high speed operation. It is because that the large centrifugal force is generated at the high speed and it can cause the mechanical stress.

To release the mechanical stress, bridges between permanent magnets (PMs) have been used for the rotor design. Although the bridge makes the mechanical safety improved, it can reduce the torque performance of IPMSM as the additional paths for flux leakage are made. When the thickness of the bridge is reduced, the magnetic reluctance of the bridges increases, and thus it makes the amount of flux leakage decreases and improves torque performance. However, the torque performance is restricted by the mechanical stress increased while the bridge thickness reduces.

In this paper, a high tensile strength steel is used to secure mechanical strength of an IPMSM. Due to its high yield strength, the steel used in the IPMSM can avoid a permanent deformation.

The rotor geometry of analysis model is presented in Fig. 1. The magnetic properties of conventional steel and a high tensile strength steel in Fig. 2. When the configuration of motor is constant, structural analysis according to the steel materials are compared in Fig. 3. As a result, the high tensile strength steel improves the mechanical performance while the electro-magnetic performance of IPMSM is remained.

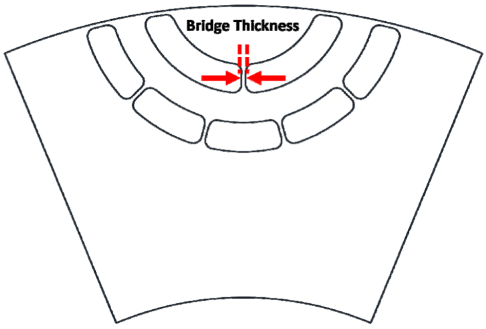

Fig. 1. Configuration of the initial model

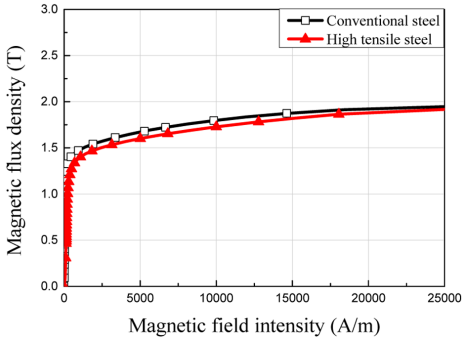

Fig. 2. Magnetic properties of steels

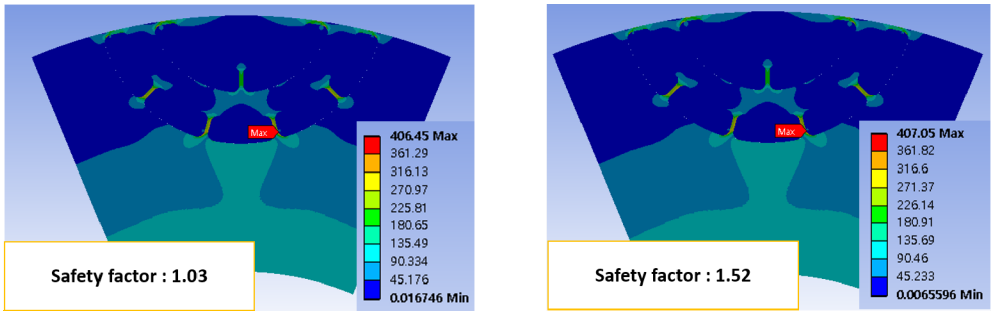

(a) (b)

Fig. 3. Structural analysis (a) conventional steel (b) high tensile strength steel steel

Preliminary Design of 10-MW Class Actively Shielded Superconducting Generator

Han-Wook Cho[1*], Kang-Hyun Jang[2], Tae-Kyoung Bang[1], Jung-In Lee[2],
Yong-Hee Lee[1], Kyung-Hun Shin[2], and Jang-Young Choi[2]
[1]Dept. of Electrical, Electronics and Comm. Eng. Edu., Chungnam National University, Korea
[2]Dept. of Electrical Engineering, Chungnam National University, Korea

With the development of superconductors and related technologies, superconducting (SC) machines offer a possible technological approach for the production of large scale direct-drive wind turbines, defense or transportation applications at a modest cost. In particular, actively shielded SC generators have the advantage of reducing the gross weight of the system because they do not have a high-weight iron core that constitutes a magnetic circuit, and can be a good design option with high specific power. In this study, the preliminary design of the 10-MW class actively shielded type superconducting (SC) generators are carried out. Selection of pole-counts and sizing, SC coil design, no-load and full load characteristics of generator will be presented. In addition, we suggest the configuration of SC generators with an active shielding SC coil. And, the actively shielded SC generator is compared to conventional SC generators with magnetic core shield and very low rotating speed. The results show that the actively shielded SC generator has lower weight, high specific power compare with conventional SC generators.

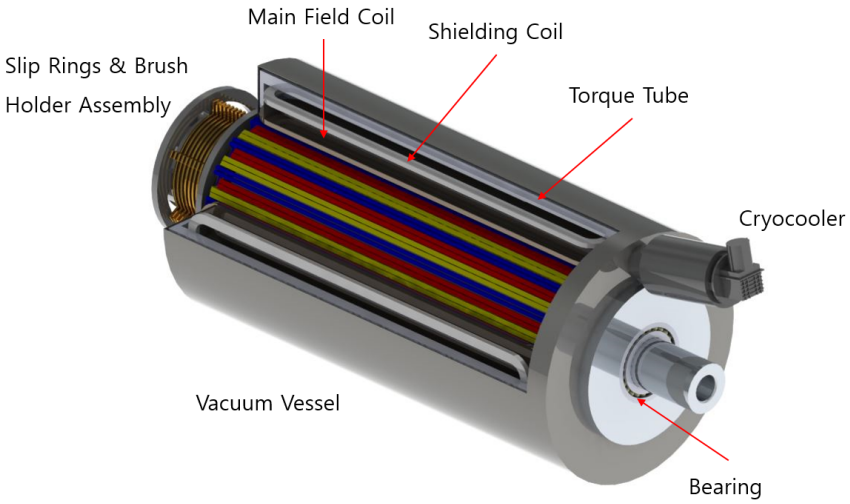

Fig. 1. Preliminary design result of 10-MW class SC generator.

International Symposium on Magnetism and Magnetic Materials 2018

Special Session V

'Spintronics I'

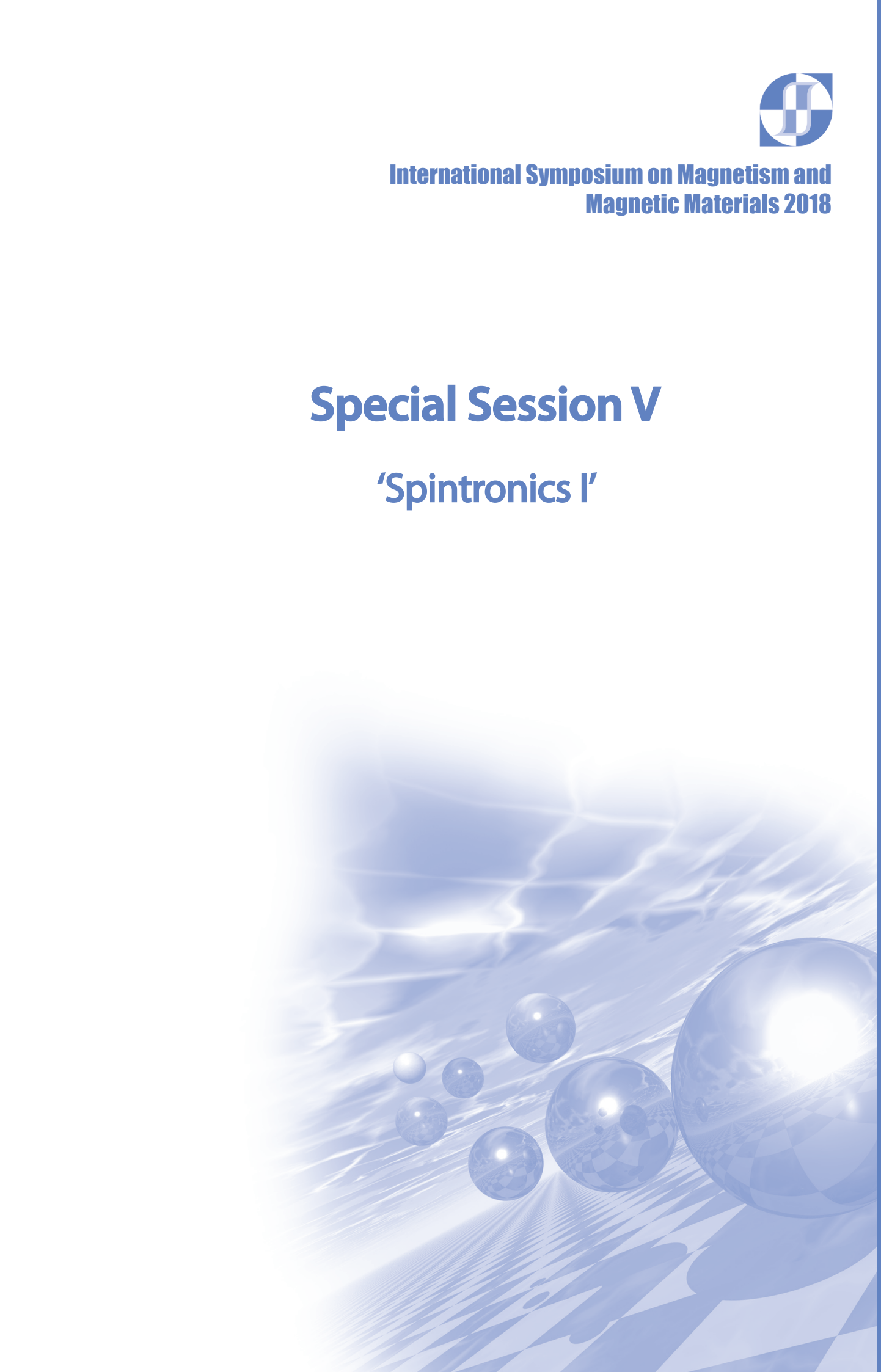

Spin Hall effect from the interplay between spin and orbital

Dongwook Go[1], Daegeun Jo[1], Changyoung Kim[2,3], Hyun-Woo Lee[1*]
[1]Department of Physics, Pohang University of Science and Technology, Pohang 37673, Korea
[2]Department of Physics and Astronomy, Seoul National University, Seoul, 08826, Korea
[3]Center for Correlated Electron Systems, Institute for Basic Science, Seoul 08826, Kora

We demonstrate theoretically that both the intrinsic spin Hall effect (SHE) and orbital Hall effect (OHE) can arise in centrosymmetric systems through momentum-space orbital texture. Unlike momentum-space spin texture, which exists only in noncentrosymmetric systems, momentum-space orbital texture is ubiquitous even in centrosymmetric systems. Thus the demonstrated mechanism is very generic. The OHE can occur even when spin-orbit coupling (SOC) is absent. When the SOC is present, the OHE is converted to the SHE. The resulting spin Hall conductivity can be sizable. This mechanism of the SHE suggests the importance of the interplay between spin and orbital degrees of freedom.

Charge-Spin Conversion in a Rashba Channel

Hyun Cheol Koo[1,2*], Joo-hyeon Lee[1,2], Won Young Choi[1,2], Hyung-jun Kim[1], Joonyeon Chang[1], Suk Hee Han[1], Seokmin Hong[1,3], Shehrin Sayed[3] and Supriyo Datta[3]

[1]Center for Spintronics, Korea Institute of Science and Technology, Seoul 02792, Korea

[2]KU-KIST Graduate School of Converging Science and Technology, Korea University, Seoul, 02481, Korea

[3]School of Electrical and Computer Engineering, Purdue University, West Lafayette, IN 47907, USA

The spin-orbit coupling has added a new dimension to semiconductor spintronics through a two-dimensional quantum well layer. In a two-dimensional Rashba system, both charge-to-spin and spin-to-charge conversions were observed. We observed three resistance states exhibiting unequal antiparallel states in a multi-terminal spin-valve-like structure on an InAs quantum well channel, where two ferromagnetic contacts were used as current terminals while a separate normal metal contact pair was used as voltage terminals. This spin-to-charge conversion result is strikingly different from conventional spin valve or magnetic tunneling junction devices, which have only two resistance states corresponding to parallel and antiparallel alignments of the ferromagnetic contacts. Surprisingly, the non-magnetic contacts to the Rashba channel reads the magnetization state of the ferromagnetic electrodes located millimeter away from the detector. From the reciprocal set-up, the ferromagnetic electrode detected a spin voltage induced by the current driven Rashba spin splitting, which confirmed charge-to-spin conversion. The temperature dependence of these experiments showed the Rashba effect induced spin splitting up to room temperature. We justify our prediction from two simple and experimentally well-established arguments which are spin voltage measurement on spin momentum locking channel and Onsager reciprocity relation. In this system, we also observed direct and inverse spin Hall effects using the FM electrode magnetized along the in-plane. We combined spin Hall and Rashba effects to provide a direct demonstration of the ballistic spin Hall effect and to demonstrate a technique for an all-electric measurement of the Datta-Das conductance oscillation. Without a perpendicular magnetization, spin Hall voltage was detected via the Rashba spin precession. Our experiments showed that charge-spin conversion can be used for efficient injection or detection of spin polarized electrons, thereby enabling the development of a spin-based electronic device.

Magnetic memristor driven by spin-orbit torque

Euna Jo[1], Hee-Gyum Park[1,2], Byoung-Chul Min[1,2*]

[1]Center for Spintronics, Korea Institute of Science and Technology, Seoul 02792, Korea

[2]Division of Nano and Information Technology, KIST School, Korea University of Science and Technology, Seoul 02792, Korea

We demonstrate a memristive device with multi-level resistance tunable by a current. The device consists of multiple nano-dots with perpendicular magnetization on a heavy-metal Hall-bar geometry. The spin-orbit torque arising from in-plane current flowing the Hall bar leads to magnetization switching of nano-dots. The switching from high to low resistance or vice versa is controlled by direction of in-plane DC current and magnetic field. The magnitude of in-plane DC current determines the number of switched dots and consequent Hall resistance of the device. The memresistive response from multiple nano-magnetic dots could serve as artificial nano-synapses.

Spin currents and spin-orbit torques in ferromagnetic trilayers

Gyungchoon Go*
Department of Materials Science and Engineering, Korea University, Seoul 02841, Korea

Magnetic torques generated through spin-orbit coupling promise energy-efficient spintronic devices. It is important for applications to control these torques so that they switch films with perpendicular magnetizations without an external magnetic field. In this talk, we demonstrate field-free switching in ferromagnetic trilayers consisting of in-plane magnetized bottom ferromagnet, non-magnet, and perpendicularly magnetized top ferromagnet[1] and show that this structure potentially reduces the switching current. This work has been done in collaboration with Byong-Guk Park, Seung-heon C. Baek, Young-Wan Oh, Geun-Hee Lee, Kab-Jin Kim from KAIST, Korea, Vivek P. Amin, M. D. Stiles from NIST, USA, and Kyung-Jin Lee, Seung-Jae Lee from Korea University, Korea.

Reference

[1] S.-h. C. Baek et al. Nat. Mater. **17**, 509 (2018).

Writing and deleting magnetic skyrmions by electric currents examined by full-field soft X-ray microscopy

Soong-Geun Je[1,2*], Min-Seung Jung[2], Weilun Chao[1], Mi-Young Im[1,2,3†], Jung-Il Hong[2†]
[1]Center for X-ray Optics, Lawrence Berkeley National Laboratory, Berkeley CA94720, USA
[2]Department of Emerging Materials Science, DGIST, Daegu, Korea
[3]School of Materials Science and Engineering, KIST-UNIST Ulsan Center for Convergent Materials, Ulsan National Institute of Science and Technology, Ulsan, Korea
[†]Correspondence to: mim@lbl.gov, jihong@dgist.ac.kr

Magnetic skyrmions and skyrmion bubbles are typical of nontrivial spin texture which have been found in various thin ferromagnetic or ferrimagnetic materials at room temperature. As the materials are compatible with current spintronic technologies, magnetic skyrmions and skyrmion bubbles are of great interest for the applications of new memory and logic devices where magnetic skyrmions serve as information carriers at a nano-scale. Recently, the concept of skyrmion-based-neuromorphic devices is also proposed, making the magnetic skyrmions more promising. From a perspective of practical utilisation of magnetic skyrmions in a device, controllable writing and deleting of magnetic skyrmion at a desired position by an electrical way is one of the criteria for the feasibility of skyrmion-based devices.

In this presentation, we will briefly review the current art of writing magnetic skyrmions in room-temperature ultrathin magnetic materials [1-5]. We then show the magnetic field-controlled creation and annihilation of magnetic skyrmions by electric currents [6-7]. The creation and annihilation of sub-100 nm magnetic skyrmions are studied using a soft X-ray transmission microscope at Advanced Light Source (XM-1, BL6.1.2) which enables the observation of in-plane and out-of-plane magnetic components with a high spatial resolution down 25 nm. We demonstrate that magnetic skyrmions can be either created or annihilated by the electric current depending on the strength of magnetic fields. The creation and annihilation rates sensitively change with respect to the applied field, suggesting the possibility of modulating the generation and annihilation rates by the addition of small magnetic field perturbation such as Oersted field. By exploiting the Oersted field, we propose a skyrmion writing/deleting device which is compatible with the skyrmion-hosting magnetic track. As our proposed scheme enables localized skyrmion writing/deleting, it might particularly be useful for the realisation of the skyrmion-based memory and neuromorphic devices.

This work was supported by Leading Foreign Research Institute Recruitment Program through the National Research Foundation (NRF) of Korea funded by the Ministry of Education, Science and Technology (MEST) (2012K1A4A3053565) and by the DGIST R&D programme of the Ministry of Science, ICT and future Planning (18-BT-02). Work at the ALS was supported by the U.S. Department of Energy (DE-AC02-05CH11231).

References

[1] W. Jiang, et al., Science 349, 283 (2015)
[2] F. Büttner, et al., Nat. Nanotechnol. 12,1040-1044 (2017).
[3] Woo, et al., Nat. electron. 1, 288-296 (2018).

[4] M. Schott, et al., Nano Lett. 17, 3006-3012 (2017).
[5] S.-G. Je, et al., Nano Lett. in press (2018)
[6] S.-G. Je, et al., Curr. Appl. Phys, 18, 1201-1204 (2018).
[7] S.-G. Je et al., in preparation (2018).

An investigation of magnetic nanostructures using synchrotron x-rays

Z. Q. Qiu*
Dept. of Physics, UC-Berkeley, Berkeley, CA 94720

X-ray Magnetic Circular Dichroism (XMCD) and X-ray Magnetic Linear Dichroism (XMLD) offer a unique technique for element-resolved investigation of ferromagnetic and antiferromagnetic nanostructures. Further development has combined XMCD/XMLD with spatial-resolved and time-resolved measurements to provide a powerful tool for the investigation of magnetic domains and spin dynamics. In this talk, I will discuss three projects we carried out at the Advanced Light Source of Lawrence Berkeley National Lab. First, I will discuss our study on exchange bias using XMCD/XMLD. Then I will present imaging study of magnetic vortices and Skyrmions using Photoemission Electron Spectroscopy (PEEM). Finally, recent development of x-ray pump-probe measurement will be discuss on the study of spin-current in magnetic nanostructures.

International Symposium on Magnetism and
Magnetic Materials 2018

Oral Session III

'Hard Magnetic Materials'

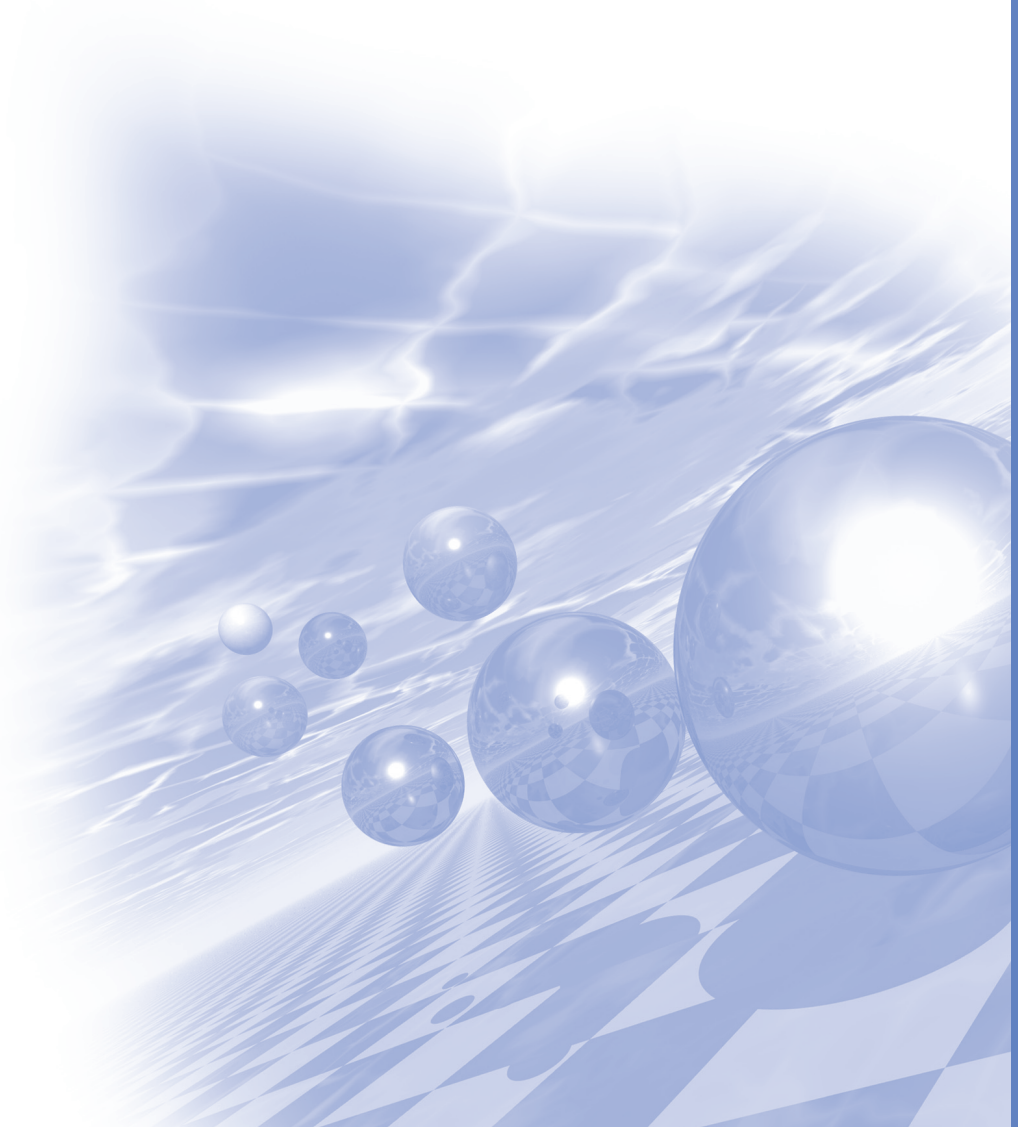

A Facile Synthesis of Peapod-like α"-$Fe_{16}N_2$ Magnetic Particles in Silica Shell

Youn-Kyoung Baek[1*], Hyun Soon Prark[2], Kyoung Min Kim[1], Jung-Goo Lee[1]
[1]Powder&Ceramic Division, Korea Institute of Materials Science (KIMS)
[2]Materials Science and Engineering, Inha University

As a possible rare-earth free permanent magnet candidate, iron nitride phase α"-$Fe_{16}N_2$ has been suggested as a possible rare-earth free PMs candidate due to abundant amount of Fe and N on the earth, its large magnetocrystalline anisotropy, and large saturation magnetization. Thus, researchers have developed the various synthesis methods such as wet chemical, ball milling and plasma process etc. The traditional approach containing ball milling has limitations in decreasing the particle size down to nanometer scale. Wet chemical or plasma based synthesis enable to fabricate fine powders with the size below than 100 nm. However, the resulting nanoparticles still exhibit low coercivity contrary to theoretical values, which might be attributed to intensive surface oxidation of the nanosized particles. Here, we developed a facile method to synthesize of α"-$Fe_{16}N_2$ nanoparticles embedded in SiO_2 shell with peapod-like structures via sol-gel process combined with hydrogen (H_2) reduction and ammonia (NH_3) nitridation. Thus, the strategy to fabricate air-stable α"-$Fe_{16}N_2$ nanoparticles will provide opportunities to realize practical Fe based permanent magnets.

This work was supported by Fundamental Research Program (PNK 5590) of Korea Institute of Materials Science (KIMS) and National Research Council of Science & Technology(NST) grant by the Korea government (MSIP) (No. CPS-18-05-KAERI).

The effects of composition on microstructure and magnetic properties of MnBi alloys

Yang Yang[1,2*], Yongho Shin[1], Hui-Dong Qian[1], Ping-Zhan Si[1], Jihoon Park[1], Oi Lun Li[2], Jong-Woo Kim[1†], Chul-Jin Choi[1†]

[1]Powder & Ceramics Division, Korea Institute of Materials Science, Changwon 51508, Republic of Korea

[2]School of Materials Science and Engineering, Pusan National University, Busan 46241, Republic of Korea

MnBi has attracted attention because of its appreciable coercivity and unusual temperature dependent magnetic properties. Doping on MnBi as well as chemical composition control has been widely employed to modify the magnetic properties. In order to obtain high purity of low-temperature phase (LTP) MnBi, Mn_xBi_{100-x} with various nominal compositions (x = 55~61.2) and Fe-/Ga-substitution on the crystal structure and magnetic properties of MnBi were studied systematically. The alloys with high portion of LTP were prepared by induction melting with subsequent low temperature annealing and low/high energy ball milling process. The $Mn_{56}Bi_{44}$ powder crushed from annealed ingot showed remarkably high magnetic property, i.e. saturation magnetization of 70.2 emu/g with a coercivity of 4381 Oe. In the meantime, it was found that the Ga-doping increased the Curie temperature of $Mn_{55}Bi_{45-x}Ga_x$ for $x \leq 5$ and the phase transformation temperature of LTP-MnBi to HTP-MnBi. The Curie temperature is elevated by ~25 K for 5 *at*.% doped Ga. In this presentation, fabrication and optimization process for MnBi compositions and transition metal elements doped MnBi will be discussed in detail.

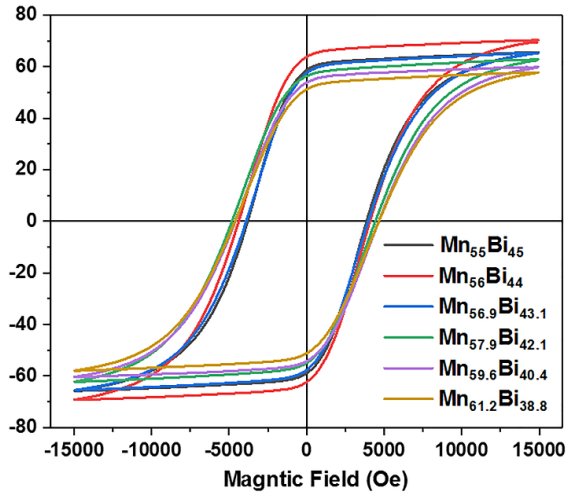

Fig. 1. The hysteresis loops of MnBi crushed annealed ingot powders.

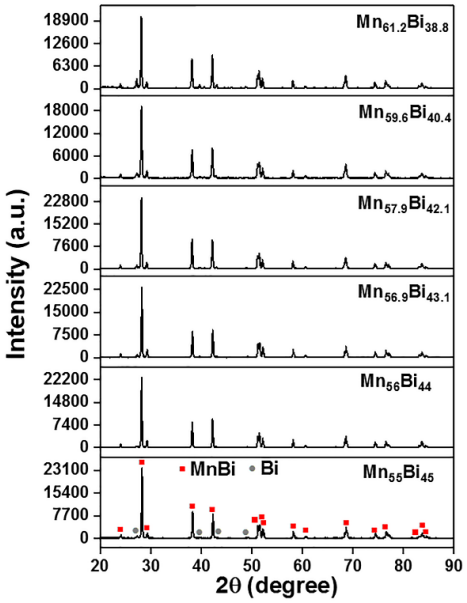

Fig. 2. XRD patterns of the MnBi ingots after annealing at 573 K for 72 hrs.

Preparation and Characterization of Fe-rich compound for permanent magnetic materials

Jung Tae Lim*, Hui-Dong Qian, Jihoon Park and Chul-Jin Choi
Powder & Ceramic Division, Korea Institute of Materials Science, Changwon, Korea

Recently, the iron-rich rare-earth alloys of $ThMn_{12}$-type structure have attracted attention as permanent magnetic material due to the high anisotropy field, saturation magnetization (M_s), and curie temperature (T_C). Especially, Sm-Fe-Co-Ti materials have been extensively studied because of the enhanced magnetic anisotropy by Co substitution [1]. In this study, the $Sm(Fe_{0.8}Co_{0.2})_{11}Ti$ sample were synthesized by arc-melting. We have investigated the crystal structure, phase purity and magnetic properties of $Sm(Fe_{0.8}Co_{0.2})_{11}Ti$ sample by using x-ray diffractometer (XRD) with Cu-$K\alpha$ radiation source, field emission scanning electron microscopy (FE-SEM), and vibrating sample magnetometer (VSM). The $Sm(Fe_{0.8}Co_{0.2})_{11}Ti$ ribbons were used high-purity Sm (99.95%), Fe (99.99%), Co (99.95%), and Ti (99.95%) pieces as starting materials and were prepared by using arc-melting and melt spinning methods. These were sealed in evacuated quartz tube of 10^{-2} torr and heat treated at 800 °C for various times.

The refined XRD patterns by using Rietveld refinement method, revealed that $Sm(Fe_{0.8}Co_{0.2})_{11}Ti$ sample exhibited tetragonal structure with the space group *I4/mmm* and the lattice constant a_0 and c_0 were 8.486 Å and 4.885 Å, respectively. Also, Ti and Co were found to be located at 8*i* and 8*f*-site, respectively.

From the magnetic hysteresis curves up to 20 kOe at 295 K, we found the M_s and intrinsic coercivity (H_c) of the heat-treated at 800 °C for 4 h sample to be M_s = 107.43 emu/g and H_c = 2399.3 Oe, respectively.

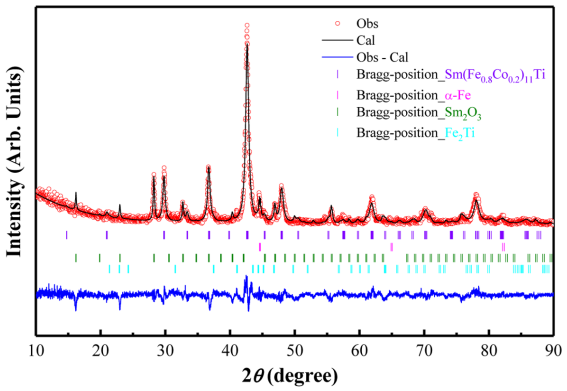

Fig. 1. XRD patterns of $Sm(Fe_{0.8}Co_{0.2})_{11}Ti$ refined by using the Rietveld refinement method.

Acknowledgements

This research was supported by Future Materials Discovery Program through the National Research Foundation of Korea(NRF) funded by the Ministry of Science and ICT (2016M3D1A1027835).

Reference

[1] P. Tozman, H. Sepehri-Amin, Y.K. Takahashi, S. Hirosawa, K. Hono, Acta Mater. **153**, 354 (2018).

Structure and magnetic properties of Fe-rich permanent magnetic materials prepared by melt spinning

Hui-Dong Qian[1,2*], Jung Tae Lim[1], Yang Yang[1,2], Ping-Zhan Si[1], Jong-Woo Kim[1], Kyung Mox Cho[2], Jihoon Park[1†], Chul-Jin Choi[1†]

[1]Powder & Ceramic Division, Korea Institute of Materials Science, Changwon, Korea

[2]School of Materials Science and Engineering, Pusan National University, Busan, Korea

[†]Email: jpark@kims.re.kr; cjchoi@kims.re.kr

The rare-earth transition-metal intermetallic compounds with $ThMn_{12}$-type structure have attracted much interest for potential application as a permanent magnet because of their high saturation magnetization and anisotropy field [1]. Recently, the $ThMn_{12}$-type Sm-Fe-X magnetic materials have been intensively studied in efforts to fabricate high performance permanent magnets by controlling the doping element and grain sizes [2]. In this work, we prepared the Sm-Fe-Ti alloys by using arc melting and melt spinning methods (32.7 m/s) starting from high purity Sm, Fe, Ti. After grinding the as-prepared ribbons, we obtained the best powdered sample with intrinsic coercivity of 2877 Oe and saturation magnetization of 113 emu/g at maximum applied magnetic field of 4 T. The structure, magnetic properties, and phase transformation of the Sm-Fe-Ti powders were systematically studied by using X-ray diffraction (XRD), scanning electron microscope (SEM), transmission electron microscopy (TEM), and physical property measurement system (PPMS).

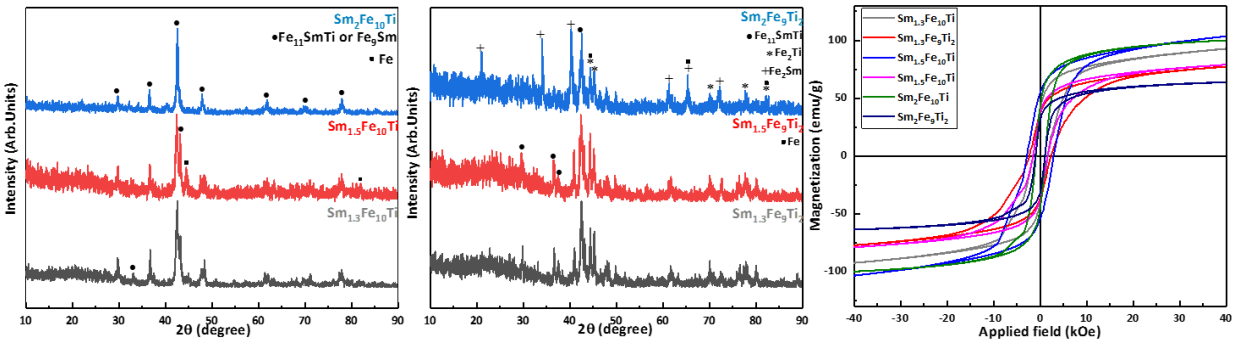

Fig. 1. XRD and magnetic hysteresis loops of Sm-Fe-Ti powders.

Acknowledgements

This research was supported by Future Materials Discovery Program through the National Research Foundation of Korea(NRF) funded by the Ministry of Science and ICT (2016M3D1A1027835).

References

[1] P. Tozman, H. Sepehri-Amin, Y.K. Takahashi, S. Hirosawa, K. Hono, Acta Mater. **153**, 354(2018)

[2] Y. Hirayama, Y.K. Takahashi, Shirosawa, K. Hono, Scripta Mater. **138**, 62(2017)

The influence of Sm-Fe-Cu-Al eutectic binder on the magnetic properties and microstructure of $Sm_2Fe_{17}N_3$ sintered magnets

Hee-Ryoung Cha[1*], Wataru Yamaguchi[2], Kenta Takagi[2], Jung-Goo Lee[1]
[1]Powders& Ceramics Division, Korea Institute of Materials Science, Korea
[2]Magnetic Powder Metallurgy Research Center,
National Institute of Advanced Industrial Science and Technology, Japan

$Sm_2Fe_{17}N_3$ phase possesses excellent intrinsic hard magnetic properties comparable to that of $Nd_2Fe_{14}B$. However, the use of $Sm_2Fe_{17}N_3$ powder has been limited to polymer-bonded magnets, which has much lower magnetic properties than that of the original powder, due to the low decomposition temperature of $Sm_2Fe_{17}N_3$ phase about 600℃ which rules out the possibility of using conventional sintering techniques. The hot-pressing technique with low melting point metal binder is an alternative sintering route to produce high performance $Sm_2Fe_{17}N_3$ bulk magnets. However, although $Sm_2Fe_{17}N_3$ powder have successfully sintered at a temperature lower than the decomposition temperature, it's the resultant coercivity usually significantly decreased due to redox reactions on powder surfaces. Recently, it is reported that Sm-based eutectic binder prevents the coercivity deterioration after sintering and enhances the density of the sintered magnet. However, there is insufficient explanation on the reason ~~of~~ why the coercivity of sintered magnet maintained to that of original powders.

In this study, we have consolidated the $Sm_2Fe_{17}N_3$ powders with $Sm_{63}Fe_5Cu_{22}Al_{10}$ (at.%) eutectic binder to investigate the influence of Sm-Fe-Cu-Al eutectic binder on the magnetic properties and microstructure of $Sm_2Fe_{17}N_3$ sintered magnets. The binder was coated on $Sm_2Fe_{17}N_3$ powder by sputtering process. The sputtering coated powder ~~is~~ was hot-pressed by a current sintering apparatus at various sintering temperatures from 300 to 600℃. In the results, the sintered magnet with sputtering coated powders showsed higher coercivity than that of non-coated powders. XRD analysis suggestsed that the $Sm_{63}Fe_5Cu_{22}Al_{10}$ eutectic binder restrained precipitation of the α-Fe phase, which causesed the decrease of coercivity.

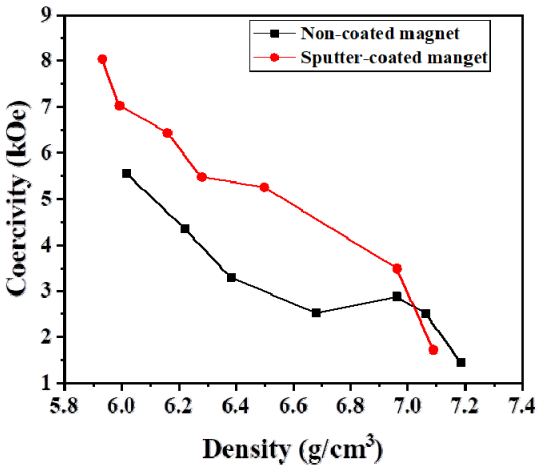

Fig. 1. Dependence of the coercivity on the density of non-coated and sputter-coated magnets.

O-III-6

A comparison of the magnetic properties and hot-deformation behavior of Nd-Fe-B magnets made from melt-spun and HDDR powder

Jae-Gyeong Yoo[1,2*], Ga-Yeong Kim[1], Hee-Ryoung Cha[1], Youn-Kyoung Baek[1], Dongyun Lee[2], Hae-Woong Kwon[3], and Jung-Goo Lee[1]

[1]Powder & Ceramics Division, Korea Institute of Materials Science, Changwon, Korea

[2]Department of Nano Fusion Technology, Pusan National University, Busan, korea

[3]Department of Materials Science and Engineering, Pukyong National University, Busan, Korea

Nd-Fe-B permanent magnet is widely used in a variety of applications such as traction motor of hybrid and electric vehicles due to the highest maximum energy product (BH)max. To achieve high (BH)max, strong (001) texture must be introduced somewhere in the course of processing. Unlike the conventional sintering process of magnetically aligned monocrystalline powders, hot-deformation process is another method being used to align the ultra-fine grains such as melt-spun (~50nm) and HDDR (~300nm) powder. Especially, since the hot-deformed magnets have smaller average grain size than those of sintered magnets, hot-deformed magnets have greater potential to obtain high coercivity and improve its temperature dependence even without using heavy rare earth elements which is usually used to obtain high coercivity in the sintered magnets. On the other hand, the mechanism of texture formation by the interface-controlled solution-precipitation-creep process and grain boundary sliding during hot-deformation has been extensively studied and well-known for melt-spun powder. However, there were only a few studies examining texture formation HDDR powder during hot-deformation. Thus, we compared hot-deformation behavior between HDDR powder and melt-spun powder under the same composition and deformation condition to understand texturing mechanism of HDDR powder during hot-deformation.

In this study, the Nd-Fe-B bulk magnets were produced by hot-deformation process using HDDR powders with the same composition of commercial MQU-F powder which is $Nd_{13.6}Fe_{73.6}Co_{6.6}Ga_{0.6}B_{5.6}$. The magnetic properties and microstructure of hot-deformed magnet were analyzed by VSM and FE-SEM. Then, we compared magnetic properties and microstructure of hot-deformed magnets and strain-stress curve during hot-deformation between MQU-F and HDDR powder.

The remanence of hot-deformed magnets from melt-spun and HDDR powder increased with increasing strain regardless of the strain rate. More interestingly, the remanence of hot-deformed magnet with HDDR powder was linearly increased at slow strain rate of $\varepsilon' = 0.001\ s^{-1}$. On the contrary, the remanence of hot-deformed magnet with MQU-F powder was linearly increased at fast strain rate of $\varepsilon' = 0.1\ s^{-1}$. Additionally, strain rate dependent strain-stress behavior was significantly different between MQU-F and HDDR powder during hot-deformation. Based upon these results, hot-deformation behavior of Nd-Fe-B hot-deformed magnet with melt-spun and HDDR powder will be discussed.

Effect of iron content of rare earth-substituted Sr M-type hexagonal ferrites synthesized by solid-state reaction

Kang-Hyuk Lee*, Sang-Im Yoo†
Department of Material Science and Engineering, Research Institute of Advanced Materials (RIAM),
Seoul National University, Seoul, Korea

M-type hexaferrites were reported to exhibit high saturation magnetization (M_S) and coercivity (H_C) comparable with M-type hexaferrites. They have several advantages of excellent magnetic properties, chemical stability, and low cost compared with other magnetic materials. There have been various attempts to improve the magnetic properties of M-type hexaferrites such as divalent and trivalent cations can be substituted for these Fe^{3+} sites or A site.

In this study, we tried to synthesize Y^{3+}-substituted Sr M-type hexagonal ferrites. A study of yttrium substituted Sr M-type hexagonal ferrites remain unexplored. The nominal compositions of $Sr_{(1-x)}Y_xFe_yO_{19}$ (x = 0.0-0.5) (y = 10-12) were prepared by solid state reaction in air using strontium carbonate ($SrCO_3$), yttrium oxide (Y_2O_3) and iron oxide (Fe_2O_3) as raw materials. The raw materials were ball-milled for 24 h and calcined at 1100~1300 °C for 10 h in air. As-calcined powder was pressed into pellets and sintered at 1200~1300°C for 4 h in air. The samples were characterized by X-ray diffraction (XRD), vibrating sample magnetometer (VSM), and scanning electron microscope (SEM). The powder XRD patterns of $Sr_{0.5}Y_{0.5}Fe_{10}O_{19}$ calcined at 1200 for 10 h exhibited a single phase. The maximum saturation magnetization value of 66.8 emu/g and coercivity value of 3755 Oe was obtained from the $Sr_{0.5}Y_{0.5}Fe_{10}O_{19-\delta}$ sample sintered at 1300˚C for 4h in air. Details will be presented for a discussion

Keywords: Yttrium-substituted Sr M-type, Hexaferrite, magnetic property

Study of Magnetic properties and MCA Strain effected $Fe_{13}Co_3$

Jin Sik Park*, S. H. Rhim†, and Soon Cheol Hong†
Department of Physics and Energy Harvest Storage Research Center,
University of Ulsan, Ulsan 44610, Republic of Korea
†Corresponding authors: sonny@ulsan.ac.kr, schong@ulsan.ac.kr

Permanent magnet is one of key components in many modern technologies. FeCo alloys have attracted interesting for a possible permanent magnet because of high saturation magnetization and high temperature. Especially, $Fe_{13}Co_3$ has most highest magnetic moment in a previous DFT study[1]. Since the alloys are well known as a soft magnet, enhancement of magnetocrystalline anisotropy (MCA) of the alloys is required to be used as a permanent magnet.

In this study, we focus on strain effects to find a way how to enhance the MCA of $Fe_{13}Co_3$. We adopt the first-principles calculational method of Vienna Ab-initio Simulation Package (VASP). The generalized gradient approximation is employed as parametrized for the exchange-correlation potential. The k-mesh of 12x12x12 is used in the Monkhorst-Pack scheme. For the wave function expansion, a plane-wave basis set with a cutoff energy 450 eV is used. First all, we get equilibrium lattice constants of a= 5.69 Å and c= 5.68 Å from total energy calculations. Calculated average magnetic moments per atom are 2.356 μ_B of Fe and 1.714 μ_B of Co, respectively. The average magnetic moments are converted to the saturation magnetization $\mu_0 M_S$ of 2.32 T. And calculated MCA energy is +0.02 meV/cell without strain, quite low as expected. Here + and - signs indicate uniaxial and planar MCA, respectively.

We consider strain effects by calculating magnetic moments and MCA's at a=5.52 Å and 5.86 Å, which are shorter and longer by 3% than the equilibrium a=5.69 Å, respectively. For the shorter a=5.52 Å, the calculated c is 5.86 Å or c/a=1.06. Total magnetic moment is reduced by 2.19% but MCA is calculated to be +0.66 meV/cell, which implies uniaxial MCA. On the other hand, for the longer a=5.86 Å the calculated c is 5.56 Å or c/a=0.95. Total magnetic moment is enhanced by 2.48% but MCA is obtained to be -0.45 meV/cell, which means planar MCA. The results imply that the elongation along the c-axis is required for $Fe_{13}Co_3$ to be a permanent magnet. We will also discuss the way to further enhance MCA of the FeCo alloys by inserting some 2p-elements.

Keywords: $Fe_{13}Co_3$, Strain effect, Permanent magnet

Reference

[1] Dangxin Wu, Qiming Zhang, J. Ping Liu, Dingwang Yuan, and Ruqian Wu, Appl. Phys. Lett. **92**, 052503 (2008).

International Symposium on Magnetism and Magnetic Materials 2018

Poster Session

Monte-carlo simulation for X-ray photon counting using SiPM detector

Seung-Jae Lee[1], Cheol-Ha Baek[2,3*]
[1]Department of Radiological Science, Dongseo University
[2]Department of Radiological Science, Kangwon National University
[2]Department of Medical Health Science, Kangwon National University

The detector for X-ray photon counting was designed using SiPM (Silicon photomultiplier) array and the detector characteristics were evaluated through simulation. GATE (Geant4 application for emission tomography) was used to obtain the position where the X-ray and the scintillation interacted, and this position was used as the light generation position of DETECT2000. 0.5 mm and 1 mm thick GAGG scintillators were used and the light generated through a 4 x 4 array of MPPCs was acquired. The spatial resolution of the designed detector was evaluated by reconstructed image using the light signal acquired for each channel. We obtained images of more than 2 lp/mm in both 0.5 mm and 1 mm thick GAGG scintillation. When this detector is used in a X-ray system, a low-cost system capable of photon counting can be made.

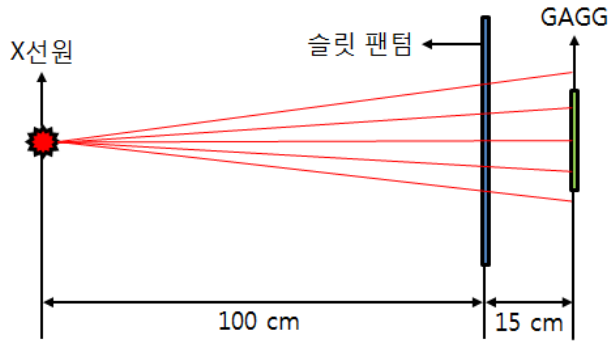

Fig. 1. Geometry of GATE simulation

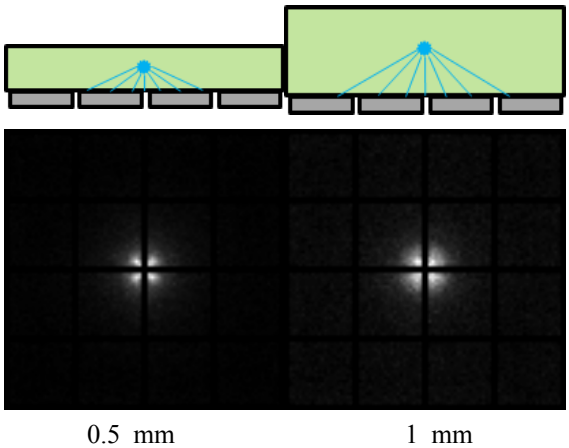

Fig. 2. Light distribution in 0.5 and 1 mm GAGG.

BM02

Influence of a nonuniform transverse magnetic field on dose distributions of MV photon beams in inhomogeneous medium

Woo Sang Ahn[1*], Wonsik Choi[1], Jungwon Kwak[2], In-Hye Jung[1], Seong Soo Shin[1]

[1]Department of Radiation Oncology, Gangneung Asan Hospital, University of Ulsan College of Medicine, Gangneung 25440, Korea

[2]Department of Radiation Oncology, Asan Medical Center, University of Ulsan College of Medicine, Seoul 05505, Korea

Radiotherapy based on magnetic resonance imaging (MRI) has emerged as a promising ability to provide real-time image-guidance during radiotherapy treatments due to excellent discrimination of tumor site and associated normal tissues. However, the use of a magnetic field during beam delivery causes fluctuations of radiation dose distributions especially in the presence of inhomogeneous regions such as the lung. This work investigated the effect of dose deposition caused by a magnetic field transverse to the incident beam by means of EBT3 film dosimetry.

The solid water phantoms with PMMA material consisted of a full water phantom and water-air-water phantom as a simplified lung. The dose distributions of 6-MV and 10-MV photon beams of a Varian TrueBeam linear accelerator were measured for different square field sizes of 1.5×1.5 cm^2 and 3.0×3.0 cm^2. Measurements using a Gafchromic self-developing radiochromic dosimetry film were performed with and without a transverse magnetic field of 0.5 T.

When a 0.5 T field is applied, the improvement of the dose to the proximal interface is most significant for the field size of 3.0×3.0 cm^2. The higher beam energy creates a more extended dose enhancement. Also, the effect of dose reduction showed in front of the distal region along the beam axis.

These dose effects potentially can be used to provide higher doses to the tumor and lower doses to adjacent normal tissues in radiation therapy.

Effects of Pulse Magnetic Field in Capillary Blood Vessel of In-vivo and In-vitro

Jinwon Mok*, Seunghwan Bang, Hyoje Ahn, Kyounghun Shin, Yonghyeok Jo, Hyunsook Lee
Department of Oriental Biomedical Engineering, College of Health Science, Sangji University,
Wonju 26339 South Korea

Introduction: Capillaries are an important vascular system in which gas and substance exchange takes place in the body. Depending on the shape of capillary blood vessels, health conditions such as blood pressure and circulation will be changed. The capillary blood vessel for a healthy person has fast blood circulation and no clogging or winding. According to previous research, the pulse magnetic field(PMF) has a positive effect on capillary blood vessels. We investigate the effects of PMF on blood flow by fabricating artificial micro-channels using PDMS and compare with capillary blood vessel.

Method: The capillary blood features and flow were observed in-vivo, with applying 0.05ml of immersion oil to the middle finger's nailfold capillary, using a capillary microscope. And we compared images of capillary loop before and after PMF stimulus of 0.27 T for 10 minutes on the palm. This method was repeated five days a week for six months to obtain continuous changes as well as transient changes. Total ten volunteers participated in the study and were obtained the written consent before the study. For in-vitro experiment, artificial micro-channels imitating a capillary blood vessel were made with PDMS. With 0.5ml of blood before and after PMF stimulus, each blood was injected into the artificial micro-channel using a syringe pump to observe changes in blood flow.

Result: In in-vivo experiments, it was found that the capillaries are became normal range after PMF: the numbers are 9±1, the lengths are about 250±10μm, and diameter inlet and outlet vessel ratios are 1: 1.5. In in-vitro, blood flow and velocity were faster than before PMF. We have demonstrated that the PMF has a positive effect on in-vivo capillary blood vessel as well as on in-vitro. Therefore, it is expected that PMF would be of great help in treating patients with blood circulatory disease.

Characteristics of systolic blood pressure and systolic time depending on the effect of thermal stimulation therapy using magnetic Hall sensor pulsimeter

Gyu-Sun Lee*, Ju-Young Kim, and Sang-Suk Lee
Department of Oriental Biomedical Engineering, Sangji University, Wonju 26339, Korea

The modern life expectancy of modern people has increased more than the past life expectancy due to various factors such as the development of medicine and improvement of nutritional status. Therefore, the diseases caused by the aging of the population have increased, and the medical burden to be used for the treatment of diseases has increased. In order to reduce the burden of such medical expenses, many self-treatment are being performed, and a home thermal stimulation therapy apparatus is widely used as an alternative to such self-treatment. We decided to see what effect the home thermotherapy device has on our bodies. There are various models of the thermal medicine used in the market today, but the N5 model of thermal stimulation therapy apparatus of the Nuga Best company is used (Fig. 1).

Fig. 1. How to use for the measurement by using the thermal stimulation therapy apparatus (Model N5) of the Nuga Best company.

In this study, we decided to conduct an experiment to measure the effect of the radial artery pulse wave as an index to see how the thermotherapy device affects our body. The clip-type pulsimeter equipped with a Hall sensor has a permanent magnet put on the center of a radial artery. In the experiment, the systolic blood pressure, ECG, oxygen saturation, and body temperature were measured for 40 subjects for 2 persons. It was measured by measuring the systolic time from the pulse wave data of the radial artery using the clip-type pulsimeter. The pulse wave data were collected by measuring the pulse wave before and after the use of the thermal stimulation therapy apparatus and after use, and the waveforms were shown in a graph.

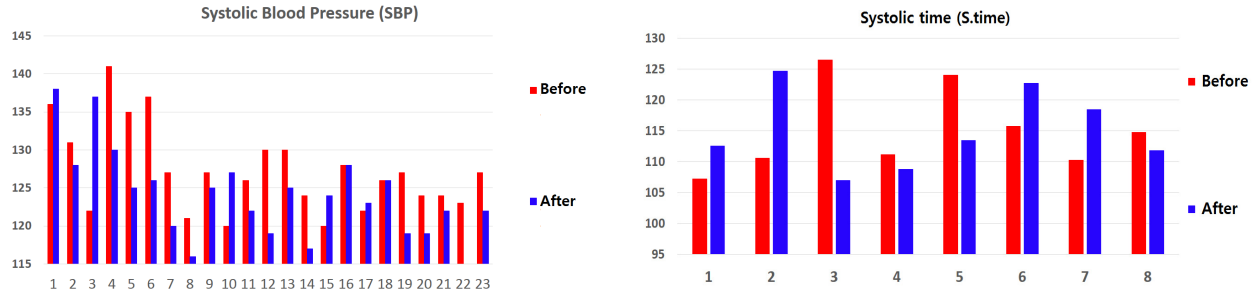

(a) (b)

Fig. 2. Analysis plots for (a) the systolic blood pressure (SPB) and (b) the systolic time (S.time) using the thermal stimulation therapy apparatus and the clip-type pulsimeter, respectively

As a result of the experiment, the temperature and the saturation degree of the human body tended to increase more, and the systolic blood pressure and the systolic time were also decreased more than those before the use of the medical apparatus, as shown in Fig 2(a) and (b). The findings of this research may be useful for developing a oriental-western biomedical signal storage device, that is, the new and fusion patient monitor, for a U-health-care system. Therefore, it is thought that the use of a thermal stimulation therapy apparatus has shown a positive result which is considered to have a positive effect on the body.

Acknowledgment: This work was supported by the Graduation Design Program of Department of Oriental Biomedical Engineering of Sangji University.

References

[1] Dae-Hui Lee, Yu-Sik Hong, and Sang-Suk Lee, “Development of Oriental-Western Fusion Patient Monitor by Using the Clip-type Pulsimeter Equipped with a Hall Sensor, the Electrocardiograph, and the Photoplethysmograph”, Journal of the Korean Magnetics Society 23(4), 135-143 (2013).

[2] Dong Jin Lee, Su-Hee Kim, Jae-Han Jeong, and Sang-Suk Lee, “The Estimation Equation of Systolic Blood Pressure Dependent on the Systolic Time of the Radial Artery Wave Measured by Wrist Wearable Pulsimeter Equipped with a Magnetic Hall Device”, Journal of the Korean Magnetics Society 28(3), 105-110 (2018).

Effect of the carbon content of $Mn_{50}Al_{50-x}C_x$ on its magnetic properties and phase stability

Sumin Kim, Hyun-Sook Lee*, and Wooyoung Lee*
Department of Materials Science and Engineering, Yonsei University,
50 Yonsei-ro, Seodaemun-gu, Seoul, 03722, Republic of Korea
*Corresponding authors. E-mail addresses: wooyoung@yonsei.ac.kr (W. Lee), h-slee@yonsei.ac.kr (H.-S. Lee)

We have investigated the effect of carbon content in $Mn_{50}Al_{50-x}C_x$ (x = 0, 1.56, 2.35, and 3.12 at.%) on the magnetic properties and phase stability. We prepared a high content of the ferromagnetic τ-phase with different particle sizes in the powders. From the phase analysis using XRD, we found that the carbon content is critical for the stability of the τ-phase formation. The highest saturation (96.6 emu/g) and remanence (47.1 emu/g) magnetizations are observed at x = 2.35. These are the highest values reported so far. This is attributed to the high fraction of the τ-phase (~94 wt%) at this carbon content. The coercive field of $Mn_{50}Al_{50-x}C_x$ shows particle-size dependence. A high coercive field is observed at a smaller size of particles. From the analyses of the phase and magnetic properties, the solubility limit of carbon in $Mn_{50}Al_{50-x}C_x$ that yields the high-quality τ -phase was found to be x = ~2.35.

Keywords: Mn-Al-C alloy; carbon addition; phase stability; magnetic properties; permanent magnets

Enhancing the coercivity of Nd-Fe-B sintered magnets by consecutive heat treatment-induced formation of Tb-diffused microstructures

Sumin Kim[1*], Dong-Su Ko[2], Donghwan Kim[3], Jong Wook Roh[4†], and Wooyoung Lee[1†]

[1]Department of Materials Science and Engineering, Yonsei University, Seoul 03722, Republic of Korea

[2]Platform Technology Lab, Samsung Advanced Institute of Technology, Samsung Electronics, Gyeonggi-do 16678, Republic of Korea

[3]Sunglim Group, Daegu 42714, Republic of Korea

[4]School of Nano & Materials Science and Engineering, Kyungpook National University, Gyeongsangbuk-do 37224, Republic of Korea

[†]Corresponding authors. Emails: wooyoung@yonsei.ac.kr (W. Lee) and jw.roh@knu.ac.kr (J. W. Roh)

The realization of efficient electric vehicle motors or power generation systems for wind turbines necessitates the development of high-performance permanent magnets, which is associated with a number of challenges. Since their discovery in 1984, high-coercivity sintered Nd-Fe-B magnets have found numerous practical and industrial applications, e.g., as components of actuators, motors, generators, and microwave/telecommunication equipment. However, the above applications require long-term magnet operation in high-temperature environments without any coercivity decrease, which is a non-trivial criterion. Generally, the coercivity of Nd-Fe-B magnets at room temperature can be enhanced by the partial replacement of Nd by Dy, Tb, or both; however, the high cost and scarcity of these rare earths preclude the widespread application of this method and necessitate the development of more economically viable alternatives. One of such alternatives is the reduction of heavy lanthanide (e.g., Dy and Tb) usage and minimization of remanence and energy product loss via the utilization of the grain boundary diffusion process (GBDP, developed in 2005).

However, many studies were carried out using only small-scale magnets, and the developed methods may therefore not be suitable for the conventional fabrication of large-size industrial Nd-Fe-B magnets. Despite the importance of understanding the grain boundary diffusion mechanism in such large magnets, no systematic investigations have addressed this issue so far.

Herein, we employ consecutive heat treatment-driven TbH diffusion to fabricate large-size Nd-Fe-B magnets exhibiting enhanced coercivity without any decrease of remanence (B_r) and energy product ((BH)$_{max}$). Furthermore, we systemically investigate the microstructure of Tb-diffused Nd-Fe-B magnets, revealing the relationship between Tb-diffused area and enhanced coercivity.

Magnetic performance of die-upset hybrid magnet composed of Nd-Fe-B and (Nd,Ce)-Fe-B materials

Dagus Resmana Djuanda[1], M. S. Kang[1*], H. W. Kwon[1], J. G. Lee[2], J. H. Yu[2], and D. H. Kim[3]
[1]Pukyong National University, Busan, Republic of Korea 48513
[2]Korea Institute of Materials Science, Changwon, Republic of Korea 51508
[3]Star-group Ind. Co., Daegu City, 42714, Republic of Korea

$R_2Fe_{14}B$ compound based on light rare earth atom, such as Nd and Pr, is the best fit for being a good hard magnetic compound, and high performance of R-Fe-B-type (R = mostly Nd, Pr) magnet derives from excellent intrinsic hard properties of the $R_2Fe_{14}B$ compound. In the magnet, the rare-earths play a key role for having high magnetocrystalline anisotropy, albeit their content is small. Those light rare earths are mostly refined from rare-earth ores of Bastnasite and Monazite. In point of fact, the most abundant rare earth element in the ores is cerium: content of cerium oxide in those ores is typically more than three times as much as that of Nd-oxide or Pr-oxide. Although the abundant Ce has wide range of applications, such as batteries and phosphor, the market supply of Ce far exceeds the demand in the market. Ce is still considered to be the most marginalized element in the rare earth family, so Ce fetches a much more charm price than Nd and Pr. It would be preferable, therefore, if the more abundant and cheaper Ce could be used as rare-earth part of the R-Fe-B-type magnet. Ce-based $R_2Fe_{14}B$-type compound, however, has disappointingly poor intrinsic hard magnetic properties for being a base compound for permanent magnet. Instead, Ce has been used as a substituent for Nd in the Nd-Fe-B-type magnet with the intention of lowering material cost. In this study, we prepared Ce-containing Nd-Fe-B-type die-upset hybrid magnet composed of melt-spun material and HDDR powder, and its magnetic performance was investigated. (Nd-Fe-B + (Nd,Ce)-Fe-B) hybrid magnet was fabricated by hot-pressing and then die-upsetting the mixture of Nd-Fe-B-type melt-spun flake (MQU-F: $Nd_{13.6}Fe_{73.6}Co_{6.6}Ga_{0.6}B_{5.6}$) and HDDR powder ($(Nd_{0.55}Ce_{0.45})_{15}Fe_{72.2}Co_{6.6}Ga_{0.6}B_{5.6}$). Overall magnetic performance of the hybrid magnet was improved with increasing vol % of the melt-spun material (Fig. 1). Texture

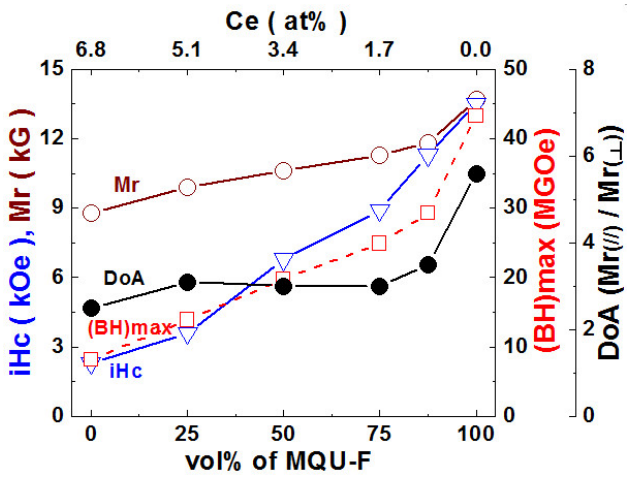

Fig. 1. Magnetic performance vs. vol% of MQU-F for the (Nd-Fe-B MQU-F + (Nd,Ce)-Fe-B HDDR) hybrid magnet.

(presented by degree of alignment) in the hybrid magnet was dependent upon mixing ratio of the magnetic particles; texture stayed low and almost constant up to 75 vol% MQU-F, after which it increased drastically. Demagnetization curve of the hybrid magnet showed single phase-like demagnetization behavior regardless of mixing ratio, indicating good interaction between the two constituent materials. The hybrid magnet with optimum composition exhibited reasonably sound magnetic performance: ${}_iH_c$ = 6.8 kOe, M_r = 10.6 kG, and $(BH)_{max}$ = 19.8 MGOe for 50 vol%MQU-F - 50 vol%HDDR hybrid magnet (3.4 at% Ce).

Magnetic properties and microstructure of hot-deformed RE-Fe-B magnets (RE = Nd, Ce, La)

Ga-Yeong Kim[1,2*], Jae-Gyeong Yoo[1], Hee-Ryoung Cha[1],
Yang-Do Kim[2], Hae-Woong Kwon[3] and Jung-Goo Lee[1†]

[1]Powder&Ceramics Division, Korea Institute of Materials Science, Changwon, Korea
[2]Department of Materials Science and Engineering, Pusan National University, Busan, Korea
[3]Department of Materials Science and Engineering, Pukyong National University, Busan, Korea

Nd-Fe-B permanent magnets have been widely used in various applications such as computers, household electrical appliances, hybrid vehicles and ~~to~~ wind generators. However, Nd-Fe-B magnets usually include 30-33wt.% of rare earth elements such as Nd, Pr and Dy, which are scarce natural resources, increasing price of magnets. Considering the cost reduction and the unbalanced use of rare earth metals, there is an urgent and growing requirement for usage of abundant rare earth metals such as Ce, La, and misch-metal in Nd-Fe-B permanent magnets. Recently, incorporating Ce and La which are abundant light rare earth elements compared to Nd, into Nd-Fe-B sintered magnets researchers has attracted much attention. However, magnetic properties of Ce substituted Nd-Fe-B magnet are much inferior to those of Nd-Fe-B magnets because of the lower intrinsic magnetic properties for $Ce_2Fe_{14}B$ phase and the formation of the CeFe2. On the other hand, the melt spinning technique has been employed as the most useful The microstructure of melt spun powders such as grain size and phase formation depend on the melt-spinning conditions such as wheel speed, ?, and ?. The hot-deformation process is a well-known method to prepare anisotropic Nd-Fe-B magnets, which are composed of platelet shaped 2:14:1 main phase grains surrounded by thin Nd-rich intergranular phase. Compared to conventional sintering process, the stable precursor and lower hot-deformation process temperature (600 to 900 ℃) may contribute to prepare high performance Ce/La-substituted RE-Fe-B magnets since $Ce_2Fe_{14}B$ and $La_2Fe_{14}B$ phases are unstable under high temperature. In this work, the magnetic properties and microstructure of the hot-deformed RE-Fe-B magnets (RE = Nd, Ce, La) were studied. The melt spun ribbons with composition of $(Nd_{1-x}M)_{30}GaCo_6Fe_{63}B$ (M = Ce/La and x = 0-30) were prepared at a wheel speed of 22 to 28 m/s in an argon atmosphere and then were ground to powders. With increasing Ce/La mass, magnetic properties decrease which mainly results from the lower intrinsic magnetic properties of $Ce_2Fe_{14}B$ and $La_2Fe_{14}B$ phase. Furthermore, the XRD result reveals that 2:14:1 phase is the primary phase and a few $CeFe_2$ phases could be observed in powders with increased Ce. After hot-deformation process, the coercivity of the hot-deformed sample was decreased, and the remanence increased. It is expected that the high remanence was resulted from alignment of the c-axis along the pressing direction during the hot-deformation.

Magnetic properties of Sr-La-Co m-type hexaferrite synthesized by solid-state reaction

Jun-Ho Park*, Kang-Hyuk Lee and Sang-Im Yoo†
Department of Materials Science and Engineering, Seoul National University,
Research Institute of Advanced Materials (RIAM), Seoul 151-744, Korea

M-type hexaferrites have been used for many applications as permanent magnets, data storage materials, electrical devices, and microwave devices because of its merit. In order to increase their magnetic properties, researches on the site substitution of M-type hexaferrites are being widely performed. There have been several reports of substitution Sr and Fe with La and Co to improve the magnetic properties of Sr m-type hexaferrites. Many industries have used Sr-La-Co m-type hexaferrites (SLC m-type), because of their high magnetic properties ($BH_{(\max)}$). In this study, we found the optimized thermal condition of SLC m-type and investigated the magnetic properties of SLC m-type by changing the rate of La and Co. First, we determined calcination and sintering temperature with $Sr_{0.85}La_{0.15}Fe_{11.85}Co_{0.15}O_{19}$ (calcination at 1250 ~ 1300 ℃ for 2h in air, sintering at 1200 ~ 1250 ℃ for 1h in air). And then, we got the value of x with the highest magnetic properties($BH_{(\max)}$) of $Sr_{1-x}La_xFe_{12-x}Co_xO_{19}(x=0.1,0.15,0.2,0.3)$. Samples were characterized by X-Ray Diffraction (XRD), Scanning Electron Microscope (SEM) and Vibration Sample Magnetometer (VSM). The XRD data revealed single m-type hexaferrite phase at all temperature and x ranges. Lattice parameter α is smiliar all ranges, while and unit cell volume tended to decreased. The coercivity tended to linearly increase with increasing x. Other research paper also showed this tendency. other papers showed highest magnetic properties at x =0.1 or x= 0.3. However, our study showed that the sample with x = 0.15 ($Sr_{0.85}La_{0.15}Fe_{11.85}Co_{0.15}O_{19}$ calcination 1280 ℃ for 2h in air, sintering 1230 ℃ for 1h in air) exhibited the highest magnetic properties of M_s= 70.7 emu/g, H_c = 3711 Oe, $BH_{(\max)}$ = 0.92 MGOe. Details will be presented for a discussion.

Keywords: M-type hexaferrite, La-Co, saturation magnetization (Ms), coercivity (Hc)

Crystallographic and magnetic properties of $Sr_{1-x}Ca_xFe_{12}O_{19}$ (x=0, 0.5) prepared by auto-combustion method

Sunghyun Yoon*
Department of Physics, Gunsan National University, Gunsan 54150

Crystallographic and magnetic effects of Ca^{2+} substitution in Sr hexaferrite were investigated in this study. $Sr_{1-x}Ca_xFe_{12}O_{19}$ (x=0, 0.5) powders were prepared by citrate auto-combustion method and subsequently sintered at 1200℃ under the atmosphere for 12 h. Crystallographic and composition analysis were done by using SEM, EDS, and XRD. Microscopic and macroscopic magnetism were examined by Mössbauer spectroscopy and VSM, respectively.

The particle sizes distributed widely up to several ㎛ and the samples were confirmed to be single phase M-type hexaferrite. Both the saturation magnetization (M_S) and the coercivity (H_C) decreased 14% and 22%, respectively as half of Sr^{2+} ions were replaced by Ca^{2+}. Meanwhile, the decrease of coercivity with the substitution of Ca^{2+} could be explained by the decrease of effective magnetic anisotropy constant (K_{eff}). These aspects were related with the distortions of 2b and $4f_2$ crystallographic sites, which were also confirmed by XRD and Mössbauer spectroscopic characterizations.

Table 1

x	a (Å)	c (Å)	Ms** (emu/g)	Hc (G)	K_{eff} (erg/cc)
0	5.8776	23.0374	50.8	3862	3.02×10^6
0.5	5.8793	23.0030	43.6	2987	2.45×10^6

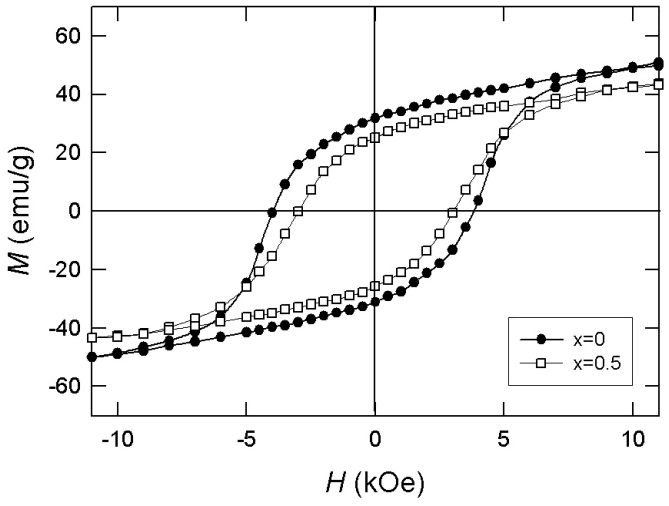

Fig. 1.

Structural and magnetic properties of $Ba_{1-x}La_xFe_{12}O_{19}$ hexaferrites

N. Tran*, H. H. Nguyen, T. L. Phan, B. W. Lee†
Department of Physics and Oxide Research Center, Hankuk University of Foreign Studies,
Yongin 17035, South Korea
†Corresponding author: bwlee@hufs.ac.kr

$Ba_{1-x}La_xFe_{12}O_{19}$ (x = 0-0.5) nanocrystallline samples were synthesized by using co-precipitation method combining with heat treatment. Both X-ray diffraction (XRD) and Raman spectroscopy (RS) studies indicated that all samples mainly crystallized into the M-type hexaferrite structure (the space group $P6_3/mmc$). Specifically, the samples with $x \leq 0.2$ were single phase without any impurity while those with $x > 0.2$ had a trace of a secondary phase Fe_2O_3. The volume fraction of Fe_2O_3 increased with increasing of La-doping concentration. Electronic-structural analyses basing on the Fe *K*-edge X-ray absorption spectra proved the oxidation state of Fe in $BaFe_{12}O_{19}$ to be 3+. For $Ba_{1-x}La_xFe_{12}O_{19}$ compounds, while the oxidation state of Ba is stable, that of Fe is changed with an appearance of a small amount of Fe^{2+} ions (beside pre-existing Fe^{3+} ions) when La-doping content (x) changes. The magnetic properties of these samples have been studied by using a vibrating sample magnetometer (VSM) with the external field up to 10 kOe. The results show that the saturation magnetization M_s of the samples with $x \leq 0.2$ were almost unchanged, about 39 emu/g, while the coercivity H_c slightly increased from 4.98 kOe for $x = 0$ to 5.26 kOe for $x = 0.2$. For the samples with $x > 0.2$, M_s gradually decreases to 28.5 emu/g. This can be attributed to the appearance of Fe_2O_3. Notably, the square ratio M_r/M_s of all the samples is higher than 0.8, making them more suitable for rare-earth-free magnet applications.

Key words: M-type hexaferrites, electronic structure, magnetic property

Synthesis and Densification of Hybrid Magnet based on Magnetite Nanoparticles

Kyung Min Kim*, Youn-Kyoung Baek†, Jung Goo Lee, Young Kuk Kim
Korea Institute of Materials Science, Changwon 51508, South Korea

The use of rare-earth magnets is rapidly increasing in technology today. However, rare-earth elements used in rare- earth magnets are limited to certain regions, which may result in unstable supply and high prices. On the other hand, iron oxide is not only rich in earth, but also inexpensive. In addition, iron oxides are known to exist in various crystal structures and display a wide variety of magnetic behaviors. Especially, ε-Fe_2O_3 is known to exhibit a large coercivity (>20 kOe) at room temperature. In this study, we fabricated the hybrid magnet by uniformly mixing the ε-Fe_2O_3 and Fe_3O_4 nanoparticles. Characterization of the synthesized ε-Fe_2O_3 and Fe_3O_4 nanoparticles was confirmed by X-ray Diffraction (XRD), Scanning Electron Microscopy (SEM), Transmission Electron Microscopy (TEM) and Vibrating Sample Magnetometer (VSM). The hybrid magnets are expected to exhibit excellent magnetic properties due to the exchange-coupling interaction between ε-Fe_2O_3 and Fe_3O_4.

Temperature dependent plastic deformability of gas atomized Nd-Fe-B alloys

Ju Young Cho[1,2*], Yong Ho Choa[2], Taek Soo Kim[1,3]
[1]Korea Institute of Industrial Technology, Korea Institute for Rare Metals, Incheon, Korea
[2]Hanyang university, Department of Materials Science and Chemical Engineering, Ansan, Korea
[3]University of Science and Technology,
Critical Materials and Semi-Conductor Packaging Engineering, Daejeon, Korea

NdFeB permanent magnet are widely used in industries such as electric vehicles, wind generators, MRI and motors etc. due to their excellent magnetic properties. The NdFeB permanent magnets are commonly fabricated by sintering using pulverized strips and ribbons. But these methods are complex and fabricated powder can be easily oxidized. Alternatively, we suggest a new method for fabrication of NdFeB permanent sintered magnet using gas atomized powder rather than ribbons.

To support our approach experimentally, we observed plastic deformability of $Nd_{12}Fe_{82}B_6$ atomized powder using high temperature hardness. We also performed plastic deformation of $Nd_{12}Fe_{82}B_6$ powder using spark plasma sintering at temperature. The structural, microstructural properties and aligning properties were observed by XRD and SEM. We found out that plastic deformability and orientation factor values increased with increasing the plastic deformation temperature.

Enhanced Uniaxial Magnetic Anisotropy in Metastable FePt

Chang Geun Park[1*], D. Tuvshin[1], T. Ochirkhuyag[1], D. Odkhuu[1], and S. C. Hong[2]
[1]Department of Physics, Incheon National University, Incheon 22012, South Korea
[2]Department of Physics and EHSRC, University of Ulsan, Ulsan, South Korea

As information storage and high-speed permanent magnet motor technologies have evolved, high-performance hard magnetic properties, including large saturation magnetization and magnetic anisotropy, have become important factors. In this study, we use the density functional theory (DFT) calculations to investigate the magnetism and uniaxial magnetic anisotropy (K_u) of L10-ordered FeX alloys (X = Ni, Pd, and Pt). Our total energy calculations reveal that the body-centered tetragonal (bct) structure with c/a = 0.83-0.84 can be formed as a metastable phase in all FeX alloys. Remarkably, for all FeX alloys, both magnetization and K_u of this bct metastable phase are enhanced with respect to those for the ground state L10-phase. More specifically, the metastable FePt exhibits an unexpectedly large K_u of about 4 meV per formula unit cell, which is about 50% larger than that of the L10-phase FePt. The analyses of atom-decomposition in K_u indicate that while the Pt atom provides the dominant contribution to the total K_u, which is similar in magnitude for both the metstable bct and ground state L10 structures, the enhancement in K_u of the metstable FePt mainly comes from Fe atom. We will also discuss our recent calculations on the structural and magnetic properties of the metastable bct and ground state L10 FePt with halogen elements doping.

First-principles prediction of large uniaxial magnetic anisotropy in Pt-substituted Fe-Co alloys

Tumentsereg Ochirkhuyag[1*], Dorj Odkhuu[1], Dorjsuren Tuvshin[1], Chang Geun Park[1], and Soon Cheol Hong[2]

[1]Department of Physics, Incheon National University, Incheon 22012, South Korea

[2]Department of Physics and EHSRC, University of Ulsan, Ulsan, South Korea

High-performance permanent magnetic materials require large uniaxial magnetic anisotropy (K_u) and high saturation magnetization (M_s) at the same time. While FeCo compounds exhibit the largest M_s and relatively high Curie temperature among the 3*d* magnetic metals, the practical usage of these alloys is quite limited due to their negligibly small K_u. Using first-principles calculations, we investigate the effect of Pt doping on the structural, electronic and magnetic properties of $Fe_{1-x}Co_x$ compounds with x = 0.25, 0.5, and 0.75. For each x, we have considered the different concentrations of Pt substitutional atoms ranging from 0.25 to 0.75 for both Fe and Co sites in $Fe_{1-x}Co_xPt_y$ ternary alloys. The structural optimization was fully accomplished by total energy and atomic force calculations within the generalized-gradient approximation in Vienna *ab initio* simulation package method. We find that both the thermal stability and magnetic anisotropy can be enhanced by adding the Pt, whereas the saturation magnetization decreases for all Fe-Co compounds considered in the present study. We attribute the large magnetic anisotropy to the interplay mechanism of the strong spin-orbit coupling of the *5d* orbitals of the substitutional Pt atom and the Jahn-Teller like tetragonal distortion.

This research was supported by Future Materials Discovery Program through the National Research Foundation of Korea (NRF) funded by the Ministry of Science and ICT (2016M3D1A1027831).

High-Performance Permanent Magnet FeNi by Enhancing the Energy Product through Pt and N dopings

Dorjsuren Tuvshin* and Dorj Odkhuu
Department of Physics, Incheon National University, Incheon 22012, South Korea

We are currently in need of replacing rare earth (RE) elements included permanent magnets with *3d* magnetic materials alone with large magnetization and high Curie temperature. While $L1_0$ ordered FeNi is among cheapest in price compared to the other transition metals such as FeCo, FePd and FePt, its negligibly small uniaxial magnetic anisotropy (K_u) and low saturation magnetization ($\mu_0 M_s$) hamper a practical use of FeNi alloys in permanent magnetic and spintronics applications. In this work, our main goal is to employ first-principles calculations to explore the possibility of enhancing the uniaxial magnetic anisotropy of $L1_0$ FeNi by lowering its high-symmetry through doping with *2p*-electron elements (B, C, and N) and 5*d*-electron Pt. Our calculations reveal that the interstitial N exhibits the thermal stability and magnetic properties better than the other B and C dopant elements, where the presence of 12.5 at.% N in FeNiN alloys enhances K_u by more than 3 times while keeping $\mu_0 M_s$ and thermal stability. More interestingly, extremely large K_u up to 2.2 meV and 3.4 μ_B per formula unit cell are predicted in FeNi by substituting the half of Ni site with Pt. These enhanced magnetic anisotropy and magnetization are discussed in connection with the Jahn-Teller like tetragonal distortion and the strong Fe 3*d*-Pt 5*d* and Fe 3*d*-N 2*p* hybridizations. We will also discuss on the even more enhanced thermal stability and hard magnetic properties of FeNi with Pt and N dopings at the same time.

This research was supported by Future Materials Discovery Program through the National Research Foundation of Korea (NRF) funded by the Ministry of Science and ICT (2016M3D1A1027831).

Effect of reductive annealing on electronic and magnetic properties of polycrystalline $SrFe_{12}O_{19-x}$

Kungwan Kang* and Hyoungjeen Jeen†
Department of Physics, Pusan National University, Busan, 46241, Korea

M-type hexaferrites are famous for its commercial use in small motors and actuators. One of disadvantages for these materials is its low saturation magnetization due to its ferrimagnetism. Thus, perturbing exchange interactions is one of important way to enhance its magnetism. One intuitive idea is change of chemical doping. In this work, we changed oxygen contents of polycrystalline SFO to see the relation between oxygen content and total magnetic moments. For this study, we used solid state reactions. X-ray diffraction and refinement tell us macroscopic and local structural information. Using vibrating sample magnetometer, we measured magnetic hysteresis of samples depending on thermal treatments. One last thing we will try is capacitance measurements to see the changes in dielectric constant, which may infer its potential ferroelectricity.

MO02

Effect of reductive annealing on physical properties in polycrystalline $PrBaCo_2O_{5.64-x}$

Yun-Seok Heo*, Han Sol Kwon, Hyoungjeen Jeen†
Department of Physics, Pusan National University, Busan 46241 Korea

A-site double perovskites have gotten great attentions, since they have been believed as a promising cathode material for solid oxide fuel cells. Moreover, because of magnetic elements and tunability of oxygen contents in this double perovskites, it would also be interesting to see the relation between oxygen contents and magnetism. Among many double perovskites, we chose $PrBaCo_2O_{5.64-x}$ (PBCO), since it is known that it has spin state transition, superior oxygen exchange behavior at the elevated temperature, arguable magnetic ground state, tunable magnetism by oxygen contents. We used solid state reaction for polycrystalline PBCO. From magnetometry data, we could stabilized the oxygen contents of our air-sintered PBCO is at least x = 5.64. For tuning oxygen contents, we used reductive thermal treatments in 3% H_2 forming gas. In this presentation, we will address the oxygen-content-driven variations in structure and magnetism by powder x-ray diffraction, Rietveld refinement, SQUID magnetometry.

Growth of LaCoOx doped SrRuO3 thin film for higher magnetoresistance

Chang Uk Jung*
Department of Physics and Oxide Research Center, Hankuk University of Foreign Studies, Yongin 17035, Korea

Previously, we reported a large magnetoresistance in LaFeO3-substituted SrRuO3 epitaxial thin films. Generally LaFeO3 doping resulted in the increase of resistivity and weakening of ferromagnetic properties. The thin film of Sr1-xLaxRu1-xFexO3 with x = 0.2 showed a clear metal-insulator transition at low temperature. The observed magnetoresistance was proportional to the doping concentration x and the value reached -35% for the film with x=0.3. Previous works by others using polycrystalline sample showed that LaCoO3 doping at SrRuO3 can result in faster increase of resistivity compared to LaFeO3 doping at SrRuO3. Usually the higher zero field resistivity tend to result in higher magnetoresistance in magnetic perovskite metal oxide system. Thus we decided to make thin film and to study the physical properties of LaCoO3-substituted SrRuO3. Thin film of Sr1-xCoxRu1-xFexO3 with x = 0~0.3 was grown using pulsed laser deposition method. The three lattice constant values were determined by using high-resolution XRD and surface morphology was studied for these films using an atomic force microscopy. All films were grown coherently with the in-plane lattice constants of the films the same as those of the underlying SrTiO3 substrate.

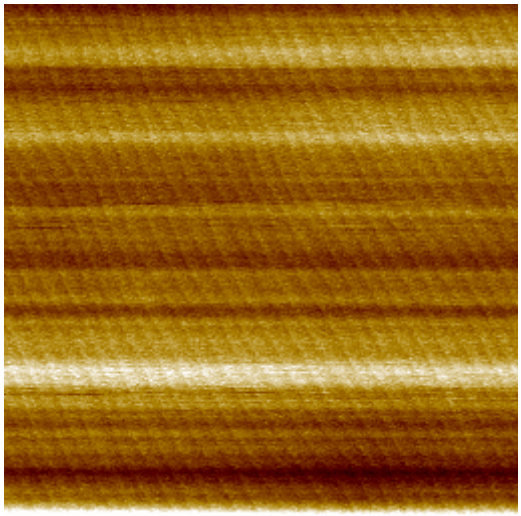

Fig. 1. Atomically smooth surface of the thin film of Sr1-xCoxRu1-xFexO3 with x = 0.3

MO04

Role oxygen vacancies in physical properties of $Ga_{0.5}Fe_{1.5}O_{3-x}$ thin films

Hyunjung Kim*, Daekil Cho and Hyoungjeen Jeen†
Department of Physics, Pusan National University, Busan, 46241, Korea

$(Ga,Fe)_2O_3$ has gotten great attentions due to a possible candidate for permanent magnets and its multiferroism. However, its saturation magnetization value is quite low due to its ferromagnetic nature. In a recent first principles-based study predicts $Ga_{0.5}Fe_{1.5}O_3$ would have the highest magnetic moment due to its selectivity in Ga position. In this presentation, $Ga_{0.5}Fe_{1.5}O_3$ (GFO) epitaxial films were fabricated on (001) YSZ substrates using RF magnetron sputtering. Then we studied the effects of oxygen contents on its physical properties. X-ray diffraction and reflectometry confirmed that epitaxial 010 GFO thin films are stabilized on (001) YSZ substrates and its clear Kiessig fringes indicates well-defined interfaces. One thing we found is that oxygen annealing as post-process leads the reduction in out-of-plan lattice constant. In special case, both oxygen rich phase and oxygen deficient phase could be stabilized. We studied physical properties of three distinct films, i.e. oxygen deficient GFO, oxygen-rich GFO, and phase separated GFO, by SQUID, XMCD, capacitance, and spectroscopic ellipsometry. We discuss the huge changes in magnetism by oxygen vacancy content. This work was supported by National Research Foundation of Korea (NRF-2018R1D1A1B07045462).

Interconversion between a magnetic skyrmion and two Bloch lines in ferromagnets

Ik-sun Hong[1*] and K. J. Lee[1,2]
[1]KU-KIST Graduate School of Converging Science and Technology, Korea University, Seoul, Korea
[2]Department of Materials Science and Engineering, Korea university, Seoul, Korea
Email: kj_lee@korea.ac.kr (K.-J. Lee)

Magnetic skyrmion are vortex-like spin texture that are topologically protected. The magnetic skyrmions are received considerable interest as information carrier because of their small size, high speed, low driving current. Topologically protected skyrmions are characterized by the topological number , that means the magnetization wrapping along the solid angle. Bloch line also treated as a topological soliton which has one half of the topological number [1].

We study about interconversion between the skyrmion and Bloch line in ferromagnetic thin film by using micromagnetic simulation. We found that the Bloch line pairs are created when the skyrmion is absorbed to the domain wall. Note that these process is irreversible, so topologically protected skyrmions can be easily annihilated by the domain wall and created by the Bloch line pairs. We will dicuss about the topological number of Bloch line and skyrmion in detail.

Reference

[1] S. K. Kim and Y. Tserkovnyak, Phys. Rev. Lett. 119, 047202 (2017)

Image Based Study of PET Detector Module for Hybrid MRI System

Shinae Lee[1*], Jaeseong Lee[2], Yeunchul Ryu[3]
[1]Department of Health Sciences and Technology, GAIHST, Gachon University, Incheon 21999, Korea
[2]Department of Biomedical Sciences, Seoul National University, Seoul 03080, Korea
[3]Department of Radiology, Gachon University, Incheon 13120, Korea

Introduction The early and accurate diagnosis of human disease in the clinical criteria is essential to provide appropriate treatment plan of the disease. The currently employed non-invasive imaging modalities such as computed tomography (CT), magnetic resonance imaging (MRI), and positron emission tomography (PET) require the hybrid imaging systems providing morphological and functional image. The PET is a nuclear medicine functional imaging technique that is used to observe metabolic processes and provide physiological, chemical, and functional images of the human body in three dimensions. On the other hand, the MRI uses high-resolution anatomical and spectral analysis images to provide anatomy and biochemical information. The PET and MRI are complementary, and the combination of the two devices can offer optimal biological and anatomical imaging techniques.

But, there is an electromagnetic (EM) interference between two systems due to the presence of magnetic fields. This EM interference can have a negative effects on both systems. Generally, PET scanner is sensitive to magnetic fields, so that strong RF transmission of MRI can degrade PET signal acquisition. The PET detector can be affected by the magnetic field because it exists inside or near the MR magnet bore. Therefore, PET electronics should be enclosed in a metal housing using a copper plate to shield it from external high frequency. The signal degradation occurs due to the shielded PET detector module, and the Silicon photomultipliers (SiPM) is applied to solve the PET signal reduction. The PET detector module uses SiPM which is not sensitive to magnetic field. The SiPM detectors offer performance comparable to the photomultiplier tube (PMT) and are insensitive to magnetic fields [1]. The microscopic differences in the magnetic field caused by PET electronics cause inhomogeneity in the internal main magnetic field (B_0-field) of MRI bore, distorting MR images. This means that the noise current can be transferred to the RF coil circuitries for the MRI by placing PET detector module inside MRI scanner bore. Potential interaction mechanisms between PET and MRI systems are as follows: 1) eddy currents, 2) degradation of gradient coil, 3) RF noise or signal loss, and 4) B_0-field inhomogeneity.

PET detector can be shielded to minimize interference, but it cannot be completely removed. In this study, the impact assessment for simultaneous PET-MRI imaging is presented [2]. PET detector is located inside the copper shielding module. In a commonly used PET-MRI, the detector module is embedded in MR gantry. In particular, we can examine the effect of PET detector module insertion and shielding on MRI imaging.

Methods *PET system* The shielding materials of PET detector module were all made of copper. The thickness of shielding material is mainly determined by RF noise frequency range. The amplitude of EM wave incident on the conductive medium decreases exponentially with the depth of the conductor. When frequency is greater than 1 MHz, the effective depth of shielding does not vary significantly over the temperature range of interest. Temperature effects are more important in the KHz range [3]. The effects of copper shielding module on MR

images were compared. The distance between PET detector modules is 1 mm, 20 mm intervals. The dimensions of the module are 14.4 cm, 4.4 cm, and 3.4 cm. PET electronics used in the study are embedded in RF coil.

MRI system All MR imaging experiments were performed with 7 Tesla MR imaging scanner (Magnetom, Siemens, Germany). The lab-built 8-channel head coil was used for the experiment. The MRI system was tuned with a shim before imaging. Images were applied using gradient echo (GRE), Magnetization Prepared Rapid Acquisition Gradient Echo (MPRAGE), and turbo spin echo (TSE) sequences (128 x 128 matrix size, 42 x 42 FOV, 1 mm slice thickness, TR = 500 ms, TE = 4.1 ms). The signal-to-noise ratio (SNR) for MRI was calculated by selecting the signal and noise of magnitude image.

Evaluation of the interference from the PET on the MRI To demonstrate the potential on MR image quality, experiments were conducted with phantom to evaluate the SNR and signal homogeneity. The homogeneity of B_0-field was also evaluated. PET date was collected without power source, and the PET detector module measured the potential interference to the MRI. The comparative measurements were obtained without mounting PET in the MRI system. MR measurements were performed by automatic shimming of the B_0-field optimized for the inserted PET detector module.

B_0-field homogeneity The homogeneity of the B_0-field was measured using a spherical phantom. The phantom was placed inside the coil. Measurements were performed using real model modules without installing actual PET inserts in the MRI system. The three sequences (GRE, MPRAGE, TSE) were applied to capture the phase image.

MRI signal-to-noise ratio and image homogeneity The uniformity of the MR Image indicates the B_0-field inhomogeneity of MRI system [4]. The eddy currents are induced by a conductive structure, such as a shielded box, by changing magnetic field. Eddy currents affect MR image because it affects the B_0-field and generates a transient magnetic field against the gradient field [5]. A cylindrical phantom (20 cm in diameter and 24 cm in length) was inserted inside the 8-channel RF coil. MR image quality was measured in three cases (no PET module, 1 mm distance between PET module, 20 mm distance between PET module) as shown in Fig. 1.

Results In this study, the uniformity of MR images was compared on three configurations according to distance between PET module. In Figure 2, MR images was acquired using three MRI pulse sequence (GRE, MPRAGE, TSE). AS the PET module distance increased and RF pulse sequence, the distortions and artifacts of MR images was shown in Fig. 2. The Image distortion was increased with increasing distance between PET module and showed different effects depending on the RF pulse sequence.

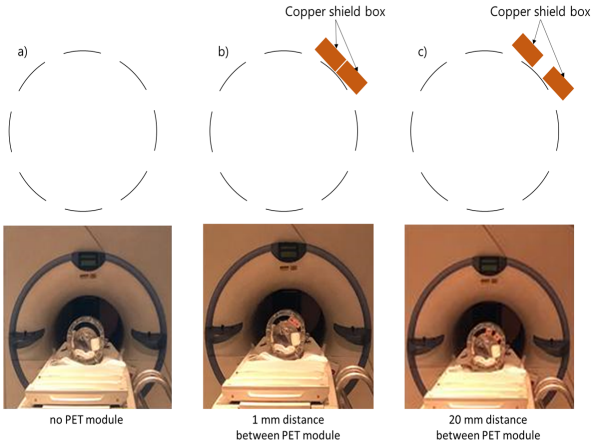

Fig. 1. The three configurations of the MR experiment according to distance between PET module

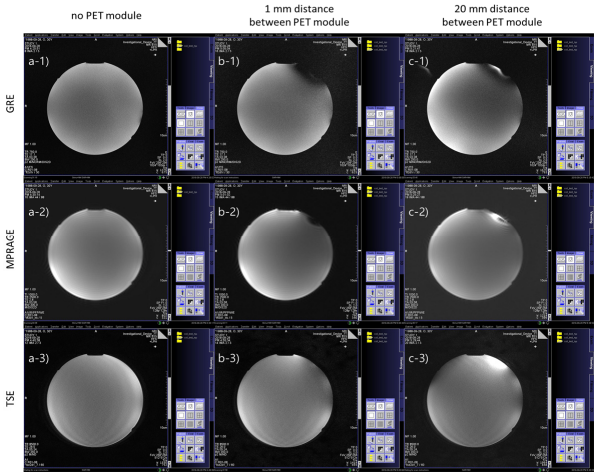

Fig. 2. MR images of GRE, MPRAGE and TSE

Conclusion Due to the automatic shimming, the field uniformity was improved when the PET detector module was installed. Phantom measurements comparing the SNR mean and standard deviation of the two PET detector modules are not significantly different between TSE and SE sequences. The MR image uniformity measurement showed lower for the homogeneity of the SE sequence when the PET module was inserted.

References

[1] Hawkes R, Lucas A, Stevick J, "Silicon photomultiplier performance tests in magnetic resonance pulsed fields", IEEE Nucl Sci Symp Conf Rec, 3400-3403, 2007

[2] Bo J Peng, Jeffrey H Walton, Simon R Cherry, Jacob Willing-Onwuachi, "Studies of the interactions of an MRI system with the shielding in a combined PET/MRI scanner", Phys. Med. Biol., 55, 265-280, 2010

[3] Vandenberghe S, Marsden PK, "PET-MRI: a review of challenges and solutions in the development of integrated multimodality imaging", Phys. Med. Biol., 60, 115-154, 2015

[4] Armin Kolb, Hans F Wehrl, Matthias Hofmann, "Technical performance evaluation of a human brain PET/MRI system", Eur Radio., 22, 1776-1788, 2012

[5] Kroot JMB, "Analysis of eddy currents in a gradient coil", PhD thesis, 182, 2005

Preliminary Study and Testing of RF Coil for Monitoring in-situ Battery Cell at 7T MR System

Danbi Song[1*], Yeunchul Ryu[1,2]
[1]Department of Health Sciences and Technology, GAIHST, Gachon University, Incheon 21999, Korea
[2]Department of Radiological Science, Gachon University, Incheon 13120, Korea

Introduction:

Lithium-ion batteries (LIBs) are currently used in many electric devices, such as mobile phones and electric vehicles. As demand for LIBs continues, efforts are ongoing to develop battery technology and to ensure safety. Recently, many studies are being conducted to confirm the state of the battery during charge and discharge using the MR system [1-3]. This provides information on how the battery changes depending on the state of charge or discharge and provides also what kind of defects are present. However, due to the structure of the loop type RF coil, there exists ununiform areas inside the cell samples and it works as a limitations in acquiring quantitative MR signal measuring from the pack of LIB battery. And the RF signals are weakened by the aluminum layer of a cell package [4]. In this paper, we propose a planar RF coil to get a uniform ^{7}Li and ^{1}H signals from this shielding-packaged battery cell in 7T MRI. To demonstrate the usefulness of our proposed planar RF coil, we compare the loop type coil and the planar type coil by comparing images and spectra acquired from each coil. We also obtain ^{1}H image and ^{1}H/^{7}Li spectroscopy and compare the results.

Material and Methods:

Loop Coil Design: The loop coils for ^{1}H and ^{7}Li were designed for 7T MRI (Fig. 1). The loop size for ^{1}H had a 20 mm inner diameter, three 22 pF capacitors and variable tune and match capacitors were set to 297.2 MHz as an operating frequency which is corresponding to the resonance frequency of ^{1}H at 7T (Fig. 1 a, c). Then, bench tests were conducted by measuring reflection coefficient S_{11} in the unloaded condition with a network analyzer. The S_{11} parameter was measured to -30.12 dB at 297.2 MHz. The loop size for ^{7}Li was a 20 mm inner diameter. Four 180 pF capacitors and variable tune and match capacitors were set to 115 MHz, the resonance frequency of ^{7}Li at 7T (Fig. 1 b, d). The S_{11} parameter was measured to -30.36 dB at 115 MHz. Each coil was matched to 50Ω.

Planar Coil Design: The planar coil for the structure of the battery cell can be considered as follows: First, the width and length of coil conductor is optimized to the size of a battery cell and to improve the SNR the gap between copper conductor is minimized to 3 mm distance. The battery cell is placed in the inner volume of this planar coil's end-corner as seen in the Fig. 2b. Second, by minimizing the 'fringe effect', which refers to a non-uniform electric field distributed around the conductor, a uniform B_1 field is formed throughout the battery cell [5]. The proposed planar ^{1}H coil that meets the above two conditions was implemented as shown in the Fig. 2. A 25 mm wide conductor strip was wrapped around the acrylic plates to form a U-shaped coil. Two acrylic plates of 110 mm x 25 mm had a gap of 3 mm, so that the battery cell could be positioned in a uniform electric field area. The size of the conductors on each acrylic plate was 40 mm x 25 mm. The currents fed to the planar coil are approximately the same in magnitude and opposite in direction. As a result, a

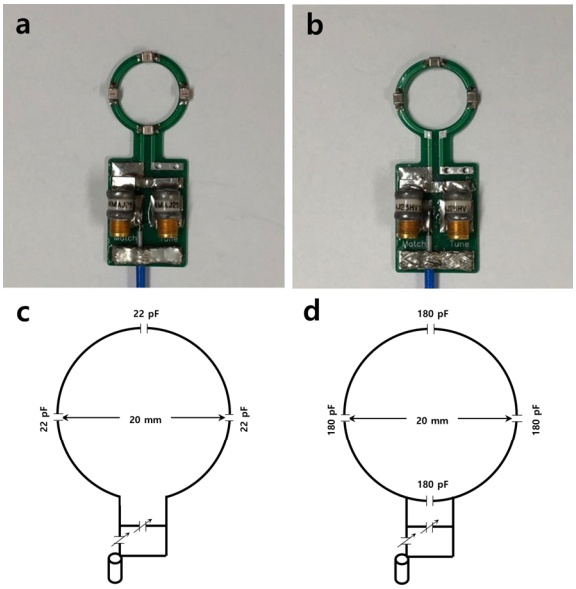

Fig. 1. a: Image of the ^{1}H loop coil. b: Image of the ^{7}Li loop coil. c: Schematic of the ^{1}H loop coil. d: Schematic of the ^{7}Li loop coil.

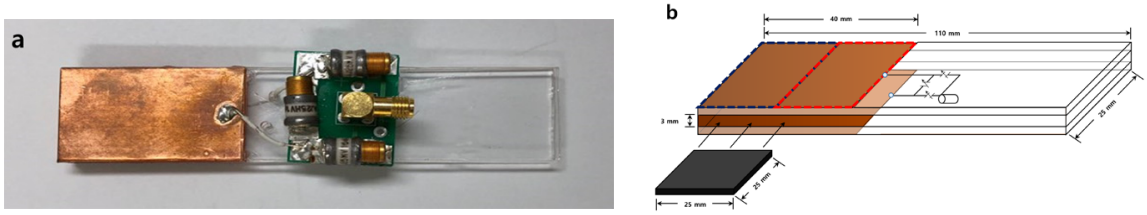

Fig. 2. The structure of proposed planar coil a: Image of implemented planar coil. b: Schematic of the planar coil.

substantially uniform current distribution is formed inside the strip, and a uniform magnetic flux density is formed inside the coil. By placing the battery cell in this area, the shape of the battery cell can be fully imaged.

MR Experiments: All experiments were performed on a 7T whole-body MRI system (Magnetom 7T, Siemens Healthcare, Erlangen, Germany). In this experiments, Polymer-packed 1M propylene carbonate - fluoroethylenene carbonate solution was used. ^{1}H gradient echo imaging and spectroscopy were performed due to the lack of a preamplifier for Li frequency.

Results and Discussion:

The proton image and spectroscopy of each coil are shown in the Fig. 3. Compared to the results of single loop coil (Fig. 3 a, b), the image and spectroscopy from proposed planar coil show better SNR (Fig. 3 c, d). And the proton spectrums according to the different bandwidth (BW) are shown in Fig. 4. However, the area outlined by the red dashed line in Fig. 2b is not suitable for acquiring images because the B_1 field distribution is not uniform over the whole object area. For this reason, in the next coil design (Fig. 5) the conductor area was 10 mm extended to the edges of the strips compared to the first planar coil, and unnecessary parts was removed for reducing the inductance of the coil. In the next research, we will try the ^{7}Li imaging and spectroscopy in 7T MRI.

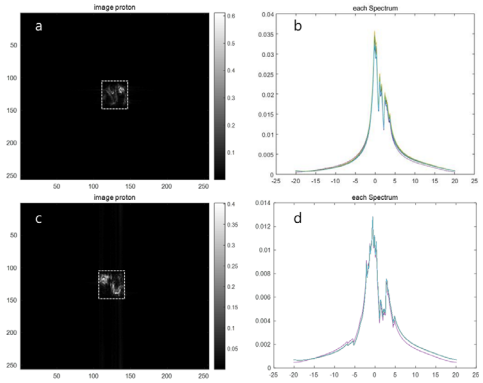

Fig. 3. ^{1}H MR image(a) and spectroscopy(b) from a single loop coil, ^{1}H MR image(c) and spectroscopy(d) from a planar coil.

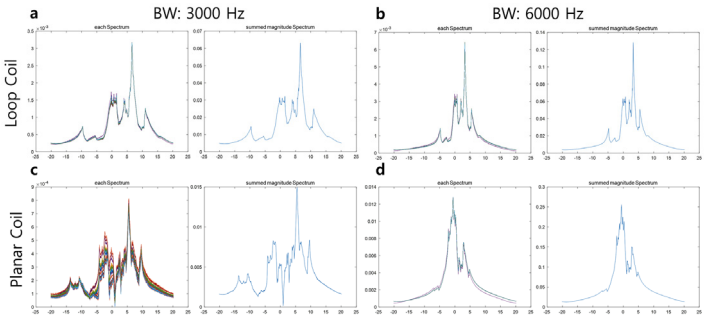

Fig. 4. ^{1}H spectroscopies from a single loop coil (a, b) and a planar coil (c, d).

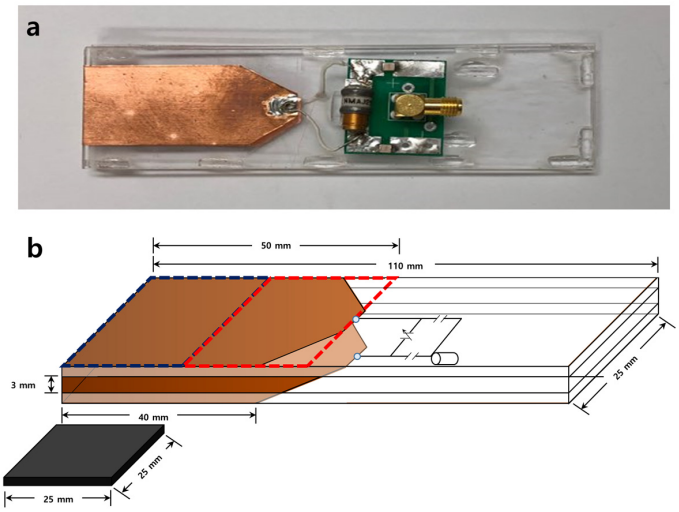

Fig. 5. The extended structure of planar coil for ^{1}H study.

References

[1] N.M. Trease, et al., Solid State Nucl. Magn. Reson. **43**:62-70 (2012).

[2] K. Shimoda, et al., Electrochimica Acta **108**:343-349 (2013).

[3] J.M. Griffin et al., Solid State Nucl. Magn. Reson. **74**:16-35 (2016).

[4] A. J. Ilott et al., Nat. Commun. **9**(1):1776 (2018).

[5] M.D. Meadowcroft et al., Magn. Reson. Med. **57**(5):835-841 (2007).

Energy Product Enhancement in Soft- and Hard-magnetic Mixtures

Namkyu Kim*, Hee-Sung Han, Dae-Han Jung, and Ki-Suk Lee†
School of Materials Science and Engineering, Ulsan National Institute of Science and Technology, Ulsan 44919, Republic of Korea

The soft- and hard-magnetic mixtures have been extensively investigated for developing rare-earth free magnet. Even though the magnetic mixtures have theoretically explicit prospect for rare-earth free permanent magnets with high energy product, no significant improvement has not been found yet because of their complicated dependence on the microstructure such as a grain size, shape, anisotropy distribution, exchange coupling among grains, and different phases. To elucidate the magnetic mixture is substantially valuable as rare-earth free permanent magnets, it is necessary to develop a clear model in which various microstructural elements are considered. In this works, we studied the magnetic mixtures composed of MnBi (hard), and FeCo (soft) by micromagnetic methods according to various ratio of two phases, their microstructures including grains, and their couplings. As a model system, we adopt the 160×160×40 nm^3 sized rectangular prism in which MnBi and FeCo phases are formed in different grains as shown in Fig. 1(a). We assumed that the easy axis of magneto-crystalline anisotropy is z-axis and the easy axis of each grains follows Gaussian distribution with standard deviation of 0.03. To estimate energy product, the hysteresis loops were calculated by applying external magnetic field ranging from -5 T to 5 T along z-axis and B- and H-fields were obtained directly from them. As shown in Fig. 1 (b), the energy product varies dramatically according to the ratio of mixture. In the presentation, we will discuss about the energy product enhancement by modulating the microstructures and the ratio of soft- and hard-magnets in mixtures.

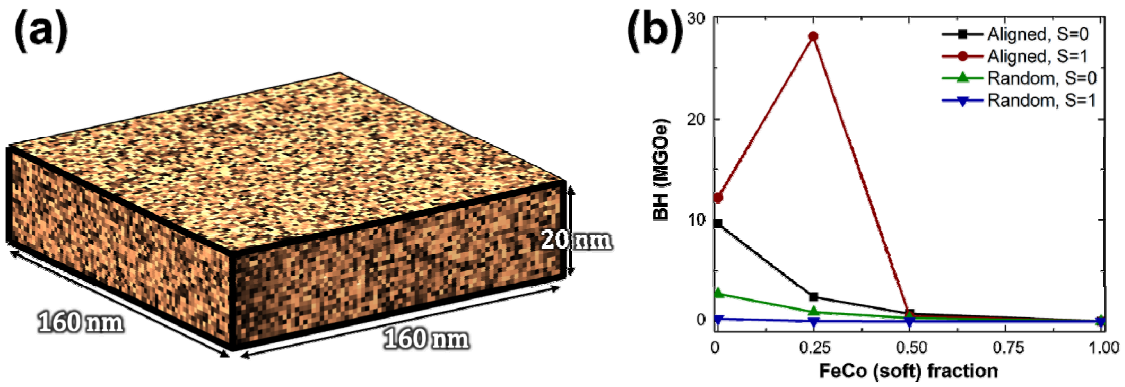

Fig. 1. (a) Model system of soft- and hard-magnetic material mixture with cubic grains. (b) Energy product of magnetic mixtures by composition.

A Limited Prediction of Maximum Energy Product from the Magnetization Hysteresis Loop

Namkyu Kim*, Hee-Sung Han, and Ki-Suk Lee†
School of Materials Science and Engineering, Ulsan National Institute of Science and Technology, Ulsan 44919, Republic of Korea

Recently, as the demand for devices using magnetic energy of permanent magnets such as electric cars and wind power generators has increased, researches have been actively carried out to develop new high-efficiency and low-cost permanent magnets. The figure-of-merit of permanent magnets is the *energy product* which is the twice the energy stored in the stray field of the magnet. It can be obtained from the volume integral of the square of the stray field outside the magnet or from the volume integral of the dot product between the demagnetizing field, $\boldsymbol{H}_{\mathrm{d}}$ and the magnetic field, $\boldsymbol{B}$ inside the magnet itself, and thus the "BH" indicates the energy product. However, this energy product of magnets is often used without a clear understanding of its definition, even though it is a basic concept that is widely known to relevant industry workers and researchers. Basically, the energy product BH corresponds to the energy stored in the stray field produced by the magnet itself. Consequently, it should be measured from $\boldsymbol{H}_{\mathrm{d}}$ and $\boldsymbol{B}$ at the remanent state, i.e., without any external field. Since the demagnetizing field depends on the shape of magnet, the energy product varies with the shape and thus, its maximum value (BH_{max}) can be obtained from the remanet state in the various shape of magnet. However, it has been found occasionally that the BH and BH_{max} are obtained from the BH loop, even from the MH loop. Here, we will discuss how to measure the energy product and how to predict correctly its maximum value (BH_{max}) from the loop.

Ferrimagnetic Domain Wall Motion Induced by Damping-like Spin-orbit Torque

Se-Hyeok Oh[1*], and Kyung-Jin Lee[1,2,3]

[1]Department of Nano-Semiconductor and Engineering, Korea University, Korea

[2]Department of Materials Science and Engineering, Korea University, Korea

[3]KU-KIST Graduate School of Converging Science and Technology, Korea University, Korea

We theoretically and numerically investigate ferrimagnetic domain wall motion driven by damping-like spin-orbit torque. We find that the damping-like spin-orbit torque combined with the interfacial Dzyaloshinskii-Moriya interaction efficiently drives the ferrimagnetic domain wall especially at the angular momentum compensation point. We obtain the analytic expression of the domain wall velocity with respect to the current density and the net spin density, which is in agreement with numerical simulation. The analytic expression is applicable to arbitrary compensation conditions, ranging from the ferromagnetic limit to the antiferromagnetic limit, and is thus useful to design and interpret ferrimagnetic domain wall experiments at various temperatures or compositions.

Figure 1 shows the velocity of ferrimagnetic domain wall as a function of δ_s at various current densities. Symbols obtained from numerical calculation are in good agreement with the analytical solution. In low current regime, the velocity is almost constant, whereas in high current regime it shows the maximum at the angular momentum compensation point (i.e., $\delta_s = 0$). This tendency is caused by decoupling between linear momentum and angular momentum of domain wall at the angular momentum compensation point. Figure 2 shows the domain wall angle φ as a function of δ_s at various current densities. The DMI sets the initial angle as $\varphi = 0$ for these calculations. There is no domain wall angle tilting at the angular momentum compensation point. For finite δ_s, the domain wall angle tilting increases with the magnitude of δ_s. For a positive (negative) δ_s, the domain wall angle φ tilts counterclockwise (clockwise). The large DMI suppresses the angle tilting strongly. In this presentation, we show

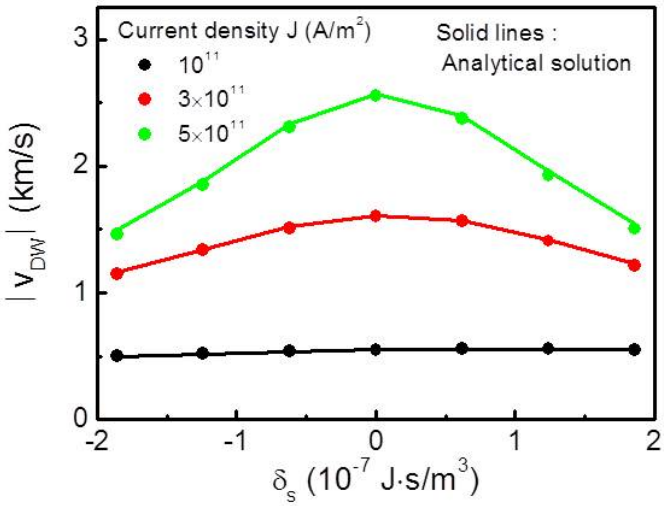

Fig. 1. The domain wall velocity as a function of the net spin density δ_s. Symbols are the numerical results, and the solid lines represent the analytical solution. The DMI constant is 0.05 (meV).

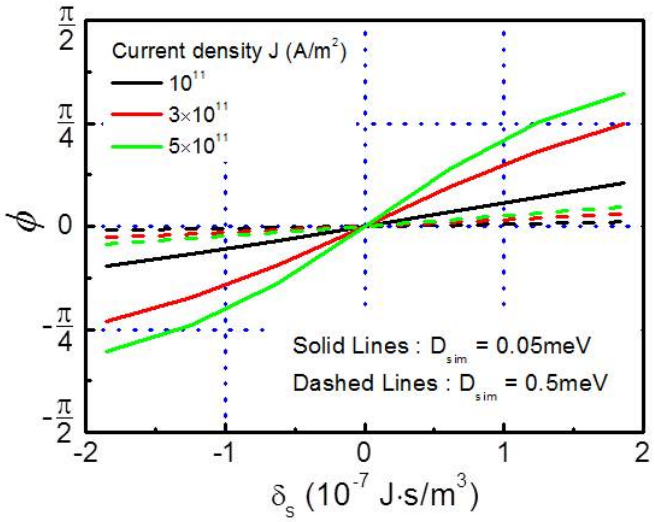

Fig. 2. The domain wall angle ϕ as a function of the net spin density δ_s.
The DMI constant is 0.05 (meV) for solid lines and 0.5 (meV) for dashed lines.

the dynamics of ferromagnetic domain wall induced by damping-like torque that the maximum of domain wall velocity appears at the angular momentum compensation condition. We expect that employing ferrimagnets offers the opportunity to realize fast dynamics of domain wall driven by current experimentally.

Chiral-induced antiferromagnetic switching in a confined nanowire

T. H. Kim[1*], S. H. Han[2], and B. K. Cho[1†]

[1]School of Materials Science and Engineering, Gwangju Institute of Science and Technology (GIST), Gwangju 61005, Republic of Korea

[2]Division of Navigation Science, Mokpo Maritime National University, Mokpo 58628, Republic of Korea

[†]Correspondence and requests for materials should be addressed to B. K. Cho. (chobk@gist.ac.kr).

In antiferromagnetic pendulum dynamics, the resonant frequency softening as the nonlinear phenomena makes it difficult to achieve a timing match between external torque and spin precession and limits the reduction of threshold torque strength, although precessional switching is adopted as fastest way to manipulate antiferromagnets. Also, overshooting problem of magnetization in a low damping system requires careful adjustment in torque strength. We investigate spiral soliton dynamics analytically and numerically in the presence of interfacial Dzyaloshinskii-Moriya (DM) interaction in the thin film. As DM interaction is induced and controlled by an electric field, the resulting spiral phase can be utilized to switch the antiferromagnet spins by perturbing the initial soliton phase through spiral-induced anisotropy modulation, and relaxing into a switched configuration. Without involving external torque, both phase mismatching and overshooting can be overcome. Our findings provide promising opportunities to realize rapid and energy-efficient electrical manipulation of magnetization for future spin-based electronic devices.

New type of skyrmion in in-plane magnetized materials

J. Yoon, K.-W. Moon*, C. Kim, and C. Hwang
Spin Convergence Research Team, Korea Research Institute of Standards and Science,
Daejeon 34113, Republic of Korea

Magnetic skyrmion have been extensively studied for the realization of information carrier due to its topological characteristics. In bulk or interfacial Dzyaloshinskii-Moriya interaction (DMI), two types of skyrmions are known to be formed such as Bloch (bulk DMI) and Néel (interfacial DMI) skyrmions, respectively. Both types of a single skyrmion cannot have two topological numbers Q of +1 and -1 in the fixed background magnetization. Consequently, if the background magnetization is fixed, the direction of the skyrmion motion has been determined depending on the sign of the resultant topological number. Here, we propose new types of skyrmions in in-plane magnetized materials with bulk or interfacial DMIs in micromagnetic simulations (hereafter called meteor-skyrmion). In contrast with Bloch and Néel skyrmions, a single meteor-skyrmion can have topological numbers Q of +1 and -1 at the same time in the fixed background magnetization. The z-component magnetization configurations of a meteor-skyrmion seem like the meteor in $+x$-magnetized materials with bulk or interfacial DMIs. The phase diagram of saturation magnetization versus bulk or interfacial DMIs is studied to confirm the topological stability of meteor-skyrmions. In addition, the spin-orbit-torque (SOT) or spin-magnetization-transfer-torque (SMT) driven motions are investigated systematically on bulk and interfacial meteor-skyrmions. The results present the meteor-skyrmion Hall effect corresponding to SOT or SMT. In this study, new proposed skyrmion will be provided as a wider variety of technical choices to realize skyrmion based memory or logic devices.

Non-adiabatic spin-transfer torque for ferromagnetic domain wall

Hyeon-Jong Park[1*], Hyewon Ko[2], Jung Hyun Oh[2], and Kyung-Jin Lee[1,2]
[1]KU-KIST Graduate School of Converging Science and Technology, Korea University, Seoul 02841, Korea
[2]Department of Materials Science and Engineering, Korea University, Seoul 02841, Korea

One of the most important issues for devices using domain wall motion is to find a way of threshold current density to move a domain wall. One of solutions is the non-adiabatic spin-transfer torque (NA-STT). It acts like a magnetic field for a domain wall and can move the domain wall with no threshold in ideal nanowires. In this respect, it is of critical important to understand various sources of the NA-STT. In this work, we theoretically analyze different sources of NA-STT, originating from spin mistracking [1], spin relaxation [2], and intrinsic spin-orbit coupling [3].

First, NA-STT due to spin mistracking appears for very narrow domain wall (width < 5 nm). In domain wall system, it is well known that local spin direction is not aligned exactly along the local magnetization but aligned along the effective field including the effect of magnetization gradient. This misalignment makes adiabatic spin-transfer torque. However, in narrow domain walls, the amplitude of spin precession around the effective field direction survives when it is integrated over the Fermi surface and this phenomenon contributes to the NA-STT. Non-adiabaticity (β_{mis}) for this contribution is proportional to $\exp(-C\lambda_{DW}/L)$ where C is constant, λ_{DW} is domain wall width and L is characteristic length [1].

Secondly, the spin relaxation also contributes to NA-STT. In the presence of spin-dependent scattering, a local spin flips and relaxes toward the magnetization direction. Thus, the spin relaxation of transverse spin component gives a NA-STT. The non-adiabaticity originating from the spin relaxation can be written as $\beta_{sf} = \hbar/J_{sd}\tau_{sf}$ where τ_{sf} is spin relaxation time [2].

Lastly, there is an electric-field induced NA-STT, called intrinsic spin-orbit torque. An electric field not only changes the occupation of states but also modifies the eigenstates of electrons. The latter contribution gives an additional non-adiabaticity to conduction electron spins [3], which is given by $\beta_{int} = \hbar/J_{sd}\tau$ where τ is momentum relaxation time.

As a result, both contributions from spin relaxation and intrinsic spin-orbit coupling are independent of the domain wall width whereas a contribution from spin mistracking enhances for a narrower domain wall. Moreover, a contribution from intrinsic spin-orbit coupling is independent of spin-dependent scattering whereas that from spin relaxation is. These different dependences allow us to separate NA-STT into three pieces of different origin. We numerically compute each contribution based on a linear response theory and evaluate an effective non-adiabaticity (β_{eff}) for a quantitative analysis. Figure 1 shows that the effective non-adiabaticity decreases with longer domain wall width. That is because the effect of spin mistracking decreases rapidly with increasing domain wall width. We also obtain an offset in β_{eff}, which is independent of the wall width and thus is the sum of β_{sf} and β_{int}. We can also divide the contributions from spin relaxation and intrinsic spin-orbit coupling by changing a disorder potential. In the presentation, we show how each non-adiabaticity varies with tight-binding parameters.

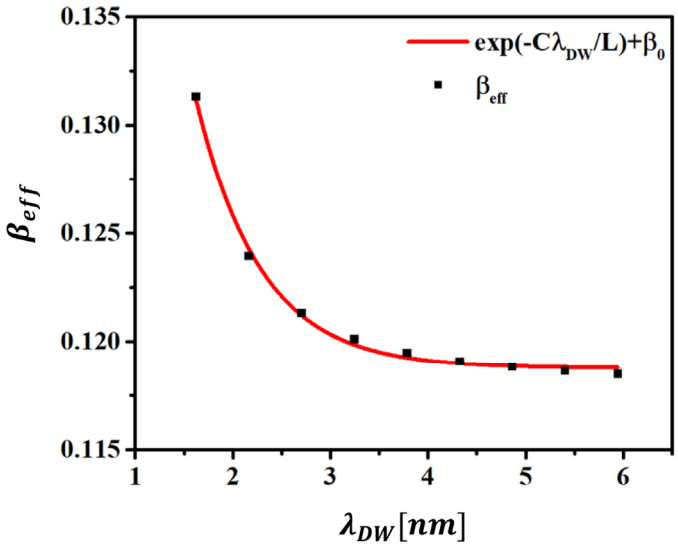

Fig. 1. Effective non-adiabaticity (β_{eff}) by domain wall width (λ_{DW})

References

[1] J. Xiao et al., Phys. Rev. B 73, 054428 (2006).

[2] S. Zhang et al., Phys. Rev. Lett. 93, 127204 (2004).

[3] K.-W. Kim et al. Phys. Rev. B 92, 224426 (2015).

Skyrmion manipulation by a rotating current

Hee-Sung Han*, Dae-Han Jung, Sooseok Lee, Namkyu Kim, Ki-Suk Lee
School of Materials Science and Engineering, Ulsan National Institute of Science and Technology, Ulsan, Republic of Korea

Magnetic skyrmion, which is one of the topologically stable magnetic configurations, has been regarded as a good candidate to develop future spintronic devices due to its rich dynamic properties and tiny size [1]. It can be created by using a material defect, or the geometrical constriction [3, 4]. However, most of the study on the creation of magnetic skyrmion has been considered the magnetic skyrmion in a film or a nanowire, not a patterned disk although the magnetic skyrmion in a patterned disk has lots of unique dynamic excitations such as gyrotropic and breathing modes [3]. Here, we propose novel method to generate skyrmions in a patterned disk with desire direction from micromagnetic studies. We modeled conventional multilayer structure of [Pt (3 nm)/$Co_4Fe_4B_2$ (0.8 nm)/MgO (1.5 nm)]$_{20}$ with material parameters in Ref. [5]. To explore the generation of the skyrmions in a patterned disk, various time-varying currents were applied along in-plane direction. We found that the rotating current generate the magnetic skyrmions from the labyrinth domain, and the rotational direction of the electrical current determines a polarization of magnetic skyrmion. The detailed manipulation process of magnetic skyrmion will be discussed at the presentation.

References

[1] J. Sampaio et al., Nat. Nanotech. 8, 839-884 (2013)
[2] W. Jiang et al., Science 349, 282-286 (2015)
[3] F. Büttner et al., Nat. Nanotech. 12, 1040-1044+ (2017)
[4] T. Shiino et al., Sci. Rep. 7, 13993 (2017)
[5] S. Woo et al., Nat. Commun. 8, 15573 (2017)

Spin Wave Phased Array Antenna

Moojune Song[1*], Kyoung-Woong Moon[2], Chanyong Hwang[2] and Kab-Jin Kim[1]
[1]Department of Physics, Korea Advanced Institute of Science and Technology, Daejeon 34141, Republic of Korea
[2]Spin Convergence Research Team, Korea Research Institute of Standards and Science,
Daejeon 34113, Republic of Korea

A phased array antenna is a phase-controlled system of antennas which work together as a single antenna. The phased array antenna is widely used in military radar applications which require a highly-directional micro/millimeter electromagnetic waves. A spin wave is a propagating collective excitations of electron spins in magnetic materials. In the rising field of "magnonics", the manipulation of the spin wave is an important issue, because the spin wave can be utilized as an information carrier. Here we apply the concept of the phased array antenna to the spin wave, to generate highly-directional spin wave. To this end, we perform the micromagnetic simulations using OOMMF simulator. We find that the phase-controlled spin wave array source can generate a spin wave in any direction over a wide angle, without physically changing the system. Furthermore, the phased spin wave array enables to focus the spin wave in a specific position with enhanced amplitude. Our work therefore suggests that the idea of phased array antenna can be readily applied to the magnetic systems, providing an efficiency way to control the spin wave, which could be an important step towards the magnon-based spintronic applications.

Abnormal anti-crossing effect in photon-magnon coupled system

Biswanath Bhoi*, Bosung Kim, Seung-Hun Jang, Junhoe Kim,
Jaehak Yang, Young-Jun Cho, and Sang-Koog Kim†
National Creative Research Initiative Center for Spin Dynamics and Spin-Wave Devices, Nanospinics Laboratory,
Research Institute of Advanced Materials, Department of Materials Science and Engineering,
Seoul National University, Seoul 151-744, South Korea

Understanding and exploiting the interactions of excited modes in hybrid quantum systems are the keys to achieve the ambitious goal of quantum information processing [1-2]. Therefore, collectively excited modes (i.e., magnons) in ferromagnets, being coupled to elementary excitations of electromagnetic waves (photons), have increasingly been studied in a variety of hybrid structures of two or more different systems [3-5]. The interaction (coupling) between the magnon and photon modes usually demonstrated by showing the modes' splitting near their common resonant frequency within the so-called anti-crossing region or the level repulsion, as described well by a classical model for coupled oscillators [4] and also by a two-level quantum model [5].

Recently a new phenomenon of quantum back-action evading (QBAE) [6] whereby a positive-energy mode is coherently coupled to a negative-energy one (which is equivalent to oscillators with negative mass) has theoretically been predicted. Strikingly, if one mode has a negative energy (mass), the eigenfrequencies of the coupled modes become complex and such an anti-crossing effect, thus, becomes unstable [7-8]. Consequently, the eigenstates of the systems are out-of-phase to each other and the corresponding real components of the eigenfrequencies pull towards each other to meet at two points called the exceptional points [7-8]. This behavior is known as level attraction or anti-phase anti-crossing of coupled modes. In fact, such a concept of negative or complex energy in real space is practically impossible but recently has been discussed within the specific context of quantum optomechanics and demonstrated at a temperature of less than 50 mK using a complicated experimental setup wherein a nano-mechanical oscillator is dispersively coupled to a driven optical cavity [8]. Although Grigoryan et al. [9] presented a theoretical framework for observation of such anti-phase anti-crossing effect in a spin-photon system, this phenomenon has not yet been found experimentally.

In this work, we report the first convincing experimental demonstration of the abnormal anti-phase anti-crossing phenomenon in a photon-magnon-coupled real system that consists of an inverted pattern of split-ring resonator (hereafter noted as ISRR) and a Yttrium Iron Garnet (YIG) film in a planar geometry. The details on the fabrication of the ISRRs and the measurement of photon-magnon coupling were reported in Ref. [4]. It is found that the normal shape of the anti-crossing effect typically observed in photon-magnon coupling is changed to its opposite anti-crossing shape just by changing the orientation of the ISRR's split gap from the perpendicular to the parallel with respect to the microstrip line axis along which ac microwave currents are applied. To quantitatively analyze the similarity and difference of such experimentally observed contrasting behaviors of the normal and abnormal anti-crossing shapes, we made analytical derivations based on fundamental electromagnetic interactions (Faraday's induction and Ampere's circuit laws) between the YIG film and the ISRR, taking into account the orientation of the ISRR's split gap. By combining the RLC and Landau-Lifshitz-Gilbert equations for the ISRR current J and dynamic magnetization m, respectively, we get the following eigenvalue equations as:

$$\begin{pmatrix} \omega-\omega_r+i\alpha\omega & -i\omega_m\left(1+\delta e^{i\varphi}\right)K_A \\ iK_F\omega^2 & \omega^2-\omega_{ISRR}^2+2i\beta\omega\omega_{ISRR} \end{pmatrix}\begin{pmatrix} m^+ \\ J^+ \end{pmatrix}=\begin{pmatrix} 0 \\ 0 \end{pmatrix} \quad (1)$$

where $\omega_r=\gamma\sqrt{H\left(H+\mu_0 M_S\right)}$ and $\omega_m=\gamma M_S$ with saturation magnetization M_s, and gyromagnetic ratio γ. Equation (1) describes the coupling between the YIG's magnon mode (ω_r) and the ISRR's photon mode (ω_{ISRR}), which have an intrinsic damping rate of α and β, respectively. The K_F term arise from Faraday's law which describes the effect of the dynamic magnetization on the rf current in ISRR. The term K_A comes from Ampere's law which shows that the current produces the rf magnetic field, which drives the magnetization in YIG film. Here, the magnetizations in the YIG are influenced by the effective field, which is the sum of two time-dependent rf magnetic fields from the feeding line (h_{line}) and from the ISSR split gap (h_{ISRR}), where ϕ is the phase difference between them, and δ is the ratio between their amplitudes. These two parameters ϕ and δ can be controlled by changing the orientation of the ISRR's split gap with respect to the microstrip line axis. For the case of ISRRs' split gap being perpendicular to the microstrip line, both hline and hISRR are in the equal phase. On the other hand, for the case of ISRRs' split gap being parallel to the microstrip line, both the fields are out of (π) phase.

We derive an analytical expression to estimate the strength of coupling of the ISRR mode to the magnon mode for different types of anti-crossing from the determinant of eq. (1) for which we can define the upper (ω_+) and lower (ω_-) branches is given by

$$\omega_\pm=\frac{1}{2}\left[\left(\omega_r+\omega_{ISRR}\right)\pm\sqrt{\left(\omega_r-\omega_{ISRR}\right)^2+\left(4\pi\Delta\right)^2}\right], \quad (2)$$

where Δ is the net coupling strength as given by $\Delta\equiv\frac{1}{2}\left(\frac{\omega_+-\omega_-}{2\pi}\right)=\frac{1}{2}\left(\frac{g_{eff}}{2\pi}\right)\sqrt{1+\delta\cos\phi}$ with $g_{eff}/2\pi=\sqrt{2K^2\omega_m\omega_{ISRR}}$ and $K^2\cong K_A K_F$. From the fitting of Eq. (2) to the lower and higher frequency branches of the experimental data shown in Fig. 1, we obtained the black-color solid lines with the fitting value of Δ = 90 MHz for both the normal and opposite anti-crossing. The analytical form of Eq. (2) along with the fitting result of Δ = 90 MHz predicts well the experimental results.

The behavior of anti-crossing effect was further investigated by plotting the $|S_{21}|$ power spectra on the ω/ω_{ISRR} - H/H_{cent} plane according to different values of δ and ϕ. The shapes of anti-crossing effect, including the dispersion, linewidth, and net coupling strength of the two coupled modes are remarkably variable and controllable with changing the relative strength and phase of the oscillating magnetic fields generated from both the ISRR's split gap and the microstrip feeding line. The experimentally observed opposite anti-crossing effect and analytically calculated anti-crossing of various dispersion types which fundamentally differs from the typically observed normal anti-crossing demonstrate the potential and great flexibility of photon-magnon systems to explore the unrevealed phenomena of light matter interaction. Furthermore, the orientation of an ISRR's split gap provides a robust means of controlling the damping and anti-crossing effect in a photon-magnon coupling, thereby offering more opportunity for advanced designs of microwave devices. The results are also interesting from the viewpoint of our simple experimental design and analytical derivations which offers a tunable macroscopic quantum platform for exploring the physics of other different coupled systems i.e. magnon-phonon, plasmon-magnon and exciton-photon systems.

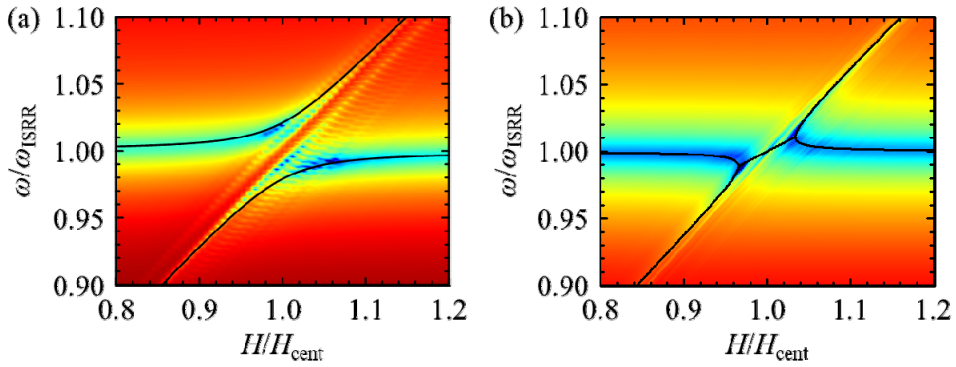

Fig. 1. A sample line graph S21| power on the plane of normalized microwave angular frequency and magnetic field (ω/ω_{ISRR}-H/H_{cent} plane) of ISRR-YIG hybrid for different orientations of ISRR split-gap with respect to microstrip feeding line: (a) case-I: orthogonal; (b) case-II: parallel. The black solid lines in (a) and (b) correspond to fitting results of Eq. 2 to the higher and lower branches.

References

[1] H. J. Kimble, Nature, 453, 1023 (2008).

[2] Z. Xiang, S. Ashhab, J. You, and F. Nori, Rev. Mod. Phys., 85, 623 (2013).

[3] L. Bai, M. Harder, Y. P. Chen, X. Fan, J. Q. Xiao, and C.-M. Hu, Phys. Rev. Lett., 114, 227201 (2015).

[4] B. Bhoi, B. Kim, J. Kim, Y-J. Cho, and S-K. Kim, Sci. Rep., 7, 11930 (2017).

[5] M. Harder, L. Bai, C. Match, J. Sirker, and C. M. Hu, Sci. China Phys. Mech. Astron., 59, 117511 (2016).

[6] K. Fang, J. Luo, A. Metelmann, M. H. Matheny, F. Marquardt, A. A. Clerk, and O. Painter, Nat. Phys., 13, 465 (2017).

[7] C. F. Ockeloen-Korppi, E. Damskägg, J-M. Pirkkalainen, A. A. Clerk, M. J. Woolley, and M. A. Sillanpaa, Phys. Rev. Lett., 117, 140401 (2016).

[8] N. R. Bernier, L. D. Toth, A. K. Feofanov, and T. J. Kippenberg, Phys. Rev. A, 98, 023841 (2018).

[9] V. L. Grigoryan, K. Shen, and K. Xia, Phys. Rev. B, 98, 024406 (2018).

Excitation of multiple spin-wave modes in photon-magnon coupled system

Bosung Kim*, Biswanath Bhoi, Jaehak Yang, Seung-Hun Jang, and Sang-Koog Kim
National Creative Research Initiative Center for Spin Dynamics and Spin-Wave Devices, Nanospinics Laboratory,
Research Institute of Advanced Materials, Department of Materials Science and Engineering,
Seoul National University, Seoul 151-744, South Korea

Magnons represent quanta of spin-wave (SW) modes, i.e., collective motions of spins in magnetic ordered systems. SWs in wavelength ranges of micrometer to millimeter scales, which are so called magnetostatic spin-waves (MSWs) [1], can propagate over long distances in low-damping magnets. Owing to their potential applications to logic gates and/or information-signal processing devices, magnonics has been attracting great interests for recent decades. Since the magnonic devices operating under the external static magnetic field include a finite number of waveguides in planar geometries for the propagation of spin-waves [2], investigation of spin-waves for various angle configurations with external magnetic field is necessary to understand, however, the experimental study of SWs has been still difficult because of their low intensity and fast decay, especially in high order mode [3]. Therefore, the search for an alternative method to excite and probe higher order SW modes should be introduced. On the other hand, in hybrid systems of an inverted split-ring resonator (ISRR) and an Yttrium Iron Garnet (YIG) film, a strong coupling between photon and magnon modes show enhanced amplitudes of multiple spin-wave modes in the YIG film around fundamental ferromagnetic resonance (FMR) mode [4]. In particular, higher-order spin-wave modes also showed enhanced signals and very contrasting dispersion characteristics depending on the external magnetic field direction.

In this work, we investigated excitations of multiple spin-wave modes with amplified signals for different external field directions over all the solid angles in an YIG film coupled with an inverted spilt-ring resonator at room temperature. Using magnon-photon coupling, the effective and convenient method to observe multiple spin-wave modes in the YIG film was introduced. Transmission coefficient $|S_{21}|$ spectra for the ISRR-YIG hybrid sample for different angles of applied static magnetic fields were measured by a calibrated two-port vector network analyzer. It is shown that the SW modes were strongly enhanced by the magnon-photon coupling and

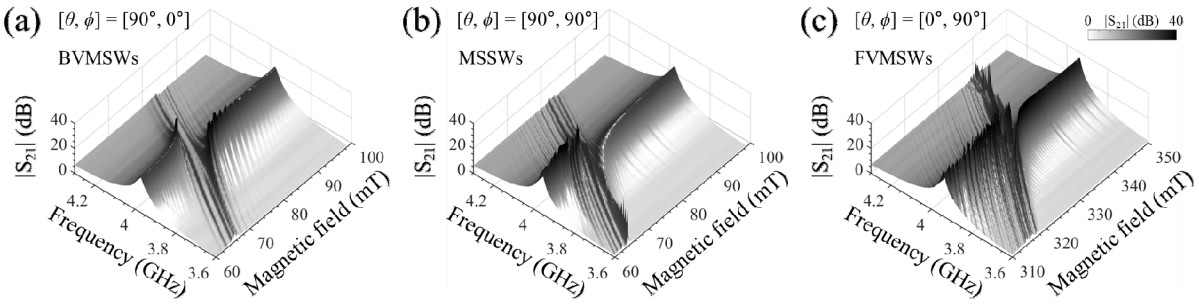

Fig. 1. Transmission coefficient $|S^{21}|$ contour plots on the plane of microwave frequency and magnetic field (f - H) for three different static field directions, as indicated by (Θ, ϕ) = (a) (90°, 0°), (b) (90°, 90°), and (c) (0°, 90°), which angle sets correspond to BVMSW, MSSW, and FVMSW modes, respectively.

their dispersion relation. Also, three types of SW modes, Backward Volume Magnetostatic Waves (BVMSWs), Magnetostatic Surface Waves (MSSWs), and Forward Volume Magnetostatic Waves (FVMSWs) (shown in Fig. 1) as well as the continuous nature of the change from one to another were clearly observed.

From the analysis, it was found that the group velocity of the spin-wave equals to zero at a certain angle, defined as the critical angle. Using the spin-wave dispersion equation [5], experimentally observed critical angles were well explained and the correlation between the critical angle set (θ_c, ϕ_c) was analytically estimated as,

$$\sin\theta_c = \left(H_i / H\right)\left\{2 - \left(1 + \mu_0 M_s / H_i\right)\sin^2\phi_c\right\}^{-0.5} \quad (1)$$

where H is the external static magnetic field, H_i is the vector sum of the effective fields in the YIG film, and $\mu_0 M_s$ is the saturation magnetization of an YIG film. As the magnetic field angle approaches the critical angle the subsidiary peaks of spin-wave modes came close to one single peak and eventually disappeared at the critical angle. It implies that only the uniform precession of the magnetization in the whole volume of the film can be excited at the critical angle, the singularity in the spin-wave spectra.

Our results not only show that magnon-photon coupling can be a powerful tool for investigation of the SWs but also offer fundamental knowledge in operation of the planar quantum computing devices using a magnon-photon coupling. They allow understanding of multiple spin-wave modes excitation for all magnetic field angles and propose a controllability of the number of the multiple magnon-photon coupling channels by changing only the direction of externally applied magnetic fields.

This research was supported by the Basic Science Research Program through the National Research Foundation of Korea (NRF) funded by the Ministry of Science, ICT & Future Planning (NRF-2015R1A2A1A10056286). The Institute of Engineering Research at Seoul National University provided research facilities for this work.

References

[1] J. R. Eshbach and R. W. Damon, Phys. Rev., **118**, 1208 (1960).

[2] Y. K. Fetisov and C. E. Patton, IEEE Trans. Magn., **35**, 1024 (1999).

[3] M. H. Francombe, Thin Film for Advanced Electronic Devices: Advances in Research and Development (Academic Press, 2016).

[4] B. Bhoi, B. Kim, J. Kim, Y.-J. Cho, and S.-K. Kim, Sci. Rep., **7**, 11930 (2017).

[5] B. A. Kalinikos and A. N. Slavin, J. Phys. C: Solid State Phys., **19**, 7013 (1986).

Effect of intermixing on Gilbert damping in Pt/Ni80Fe20/Pt trilayers

Yongsub Kim*, Bosung Kim, Biswanath Bhoi and Sang-Koog Kim
National Creative Research Initiative Center for Spin Dynamics and Spin-Wave Devices, Nanospinics Laboratory,
Research Institute of Advanced Materials, Department of Materials Science and Engineering,
Seoul National University, Seoul 151-744, South Korea

The dynamic properties of magnetization is determined by the Gilbert damping constant α, which plays a crucial role in performance of the spintronic devices. In order to realize high-performance spintronic devices, it demands low Gilbert damping constant even in complex nanostructures with various interfaces. To achieve this goal, it is important to understand of the interfacial effect on magnetization damping. Many studies on FM/NM interfaces composed of different FM and NM materials have been reported. However, most studies assume samples of well-defined sharp interfaces, even though they are rarely ideal, including intermixing and alloying of constituent materials, interface roughness. Therefore, it is necessary to conduct appropriate study on the intermixing effect on the Gilbert damping constant. Although annealing effect on magnetization damping[1] have been studied, understating them in terms of interfacial intermixing is still lacking.

In this work, we investigated intermixing effect on Gilbert damping constant of sputter-grown Pt/Py/Pt trilayer films. In order to make intermixing at both Pt/Py interfaces, we post annealed them in the same vacuum environment for 30 min by varying annealing temperature up to 800 K. We examined the structural change between all the samples by X-ray diffractometry(XRD) and the magnetic properties using VSM measurement; and then the Gilbert damping constant was obtained by VNA-FMR technique. According to the VNA-FMR results, it was found that α_{eff}= 0.0206 for as-deposited sample and α_{eff}= 0.0932 for the sample annealed at 800 K.

In the annealing temperature range upto 600 K, the Gilbert damping constant is nearly unchanged from 0.0206 to 0.0212. This can be explained by the competition between spin pumping effect and the sharp interface effect on Gilbert damping constant. Above 600 K annealing temperature, the Gilbert damping constant begin to increase and it shows a drastic increase from 0.0329 to 0.0932 in the annealing temperature range of 700 - 800 K. Such an increase in the Gilbert damping constant can be accounted for intermixing, the stoichiometric compound and non-magnetic dead layer formation at the interface. The XRD reveals that the crystallinity of the interface increase upto 600 K annealing temperature, however, shows an increase the roughness of the interface and degradation of the crystallinity and texture of Pt phase above 600 K annealing temperature. In addition, formation of stoichiometric compound between Py and Pt and the structural transformation from the ordered-L12-FCC to disordered-A1-FCC[2] were observed above 700 K annealing temperature. Furthermore, the calculated average diffusion length[3,4] of each atoms provides a consistent tendency with the structural change from XRD.

This research establishes that the intermixing effect on Gilbert damping, thereby allowing for understanding of the interfacial effect and give an insight to the optimization of a complex multilayed spintronic devices with low damping constant with various interfaces.

References

[1] A. Conca and B. Hillerbrands, Appl. Phys. Lett., 104, 182407 (2014)
[2] I.V. Vernyhora and S. M. Bokoch, ISRN Thermodynamics, 2012, 917836 (2012)
[3] V.D. Divya and A. Paul, J. Mater. Res., 26, 18, 2384-2393 (2011)
[4] T. Kaiser and W. Jäger, J. Appl. Phys., 103, 063913 (2008)

Atomistic model study of resonant frequency of ferrimagnetic GdFeCo nanoparticles across the compensation points

Jaegun Sim*, Jae-Hyeok Lee, and Sang-Koog Kim
National Creative Research Initiative Center for Spin Dynamics and Spin-Wave Devices, Nanospinics Laboratory,
Research Institute of Advanced Materials, Department of Materials Science and Engineering,
Seoul National University, Seoul 151-744, South Korea

A central motivation for antiferromagnetic spintronics is the expectation that antiferromagnetic spin dynamics are much faster than their ferromagnetic counterpart[1] and that the antiferromagnet has no magnetic stray field, which properties are beneficial for integrated circuits due to the fact that the stray field is the primary source of detrimental magnetic perturbations.[2] However, for realization of such magnetic memory devices in the future, it is necessary to understand the intrinsic mechanism of the dynamics. The fast dynamics of the antiferromagnet also are observed in the ferrimagnet, which fact is very helpful for understanding antiferromagnetism, owing to its ease of measurement.[3] Ferrimagnetic GdFeCo[4] material is one of the robust model systems for the study of the ferrimagnetic resonance (FMR) dynamic modes as a function of Gd atomic content across the magnetization and angular momentum compensation points. The experimental observations of FMR near both compensation points are not consistent with the theoretical predictions.[5]

Here, as further work, we calculated the temperature dependence of sublattice magnetizations and resonant magnetization dynamics over a given Gd-concentration range (0-48%) [6]. In this calculation, we used the VAMPIRE software package, which uses a simple text file format to define and run an atomistic simulation [7]. The magnetization directions of FeCo and Gd are opposite to each other, and therefore they exhibit antiferromagnetic coupling between the sublattices. The magnetization(T_M) and angular momentum(T_A) compensation points exist within a Gd-concentration range of 24-44% and increase linearly with that concentration [8]. According to the literature,[9-11] g_{FeCo}(~2.2) is slightly larger than g_{Gd}(~2), owing to the spin-orbit coupling of FeCo and the zero orbital angular momentum of the half-filled 4f shell of Gd. T_A is expected to be higher than T_M in GdFeCo. We confirmed that the correlation of the resonance frequency of magnetization dynamics is a function of the sublattice composition and thermal fluctuations. We also confirmed that atomistic simulations of magnetic materials are useful for understanding the mechanism of the fast dynamics of the ferrimagnet and their applications to other systems.

References

[1] F. Keffer, C. Kittel, Phys. Rev. 85, 329 (1952).
[2] T. Shiino, S. H. Oh, P. M. Haney, S. W. Lee, G. Go, B. G. Park, and K. J. Lee, Phys. Rev, Lett. 117, 087203 (2016).
[3] S. Kim, Y. Tserkovnyak, Appl. Phys. Lett. 111, 032401 (2017).
[4] K. Vahaplar, A. M. Kalashnikova, A. V. Kimel, D. Hinzke, U. Nowak, R. Chantrell, A. Tsukamoto, A. Itoh, A. Kirilyuk, and Th. Rasing, Phys. Rev. Lett. 103, 117201 (2009).
[5] A. Tuskamoto, T. Sato, S. Toriumi, and A. Itoh, J. Appl. Phys. 109, 07D302 (2011).

[6] T.A. Ostler, R.F.L. Evans, R.W. Chantrell, Phys. rev. B. 84, 024407 (2011).
[7] R.F.L. Evans, W.J. Fan, P. Chureemart, T.A. Ostler, M.O.A. Ellis, R.W. Chantrell, J. Phys.: Condens. Matter 26, 103202 (2014).
[8] P. Hansen, C.Clausen, G.Much, M. Rosenkranz, J. Appl. Phys. 66, 756 (1989).
[9] C. Kittel, Phys. Rev. 76, 743-748 (1949).
[10] G. G. Scott, Rev. Mod. Phys. 347, 102-109 (1962).
[11] B. I. Min and Y. R. Jang, J. Phys. Condens. Matter 3, 5131-5141 (1991).

Spin wave modes and rotational motions of magnetic skyrmion in magnetic nanotubes

Jaehak Yang*, and Sang-Koog Kim

National Creative Research Initiative Center for Spin Dynamics and Spin-Wave Devices, Nanospinics Laboratory, Research Institute of Advanced Materials, Department of Materials Science and Engineering, Seoul National University, Seoul 151-744, South Korea

We study spin wave modes of magnetic skyrmion activated by microwave magnetic fields in low aspect ratio of magnetic nanotubes with radial anisotropy and interfacial Dzyaloshinskii-Moriya exchange interaction. Two peaks of spin wave resonances are found for in-plane ac magnetic field where CCW (CW) gyration mode occurs in low (high) frequency regime. Directions of the circulations are opposite between these two modes: distributions of the out-of-plane spin components near the core circulate CW and CCW direction, respectively. A breathing-type mode is also found for an out-of-plane ac magnetic field based on the skyrmion core. By intensively activating the CCW gyration mode, a spiral rotating motion of magnetic skyrmion is achieved along the circumference of the nanotube. Moreover, we found that the multiple skyrmions can also be dragged by excitation of CCW spin wave modes. This finding provides physical insight into the skyrmion dynamics in the curvature system and would be of use to potential skyrmion-based 3D racetrack memory applications.

References

[1] Fert, A., Cros, V., and Sampaio, J. Skyrmions on the track. Nature Nanotech. **8**, 152 (2013).

[2] Mochizuki, M. Spin-wave modes and their intense excitation effects in skyrmion crystals. Phys. Rev. Lett. **108**, 017601 (2012).

[3] Onose, Y. et al. Obervation of magnetic excitations of skyrmion crystal in a helimagnetic insulator. Phys. Rev. Lett. **109**, 037603 (2012).

[4] Yan, M. et al. Fast domain wall dynamics in magnetic nanotubes, Appl. Phys. Lett. **99**, 122505 (2011).

[5] Pylypovskyi, O. V. et al. Coupling of Chiralities in Spin and Physical Spaces: The Möbius Ring as a Case Study, Phys. Rev. Lett. **114**, 197204 (2015).

[6] Otálora, J. A. et al. Curvature-Induced Asymmetric Spin-Wave Dispersion, Phys. Rev. Lett. **117**, 227203 (2016)

[7] Abert, C. et al. magnum.fe: A micromagnetic finite-element simulation code based on FEniCS. J. Magn. Magn. Mat. **345**, 29-35 (2013)

Spin-wave modes excited in Magnetic domain walls and their application to Magnetic logic operation

Jong-Hyuk Lee*, Jaehak Yang, and Sang-Koog Kim
National Creative Research Initiative Center for Spin Dynamics and Spin-Wave Devices, Nanospinics Laboratory,
Research Institute of Advanced Materials, Department of Materials Science and Engineering,
Seoul National University, Seoul 151-744, South Korea

In the field of magnonics, devices based on spin-wave logic gates are of considerable interest, as the wave character of spin waves holds promise for application to information-processing and high-efficiency computing platforms. In this study, a magnetic logic operation is presented along with an approach by which the spin wave can be propagated in a nano-sized magnonic waveguide. It is shown through micromagnetic simulation that the channeling of the localized spin wave in domain walls is realized in a specific type of nano-magnonic waveguide, which fact allows for the spatial superposition and interference of the confined spin-wave modes. The dynamics of the vortex generated in the proposed structure and the interaction of the spin wave with it are analyzed, and the scattering of the spin wave into the magnonic waveguide is demonstrated. The proposed concept features the utilization of the Damon-Eshbach spin-wave mode in modern wave-based logic devices and suggests a route by which the limitations of the previous approaches can be overcome. The present study not only proposes the operation mechanism underlying a majority gate function encoded in the phase of the transmitted spin waves, but also presents a library of logic gates as a function of amplitude.

Vortex-polarity switching in magnetic-dot arrays by gyration signals and its application to SR latch

Young-Jun Cho* and Sang-Koog Kim
National Creative Research Initiative Center for Spin Dynamics and Spin-Wave Devices, Nanospinics Laboratory,
Research Institute of Advanced Materials, Department of Materials Science and Engineering,
Seoul National University, Seoul 151-744, South Korea
Corresponding author: sangkoog@snu.ac.kr

In recent years, magnetic vortices in geometrically confined magnetic dots have drawn much attention owing to their strong potential applications to information storage and logic devices as well as microwave oscillators [1-5]. Magnetic vortices have unique static spin configurations that are characterized by a clockwise or counter-clockwise curling in-plane magnetization (chirality) around a single core being magnetized perpendicularly either upward or downward (polarity). Especially, they have unique dynamic modes, such as gyration that represents the translational motion of a core in the dot plane around its center position at a characteristic resonance frequency. Vortex-core switching can be accomplished with low power consumption by resonant excitation of the gyration mode. Furthermore, it is known that the core gyration motion can be used as an information signal in coupled vortex arrays.

In the present study, we explored a new way to switch vortex cores controllably by gyration signals in a magnetic-dot network. First, we designed such a device using micromagnetic simulations. We used a Permalloy ($Ni_{81}Fe_{19}$) model system of three dipolar coupled, but physically separated, vortex-state disks of identical diameter D=303nm, thickness t=30nm, and edge-to-edge distance D_{int} = 3nm. The spatial correlation of the dynamic motions of individual cores was extracted from the inverse fast Fourier transformation of each peak of the coupled modes. We found that each disk have different core-gyration velocity, which fact reinforces core-velocity control to achieve the critical core velocity [6]. We could switch vortex cores directly via gyration signals excited from neighboring disks by controlling coupled modes. This makes a magnetic-vortex-state network to operate as a latch device which is a fundamental storage building block of sequential logic. Vortex network latch has non-volatility since vortex core polarities can be maintained at a ground state of either upward or downward. This work paves the way for a non-volatile sequential logic based on magnetic-vortex-state networks and direct gyration signals.

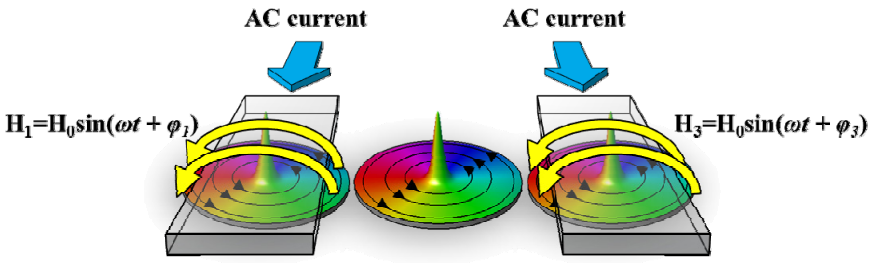

Fig. 1. Schematic illustration of a SR latch device concept. The streamlines and colors of the disks represent the in-plane curling magnetizations, and the height indicates the out-of-plane magnetizations. Gyration signals in the neighboring disks are excited by applied magnetic fields (marked by red arrows).

References

[1] H. Jung, K.-S. Lee, D.-E. Jeong, Y.-S. Choi, Y.-S. Yu, D.-S. Han, A. Vogel, L. Bocklage, G. Meier, M.-Y. Im, P. Fischer, and S.-K. Kim, Sci. Rep. 1, 59 (2011).

[2] S.-K. Kim, K.-S. Lee, Y.-S. Yu, and Y.-S. Choi, Appl. Phys. Lett. 92, 022509 (2008).

[3] S. Sugimoto, Y. Fukuma, S. Kasai, T. Kimura, A. Barman, and Y. Otani, Phys. Rev. Lett. 106, 197203 (2011).

[4] M. Rahm, J. Stahl, and D. Weiss, Appl. Phys. Lett. 87, 182107 (2005).

[5] A. Dussaux, B. Georges, J. Grollier, V. Cros, A. V. Khvalkovskiy, A. Fukushima, M. Konoto, H. Kubota, K. Yakushiji, S. Yuasa, K. A. Zvezdin, K. Ando, and A. Fert, Nat. Commun. 1, 8 (2010).

[6] K.-S. Lee, S.-K. Kim, Y.-S. Yu. Y.-S. Choi, K. Y. Guslienko, H. Jung, and P. Fischer, Phys. Rev. Lett. 101, 267206 (2008).

Motion phenomena and MR properties of magnetic beads and fluorescent magnetic nano-particle clusters embedded in PBS

Byeong-Uk Kang, Sang-Heon Choi, Jong-Gu Choi*, and Sang-Suk Lee
Department of Oriental Biomedical Engineering, Sangji University, Wonju 26339, Korea

The superparamagnetic bead used in this study is a Co-Si-OH structure with a diameter of 1 μm and a volume of 50 mg per ml. Fluorescent magnetic nano-particles are manufactured the SPHEROTM, FCM-0552-2H by Spherotech of Illinois State Lake Forest City, USA. The average diameter of magnetic nano-particles with carboxyl (-COOH) groups is about 460 nm [1]. The scanning electron microscope (SEM) image of the magnetic particles supported by the purchasing company is shown in Fig. 1(a). As shown in the Fig. 1(b), we selected a fluorescent color with a iron (Fe, Iron) in the center, a -COOH beside it, and a nile red one of green, yellow, pink or nile red.

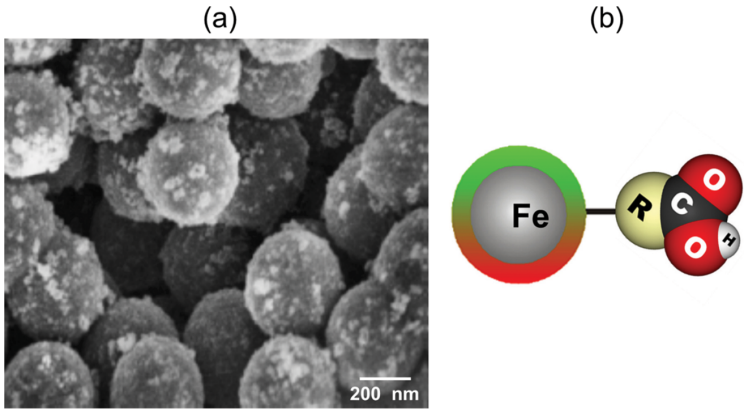

Fig. 1. (a) SEM photo of Spherotech Cat. No. FCMseries (Carboxyl Magnetic Particles, concentration of 0.5 % w/v, mean magnetic nano-particle size of 0.46 μm, total liquid volume of 2 mL, and storage buffer of deionized water with 0.05% sodium azide). (b) Structure of one fluorescent (green, yellow, pink, or nile red color) carboxyl (-COOH) magnetic particle composed of with one high Iron (Fe).

The magnetic particles contained in the 2.5 ml container are maintained at a concentration of 0.5% w/v and stored at room temperature in distilled water containing 0.05% sodium azide as a buffer. These fluorescent magnetic nano-particles are used during biomolecule separation and affinity purification in a wide range of analytical and application fields and contain carboxylic acid groups that can be used for carbodiimide activation (ex: EDC(endocrine disrupting chemicals)) for covalent bonding. It is also coupled to a primary amino group of a nucleic acid, peptide, protein or other target molecule [2-4]. The acrylic plate was processed to make a water tank capable of filling a 20 cc physiological saline solution (PBS). The experimental results show that the magnetic beads and the magnetic nano-particles embedded in PBS were observed with the external magnetic field. The results are shown in Fig. 2(a), 2(b), 2(c), and 2(d). The cluster motion phenomenon showed a distinct

difference according to the change of the external magnetic field. In addition, the magnetoresistance (MR) curves were quantitatively analyzed because the magnetic beads and magnetic nano-particles cluster movements have various characteristics that the MR curve according to the external magnetic field changes sensitively.

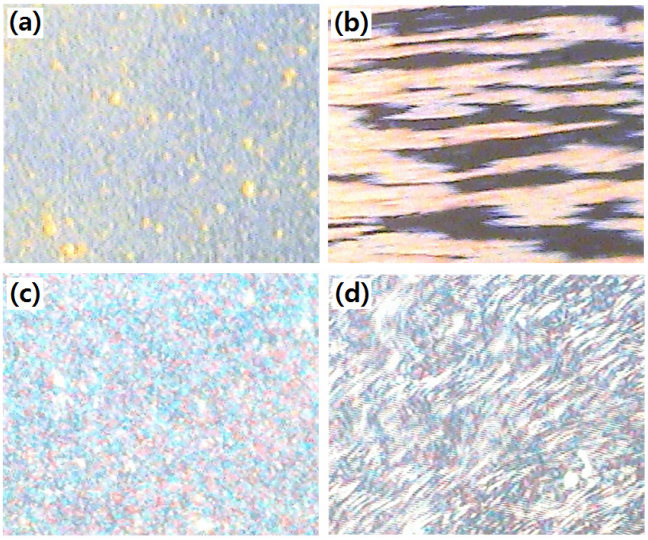

Fig. 2. Optical microscope images of the magnetic beads (a) without and (b) with and the fluorescent magnetic nano-particles (c) without and (d) with an external applied magnetic field.

Acknowledgment: This work was supported by the National Research Foundation of Korea (NRF) funded by the Korea government (Ministry of Education) with the Grant No. of NRF-2016R1D1A1B03936289.

References

[1] J. Y. Shin, S. H. Choi, D. W. Choi, Y. J. An, J. H. Seo, J. G. Choi, and S. S. Lee, J. Korean Magn. Soc. 28, 111 (2018).

[2] Fluorescent Magnetic-Spherotech, http://www.spherotech.com/fluor_mag_par.htm.

[3] SPHEROTM Magnetic Particles, http://www.spherotech.com/new%20downloadable% 20notes/Magnetic% 20Particles%202008-2009.pdf.

[4] P. L. Johansen, F. Fenaroli, L. Evensen, G. Griffiths, and G. Koster, Nature Commun. 7, Article number: 10974, 1 (2016).

Transition on parametric spin wave property of Permalloy nanowire by electric current control

Seong Hwang*, and Beongki Cho†
School of Materials Science and Engineering, Gwangju Institute of Science and Technology (GIST), Gwangju 61005, Republic of Korea

Dependency of parametric property of 30 nm thick Permalloy nanowire on electric current power density was intensively studied by micro-Brillouin light scattering (μ-BLS). Parametric pumping is a nonlinear wave phenomena and one of the promising spin wave exciting techniques having threshold characteristic and high excitation efficiency for spin wave with large wave vector. In experimental structure, we directly measured parametric pumping of main mode and two higher-order modes. Figure 1 show parametric spin wave spectrum for different electric current power. As shown in Fig. 1(b) without electric current, three specific modes were detected, f_0 related to fundamental mode with the lowest threshold microwave power and f_1, f_2 corresponding with Backward-Volume (BV) spin wave and Damon-Eshbach (DE) spin wave mode, respectively. In the presence of electric current, distinct transition of threshold property of each modes was identified in Fig. 1(a) and (c). Especially, f_1 mode have a largest sensitive transition at ± 6 mA. For discussion in this transition, we have used a time-resolved measurement and some calculation process from obtained time domain to extract an ellipticity of each modes for evidence that relation with parametric property and electric current power density.

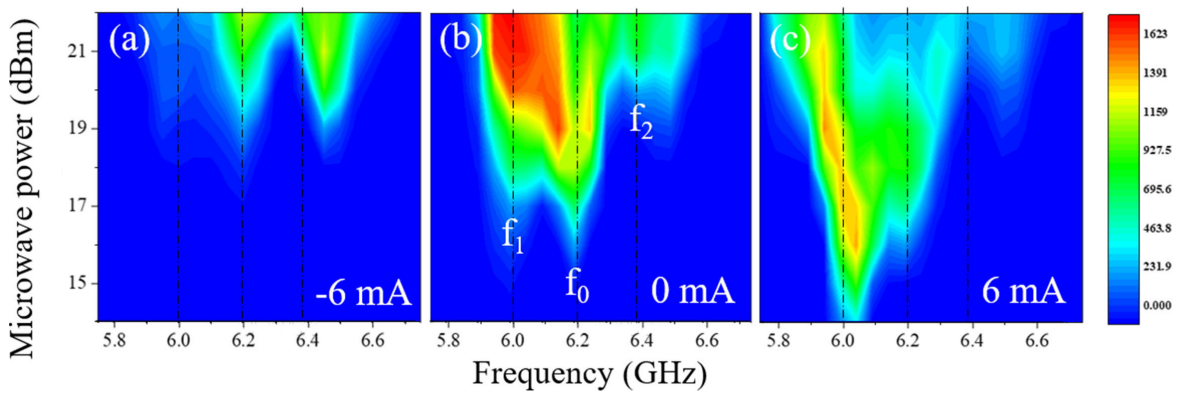

Fig. 1. Parametric spin wave spectrum obtained by μ-BLS in presence of electric current (a) at -6 mA, (b) at 0 mA, and (c) at 6 mA

Magnetic Tunnel Junction as a Stochastic Spiking Neurons with Fokker-Planck Equation

Eunchong Baek*, Purnama Indra, Chun-Yeol You†
Daegu Gyeongbuk Institute of Science and Technology, Korea

As research on the human brain related develops, studies on deep learning in the software field and neuromorphic in the hardware field are actively under way. Neuromorphic technology aims to overcome the disadvantages of modern computing technology using the von Neumann scheme by mimicking the human nervous system at the circuit and device level. The nervous system consists of synapses, which are the connections between neurons and neurons. Neuromorphic technology wants to mimic neurons and synapses at the device level and merge them at the circuit level to create an artificial neural network (ANN). Until recently, studies based on CMOS neurons and memristors synapse have been actively conducted and research on spintronics-based magnetic materials are under way. Both studies are focused on implementing Spiking Neural Networks (SNNs).

Spintronics-based research has been actively pursued in magnetic tunnel junctions (MTJs). Non-volatile features and nonlinear dynamics systems of MTJ are suitable for neurons and synaptic mimics. Furthermore, probabilistic magnetization switching of MTJ is an important feature that can mimic stochastic neurons. Sengupta *et al.* [1] shows the Stochastic Cortical Spiking Neuron imitation using MTJ. This paper assumes the MTJ structure with in-plane magnetic anisotropy and solves the LLG equation for the magnetization of the free layer of MTJ. The additional thermal field was added to explain the stochastic magnetization reversal by thermal noise.

We reproduce the results of [1] using the Fokker-Planck Equation (FPE). FPE is used to understand the effect of thermal fluctuations on the MTJ [2]. We obtained the non-switching probability and the probability distribution of magnetization of free layer with perpendicular magnetic anisotropy. We can compare those results under various conditions like energy barrier or pulse width using FPE. For stochastic spiking neurons, we obtained the switching

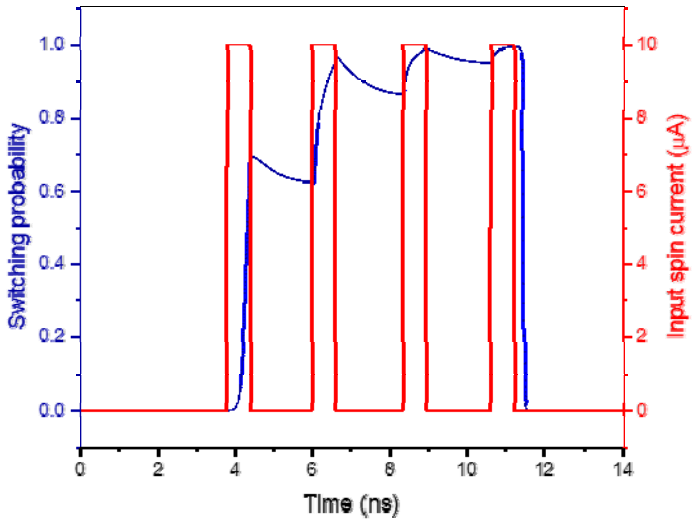

Fig. 1. Switching probability of magnetization of free layer for four input pulses. It increases with the integration of input pulses and starts leaking when pulse is removed.

probability of magnetization for pulse current as shown in Fig 1. Figure 1 shows that the switching probability has the leak and integration components of the biological neuron and refractory period with reset current. We expect these results to be helpful in developing the MTJ for neuromorphic device.

References

[1] A. Sengupta, P. Panda, P. Wijesinghe, Y. Kim, K. Roy, Sci. Rep., vol. 6, Jul. 2016.

[2] W. H. Butler et al., IEEE Trans. MAG 48, 4684 (2012).

Electrical characterization of Magnetic properties of Ultrathin Mn films

Tae Hee Kim[1,2*], Pham Thi Kim Hang[1,2], Do Thi Nga[1,2]

[1]Center for Quantum Nanoscience, Institute for Basic Science, Ewha Womans University, Seoul, 120-750, Korea

[2]Department of Physics, Ewha Womans University, Seoul, 120-750, Korea

Novel concepts using antiferromagnets for spintronic technologies and applications have emerged drastically in order to realize high-speed all-electrical devices [1]. Advantageous properties of antiferromagnets are: they do not generate any stray field, which limits the pack density of ferromagnetic elements, and exhibit intrinsic high frequency dynamics. However, a lot of questions remain to be answered, which trigger magnetic research community to look into fundamental aspects of antiferromagnetism.

Here, we report the surface (interface) microstructure of Mn thin films determined by Atomic Force Microscopy (AFM), and transport properties of 3 nm Pt/x nm Mn (x = 2.5, 5.0 and 8.0 nm) thin films which were successively deposited at room temperature using Ultra High Vacuum-Molecular Beam Epitaxy (UHV-MBE). The Mn thin films with thickness of thicker than 2.5 nm reveal an excellent layer structure toward Frank-van der Merwe growth, while thin film of 2.5 nm thickness shows Volmer-Weber island growth mode with remarkable surface roughness. The impact of the films morphology on electrical and magnetic properties was accessed via resistivity measurements of the Pt upper layer under applied magnetic field. The Néel temperature and noncollinear antiferromagnetic structure at the interface were characterized as the Mn thickness varies. Our results can provide further insight on the nature of the so-called “finite size effects” in magnetism.

Reference

[1] P. Wadley et al., Science 351, 587-590 (2016).

Aging effect of Co/Pd multilayers reduced by proton irradiation

Jeeseung Lim*, Jongill Hong†
Materials Science and Engineering, Yonsei University, Seoul 03722, Korea

Spin device needs a ferromagnet with perpendicular magnetic anisotropy (PMA) which secures high thermal stability for high degree of integration. Interfacial PMA can be easily induced in Co/Pd multilayers by changing the number of a repetition of [Co/Pd] and the individual thickness of elements in Co/Pd layer. In addition, PMA can be enhanced by controlling defect, strain, and roughness at the Co/Pd interface.

We successfully enhanced the PMA of Co/Pd multilayers by low-energy proton irradiation which can selectively remove oxygen atom from Co_3O_4/Pd multilayers. We found changes in electromagnetic properties for the reduced sample as time elapsed. For example, magnetic moment decreased but coercivity increased over time. The tendency of anomalous Hall resistance that changed with time was similar to that of the magnetic moment. To analyze the cause of such an aging effect, following experiments such as re-irradiation of reduced sample that saturated the magnetic moment, hydrogen plasma treatment on metallic Co/Pd multilayer, and the heat treatment on the reduced sample were carried out. In this presentation, we compare electromagnetic properties between reduced and metallic Co/Pd multilayers and discuss the aging effect of the reduced multilayer on the electromagnetic properties.

Magnetocaloric effects of $GdVO_4$ nanopowders

Sung-myung Ryu[1*], Jae-woong Lee[2], Myung-suk Song[2], Beong-Ki Cho[2], and Chunghee Nam[1]
[1]Department of Photonics and Sensors, Hannam Univ., Korea
[2]School of Materials Science and Engineering, GIST, Korea

Steam compression refrigeration technology, which is the most widely used cooling method, has a disadvantage of causing environmental destruction due to the freon gas. It is necessary to study new cooling technology to replace the past cooling technology. In this study, we focused on Magnetocaloric effect (MCE) which is the basis of magnetic refrigeration. $GdVO_4$ was selected from the promising RVO_4 (R = Gd, Ho, Er and Yb) series for cryogenic refrigeration and synthesized using microwave based hydrothermal methods. The synthesized $GdVO_4$ was a nanopowder of ellipsoidal particle size of about 100 nm. The morphological analysis was carried out by SEM and TEM analysis. Crystallinity of fabricated nanopowder was confirmed by XRD, and magnetic properties were confirmed by MPMS analysis. In the $GdVO_4$ nanopowder, the M-T graph shows that AFM to PM magnetic transition occurs at about 2.20 K. The relative cooling power (RCP) was 138.93 J kg^{-1} when the magnetic field was 50 kOe and the maximum magnetic entropy variation was 35.17 J kg^{-1} K^{-1}. The second-order magnetic transition was observed through the Arrot-plot, and the magnetization hysteresis for the change of the magnetic field was hardly confirmed.

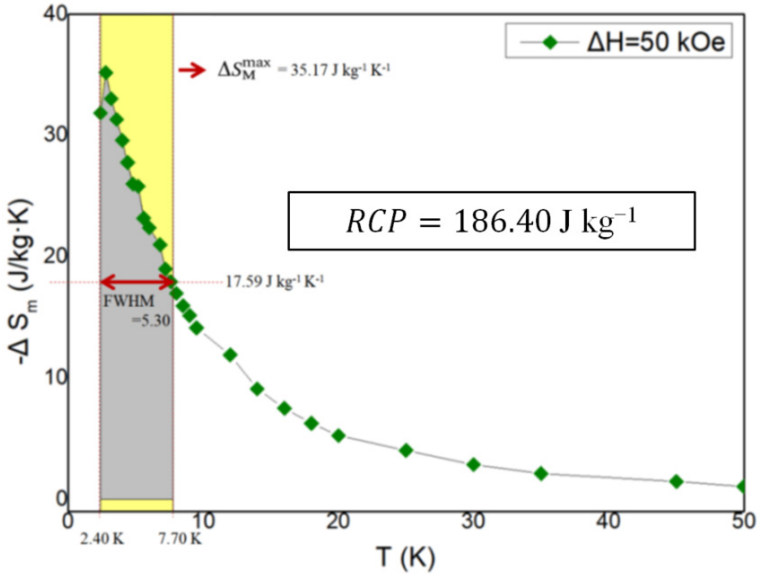

Fig. 1. The magnetic entropy variation of fabricated $GdVO_4$.
The external magnetic field is 50 kOe. The relative cooling power (RCP) can be derived from the product of the maximum magnetic entropy change and the operating temperature range.

Neutron Scattering Method for Fe-based Magnetic Materials

June Hyuk Lee[1*], Youn-Kyoung Baek[2], Jung-Goo Lee[2], Hyungsub Kim[1], Seongsu Lee[1]
[1]Neutron Science Center, Korea Atomic Energy Research Institute, Daejeon, Korea
[2]Powder&Ceramics Division, Korea Institute of Materials Science, Changwon, Korea

Next-generation high-performance magnets are essential components for electric vehicles, robots, wind power plants, and generators. To develop novel magnets without rare earth elements or improve current Nd-Fe-B magnet synthesis processes, neutron scattering method can be utilized by identifying the crystal structure and probing magnetic order in nano- to micro- scale. Neutron exhibits unique magnetic spin and transmission characteristics, and can analyze crystal structure, microstructure and magnetic domains through scattering and diffraction. In this presentation, we will introduce the application of neutron scattering on Fe-based magnet research using HANARO and foreign neutron facilities. Examples of neutron powder diffraction (HRPD), magnetic small angle scattering (SANS), and reflectivity measurement (REF) for bulk and thin film magnets will be presented.

Accuracy of automatic matching of Catphan 504 phantom in cone beam computed tomography for tube current-exposure time product

Dong-heun Kim[1*], Chae-yeon Park[1], Jun-seoug Lim[1], Won-hee Jung[1],
Hee-su Won[2], Man-seok Han[1]

[1]Kangwon National University, Department of Radiology

[2]Bundang Seoul National University Hospital Department of Radiation Oncology

The purpose of this study is to evaluate the accuracy of automatic matching in cone-beam computed tomography (CBCT) images relative to the reduction of total tube current-exposure time product (mAs) for the X-ray imaging (XI) system. The CBCT images were acquired with the Catphan 504 phantom various total mAs ratios such as 1.00, 0.83, 0.67, 0.57, and 0.50. For studying the automatic match-ing accuracy, the phantom images were acquired with a six-dimensional shifting table. The image quality and correction of automatic matching were compared. With a decreasing total mAs ratio, the noise of the images increased and the low-contrast resolution decreased, while the accuracy of the automatic matching did not change. Therefore, this study shows that a change of the total mAs while acquiring CBCT images has no effect on the automatic matching of Catphan 504 phantom in XI system.

For radiation therapy using Tomotherapy, evaluation of usefulness of fixation mechanism that increases patient reproducibility

Hee Young Lee[1*], Sang Hee Park[1], So Yeon Kim[1], Gyu Tae Park[1], Man-Seok Han[1], Jae-Uk Jang[2]

[1]Kangwon National University, Department of Radiology

[2]Chungnam University School Hospital radiotherapy

Background & Purpose : Recently, radiotherapy is a special type made by mixing the concept of ultra-high pressure computed tomography and linear accelerator therapy equipment using computed tomograpy (CT) images for century-regulated radiotherapy such as Tomotherapy Treatment techniques were introduced. Patients receiving Tomotherapy radiotherapy cause postural changes due to prolonged treatment and cause changes in dose distribution. Therefore, in order to minimize radiation therapy errors and long-term movements, and to increase the position reproducibility of the target volume within the patient positioning and irradiation area, development of a patient's fixation device Appropriate use is important. I tried experiments by making aquaplast and vac-lok which are representative fixation mechanisms which are often used frequently, let's examine whether the use of the fixation device is practical clinical

Materials and methods

1. Experiment object

In this study, we surveyed 100 patients with radiotherapy using Tomotherapy from 2015 to 2017. Patient was fixed using vac-lok (30 people) with a fixation mechanism for radiotherapy of the remaining part using aquaplast (70 persons) in the fixation mechanism for radiotherapy of the head and neck of this patient After that, radiation therapy was done.

2. Experimental method

In order to investigate arbitrary changes of patients after radiotherapy, MVCT was performed to fuse images with KVCT. For analysis, we analyzed the three axes on the space, X axis, Y axis, Z axis and measured the value of the Vector on the space to confirm the patient's

Results : Errors due to movement of patients treated with radiation using aquaplast after radiation treatment are confirmed with X axis - 0.507 ± 6.632 mm, Y axis 1.344 ± 8.820 mm, Z axis 3.77 ± 5.920 mm, vector 5.622 ± 6.054 mm It was done. Errors due to motion of patients who had radiotherapy using vac-lok were confirmed with X axis -2.182 ± 3.747 mm, Y axis 0.458 ± 4.450 mm, Z axis 9.104 ± 7.730 mm, vector 11.932 ± 6.250 mm. Conclusion: From the present study, evaluation of the posture reproducibility of the patient by using the fixation mechanism was relatively well measured, but from the aquaplast used for the treatment of the head and neck, treatment of the chest, abdomen and pelvis Vac - lok used for the measurement was measured with relatively large error. Therefore, in treatment using Vac-lok, it is judged that image-guided radiation therapy (IGRT) additionally

Key words: Tomotherapy, CT, aquaplast, vac-lok, vector, IGRT

Detection of Rashba-Edelstein effect in InAs 2DEG using local/non-local geometry

Won Young Choi[1*], Hyung-jun Kim[1], Joonyeon Chang[1], Suk Hee Han[1] and Hyun Cheol Koo[1,2]
[1]Center for Spintronics, Korea Institute of Science and Technology, Seoul, 02792, Korea
[2]KU-KIST Graduate School of Converging Science and Technology, Korea University, Seoul 02841, Korea

Rashba spin-orbit coupling plays an important role not only in a 2-dimensional electron gas structure but also in a ferromagnet / heavy metal bilayer structure. In 2DEG, it is an indispensable element of spin FET fabrication because of spin precession and spin Hall effect. In addition, Rashba spin-orbit coupling is expected to have a great impact on ferromagnet / heavy metal bilayer as well as the conventional bulk spin Hall mechanism. The Rashba-Edelstein effect, on the other hand, causes spin polarization within the channel, resulting in a very large spin signal through potentiometric measurements. And it also has the potential as a spin transistor. In this research, local and non-local characteristics will be discussed through the potentiometric measurement of the Rashba-Edelstein effect.

Magneto-conductance of InAs nanowire tunable by gate-voltage

Jeehoon Jeon[1,2*], Taeyueb Kim[3], Sangsu Kim[1], Sungjung Joo[3], Min Hyeok Jo[4], Jae Cheol Shin[4], Hyun Cheol Koo[2,5], Jinki Hong[1]

[1]Department of Applied Physics, Korea University, Sejong, 30019, Korea
[2]Spin Convergence Research Center, Korea Institute of Science and Technology, Seoul, 02792, Korea
[3]Center of Electricity and Magnetism, Korea Research Institute of Standards and Science, Daejeon, 34113, Korea
[4]Department of Physics, Yeungnam University, Gyeongsan 38541, Korea
[5]KU-KIST Graduate School of Converging Science and Technology, Korea University, Seoul, 02792, Korea

Large magneto-conductance effect on switching device has received considerable attention because of their interesting physical phenomenon and potential applications such as nonvolatile memories, sensors and magneto-logic electronics. Recently, a new type of transistor has been proposed in which electric switching function is manipulated by magnetism instead of electricity. We investigate magneto-transport in an InAs nanowire to utilize as multifunctional nonvolatile logic device. The characteristic feature of our devices comes from magnetic field dependent carrier generation and recombination in non-magnetic semiconductor nanowire. This device shows that the magneto-conductance can be controlled by the transverse electric field by the gate bias voltage. In addition, the device shows abrupt increase of the current as the magnitude of magnetic field decreases. Our device exhibited more than four orders of magneto-conductance change. The huge difference in current values near the threshold magnetic field in the present device can give rise to a large ON/OFF ratio as a switching device. Also, large magneto-conductance effect is controlled by tuning recombination rate in accordance with the magnetic field orientation. It can be show the possibility of application as nonvolatile memory. This novel device can be a good candidate as an electrical switching device controlled by a magnetic field.

References

[1] Magnetic-field-controlled reconfigurable semiconductor logic. Nature, 494, 72-76 (2013)

[2] Large, Tunable Magnetoresisstnace in Nonmagnetic Ⅲ-Ⅴ nanowires. Nano Lett, 15(12), 8026-8031 (2015)

Displacement sensor using mutual inductance of two coils

Hyung-guen Kim*, Kyeong-Won Kim, Kwang-Ho Shin†
Kyungsung University, Korea

Displacement sensors have been used in various areas, and in particular, there has been a demand for development of a displacement sensor having both high precision and high reliability as automobiles are becoming more sophisticated. A common method for measuring displacement is to use an eddy current of a metal, or to use a Hall sensor and a magnet with a suitable magnetic field. However, in the case of an eddy current sensor, the output dependent on displacement is nonlinear, which is more suitable for a displacement switch than a displacement sensor. When a hall sensor is used, it is not suitable to use in a space contaminated with magnetic powder because a magnet generating a large magnetic flux to be used together. In this study, we proposed a displacement sensor composed of two coils of which mutual inductance could be changed by displacement. The coils were connected to capacitors to adjust the resonant frequency. Since the coils were coreless, they have high quality factors. Therefore, high sensitivity could be achieved at near the resonant frequency. Fig. 1 shows the frequency dependence of the output voltage measured.

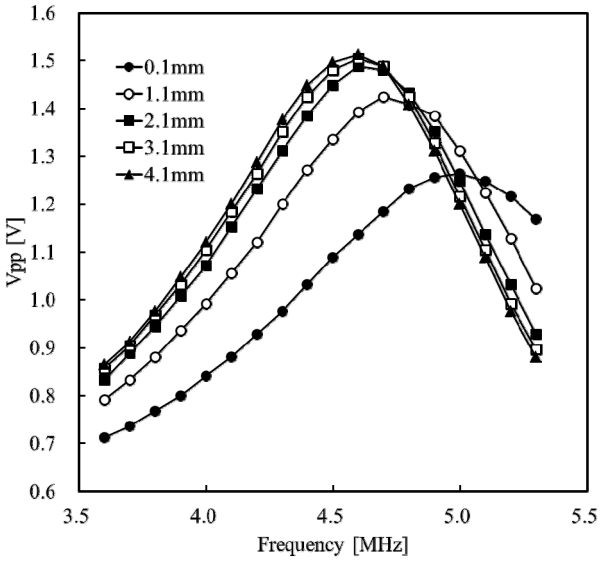

Fig. 1. Frequency dependence of output voltage measured according to distance of two coils. The coils were connected to capacitors to adjust the resonant frequency.

Fabrication and Analysis PHR sensor on flexible substrate

Mijin Kim[1*], Yumin Kang[2], Junil Kim[2], Jaehoon Jeong[2], Geunha Kim[2],
Taehyeong Jeon[1], Cheol Gi Kim[1†]

[1]Department of Emerging Materials Science, DGIST, Daegu, 711-873, Republic of Korea
[2]School of undergraduate studies, DGIST, Daegu, 711-873, Republic of Korea
[†]Email: cgkim@dgist.ac.kr

Flexible devices have garnered significant interest over the past decades, because their application range is not only permitted to electrics, electronics and displays but also expanded to bio-applications in implantable types of devices. In particular, flexible device manufacturing techniques enables their applicability range in mobile devices, biosensors and soft robots which are the core of information and communication technologies. Recently, commercialized products such as flexible, foldable smart phones and TVs are also emerging.

In addition, as the design of these devices is constantly becoming slimmer and also sensors for mobile electronic components becomes more and more vulnerable to warping. In the future, the flexibility of various sensors such as GPS sensor, geomagnetic sensor, acceleration sensor, gyro sensor is expected to be highly demanded.

In this experiment, we have fabricated flexible magnetic sensors using PDMS and Parylene C polymers as substrate instead of Si/SiO_2 mainly because the later being a hard substrate, cannot with-stand external stress. Here, we have also analyzed the performance of flexible magnetic sensors by using the effect on tensile stress due to the curvature of polymer substrates. Furthermore, mechanical and thermal properties were investigated which included measuring stress, reversible bending behavior, and temperature stability. The demonstrated flexible magnetic sensor was fabricated as PHR (Planar Hall Magnetoresistance) sensor which has advantages like higher signal-to-noise ratio, low offset voltage, almost zero hysteresis signal and good linearity. The magnetization behavior of sensors based on external magnetic field and human body temperature variation have been studied here and the magnetic properties of the magnetoresistive sensors were also investigated.

Flexible spin-caloritronic devices

Min-Sun Jang*, Hye-Jin Ok, and Ki-Suk Lee
School of Materials Science and Engineering, Ulsan National Institute of Science and Technology (UNIST), Ulsan 44919, Republic of Korea

Flexible thermoelectric generator (TEG) [1] is a fast-evolving research field in a future sustainable energy technology as well as an internet of things (IoT). One of the prominent candidates for a flexible TEG is a spin Seebeck effect (SSE) device [2] which has a device-design flexibility and scaling capability [3]. Here we proposed a novel method for fabricating substrate-free flexible YIG sheet through the sol-gel synthesis which enables low-cost mass production. Through the optimization of the heat treatments and adding newly-developed mechanical process in a conventional sol-gel synthesis process, we obtained considerable enhancement of the saturation magnetization and the thermoelectric efficiency of flexible YIG sheet compare to them of a polycrystalline YIG sheet [4]. For converting spin to charge current through the inverse spin Hall effect, a gold (Au) electrode was sputtered on the surface of three different YIG sheets. To magnetize YIG sheet along the film surface direction, 400-Oe magnetic field was applied. Temperature gradient was applied perpendicular to the magnetization direction of an YIG sheet and parallel to the flow of spin currents, which is well-known the longitudinal configuration of SSE. In this study, for temperature difference (ΔT) of 40 K, our flexible SSE devices reliably generated thermoelectric voltages as shown in Fig. 1(b). Flexible substrate-free SSE device fabricated by the sol-gel synthesis will pave the way for harnessing spin caloritronic to energy harvesting devices for next-generation smart network devices which related to IoT.

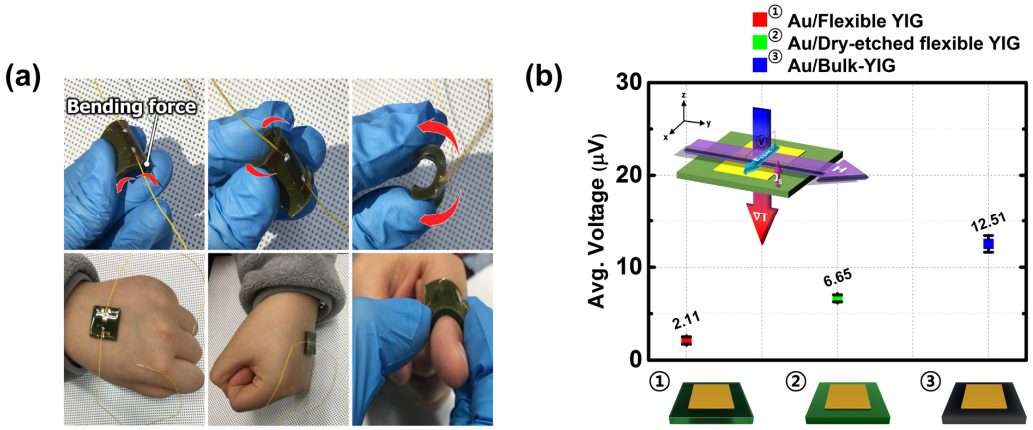

Fig. 1. (a) Bending demonstration of flexible spin-thermoelectric device; Au/Flexible YIG system. (b) thermoelectric voltage measurements of YIG sheets; a flexible YIG, a dry-etched flexible YIG, and a bulk-YIG. Insert schematic shows the LSSE geometry formed 400-Oe H-field is perpendicular to the temperature difference of 40 K and the spin current.

Reference

[1] K. Uchida, et al., Nat. Mat. **9**, 894 (2010). [2] K. Uchida, et al., J. Phys.: Condens. Matter **26**, 343202 (2014). [3] N. B. Ibrahim, et al., J. Magn. Magn. Mater. **220**, 183 (2000). [4] M.-S. Jang, et al., J. Alloys Compd. **711**, 693 (2017).

Hybrid PHE-GMR sensor based on ferromagnetic bilayers

A. D. Talantsev*, A. A. Elzwawy, C. G. Kim
Department of Emerging Materials Science, DGIST, 42988, Daegu, Republic of Korea

Magnetic field sensors, based on planar Hall effect (PHE-sensors), are extensively used for detection of magnetically labeled nanoparticles and biomolecules, because of high linearity of response of these sensors to tiny variations of magnetic field. Giant magnetoresistive sensors (GMR sensors) are of less linearity, but the amplitude of their response is higher. Combining GMR and PHE together in one device looks promising to achieve high linearity and strong signal amplitude, both. In this work we have fabricated PHE cross-junctions, based on NiFe/M/NiFe trilayers, using Ta, Au and Ag as a non-magnetic (M) layer material [**1**]. We have found, that, GMR and PHE components of the sensor's output signal can contribute either oppositely, or additively, dependently on the angle between easy magnetization axis and applied magnetic field. When this angle is 45 degrees and applied magnetic field is within the range, correspondent to reversible magnetization process, the sensor's output is linear to applied magnetic field. When the applied field is larger than the critical field of domain unpinning in sensor's ferromagnetic layers, stepwise change of PHE voltage with magnetic field has been observed. The stepwise PHE response has been compared with an AMR (anisotropic magnetoresistance) response (two-points measurement was

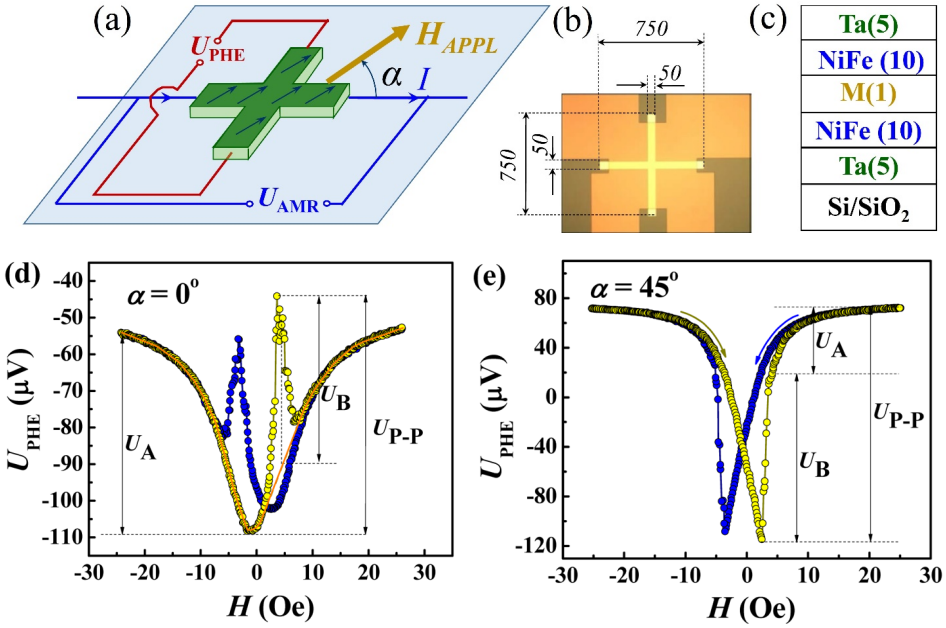

Fig 1. (a) The scheme of connection of the cross-type junction for AMR and PHE measurements; α - angle between applied magnetic field H_{APPL} and current I directions, U_{PHE} - planar Hall voltage response, U_{AMR} - the voltage response to anisotropic magnetoresistance, measured by two-point measurement technique; the arrows on the cross correspond to the magnetization direction. **(b)** The microphotograph of the junction; dimensions are given in microns; **(c)** the layer constitution of the cross-type junction. **(d, e)** Magnetic field dependence of PHE voltage for (d) α = 0° and (e) α = 45° orientations of the applied in-plane magnetic field with respect to the current direction.

used for AMR) in the correspondent field range. The jumps on PHE and AMR were found to be either correlated, on uncorrelated, dependently on the direction on applied magnetic field in respect to cross-junction's easy magnetization axis. Effect of interlayer non-magnetic material on PHE output voltage range has been studied. Among the three materials, Ag, Ta and Au, used as NM spacer in NiFe/NM/NiFe junctions, the use of Au spacer results in best performance of the junction, characterized by highest linearity and lowest magnetic field detection limit. The magnetic field detection limit of the junction with Au spacer is up to 2 times higher than the one for junctions with Ag spacer layers.

Reference

[1] A. Elzwawy, A. Talantsev, and C. Kim, J. Magn. Magn. Mater. **458**, 292 (2018).

Magnetic nanoparticles based portable Microfluidic device for detection of cancer biomarker

K. Krishna Chaitanya Satish Babu*, Sri Ramulu Torati, Yunji Eom, Cheol Gi Kim†
DGIST, Korea
Corresponding author: cgkim@dgist.ac.kr

Early stage of detection is very important to succeed in any cancer treatment [1]. Recently, microfluidic approach makes the miniaturization of bioassay for the early detection of nucleic acids or proteins. Hence, the microfluidic approach can be a suitable candidate for the detection of cancer. The sensitivity will be further increased if we deposit magnetic materials one the sensor's surface.

A miniaturized Magnetic sensor biochip, for the detection of cancer biomarkers was demonstrated [2]. Initially, Fe_3O_4 nano particles were synthesized using wet chemical reduction method [3]. Then, we fabricated microelectrode system on chip by conventional lift-off technique. The microelectrode modified with synthesized Fe_3O_4 Nano particles dispersed in Chitosan polymer solution by drop casting method to enhance the surface area of the electrode, which ultimately increase the sensitivity of the sensor. After that, we integrated the monolithic micro-fabricated valves and micro-channels into the electrochemical microchip [4]. We have immobilized the capture antibodies on the Fe_3O_4 microelectrodes by operating the micro pumps, and the target antigen was flowed over the immobilized receptor molecules, which gives the sensor signal. Electrochemical techniques used to measure every modified steps.

References

[1] S.R. Torati et.al, Sensors and Actuators B: Chemical 2017, 243, 64
[2] Mei Hu et.al, ACS Nano 2010, 4, 488
[3] S H Chaki et.al, Adv. Nat. Sci.: Nanosci. Nanotechnol. 2015, **6,** 035009
[4] David.C. Duffy et.al, Analytical Chem. 1998, 70, 23, 4974

Seed and Capping Layers Effects on Planar Hall Voltage Response and Exchange Bias in NiFe/Au/IrMn Trilayer Structures

Amir Elzwawy[1,2*], Artem Talantsev[1,3] and Cheol Gi Kim[1†]
[1]Daegu Gyeongbuk Institute of Science and Technology (DGIST), Daegu, Republic of Korea
[2]National Research Centre (NRC), Cairo, Egypt
[3]Institute of Problems of Chemical Physics, Moscow, Russia
[†]Corresponding author's email: cgkim@dgist.ac.kr

The Planar Hall effect sensors are promising type of magnetoresistive sensors. Their benefits as enhanced signal to noise ratio (SNR) and low offset as well as high linearity at small field values nominate them to play a crucial role in biosensing and lab-on-a-chip applications. The insertion of non-magnetic layer in the ferromagnetic/antiferromagnetic interface results in an increased sensors sensitivity. Moreover, the introduction of NiFeCr as an underlayer compared to the well-known Ta has a reducing effect on the noise and offset. Based on the Cr content in the NiFeCr alloy, the magnetic behavior can be altered from ferromagnetic, antiferromagnetic to paramagnetic. In the high content over 30% as in our case it was in the paramagnetic state. We revealed the underlayer and capping layer effects on the coercivity (H_C), exchange bias (H_B), and output voltage for (NiFe/Au/IrMn) trilayer structure. The mechanical effects due to scatterings and collisions of atoms during sputtering were evaluated. As for the discussed results, an optimized and adjustable output voltage, field range, noise level, and surface topography can be depicted based on these two layers (i.e. capping and underlayers). The substitution of Ta with NiFeCr in the underlayer case results in 30% enhancement of the exchange bias values, whereas the same substitution for the capping layer gives rise to 3 times of the bias values. We demonstrated the use of Ta as underlayer and NiFeCr as a capping layer in combination with NiFe/Au/IrMn trilayer structure results in better signal to noise ratio and thermal stability [1]. These structures can be integrated on chips to show real on-hands experiments for magnetic nanoparticles detection with high sensitivity, reproducibility and stability.

This work is supported by the grant of Ministry of Trade, Industry and Energy (MOTIE, Korea) grant 10064089.

References

[1] Talantsev, A., Elzwawy, A., Kim, C. (2018). Effect of NiFeCr seed and capping layers on exchange bias and planar Hall voltage response of NiFe/Au/IrMn trilayer structures. Journal of Applied Physics, 123(17), 173902.

[2] Hsu, J. H., Sun, A. C., & Sharma, P. (2013). Lateral grain size effect on exchange bias in polycrystalline NiFe/FeMn bilayer films. Thin Solid Films, 542, 87-90.

Enhancement of the spin Seebeck voltage in a polycrystalline bulk-YIG by controlling microstructure

Min-Sun Jang*, Hye-Jin Ok, and Ki-Suk Lee
School of Materials Science and Engineering, Ulsan National Institute of Science and Technology (UNIST), Ulsan 44919, Republic of Korea

Since the spin Seebeck effect (SSE) has been discovered [1], most of experiments has been performed on a single crystal $Y_3Fe_5O_{12}$ (YIG) fabricated by a pulsed laser deposition (PLD) method [2, 3]. This is because a single crystal YIG has been believed to be able to generate sufficiently high SSE signal [4]. However, this method is known to be very difficult to use in mass-production. In contrast, the sol-gel synthesis can provide a low-cost and mass-production method. Here, we fabricated a bulk-YIG by adopting a sol-gel synthesis and a mechanical pressing process with heat-treatments [5]. To explore the role of the grain in the SSE, the bulk YIG samples with various gran size ranging from 4 to 7 μm were fabricated by manipulating the sintering time as displayed in Fig. 1(a). To measure the longitudinal-SSE (LSSE), a platinum (Pt) electrode was deposited on the bulk-YIG sample by rf sputtering on the surface of disk-shaped YIG with 1.8 mm-thickness and 14 ∅ mm-diameter. By applying 400 Oe magnetic field parallel to the disk plane (+y direction), magnetization in bulk YIG aligned along +y direction. In order to form temperature gradient along -z direction, bottom surface was heated, and top surface was air cooled as shown in Fig. 1(b). Figure 1(c) indicates thermoelectric voltage induced by LSSE versus temperature difference, 40 K between top and bottom surfaces of the bulk YIG. It is evident that the grain size can affect significantly to the thermoelectric voltage. These results can provide the method to enhance the SSE by controlling the microstructure of a polycrystalline bulk-YIG.

References

[1] K. Uchida, et al., Nat. 455, 778 (2008).
[2] N. B. Ibrahim, et al., J. Magn. Magn. Mater. 220, 183 (2000).
[3] A. Sposito, et al., Opt. Express 3, 624 (2013).
[4] Siegel, G., et al., Sci. Rep. 4, 4429 (2014).
[5] M.-S. Jang, et al., J. Alloys Compd. 711, 693 (2017).

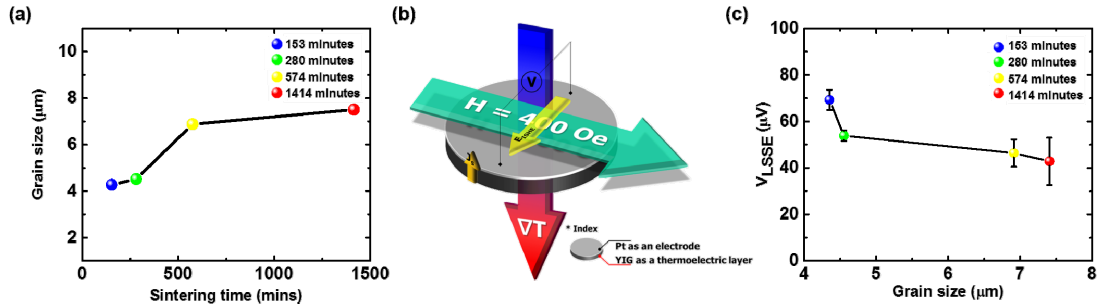

Fig. 1. (a) Grain sizes as a function of the sintering time at; for 153, 280, 574, and 1414 minutes all temperature of 1400 °C. Schematic illustration of the geometry of the longitudinal spin Seebeck effect (LSSE) in a Pt/bulk-YIG structure. The relation is H-field perpendicular to the temperature difference (△T) and the spin current. And the V_{LSSE} as function of the grain size in the (c).

High Resolution Current sensor using Differential Planar Hall Resistance Sensor

Jae Hoon Lee*, Sung Joon Kim, Cheol-Gi Kim
Department of Emerging Materials Science, DGIST, Daegu 42988, Korea

Current technologies that use sensor are used in general areas of variety of industries such as automotive sensors and bio-sensors, and are especially core technologies in industries that use magnetic sensor. Among sensor technology development, technology that uses high density and high resolution has very high value.

Development of high accuracy sensors and high resolution are very important parts of sensor detection areas and signal analysis and are an important part of various fields. Now days, studies are also being conducted to control the effects of interference on external magnetic field interference. Therefore, this study proposed a high accuracy, resolution current sensor using a PHR sensor. In this experiment a differential PHR sensor was fabricated using a DC magnetron sputter. The PHR sensor used the tri-layer structure of Ta/NiFe/Cu/IrMn/Ta. In this experiment, differential current sensor were used to compensate for external magnetic interference, a problem with existing current sensors. In addition, only highly sensitive PHR sensors were used, replacing hall sensors that use magnetic collectors. The designed sensors are designed in chip form through calibration circuits and CMOS processes.

Our Current sensor measures the 1A current level and has a performance bandwidth of 16 kHz and a nonlinear characteristic of less than 0.5%

A study on Electromagnetic-Thermal Interaction Analysis of BLDC Motor applied to EGR Valve System

Su-Jeong Lee[1*], Junyoung Chae[1], Hyo-Sung Choi[1], Ho-Young Kang[1],
Yun-Sang Jeong[2], Jun-Young Jo[2] and Sung-Kun Kim[2]
[1]Eco-friendly Auto part technology institute of Gyeongbuk Technopark, Korea
[2]Seohan Engineering Research Institute, Korea

The Exhaust Gas Recirculation (EGR) system for commercial diesel cars, which is currently in production, is a device for reducing the generation of NOx in the exhaust gas components. The EGR system is a principle of reducing the combustion chamber temperature by recirculating a part of the exhaust gas to the combustion chamber. Also, the EGR system consists of an EGR valve that controls the exhaust gas flow rate, an actuator that drives the valve, and an EGR cooler that cools the exhaust gas. The actuator that controls the EGR valve of a commercial diesel car is a small actuator using a DC motor. Large actuators using BLDC motor are not mass-produced in the domestic, so the whole quantity is imported as well as Electronic Distribution Unit (EDU).

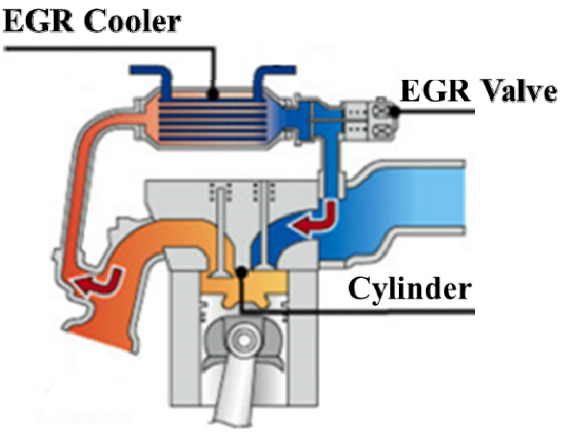

Fig. 1. Components of the EGR System

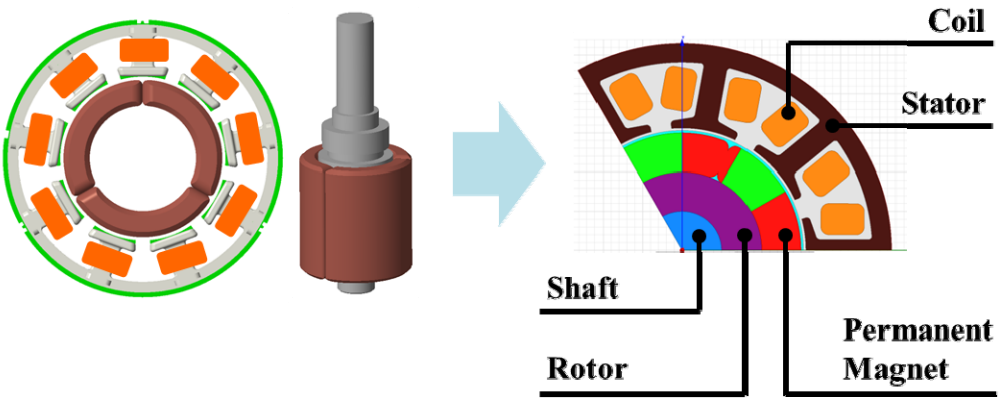

Fig. 2. 3D/2D Model of BLDC Motor

Therefore, we need to develop actuators using BLDC motors with high efficiency and high durability compared to DC motors in order to localize actuators for controlling EGR valves for commercial diesel vehicles. In this study, we designed BLDC motor using electromagnetic analysis software MAXWELL. In addition, in this paper, we visualized the heat generated by the motor and analyzed electromagnetic-thermal interactions based on the final designed motor for mass production in the future.

Acknowledgement. This research is supported by research fund of the Ministry of Trade, Industry, and Energy and Korea Evaluation Institute of Industrial Technology (KEIT) in 2017.
(Development of Actuator for EGR Valve/Turbocharger for Commercial Diesel Vehicles by using BLDC motor, '10076723')

Characterization of Ni-Zn ferrite prepared by sol-gel method

Ji-Eun Yoo*, Young-Min Kang†
Department of Materials Science and Engineering, Korea National University of Transportation, Chungju 27469, Korea

Soft magnetic Ni-Zn spinel ferrites are one of the widely used materials for telecommunication, microwave devices due to their high magnetic permeability and low coercivity, and high resistivity. The Ni-Zn ferrites can be prepared various technologies, such as typical ceramic process, coprecipitation, sol-gel, etc. and their magnetic properties strongly depend on the kind of fabrication methods. In this research, nanoparticles of $Ni_xZn_{1-x}Fe_2O_4$ (x= 0.4, 0.5, 0.6) spinel ferrites were prepared by the sol-gel method. Precursors of $Ni{\cdot}N_2O_6(6H_2O)$, $Zn{\cdot}N_2O_6(6H_2O)$, and $Fe{\cdot}N_3O_9(9H_2O)$ in desired stoichiometric amount were weighed and mixed with citric acid in 1:1 weight ratio by using minimum amount of distilled water to form an aqueous solution. Ammonia (NH_4OH) is added to the solution drop by drop to adjust the PH value 7. The final solution was stirred at 100°C, and dried at 180°C. The dried powders were sintered at 700 °C, 800 °C, 900 °C and 1000 °C for 4 h in air. Single cubic spinel phase were confirmed by X-ray diffraction (XRD) analysis for all the samples. Scanning Electron Microscope (SEM) was used for the study of microstructure. The particle size increases from 69.6nm to 228.2nm with increasing sintering temperature from 700 °C to 1000 °C for the $Ni_{0.5}Zn_{0.5}Fe_2O_4$ sample as shown Fig.1. There was no significant particle size dependence on Ni substitution, x. The magnetic properties of these samples with x = 0.4, 0.5, and 0.6 and the correlation among the properties, structure, and sintering temperature will be discussed.

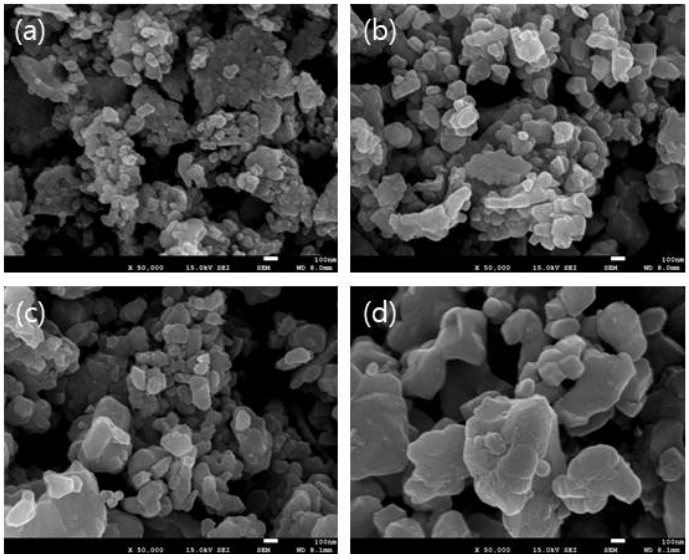

Fig. 1. Micrographs of $Ni_{0.5}Zn_{0.5}Fe_2O_4$ with different sintering temperature of 700°C(a), 800°C(b), 900°C(c) and 1000°C(d)

This work was supported by Korea National University of Transportation in 2018.

EMI Shielding Effectiveness of Sputtered NiFe /Cu Multi-layer Thin Film with High Frequency

Jung Woo Lee[1*], Jong Hwan Park[1], Ho Jun Choi[1], Tae Sung Kim[2], Jae Chul Roh[1], Chan Sei Yoo[3], Ki Hyeon Kim[4], Dae Seok Suh[1], Han Young Jeong[1], Seo Young Chang[3] and Su Jeong Suh[1†]

[1]School of Advanced Materials Science and Engineering, Sungkyunkwan University, Suwon 16419, South Korea

[2]Soution Product & Development, Samsung Electronics,
158 Baebang-ro Baebang-eup Asan si Chungcheongnam-do 31489, South Korea

[3]Korea Electronic Technology Institute, Seongnam-si, 13509 South Korea

[4]Department of Physics, Yeungnam University, 280 Daehak-Ro, Gyeongsan Gyeongbuk, 38541, South korea

We focused on the EMI shielding effectiveness of multi layer thin films, which were composed of Cu/NiFe fabricated on Si wafer (100) by DC magnetron sputtering. Scanning Electron Microscopy (SEM), X-Ray Diffraction (XRD), and Transmittance Electron Microscopy (TEM) revealed the surface morphology and interlayer d spacing (hkl) in the Copper and NiFe materials. In addition, a Vibration Sample Magnetometer (VSM) and Vector Network Analyzer (VNA) confirmed their static magnetic properties and permeability. In order to increase the EMI Shielding effectiveness, we selected copper and NiFe for their conductive properties and high permeability. This paper further studies the shielding effectiveness of a multi-layer structure with respect to laboratory measured EMI, using frequency from 700 MHz to 10 GHz. Multi-layers consisting of the conductive and magnetic material films have the same thickness of 4 um. Our result confirmed that NiFe/Cu multi layer films have thickness better than copper in a high frequency range. Additionally, we further showed that multi layer films in NiFe/Cu with ferromagnetic material and metal improved EMI shielding effectiveness for higher frequency. The result suggests that the multiple reflections and magnetic properties at the internal interfaces of Cu/NiFe/Cu/NiFe layers contribute to an increase of SE(dB).

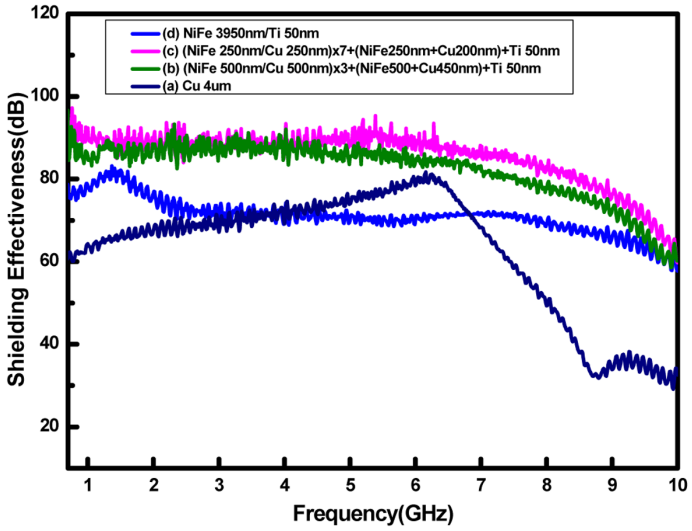

Fig. 1. EMI Shielding effectiveness of (a) Cu, (b) NiFe/Cu 8 layer, (c) NiFe/Cu 16 layer and (d) NiFe film.

Evaluation of microwave complex permeability measurements for magnetic thin films by using a shorted strip line

Wonkyu Jang[1*], Joonsik Lee[2], Ki Hyeon Kim[1]
[1]Department of Physics, Yeungnam University, Gyeongsan, Korea
[2] Composites Research Division, Korea Institute of Materials Science, Changwon, Korea

The complex permeability measurements on microwave range for magnetic thin films have an important role for the applications such as telecommunication devices, magnetic sensors, electromagnetic interference countermeasure and biosensors, etc. The permeability measurement by using coil technique could be obtained a good accuracy and reliability in the MHz frequency range. When the frequency reach higher to the GHz range, the transmission line measurement method have been employed the two-port method by measuring the transmission(S_{21}, S_{12}) and reflection (S_{11}, S_{22}) and the one-port method of the reflection (S_{11}). The permeability textures on microwave range generally employed the 7 mm-coaxial waveguide and rectangular waveguide for measuring the magnetic composites and powder materials. M. Yamaguchi et al. [1] have been developed the thin film premeameter using a side-open TEM cell and a pickup coil. Bekker et. al. [2], Y. Wu et al.[3] and Shigeru Takeda et. al., [4] developed the permeameter by using a shorted strip line. Therefore, we simulated and fabricated the shorted strip line method, which is based on IEC 60556. And it evaluated the permeability by using 228nm-thick CoFeHfO magnetic thin film [5]. The ferromagnetic CoFeHfO thin film was fabricated using sputtering method on Si (100) substrate. The effective permeability was extracted from the S-parameters through the de-embedded process of the shorted strip line by using vector network analyzer (VNA, N5222B, Keysight). The acceptable dimension of specimens for permeability measurement are 8 mm-wide to the magnetic easy direction and thickness of 2 mm. The experimental results show that the permeability is measured with high

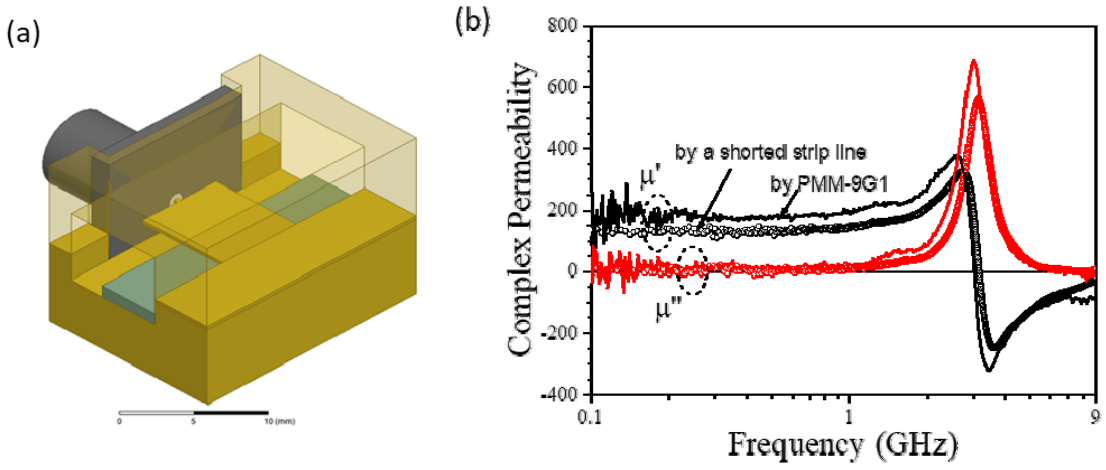

Fig. 1. (a) The schematic of a short-circuited strip line and (b) the measured complex permeability of 228 nm-thick CoFeHfO thin film by a short-circuited strip line in comparison with that of PMM-9G1.

accuracy up to 9 GHz in comparison with that of PMM-9G1 (Ryowa Ltd.). The reason of lower permeability value and higher shifted frequency of ferromagnetic resonance should be resulted from oxidation of film surface, which film has been kept in a desiccator for 10 years.

References

[1] Masahiro Yamaguchi, et al., Trans. Magn. Soc. Jpn., **3(**4), 137 (2003)

[2] V. Bekker, K. Seemann, H. Leiste, J. Magn. Magn. Mater. **270**, 327 (2004)

[3] Y. Wu, et. al., Progress In Electromagnetics Research Letters, **9**, 139 (2009)

[4] Shigeru Takeda, et. al., J. Magn. Magn. Mat. 449 530 (2018)

[5] Dong Young Kim, et. al., IEEE TRANS. MAG, **44**(11), 3115 (2008)

Magnetic properties of $Mn_{2/3-x}Zn_{1/3+x}Fe_2O_4$ spinel ferrites

Eun-Soo Lim[1*], Young-Min Kang[1†], Dong-Young Kim[2]
[1]Department of Materials Science and Engineering, Korea National University of Transportation, Chungju 27469, Republic of Korea
[2]Department of Physics, Andong National University, Andong 36729, Republic of Korea

Mn-Zn spinel ferrites are widely used materials in various electromagnetic devices, such as telecommunication, microwave devices, power transformer because of their high magnetic permeability with low magnetic loss. Electromagnetic devices operating frequency range can be classified based on the complex relative permeability. High μ' and μ"≈ 0 are ideal for applications to magnetic core and magnetic shielding sheet for a wireless charger.

In this research, $Mn_{2/3-x}Zn_{1/3+x}Fe_2O_4$ (x=0.0, 0.1, 0.2, 0.3) spinel ferrites samples were prepared by conventional solid state reaction processes. Stoichiometric quantities of the precursor powders of Fe_2O_3, $SrCO_3$, $MnCO_3$, and ZnO were weighed and ball-milled in water, dried, and pre-calcined in air at 900 °C for 4 h. The calcined powders were grinded, ball-milled again, dried, pelletized to disk and toroidal shapes, and then they are sintered at temperatures of 1300 °C for 2 h both in air and nitrogen atmospheres. X-ray diffraction (XRD) analysis revealed that all the sintered samples have single spinel phase, except for the sample of x = 0 sintered in air, where a small intensity of hematite peak is shown. Magnetic hysteresis curves were measured on the wire-wound toroidal samples by a soft B-H curve tracer. Much higher magnetic flux density and higher permeability values are obtained for the samples sintered in N_2 compared to those samples sintered in air. Highest magnetic flux density is obtained at x = 0 when the samples are sintered in air while it is found at x = 0.1 for the samples sintered in N_2. When x = 0.3, almost no magnetic behaviors are found in both case. Further studies on the microstructure and complex permeability dependence on frequency will be discussed.

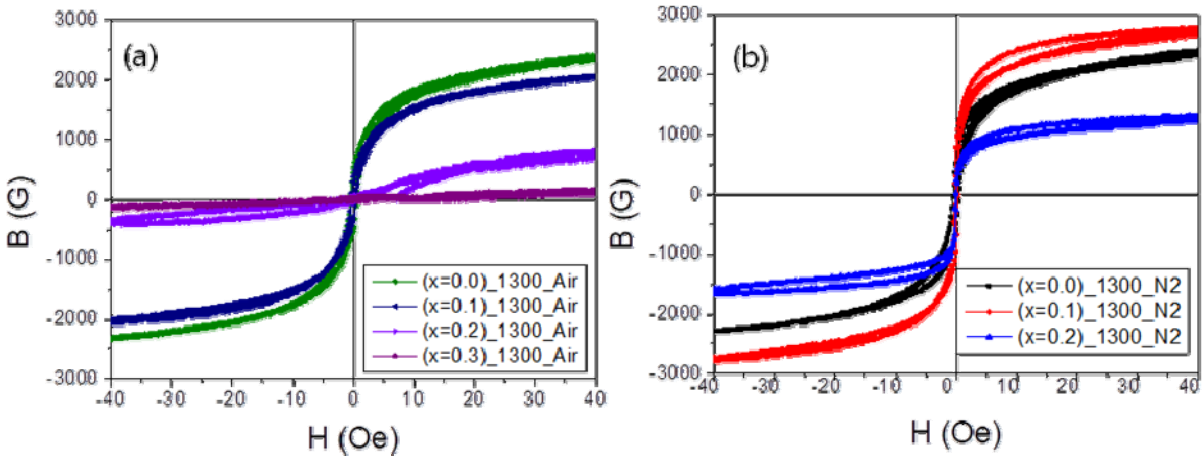

Fig. 1. B-H curves of $Mn_{2/3-x}Zn_{1/3+x}Fe_2O_4$ ferrites sintered at 1300 °C in (a) air and (b) N_2

Size Control of FeCo Nanoparticles and Characterization

Jong-Hwan Park[1*], Chan Park[2], Su-Jeong Suh[1†]
[1]School of Advanced Materials Science and Engineering, Sunkyunkwan University, Korea
[2]Department of Materials Engineering, Pukyong National University, Korea

Many researchers have been interested in FeCo nanoparticles due to the high saturation magnetization, its high permeability and curie temperature. FeCo nanoparticles are used for electromagnetic wave absorbers in high frequency.

However, synthesis of FeCo nanoparticles remains difficulty in term of controlling size. There have been many attempts to synthesize FeCo nanoparticels such as arc discharge, copricipitation, wet chemical synthesis.

Among the synthesis methods, the polyol method has many merits such as uniform particle size, control of compositions and morphology. In the polyol method, synthesis parameters are the molar concentration of metal salts, hydroxyl ion and synthesis temperature, reduction potential of polyol. The purpose of this study was to investigate how particle size affects the magnetic properties of FeCo nanoparticles using the polyol method.

The effect of Al_2O_3 insulation coating on the magnetic properties of Fe powder

Sung Joon Choi*, Sunwoo Lee, and Sang-Im Yoo

Department of Materials Science and Engineering, and Research Institute of Advanced Materials,
Seoul National University, Seoul 151-744, Korea

The soft magnetic composites (SMC) have developed for many applications such as AC and DC electromagnetic devices. It is quite well-known that AC loss of magnetic metal powder can be effectively suppressed by insulation coating due to a reduced macroscopic eddy current loss between metal particles. A thin coating of the insulator on the surface of magnetic metal powder is considered to be highly desirable for high performance SMC especially at high frequency, but reports on this topic are very few so far. In this study, we controlled the coating time to examine the microstructures and magnetic properties of soft magnetic composites (SMCs) with different coating thickness. To evaluate the core loss of samples, the toroidal cores were fabricated by mixing Al_2O_3-coated Fe powder with a resin. The microstructural analysis of Al_2O_3-coated Fe powder was conducted using field emission-scanning electron microscope (FE-SEM) and transmission electron microscope (TEM). The magnetic properties were characterized by performing inductance analysis and B-H curve analyzer. Details will presented for a discussion.

This work was supported by a Grant from world class 300 (0417-20150129).

Characteristics of current transfer dependence of NiO thickness between hybrid high temperature superconductor YBCO thin film and GMR-SV thin film

Woo-Il Yang[1], Byeong-Uk Kang[2], Jong-Gu Choi[2*], Purevdorj Khajidmaa[2], and Sang-Suk Lee[2]
[1]Department of Applied Physics and Electronics, Sangji University, Wonju 26339, Korea
[2]Department of Oriental Biomedical Engineering, Sangji University, Wonju 26339, Korea

An antiferromagnetic NiO based gaint magnetoresistance- spin valve (giant magnetoresistance-spin valve, GMR-SV) multilayer thin film of NiFe/CoFe/Cu/CoFe/NiFe was fabricated on a high temperature superconductor $Y_1Ba_2Cu_3O_{7-x}$ (YBCO) thin film by dc magnetron sputtering. The thickness of YBCO thin film was 300 nm and the thickness of NiO thin film was 5 nm to 50 nm. The characteristics of the magnetoresistance (MR) curves measured at room temperature and at liquid nitrogen temperature (77 K) below the critical temperature of superconductors were compared. The MR curve measured at 77 K for a superconductor-magnetic spin valve hybrid thin film sample showed a MR ratio of -6.0% or less as shown in Fig. 1 was explained by the four terminal method current transfer effect.

The NiO thickness was varied to observe the full current transfer effect because the residual resistance due to the NiO layer thickness was too great below the critical temperature at which the resistance of the YBCO thin film became zero. In order to remove the native oxide layer of the YBCO thin film which increases the residual resistance, the NiO thin film was deposited by rf magnetron sputtering to a thickness of 50 nm at a

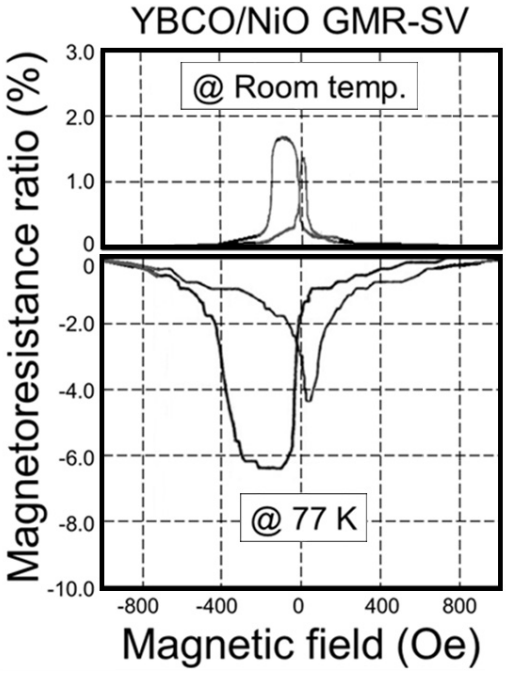

Fig. 1. Normal and inverse magnetoresistance ratios (MR(%)) versus magnetic field curves of MgO/YBCO(20 nm)/NiO(40 nm)/NiFe(5 nm)/Cu(3 nm)/NiFe(6 nm) multilayer (Ref. [1]).

thickness of 5 nm after the dry etching by an electron cyclotron resonance (ECR) Ar ion milling. The internal and residual resistances of the hybrid YBCO/NiO GMR-SV multilayer films changed nonlinearly with increasing sensing current from 1.0 mA to 12.0 mA, but the current increase did not affect the superconductivity at values below the threshold current of YBCO. Negative value MR(%) is due to the existence of NiO layer between GMR-SV multi-layer structure and YBCO thin film because the current path is different in the spin valve effect of the upper layer and the change of negative MR(%) value according to NiO thickness is investigated.

The GMR-SV structure of the YBCO/NiO GMR-SV multi-layer thin film has two states of low resistance $R_{\downarrow\downarrow}$(low) and high resistance $R_{\uparrow\downarrow}$(high) depending on the spin arrangement due to the presence of NiO layer. However, the resistance of the YBCO film is zero, The I-V curve and the residual resistance, which depend on the distance between the four terminals, and the change in MR(%) were evident. The negative MR phenomenon measured below the critical temperature of the YBCO thin film was explained by the current transfer effect of the in-plane thin film tunneling due to the current resistance depending on the thickness of NiO layer.

Acknowledgment: This work was supported by the National Research Foundation of Korea (NRF) funded by the Korea government (Ministry of Education) with the Grant No. of NRF-2016R1D1A1B03936289.

References

[1] S. S. Lee, J. R. Rhee, D. G. Hwang and K. Rhie, J. Magn. **6**, 83 (2001).

[2] W. I. Yang, J. G. Choi and S. S. Lee, New Phys.: Sae Mulli **68**, 950 (2018).

Mössbauer studies of $Ba_{0.5}Sr_{1.5}Ni_2Fe_{12}O_{22}$ Y-type hexaferrite

Jeonghun Kim*, Chul Sung Kim
Department of Physics, Kookmin University, Seoul 02707, Korea

The $Ba_{0.5}Sr_{1.5}Ni_2Fe_{12}O_{22}$ polycrystal sample of Y-type hexaferrite was prepared by polymerizable complex method using $BaCO_3$, $SrCO_3$, $Ni(NO_3)_2{\cdot}6H_2O$, $Fe(NO_3)_3{\cdot}9H_2O$ as the starting materials. The crystalline structure and phase purity of sample were confirmed X-ray diffractometer (XRD) and the measured XRD pattern was analyzed by using Rietveld refinement method with FULLPROF program. The measurements of magnetic properties were measured by using vibrating sample magnetometer (VSM) and Mössbauer spectrometer at various temperature. From the refined XRD pattern, the prepared sample was found to be rhombohedral structure with space group R-3m at room temperature and the lattice constants of sample were a_0 = 5.8306 Å, c_0 = 43.256 Å, V = 1273.45 Å^3. To determine the spin transition temperature (T_S) and Curie temperature (T_C), the temperature dependence of the zero-field-cooled magnetization curve was measured under applied 100 Oe at temperature ranging from 4.2 to 750 K. We determined T_S = 188 K which the spin structure change from the helimagnet to the ferrimagnet, and T_C = 677K which the spin structure changes from ferrimagnet to paramagnet. The Mössbauer spectra were obtained at temperature ranging from 4.2 to 295 K and fitting for six different sublattices ($3b_{VI}$, $18h_{VI}$, $6c_{IV}$, $6c_{IV}$*, $6c_{VI}$, and $3a_{VI}$). The magnetic hyperfine field and the electric quadrupole splitting of sample have shown abrupt changes around T_S.

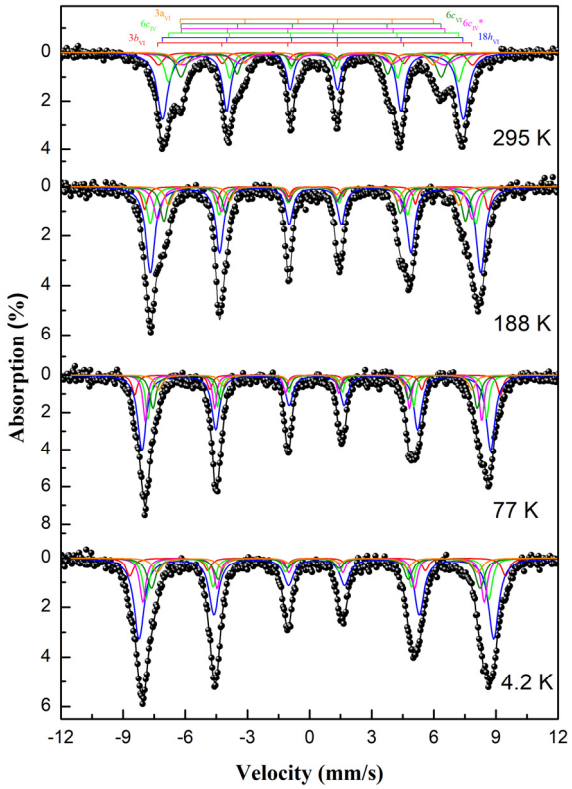

Fig. 1. Mössbauer spectra of $Ba_{0.5}Sr_{1.5}Ni_2Fe_{12}O_{22}$ at various temperatures from 4.2 to 295 K.

Three-dimensional Magnetic Vortex Structure Transformation

Sooseok Lee[1*], Hee-Sung Han[1], Namkyu Kim[1], Mi-Young Im[2], Jung-Il Hong[3], Ki-Suk Lee[1]
[1]Ulsan National Institute of Science and Technology, Korea
[2]Lawrence Berkeley National Laboratory, USA
[3]Daegu Gyeongbuk Institute of Science and Technology, Korea

A flux-closure domain structure such as a magnetic vortex structure is formed from the competition between demagnetization and exchange energies [1]. Such magnetic configuration has been studied in a two-dimensional (2D) structure. However, as increasing the thickness of the sample, a magnetic vortex structure becomes a complicated three dimensional (3D) structure [2, 3] to reduce demagnetization energy along the thickness direction. For example, with increasing aspect ratio, asymmetric Bloch wall (ABW) with Néel cap appears between two shifted vortex cores as shown in Fig. 1. In this system, two types of ABWs can be generated. Depending on the positions of the top and bottom vortex core, the ABW CW and CCW are determined: they are exactly same energy states (degenerate states). In this study, we found that 3D magnetic vortex structure can be formed even in a square disk sample under an external in-plane magnetic field from magnetic transmission soft X-ray microscopy (MTXM) measurements and micromagnetic simulations. A symmetric vortex core structure at the center of disk pattern is shifted along +y direction by applying magnetic field and it abruptly transformed to the ABW structure; top and bottom vortex core structures are separated opposite direction, +x and -x for top and bottom vortex core, respectively. And this separation direction determines the rotation sense of ABW, CCW. In this presentation, we will discuss about the detailed mechanism of 3D vortex structure transition and its related physical significance.

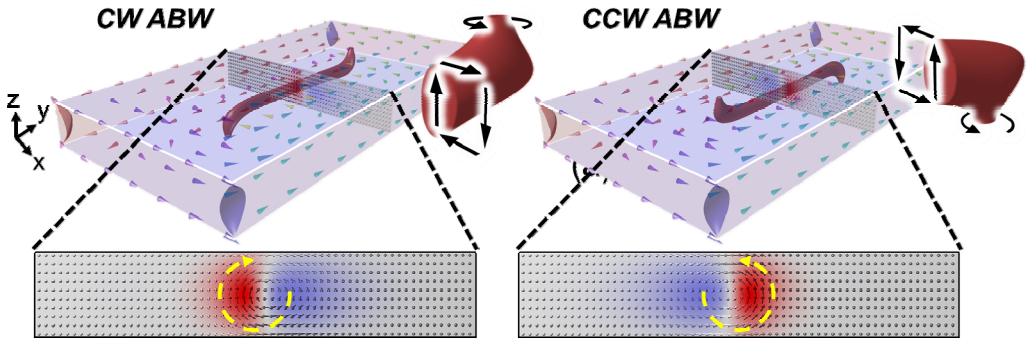

Fig. 1. The simulated images for two degenerate states of the asymmetry Bloch wall (ABW) (top) and their magnetization configuration on the cross section area of the center region (bottom). The red surface indicates the volume where $M_z/M_s > 0.8$.

References

[1] A. Hubert and R, Schäfer. Magnetic Domains. (Springer, Berlin, 1999)
[2] F. Cheynis et al., Phys. Rev. Lett. 102, 107201 (2009)
[3] A. Masseboeuf et al., Phys. Rev. Lett. 104, 127204 (2010)

Magnetic recoverable Z-scheme Au-$CoFe_2O_4$/MoS_2 catalyst for environmental purification of organic pollutants

Yuefa Jia*, Haoxuan Ma, Weiqi Zhu, Chunli Liu†
Department of Physics and Oxide Research Center, Hankuk University of Foreign Studies, Yongin 17035, Republic of Korea
*Corresponding author. E-mail address: chunliliu@hufs.ac.kr (C. Liu)

Spinel ferrite nanomaterials such as $CoFe_2O_4$, $ZnFe_2O_4$, $MnFe_2O_4$, and $NiFe_2O_4$ have been widely studied as photocatalysts due to their narrow band gap and easy availability. Furthermore, the room temperature ferromagnetism also makes it possible to magnetically recollect these photocatalysts. In this study, a magnetic recoverable Au-$CoFe_2O_4$/MoS_2 catalyst was prepared via a sol-gel and hydrothermal route. The photocatalytic performance was investigated by the degradation of methyl orange (MO) under visible light irradiation. Its photocatalytic activity was improved significantly by introducing Au nanoparticles into $CoFe_2O_4$/MoS_2, the photocatalytic performance was improved by nearly 60% in the Au-$CoFe_2O_4$/MoS_2 composite. Physical properties and photocatalytic characterizations suggested the Z-scheme charge transfer mechanism in the Au-$CoFe_2O_4$/MoS_2 composite. The photocatalyst can be recycled easily and showed very stable efficiency in degradation of MO. Because of the high activity and recyclable magnetic separation of the Au-$CoFe_2O_4$/MoS_2 composite, it has a potential application on the oxidation of other organic pollutants in wastewater.

Key words: magnetic, $CoFe_2O_4$, Z-scheme, photocatalyst

Current-Induced Magnetic Switching with Spin-Orbit Torque in an Interlayer Coupled Junction with Ta Spacer Layer

W.-Y. Kwak*, B. K. Cho†

School of Materials Science and Engineering, Gwangju Institute of Science and Technology, Republic of Korea

Manipulation and detection of magnetization in ferromagnetic layers have received continuous attention for the applications to spintronic devices, such as magnetic sensors, magnetic logic devices, and magnetic oscillators. Recently, spin-orbit torque (SOT) was designed to switch magnetization by electric current, as like spin-transfer torque (STT), in heavy metal/ferromagnet bilayers. Spin Hall effect (SHE) of the heavy metal layer generates transverse spin current that is absorbed to an adjacent ferromagnetic layer, resulting in a Slonczewski-like torque (SLT) and field-like torque (FLT). However, the in-plane magnetic field is necessary for deterministic SOT switching to break symmetry in heavy metal/ferromagnetic bilayers with perpendicular magnetic anisotropy (PMA). In terms of application for realistic devices, the external magnetic field should be eliminated because of detrimental effects on neighboring circuits, which becomes more serious as spin-devices goes to higher density.

Here, we showed current-induced magnetization switching using interlayer coupling in Pt/Co/Pt/Ta/CoFe/IrMn structure without an external magnetic field. VSM measurement and anomalous Hall effect measurement with a constant DC current and pulsed current was carried out for magnetic and electrical properties. In the structure of Pt/Co/Pt/Ta/CoFe/IrMn, switching characteristics have been investigated for two cases; CoFe pinned in x and - x direction. No current switching in Pt/Co/Pt structure and opposite switching signs in Pt/Co/Pt/Ta/CoFe/IrMn structures with CoFe pinned along ± x directions demonstrated a crucial role of interlayer coupling in zero-field switching. In addition, the current-induced switching sign of the Co layer was reversed when an in-plane magnetic field of ± 600 Oe was applied in the opposite direction against interlayer coupling, resulting from reversal of the exchange coupled CoFe with the IrMn layer. Through this experiment, it is demonstrated that the ultrathin Ta spacer can be used for robust magnetization switching induced only by current, although Ta is an element to induce the weakest exchange coupling strength in Co/transition metal multi-layers among 3d, 4d and 5d transition metals. Therefore, it is verified that proper material choice for spacer layer with appropriate interlayer coupling strength will give us wide rooms for both enhanced zero-field switching and optimizing junction functionality.

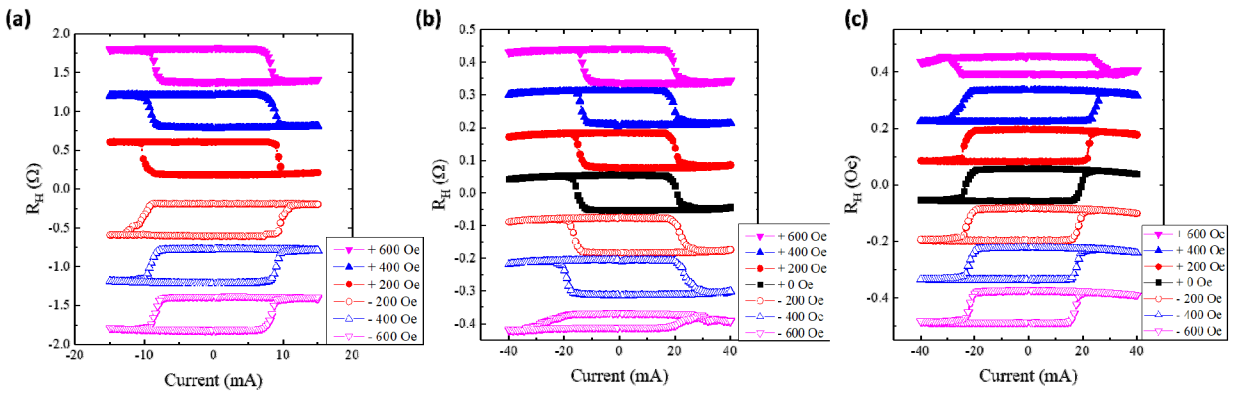

Fig. 1. Current induced magnetization switching of with and without external fields for (a) Pt/Co/Pt structure and Pt/Co/Pt/Ta/CoFe/IrMn structure with CoFe pinned along (b) x direction and along (c) - x direction.

Electrical Spin Injection and Detection in Copper with Perpendicularly Magnetized [CoSiB/Pt] Multilayer Electrodes

Pradeep Raj Sharma[1*], Young Gwang Kim[2], Tae Wan Kim[2], Hwayong Noh[1]
[1]Department of Physics and Astronomy and Graphene Research Institute, Sejong University, Korea
[2]Department of Nano and Advanced Materials Engineering, Sejong University, Korea

We report the spin injection and detection in a diffusive metallic copper with perpendicularly magnetized electrodes made from a $[CoSiB/Pt]_{N=7}$ multilayer film. The spin-dependent signal measured in a four terminal geometry with the application of a perpendicular magnetic field corresponds to 533 μΩ at 80 K and increases to 625 μΩ at 30 K. These values are about 4 times and 100 times larger than those reported with perpendicularly magnetized Co/Ni and Co/Pd multilayer electrodes, respectively [J. Appl. Phys. **116**, 073905 (2014)]. With the application of an in-plane magnetic field, we observed a decrease in the spin-dependent signal and attribute it to the Hanle precession.

Modification of interfacial Dzyaloshinskii-Moriya interaction in Ta/W/CoFeB/MgO films

Taehyun Kim[1*], In Ho Cha[1], Yong Jin Kim[1], Gyu Won Kim[1], A. A. Stashkevich[2], Y. Roussigné[2], M. Belmeguenai[2], S. M. Chérif[2], A.S. Samardak[3] and Young Keun Kim[1]

[1]Department of Materials Science and Engineering, Korea University, Seoul 02841, Korea

[2]Université Paris 13, Sorbonne Paris Cite, 93430 Villetaneuse, France

[3]School of Natural Sciences, Far Eastern Federal University, Vladivostok 690950, Russia

Development of next-generation nonvolatile spin orbit torque magnetic random access memory (SOT-MRAM) is attracting attention due to its potential application for low power and high speed Logic-in-Memory. SOT-MRAM incorporates the magnetic tunnel junction (MTJ) as its basic structure and heavy metal layer under MTJ. The interface between heavy metal (HM) with strong spin-orbit coupling and ferromagnet (FM) is a source of spin-orbit effects including the spin Hall effect (SHE) and interfacial Dzyaloshinskii-Moriya interaction (iDMI). Many research groups are investigating on different combinations of HM/FM by varying its thicknesses and materials to achieve higher performance of SHE and iDMI [1-2]. Research interest to iDMI is due to its assistance to fast domain wall movement and magnetization switching as well as stabilization of spin spirals, chiral domain walls and skyrmions [3]. In this study, we have used a W dusting layer of different thicknesses deposited between HM and FM in order to tune the iDMI energy density in a wide range of possible values.

A DC and RF magnetron sputtering system under base pressure of $5x10^{-9}$ Torr was used to deposit all samples. Each sample underwent annealing at 300°C for 1 h with a magnetic field of 6 kOe under $1x10^{-6}$ Torr. We used Ta, a strong spin orbit coupling material, as HM, $Co_{40}Fe_{40}B_{20}$ with saturation magnetization 1307 emu/cm^3 as FM, which has large tunneling magnetoresistance with MgO tunnel barrier, and Ta as capping layer. We inserted a dusting W layer between Ta and CoFeB to observe the iDMI transformation depending on the thickness of W (t_W) varied from 0 to 1 nm. The thicknesses of FM and MgO layers were fixed to control the other potential effects on iDMI. The magnetic properties were observed using a vibrating sample magnetometer (VSM) and iDMI was measured using Brillouin light scattering (BLS) spectroscopy of non-reciprocal propagation of spin waves in the Damon-Eshbach geometry, where the sample is in-plane magnetized and the wave vector is perpendicular to the magnetization [4]. The shift between the Stokes and anti-Stokes frequencies of the spin waves at a given wavelength is directly proportional to the iDMI value [3].

The Ta(3)/W(t_W)/$Co_{40}Fe_{40}B_{20}$(0.9)/MgO(1)/Ta(2) films have perpendicular magnetic anisotropy (PMA) after 300°C annealing. iDMI value starts to rapidly increase with the growing thickness of W layer. At t_W=1.5 nm we observed the maximum of the iDMI value 0.47 mJ/m^2. Although $Co_{20}Fe_{60}B_{20}$ is known to show stronger iDMI value than $Co_{40}Fe_{40}B_{20}$ does, [5] we found higher DMI value in $Co_{40}Fe_{40}B_{20}$ compared to a previous study that reported iDMI energy density of 0.2 mJ/m^2 in the structure with 2 nm of W, which is an optimum thickness of W exhibiting maximum DMI value, with $Co_{20}Fe_{60}B_{20}$ on top. [6] Our results, however, show that the combination of two different heavy metals can greatly enhance the iDMI value, which implies that further investigation is required.

References

[1] S. Fukami et al., Nat. Mat. **15**, 535 (2016)

[2] A. van den Brink et al., Nat. Comms. **7**, 10854 (2016)

[3] J. Cho et al., Nat. Comms. **6**, 7635 (2015)

[4] J.-H. Moon et al., Phys. Rev. B **88**, 184404 (2013)

[5] S. Jaiswal et al., Appl. Phys. Lett. **111**, 022409 (2017)

[6] A. K. Chaurasiya et al., Sci. Rep. **6**, 32592 (2016)

Annealing temperature and sputtering power dependence of interfacial energies in magnetic heterostructures

Woo-Yeong Kim[1*], Hyung Keun Gweon[1], Sang Ho Lim[1], Kyung-Jin Lee[1,3] and Chun-Yeol You[2]

[1]Department of Materials Science and Engineering, Korea University, Seoul 02841, Korea

[2]Emerging Materials Science, Daegu Gyeongbuk Institute of Science & Technology, Daegu 42988, Korea

[3]KU-KIST Graduate School of Converging Science and Technology, Korea University, Seoul 02841, Korea

Asymmetric exchange interaction at the interface between heavy metal (HM) and ferromagnet (FM) thin films, so called the interfacial Dzyaloshinskii-Moriya Interaction (iDMI) rises in the broken inversion symmetry combined with the large spin-orbit coupling (SOC) [1, 2]. In the presence of iDMI, spin-wave properties become asymmetric with respect to spin-wave propagation direction [3]. In this work, we investigate the correlation of iDMI and perpendicular magnetic anisotropy (PMA) associated with annealing temperature (T_a) by utilizing Brillouin Light Scattering system. PMA samples of Pt(5 nm)/Co(1.4 nm)/MgO(2 nm) and Pt(5 nm)/Co(1.4 nm)/Cu(2 nm) with various T_a are prepared using DC magnetron sputtering system, whereas MgO layer is grown by RF power density, P_{MgO}= 1.10 W/cm^2 and 4.39 W/cm^2. [4]. Here, Cu is chosen to replace MgO owing to its weak SOC and immiscibility with Co. The results are consistent with our previous reports [5, 7]. The total interfacial anisotropy ($K_{i,total}$) is ascent as T_a increases, while iDMI energy density (D) is descent for Pt/Co/MgO samples [5]. Otherwise, both D and $K_{i,total}$ for Pt/Co/Cu film decreases with increasing T_a. Decreasing $K_{i,total}$ can be explained by the intermixing of Pt and Co at the interface [6]. For the detail of the Pt/Co interface, K_i values at each interface ($K_{i,Pt/Co}$ and $K_{i,Co/MgO}$) with P_{MgO} = 1.10 W/cm^2 are obtained. Due to the diffusion of oxygen into both Pt/Co and Co/MgO interface employing high P_{MgO} [4], $K_{i,Pt/Co}$ value is not observed with P_{MgO} = 4.39 W/cm^2. Here, we show the correlation between D and $K_{i,Pt/Co}$ following change of temperature. $K_{i,Pt/Co}$ has the positive correlation in terms of D while there is no meaningful correlation between $K_{i,Co/MgO}$ and D. Note that the SOC originates both iDMI and iPMA at HM/FM interface [5, 7]. Decrease rate of D in the sample with P_{MgO} = 4.39 W/cm^2 is higher than that for sample with P_{MgO} = 1.10 W/cm^2. Details will be discussed.

References

[1] I. E. Dzyaloshinskii, Sov. Phys. JETP 5, 1259 (1957).

[2] T. Moriya, Phys. Rev. 120, 91 (1960).

[3] J. H. Moon, et al. Phys. Rev. B 88, 184404 (2013).

[4] H.-K. Gweon et al. Jpn. J. Appl. Phys. 57, 030301 (2018); H.-K. Gweon et al. Sci. Rep. 8, 1266 (2018).

[5] J. Cho et al. IEEE Trans. Magn. 54, 6, 1-4 (2018)

[6] J. M. Sanchez et al. J. Phys.: Condens. Matter 1, 491 (1989).

[7] N.-H. Kim et al. Appl. Phys. Express 10, 103003 (2017); N.-H. Kim et al. AIP Advance 7, 035213 (2017).

Observation of the anisotropic magnetoresistance in a ferromagnet-topological insulator junction

Sung Jong Kim[1,2*], Youn Ho Park[2], Chaun Jang[2], Andrzej Hruban[3], and Hyun Cheol Koo[1,2]

[1]KU-KIST Graduate School of Converging Science and Technology, Korea University, Seoul, 02481, Korea

[2]Center for Spintronics, Korea Institute of Science and Technology, Seoul 02792, Korea

[3]Institute of Physics Polish Academy of Sciences, 02-668, Warsaw, Poland

Topological insulators have a great attention in the two-dimension material device because it shows a high conductance characteristic and a high spin-momentum locking at the surface. We observed the anisotropic magnetoresistance (AMR) in a ferromagnet-topological insulator hybrid structure. Ca-doped Bi2Se3 is adopted as a topological insulator layer and a permalloy is utilized as a ferromagnetic layer. The lateral size and film thickness of the ferromagnetic electrode are 0.5 μm × 5 μm and 30 nm, respectively. The thickness of Ca-doped Bi2Se3 layer is about 100 nm. The magnetoresistance is measured with an applied magnetic field along the longer axis (x-direction). The AMR is determined by the alignment between the magnetization direction of the ferromagnetic electrode and the bias current direction. The bias current along the x-axis induces strong a spin-orbit interaction and spin-momentum locking along the y-direction at the interface of the ferromagnet-topological insulator. These results in the hybrid structure induced a large AMR of the permalloy compared to that on a single ferromagnetic layer.

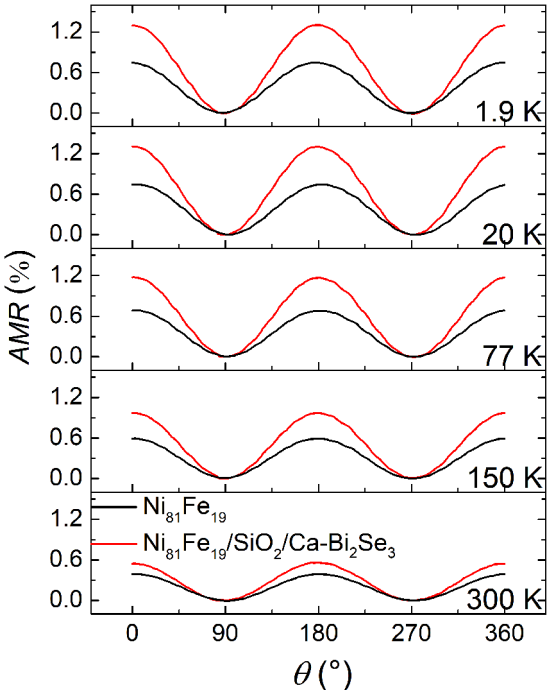

Fig. 1. Angle dependence of the magnetoresistance. Magnetoresistance as a function of the field direction for various temperatures.

Coercivity field control using magnetron sputtering energy

Changjin Yun[1*], Jiho Kim[1], Kungwon Rhie[2], Dongseuk Kim[2], and Chanyong Hwang[2]
[1]Department of Applied Physics, Korea University, Sejong 30019, Republic of Korea
[2]Department of Display and Semiconductor Physics, Korea University, Sejong 30019, Republic of Korea
[3]Quantum Technology Institute, Korea Research Institute of Standards and Science,
Daejeon 34113, Republic of Korea

The multilayer thin films with two structures were fabricated by DC and RF magnetron sputtering with Ar gas at ultra-high vacuum; the base pressure was 3×10^{-8} *torr*.

The first structure is MgO(5 nm)/CoFeB(3 nm)/Pt(5 nm)/MgO(5 nm)/Ta(2 nm) and the other is Pt(5 nm)/CoFeB(3 nm)/MgO(5 nm)/Ta(2 nm).

The conditions used for depositing all the thin films is same, except the working pressure used for depositing Pt film. The working pressure varied from 3 mtorr to 20 mtorr to control the quality of the film via sputtering energy. When the working pressure increased, the roughness of the Pt film also increased at Pt monolayer. From the VSM & TEM data, it was confirmed that the coercivity field is affected by the roughness of the thin film located below the CoFeB film. (in our case is Pt)

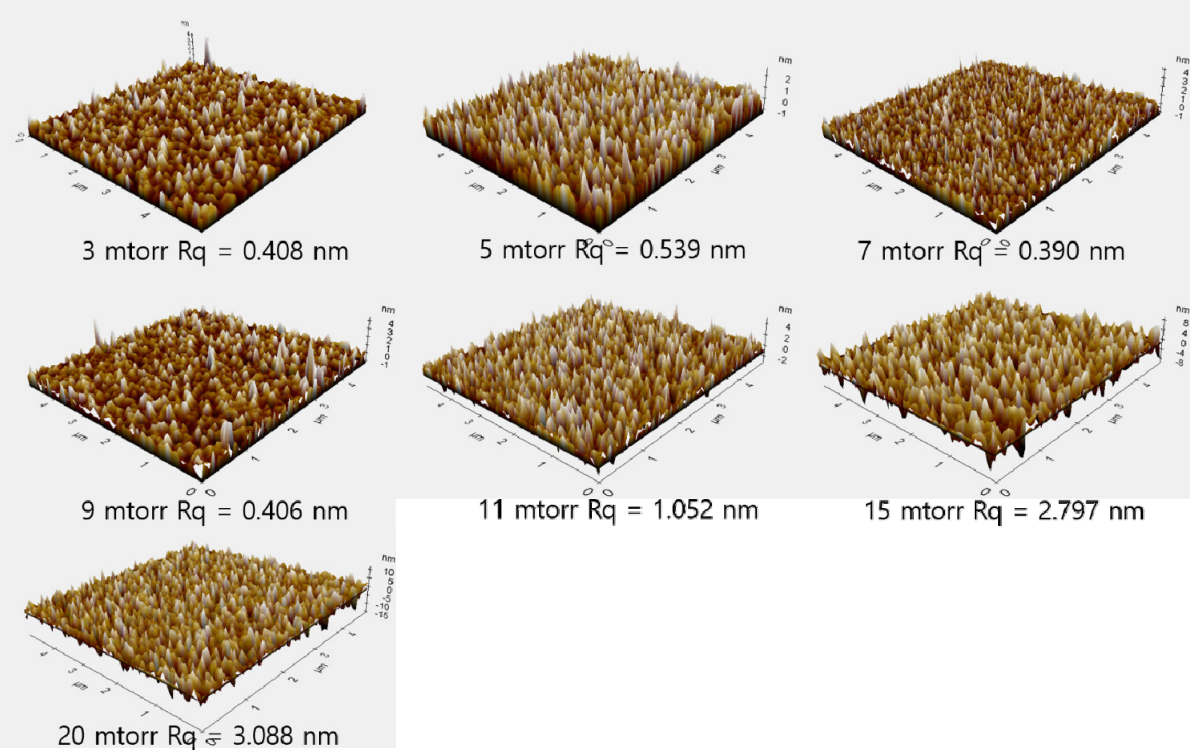

Magnetic properties of $NaFe_{0.9}Mn_{0.1}PO_4$ by Mössbauer spectroscopy

Jae Yeon Seo*, Hyunkyung Choi, Chul Sung Kim
Department of Physics, Kookmin University, Seoul 02707, Republic of Korea

Maricite-type $NaFePO_4$ is promising for use as the cathode in Na-ion batteries because it is advantages of environmental friendliness and low-cost. However, it has low electrochemical conductivity and poor performance than other materials. Mn-based phosphate has higher redox reduction potential than Fe-based phosphate. Therefore, $NaMnPO_4$ can obtain higher potential than $NaFePO_4$. In this paper, we have substituted other transition-metal ions such as Mn ions for Fe sites and investigated the hyperfine electromagnetic interaction of Fe ions. The crystal structure and magnetic properties of the as prepared materials were studied by X-ray diffraction (XRD), vibrating sample magnetometer (VSM), and Mössbauer spectroscopy. The $NaFe_{0.9}Mn_{0.1}PO_4$ sample was prepared using the ball mill method. Structure refinement of $NaFe_{0.9}Mn_{0.1}PO_4$ was analyzed using Fullprof program. The crystal structure of $NaFe_{0.9}Mn_{0.1}PO_4$ sample was found to be orthorhombic with space group of *Pmnb*. Lattice parameters of $NaFe_{0.9}Mn_{0.1}PO_4$ are as follows: a_0 = 6.866 Å, b_0 = 8.988 Å, c_0 = 5.047 Å, and V = 311.544 Å^3. The zero-field-cooled (ZFC) and field-cooled (FC) curves were examined by VSM at 100 Oe from 4.2 to 295 K. The magnetic susceptibility curves showed that antiferromagnetic behavior below Néel temperature (T_N = 14 K). We have investigated the magnetic hyperfine interaction using Mössbauer spectroscopy at various temperatures between 4.2 and 295 K. At 4.2 K, the magnetic hyperfine field (H_{hf}), the electric quadruple splitting (ΔE_Q), and isomer shift (δ) are found to be H_{hf} = 166.09 kOe, ΔE_Q = 2.18 mm/s, and δ = 1.24 mm/s. The room-temperature Mössbauer spectrum showed one-doublet with measured values of ΔE_Q = 2.20 mm/s and δ = 1.08 mm/s. We confirmed that T_N of $NaFe_{0.9}Mn_{0.1}PO_4$ are lower than those of pure $NaFePO_4$ (T_N = 15 K). This is due to the Fe-O-Mn superexchange interaction being lower than that of the Fe-O-Fe link.

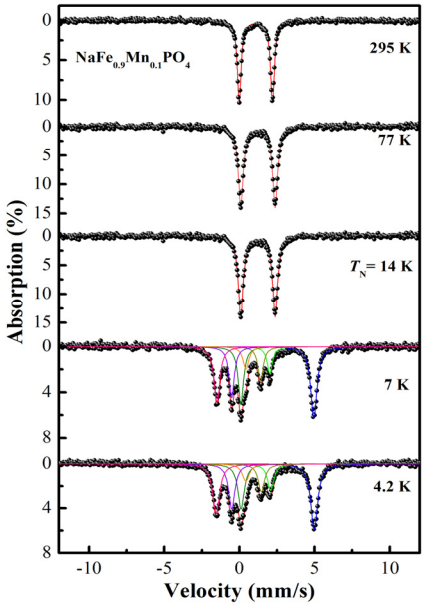

Fig. 1. Mössbauer spectra of $NaFe_{0.9}Mn_{0.1}PO_4$ at various temperature range from 4.2 to 295 K.

Mössbauer studies of ^{57}Fe doped $LiMnPO_4$ by external magnetic field

Hyunkyung Choi*, Chul Sung Kim
Department of Physics, Kookmin University, Korea

Olivine structure LiMPO$_4$ has received much attention because the covalently bonded PO$_4$ groups offer structure stability, excellent thermal, and environmentally friendly. These materials are known for their exceptionally large magnetoelectric (ME) effect. From these complex magnetic structures, LiMnPO$_4$ show the various anomaly effects. Therefore, we have substituted a small amount of ^{57}Fe ions for Mn sites and investigated the hyperfine electromagnetic interaction of Fe ions in crystal symmetry. The crystal and magnetic properties of ^{57}Fe doped LiMnPO$_4$ have been investigated by XRD, VSM, and Mössbauer spectroscopy. The pure Li^{57}Fe$_{0.01}$Mn$_{0.99}$PO$_4$ sample was prepared using the solid-state reaction method. The crystal structure is found to be an orthorhombic (space group: *Pmnb*). The determined lattice constants a_0, b_0, and c_0 are 6.1009 Å, 10.4435 Å, and 4.7427 Å, respectively. The magnetic susceptibility measured by VSM show that Néel temperature is 34 K. Mössbauer spectra of Li^{57}Fe$_{0.01}$Mn$_{0.99}$PO$_4$ have been taken at various temperatures ranging from 4.2 to 295 K. The charge state of the iron ions is ferrous in character by isomer shift. Magnetic hyperfine (H_{hf}) and electric quadrupole splitting (ΔE_Q) at 4.2 K have been studied, yielding the following results; H_{hf} = 320 kOe, ΔE_Q = 2.81 mm/s. We find an abrupt change in ΔE_Q near 8 K due to the spin ordering. Also, Mössbauer spectra under various external fields at 4.2 K were performed parallel to the direction of the gamma-ray emission. From the analysis of Mössbauer spectra, we confirmed that an increase in the canting angle between the applied and H_{hf} due to spin ordering by the strong external field.

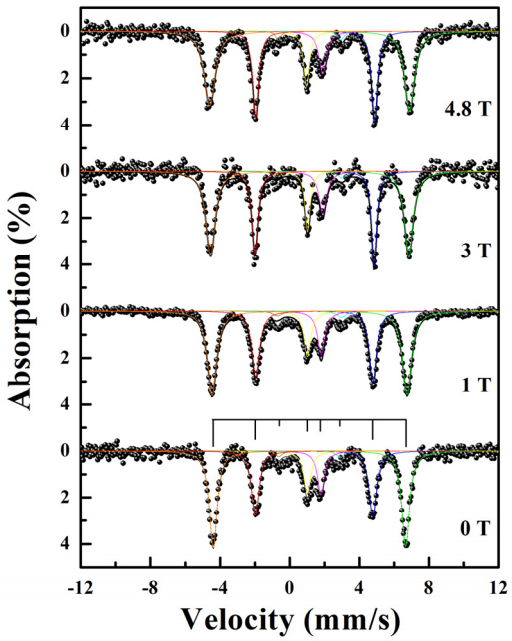

Fig. 1. Mössbauer spectra of Li^{57}Fe$_{0.01}$Mn$_{0.99}$PO$_4$ at 4.2 K under applied fields up to 4.8 T.

Changed Characteristic of Perpendicular Magnetic Anisotropy by Normal Metal

Mingu Kim*, Jiho Kim, Changjin Yun, Jinwon Seo and Kungwon Rhie
Department of Display and Semiconductor Physics, Korea University, Sejong, 30019, Korea

1. Introduction

At general magnetic material, the spin is aligned in the in-plane direction of the sample due to the shape magnetic anisotropy. Otherwise that the spin is aligned in perpendicular to the plane direction is called perpendicular magnetic anisotropy (PMA). The CoFeB / Mgo structure is a typical structure in which perpendicular magnetic anisotropy is appeared due to Oxigen of Mgo and orbital bonding of Co, Fe of CoFeB. [1, 2, 3]. To prevent the external effects, this structure has buffer layer at bottom. The properties of perpendicular magnetic anisotropy are changed by material used for buffer layer.

2. Conclusion and discussion

The structure of samples were buffer layer (2nm)/CoFeB(x)/MgO(2nm). The samples were deposited at ultra-high vacuum chamber with DC magnetron sputtering system and were annealed at 450℃ from 250℃. At M-H graph in case of FeZr used for buffer layer with annealing temperature 400℃, the properties of PMA were appeared when the buffer layer is 0.9nm<t_{CoFeB}<1.8nm. In the case of Ta with annealing temperature 250℃, the properties were appeared when the buffer layer is 1.3nm<t_{CoFeB}<1.5nm. It shows that FeZr has higher thermal stability than Ta because it can be annealed at higher temperature.

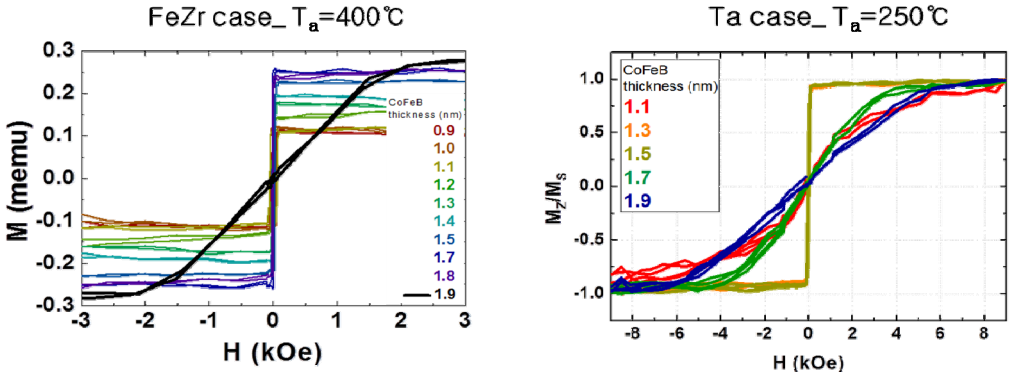

3. Rerferences

[1] Shouzhong Peng, Mengxing Wang, Hongxin Yang, Lang Zeng, Jiang Nan, Jiaqi Zhou, Youguang Zhang, Ali Hallal, Mairbek Chshiev, Kang L. Wang, Qianfan Zhang & Weisheng Zhao, Sci. Rep. 5, Article number: 17169 (2015)

[2] S. Ikeda, K. Miura, H. Yamamoto, K. Mizunuma, H. D. Gan, M. Endo, S. Kanai, J. Hayakawa, F. Matsukura & H. Ohno, Nat. Mat. 9, 721-724 (2010)

[3] Young-Wan Oh, Kyeong-Dong Lee, Jong-Ryul Jeong and Byong-Guk Park, Appl. Phys. 115, 17C724 (2014)

SMR based spin Hall measurement technique for in-plane magnetization

Jiho Kim[1*], Changjin Yun[1], Mingu Kim[1], Dongseuk Kim[2] and Kungwon Rhie[1]
[1]Department of Display and Semiconductor Physics, Korea University, Sejong, 30019, Korea
[2]Center for Nanometrology, Korea Research Institute of Standards and Science, Daejeon, 34113, Korea

Spin Hall angle measurement technique is well developed for heavy metal/ ferromagnet which has perpendicular magmagnetic anisotropy (PMA). However, a DC current based spin Hall angle measurement for in-planeanisotropy (IPA) has not been yet developed. We present a simple spin hall magnetoresistance (SMR) technique that measures spin Hall angle without any worry of artifacts which could be introduced in RF based spin Hall measurement. SMR is measured resistance with applied current and field at perpendicular to current. SMR peak shifts its maximum as applied current is increased, since spin Hall torque is added to the torque induced by transverse field. This shift yields spin Hall angle of heavy metal layer. For a Pt/CoFeB bilayer, we obtained θ_{SH}^{eff} = 0.045, l_s= 2.49 nm, which is a reasonable value.

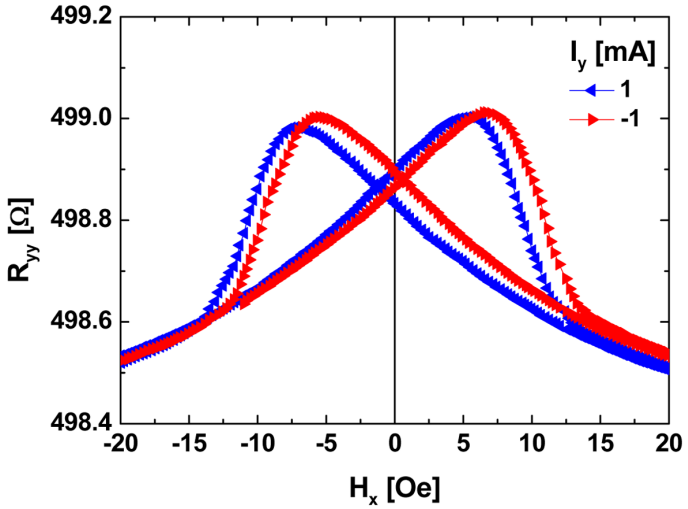

Fig. 1. The R-H curve measured with two direct current flow in the Pt/CoFeB bilayer.

Interface Engineering in Heavy metal/Ferromagnetic Heterostructures for Spin-Orbit Torque

Jungmin Park[1*], Jung-Woo Yoo[2] and Seung-Young Park[1†]

[1]Spin Engineering Physics Team, Division of Scientific Instrumentation, Korea Basic Science Institute, Daejeon, 305-806 Korea

[2]School of Materials Science and Engineering-Low Dimensional Carbon Materials Center, Ulsan National Institute of Science and Technology, Ulsan 44919, Korea

Over the last decade, electrical manipulation of magnetization using spin-orbit torque (SOT) has been a prominent theme in spintronic device because it provides miniaturization of device, low power consumption, and fast reading and writing. For highly efficient SOT memory device, a reduction of magnetization switching current is required. The spin-orbit torque is attributed to arise due to the spin accumulation at the heavy metal (HM) / ferromagnetic (FM) interface. This spin accumulation at the interface exerts the torque on the magnetization of FM. The two main phenomena generating the spin accumulation are the spin Hall effect and interfacial spin-orbit coupling, and SOT efficiency of HM/FM heterostructure strongly depends on the spin memory loss, spin mixing conductance and interfacial spin-orbit scattering of its interface. Therefore, interface engineering of HM/FM heterostructure is important to enhance SOT efficiency with reduction of magnetization switching current.

In this study, we investigate an influence of graphene interlayer in a Pt/(CoFeB, Co or YIG) interface using a FMR (Ferromagnetic resonance) injecting pure spin current into the Pt layer. Here, single, bi-, and triple layers graphene were introduced as interlayers because graphene has weak spin-orbit interaction and long spin diffusion length. The magnetic damping parameter α extracted from the ferromagnetic resonance field and the peak-peak line width obtained by fitting the absorption data. Finally, we will discuss how graphene interlayer affects SOT efficiency and magnetization switching through analyzing anomalous Hall resistance, inverse spin Hall voltage and FMR derivative spectra of Pt/graphene/(CoFeB, Co, or YIG) device.

Asymmetric Hall effect induced by canted state in epitaxial Co/Pt

Jeongchun Ryu[1,2*], Can Onur Avci[3], Makoto Kohda[1,4], Geoffrey S. D. Beach[3] and Junsaku Nitta[1,4]

[1]Department of Materials Science, Tohoku University, Japan

[2]Department of Materials Science and Engineering, KAIST, Daejeon, South Korea

[3]Department of Materials Science and Engineering, MIT, MA USA

[4]Spintronics Research Network, Tohoku University, Japan

[*]email: salsberry@dc.tohoku.ac.jp

Spin orbit torques (SOT) driven by spin Hall and interfacial effects have been broadly investigated to understand the underlying mechanism and to achieve desirable spintronic devices [1]. Recent reports suggest that spin transport and spin dephasing mechanism depend on the crystal structure of the heavy metal [2], therefore one can expect that SOT also shows a dependence on the crystal structure of the heavy metal (HM) layer in HM/ferromagnetic metal structures. In this report, we investigate the harmonic Hall voltage in epitaxial and polycrystal Pt/Co bilayers with perpendicular magnetic anisotropy. We find that an antisymmetric contribution to the Hall effect is present additional to the conventional anomalous and planar Hall effects when Pt is epitaxial. The understanding of this additional signal is crucial in the SOT characterization in epitaxially grown metallic systems.

Perpendicularly magnetized Co on poly crystal Pt (Co/Pt(P)) and epitaxial Pt (Co/Pt(S)) were deposited on MgO (100) and MgO (111) substrates, respectively. The 1st harmonic Hall voltage V_{harm} with an in-plane field sweep is typically driven by the anomalous Hall effect as well as the planar Hall effect (PHE). For Co/Pt(P), V_{harm} behaves symmetric to the sign of the in-plane magnetic field (Fig. (a)) as typically obtained in literature [3]. However, in the case of Co/Pt(S), we could observe a significant antisymmetric component in addition to conventional symmetric signal (Fig. (b)). When we separate V_{harm} into symmetric V_S and asymmetric component V_A, we find that shows dependence as expected from the PHE. On the other hand, V_A is proportional to cosϕ, which results from the crystal symmetry (Fig. (c), (d)) [4].

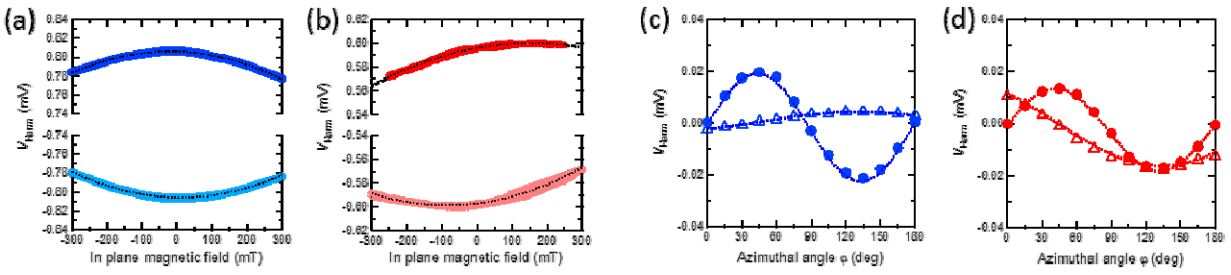

Fig. 1. (a) V_{harm} at ϕ=0 for Co/Pt (P). (b) V_{harm} at ϕ=0 or Co/Pt (S). (c) and (d) corresponds to ϕ angle dependence of V_S (dot) and V_A (triangle) in V_{harm} of Co/Pt (P) and Co/Pt (S).

References

[1] I. M. Miron et al., Nature (London) **476**, 189 (2011).

[2] J. Ryu, M. Kohda and J. Nitta, Phys. Rev. Lett. **116**, 256802 (2016).

[3] J. Kim et al., Nat. Mater. 12, 240 (2013); K. Garello et al., Nat. Nano., **8**, 587 (2013).

[4] P. K. Muduli et al., Phys. Rev. B, **72**, 104430 (2005).

Proton and Ion Beam Radiation Effects on Magnetic Tunnel Junction

June-Young Park*, Jeong-Mok Kim, Jeongchun Ryu, Jimin Jeong, Byong-Guk Park
Dept. of Materials Science and Technology, KAIST, Daejeon, 34141, Korea

Under radiation environment, microeletronic devices have been investigated to have serious issues in terms of operation reliability [1]. For example, the CMOS devices, widely utilized to current practical applications, cause distorted information or physical damage when exposed to cosmic rays. To overcome the problems, metal-based magnetic memory composed of magnetic tunnel junction (MTJ) is proposed due to its non-volatile characteristics. Previous studies on the radiation hardness of magnetic memories have mainly focused on gamma rays and neutron beams[2-5], which are secondary cosmic rays and mainly encountered in the earth. In this study, we confirmed the radiation hardness of the in-plane MTJ and the perpendicular MTJ devices for primary cosmic rays, the protons beam and the ion beam, which are mainly encountered in space.

We fabricated the in-plane MTJ structure, Ta(5)/Pt(5)/IrMn(10)/CoFeB(5)/MgO(2.5)/CoFeB(5)/Ru(5), and perpendicular MTJ structure, W(5)/CoFeB(1.2)/MgO(3.5)/CoFeB(2.2)/W(5)/Ru(5), by DC and RF magnetron sputtering system, where the parenthesis corresponds to thickness of nm. The magneto-electric properties were measured to observe the radiation hardness, before and after the irradiation of proton and Cr ion beams. Magnetic properties were confirmed by M-H curves measurement using VSM (Vibrating Sample Magnetometer) and the electrical properties were confirmed by TMR (Tunneling MagnetoResistance) measurement.

The proton beam was irradiated with 20 MeV in the Korea Multi-purpose Accelerator Center. The M-H curves, as shown in Fig. 1. (a), shows almost no change at all dose levels. In Fig. 1. (b), it shows TMR has similar size before and after proton irradiation at all dose levels, confirming that the MTJ has radiation hardness to the proton beam. Cr Ion beam was irradiated at 20 keV energy level in Korea Multi-purpose Accelerator Center. As shown in Fig. 1. (c), both the magnetic moments and the coercivities are decreased with increasing dose level. Fig. 1. (d), it shows TMR has decreased size at the high dose level, and it is found that the MTJ has relatively poor radiation hardness to the Cr ion beam and its characteristics change in proportion to the dose level. This change is presumably due to physical damage to the magnetic layer of the MTJ by ion bombardment. It is confirmed through SRIM (the Stopping and Range of Ions in Matter) code simulation. However, these ion beams are believed to be blocked by packaging at the actual device implementation stage because the penetration depth of ion beam is very thin.

In summary, we irradiated proton and Cr ion beams to the MTJ structures and confirmed its radiation hardness by measuring its magnetic and electrical properties. Our metal based device, MTJ, has good radiation hardness against the proton beam, although the proton beam has enough energy to penetrate whole sample. On the other hand, the MTJ has not enough radiation hardness to the Cr ion beam. It is assumed that originated from the physical damage by ion bombardments, and would be protected by other packaging materials in practical device applications.

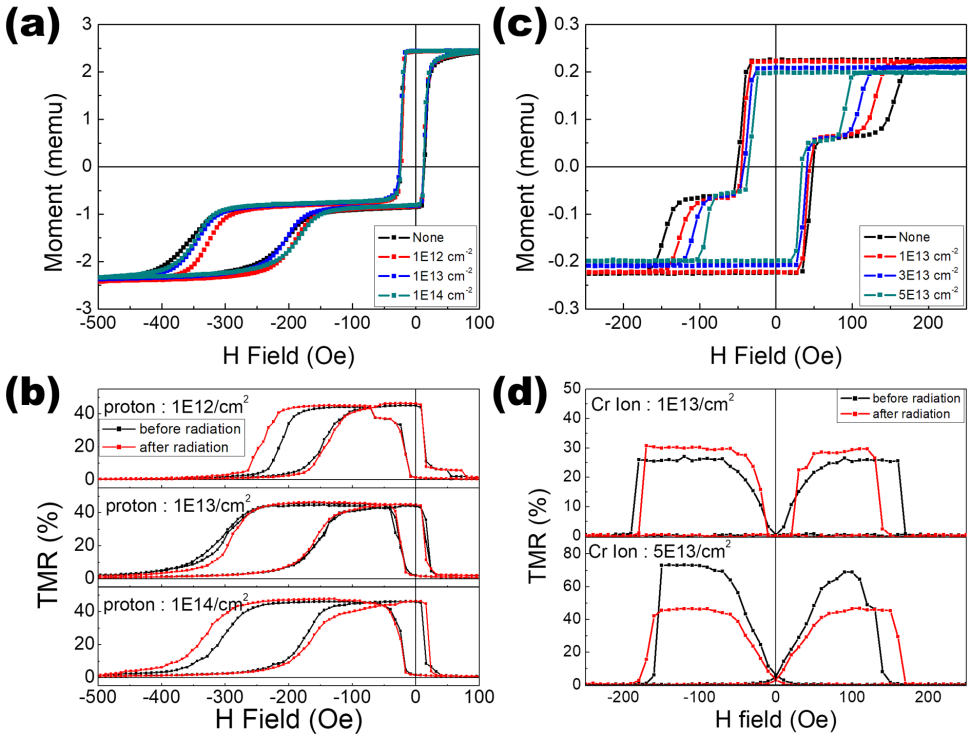

Fig. 1. (a) The change of M-H curves of in-plane MTJs depending on the dose level of irradiated proton. (b) TMR changes before and after proton irradiation with various dose levels. (c) The change of M-H curves of out-of-plane MTJs depending on the dose level of irradiated Cr ions. (d) TMR changes before and after Cr ion irradiation with various dose levels.

References

[1] Paul. E. Dodd et al., IEEE Trans. Nucl. Sci. **50**, 3 (2003)

[2] Yahya Lakys et al., IEEE Trans. Nucl. Sci. **59**, 4 (2012)

[3] D. N. Nguyen et al., 9th European Conference on Radiation and Its Effects on Components and Systems, 628-631 (2007)

[4] Romney R. Katti et al., 2009 IEEE Radiation Effects Data Workshop, 103-105 (2009)

[5] Fanghui Ren et al., IEEE Trans. Nucl. Sci. **59**, 6 (2012)

Measurement Equipment of Superconducting Magnetic Levitation Force

Young Hwan Lee[1*], Ji U Kim, Ye Bin Jo[1], Jah Ho Lee[1†], Chan Joong Kim[2†]
[1]Gajaeul High School
[2]Korea Atomic Energy Research Institute
[†]Advisor

A Meissner phenomenon in which the superconductor rejects the external magnetic force appears below the superconducting critical temperature (T_c) of the superconductor. This force causes the superconductor to levitate above the permanent magnet and vice versa. The magnetic repulsive force of the superconductor varies with the distance between the superconductor and permanent magnet, size and thickness of the permanent magnet. A device was developed to measure the force acting between the superconductor and the magnet below the critical temperature. The measuring device consists of a container for cooling the superconductor, a digital balance for measuring the repulsive force acting between the superconductor and the permanent magnet, a permanent magnet holder, and a distance controller. A 3D printer and a laser cutter were used to make the measuring device. A liquid nitrogen container for cooling the superconductor was manufactured using a 3D printer. Using this device, we were able to successfully measure the force acting between the superconductor and the permanent magnet.

Fig. 1. Magnetic force measurement equipment

Magnetic Levitation Force of YBCO superconductors at 77 K

Ji U Kim[1*], Ye Bin Jo[1], Young Hwan Lee[1], Jah Ho Lee[1†], Chan Joong Kim[2†]
[1]Gajaeul High School
[2]Korea Atomic Energy Research Institute
[†]Advisor

The repulsive magnetic force acting between the superconductor and the permanent magnet at the liquid nitrogen (LN_2) temperature was measured using the measuring instrument. An Nd-B-Fe magnet (Nd magnet) with a diameter of 25 mm and a thickness of 5 mm was used. The surface magnetic field at the center of the permanent magnet was 3,000 G. The size of the superconductor (Melt growth-processed large grain Y123 bulk superconductor) was 26 mm in diameter and 6 mm in thickness. The superconductor was cooled using LN_2. The T_c of the superconductor is 91 K, and the temperature of LN_2 is 77 K. When a superconductor is cooled using LN_2, therefore, the superconductor becomes superconducting. After fixing the Nd magnet to the holder, the distance (d) of the Nd magnet from the superconductor was adjusted. The repulsion of the superconductor is observed when d was 22 mm. As d decreased, the repulsive force of the superconductor increased. When d = 1 mm, the repulsive force was 5.3 N.

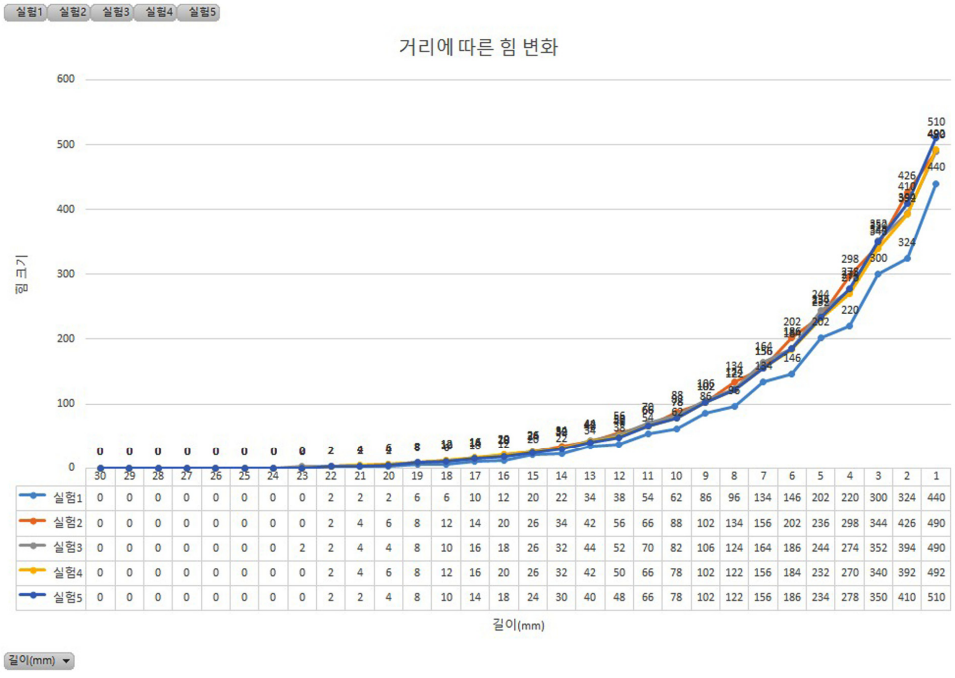

	30	29	28	27	26	25	24	23	22	21	20	19	18	17	16	15	14	13	12	11	10	9	8	7	6	5	4	3	2	1
실험1	0	0	0	0	0	0	0	0	2	2	2	6	6	10	12	20	22	34	38	54	62	86	96	134	146	202	220	300	324	440
실험2	0	0	0	0	0	0	0	0	2	4	6	8	12	14	20	26	34	42	56	66	88	102	134	156	202	236	298	344	426	490
실험3	0	0	0	0	0	0	0	2	2	4	4	8	10	16	18	26	32	44	52	70	82	106	124	164	186	244	274	352	394	490
실험4	0	0	0	0	0	0	0	0	2	4	6	8	12	16	20	26	32	42	50	66	78	102	122	156	184	232	270	340	392	492
실험5	0	0	0	0	0	0	0	0	2	2	4	8	10	14	18	24	30	40	48	66	78	102	122	156	186	234	278	350	410	510

Fig. 1. Forc-distance curve of the superconductor at 77 K

Effects of the size of an Nd-B-Fe magnet on the Magnetic Repulsive Force of YBCO superconductors at 77 K

Hee Yeon So[1*], Dong Hyun Kim[1], Yu Seong Hong[1], Jah Ho Lee[1†], Chan Joong Kim[†]
[1]Gajaeul High School
[2]Korea Atomic Energy Research Institute
[†]Advisor

The magnetic strength of the permanent magnet is proportional to the thickness and size of the permanent magnet. If the area of the superconductor and the permanent magnet facing each other is large, the repulsive force of the superconductor is large. In this study, the repulsive force of a superconductor was investigated using Nd-B-Fe permanent magnets (Nd magnets) of different diameters. Nd magnets with diameters of 15 mm, 20 mm, 25 mm and 30 mm and a surface magnetic fied of 3,000 G were used. The superconducting sample was made by the melt growth process and the dimension was 20×20×13mm. The experimental results are as follows. 1) The larger the diameter of the permanent magnet, the greater the distance that the magnetic repulsion of the superconductor appears. 2) When the diameter of the permanent magnet is large, the repulsive magnetic force of the superconductor is increased. 3) When d = 15 mm, d = 20, d = 25 mm and d = 30 mm, the maximum repulsive magnetic force of the superconductor was 4.8 N, 12.5 N, 13.8 N and 9.2 N, respectively. These values are measured at a distance of 0.1 mm between the superconductor and the Nd magnet. When the cross-sectional area of the superconductor and the permanent magnet was similar, the repulsive magnetic force was large.

Through this experiment, we have understood the relationship between the size of the Nd magnet and the magnetic repulsive force of the superconductor. It is expected that the experimental results can be used for designing the superconducting magnetic levitation train, which is the next project.

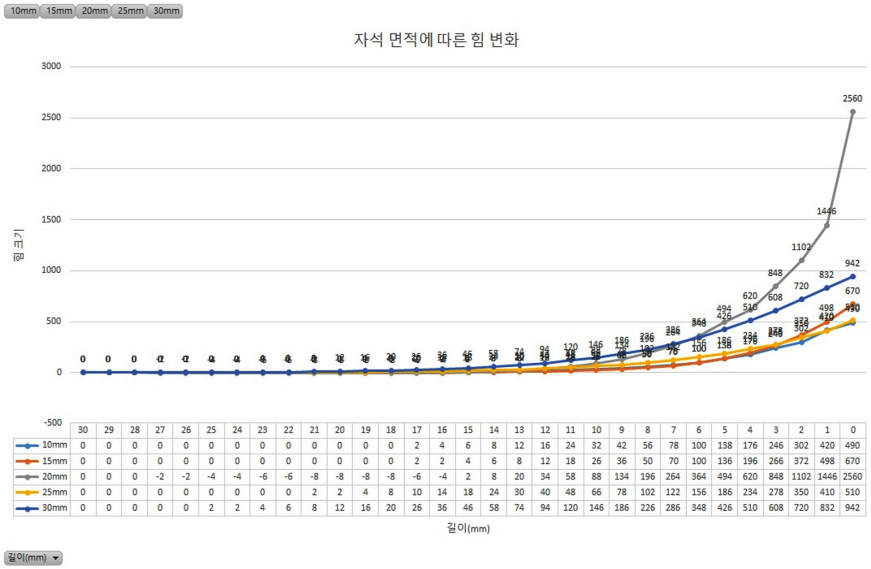

Fig. 1. Repulsive magnetic force of the YBCO superconductor at 77 K as a function of the diameter of Nd magnets

Effects of the thickness of an Nd-B-Fe magnet on the Magnetic Repulsive Force of YBCO superconductors at 77 K

Ha-Young Kim[1*], Jung-Hee Chae[1], Young-Bin Jung[1], Jah Ho Lee[1†], Chan Joong Kim[2†]
[1]Gajaeul High School
[2]Korea Atomic Energy Research Institute
[†]Advisor

The magnetic strength of the permanent magnet affects the repulsive magnetic force of the superconductor. In this study, we investigate the correlation between the thickness (t) of Nd-B-Fe permanent magnet (Nd magnet) and the repulsive magnetic force of the superconductor. A disc-shaped permanent magnet having a diameter of 25 mm and a thickness (t) of 5 mm, 10 mm, and 15 mm was used. The thickness of Nd magnet was adjusted by the number of Nd magnets. The superconductors (MG-processed YBCO superconductor, T_c = 91 K) were cooled using LN_2. The distance (d) between the superconductor and the Nd magnet was changed from 30 mm to 0.1 mm by 1 mm. The force acting between the Nd magnet and the superconductor started to be observed at d= 23 mm when using a single Nd magnet (t = 5 mm). For double Nd magnets (t = 10 mm), it was observed when d = 24 mm. For triple Nd magnets (t = 15 mm), it was observed at d = 28 mm. The maximum repulsive force (the force at 0.1 mm gap) measured for t = 5mm, 10 mm, and 15 mm was 7.4 N, 12.5 N and 13.8 N, respectively. As a result, it can be concluded that d increases as t increases and the repulsive magnetic force of the superconductor increased as t increased.

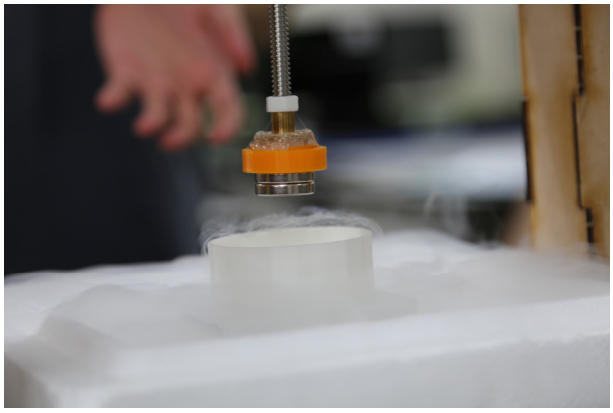

Fig. 1. Measurement of a repulsive magnetic force of the YBCO superconductor at 77 K

International Symposium on Magnetism and Magnetic Materials 2018

Special Session VI

'Spin Magnetism for Bioconvergence'

Magnetic bead signal measurement by using PHR sensors

Dong Young Kim[1*], Seok Soo Yoon[1], Jung-Woo Shin[1], Jae-Hoon Lee[2], Cheol-Gi Kim[2]
[1]Deaperment of Physics, Andong National University, Korea
[2]Department of Emerging Materials Science, DGIST, Korea

The planar Hall resistance (PHR) sensor with 100 x 200 μm^2 size was fabricated using NiFe(20 nm)/Cu(0.5 nm)/MnIr (10 nm) thin film. The magnetic field dependence of magnetic bead signals was measured by Planner Hall resistance (PHR) method and self-field (SF) method by using the PHR sensor. The magnetic bead signals measured with SF method showed about 14 times improved signal properties than one measured with PHR method. Fig.1 showed the magnetic field dependence of V_w/V_{wo} measured by SF method. V_w and V_{wo} was the measured output voltage with and without magnetic beads by SF method, respectively. High hysteresis and low stability of magnetic bead signals at H> H_{eff} was due to the magnetic hysteresis of NiFe/Cu/MnIr thin film used in PHR sensor. We obtained high and stable magnetic bead signals at H> $2H_{eff}$. Therefore, the high and stable magnetic bead signals measured by SF method at H> $2H_{eff}$ can be used to the biosensor.

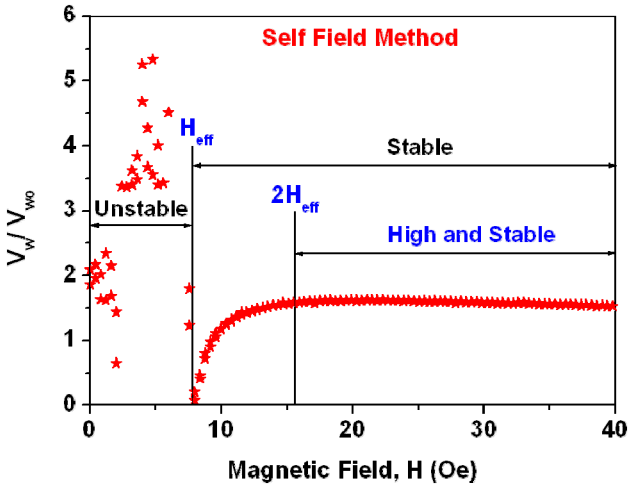

Fig. 1. Magnetic field dependence of V_w/V_{wo} measured by self-field method

Micromagnets for synchronous separation of multiple bio-functionalized particles and cells

Cheol Gi Kim*, Sri Ramulu Torati, Xinghao Hu, Byeonghwa Lim, Kunwoo Kim
Department of Emerging Materials Science, DGIST, Daegu-42988, Korea

The precise transport of biofunctionalized matters is of great interest and significant in modern biological sciences and biophysics to understand the fundamentals and its implication of cell heterogeneity and cellular mechanics. Although, significant progress has been achieved during the last decade, a parallel and automated isolation and manipulation of rare analyte, and their simultaneous on-chip separation and trapping, still remain challenging. Here, a universal micromagnet junction was fabricated for microrobotic particles to deliver the biomolecules to specific sites using a remote magnetic field (Fig.1). The nonmagnetic gap between the lithographically defined donor and acceptor micromagnets plays a crucial role and create an energy barrier to restrict particle gating. By careful designing of junction geometry, it becomes possible to transport multiple protein-functionalized particles in high resolution, as well as MCF-7 and THP-1 cells from their mixture, with high reliability and trap them in individual apartments. Further integration of this micromagnet junction with magnetophoretic circuitry elements could lead to novel platforms for the synchronous digital manipulation of particles/ biomolecules in microfluidic multiplex arrays for next-generation biochips.

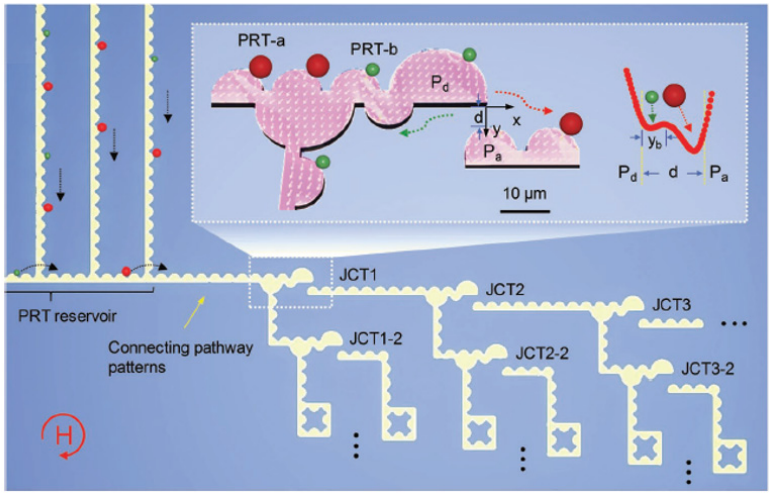

Fig. 1. Schematic representation of micromagnet junctions for autonomous separation and delivery of biofunctionalized matters to individual apartments

Complementary spin logic operation based on electric-field controlled spin-orbit torques

Seung-heon Chris Baek[1,2], Kyung-Woong Park[1,2], Kyung-Jin Lee[3,4], Byong-Guk Park[1*]

[1]Materials Science and Engineering, KAIST, Daejeon, Korea

[2]SK Hynix Semiconductor, Inc., Gyeonggi-do, Korea

[3]Department of Materials Science and Engineering, Korea University, Seoul, Korea

[4]KU-KIST Graduate School of Converging Science and Technology, Korea University, Seoul, Korea

Spintronic devices offer low power consumption, built-in memory, high scalability and reconfigurability, and could therefore provide an alternative to traditional semiconductor-based electronic devices. However, for spintronic devices to be useful in computing, complementary logic operation using spintronic logic gates is likely to be required. Here we report a complementary spin logic device using electric-field controlled spin-orbit torque switching in a heavy metal/ferromagnet/oxide structure [1]. We show that the critical current for spin-orbit-torque-induced switching of perpendicular magnetization can be efficiently modulated by an electric field via the voltage-controlled magnetic anisotropy effect (Fig. 1). Moreover, the polarity of the voltage-controlled magnetic anisotropy can be tuned through modification of the oxidation state at the ferromagnet/oxide interface. This allows us to create both n-type and p-type spin logic devices and demonstrate complementary logic operation

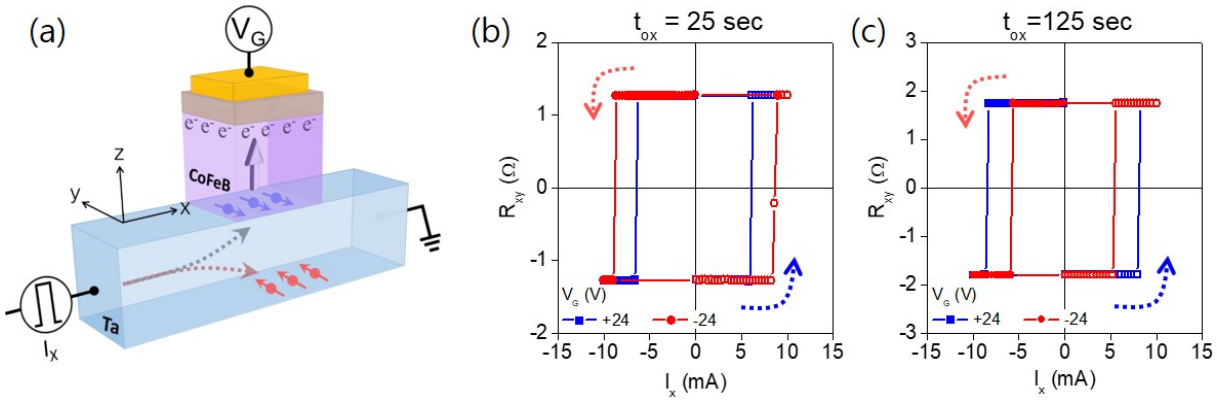

Fig. 1. (a) Schematic of the Ta(5 nm)/CoFeB(1 nm)/MgO(1.6 nm)/AlO_x(1.8 nm) sample, where the magnetization can be controlled by the in-plane current (I_x) and gate voltage (V_G). **(b, c)** SOT-induced switching experiments for samples with t_{ox} = 25 s (a) and 125 s (b). R_{xy} versus I_x under a V_G of ± 24 V. During the switching experiments, B_x = 10 mT was applied.

Reference

[1] S.C.Baek et al. Nature Electronics 1, 398 (2018)

Manipulation of Magnetic Skyrmions Motion in Confined Geometries for Potential Neuromorphic Applications

Dae-Han Jung, Hee-Sung Han, Namkyu Kim, and Ki-Suk Lee*
School of Materials Science and Engineering, Ulsan National Institute of Science and Technology, Ulsan 44919, Republic of Korea

Neuromorphic computing, inspired by the biological nervous system, has attracted enormous attention since it holds the promise of energy-efficient, intelligent, and highly adaptable computing systems [1-3]. Recently, magnetic skyrmions have been considered as promising candidates for neuromorphic computing design owing to their unique dynamic and topological characteristics such as high stability, low driving current density, and compact size in the nanometer range [4-6]. In this work, we report on a micromagnetic simulation study of the dynamics of the skyrmions and their manipulations in confined geometries, attempting to emulate the behaviors of biological synapses and neurons. By exploiting the topological characteristics in current-driven skyrmion motion accompanying with tunable geometrical potentials, we propose the design of skyrmion-based artificial neuron, mimicking the short-term plasticity and long-term potentiation functions of a biological neuron. The artificial neuron proposed here is built on a simple track-based structure in synaptic crossbar array architecture. Consequently, these results may enable to provide a dense and energy-efficient neuromorphic computing system with a simple single device implementation.

References

[1] Y. LeCun, Y. Bengio, and G. Hinton, Nature 521, 7553, 436-444 (2015).
[2] P. A. Merolla et al., Science 345, 6197, 668-673, (2014).
[3] S. H. Jo, T. Chang, I. Ebong, B. B. Bhadviya, P. Mazumder, and W. Lu, Nano Lett. 10, 4, 1297-1301 (2010).
[4] N. S. Kiselev, A. Bogdanov, R. Schäfer, and U. K. Rößler, J. Phys. D 44, 392001 (2011).
[5] A. Fert, V. Cros, and J. Sampaio, Nat. Nanotech. 8, 152 (2013).
[6] N. Nagaosa and Y. Tokura, Nat. Nanotech. 8, pp. 899-911 (2013).

Magnetic hyperthermia for removal of leukemia cells in circulatory system and thymus of mice

Hasan Al Faruque, Eun-Sook Choi, Jung-Hee Kim, Eunjoo Kim*
Companion Diagnostics and Medical Technology Research Group,
Daegu Gyeongbuk Institute of Science and Technology (DGIST), Korea

Magnetic hyperthermia has been widely applied for selective removal tumor tissues in vivo as well as in vitro cells. Leukemia is a kind of blood cancer, in which malignant tumor cells are produced from thymus and flow through body via circulating system. The method to remove leukemia cells from circulating system is chemotherapy and radiotherapy, however, the selective removal of leukemia cells has not been available until now. In this study, targeted therapy by using magnetic hyperthermia is applied to remove leukemia cells, directly from circulating system. Magnetic nanoparticles (MNPs) are modified by anti-EpCAM antibody, which is specifically bound to the leukemia cell surface. AKR mice (leukemia model) injected with anti-EpCAM-modified MNPs showed increased removal of leukemia cells from whole blood under the irradiation of magnetic field to whole body, compared to that of bare MNPs. This result is promising to selective removal of leukemia cells, thus the side effects from chemotherapy or radiotherapy could be avoided by biomedical treatment of MNPs.

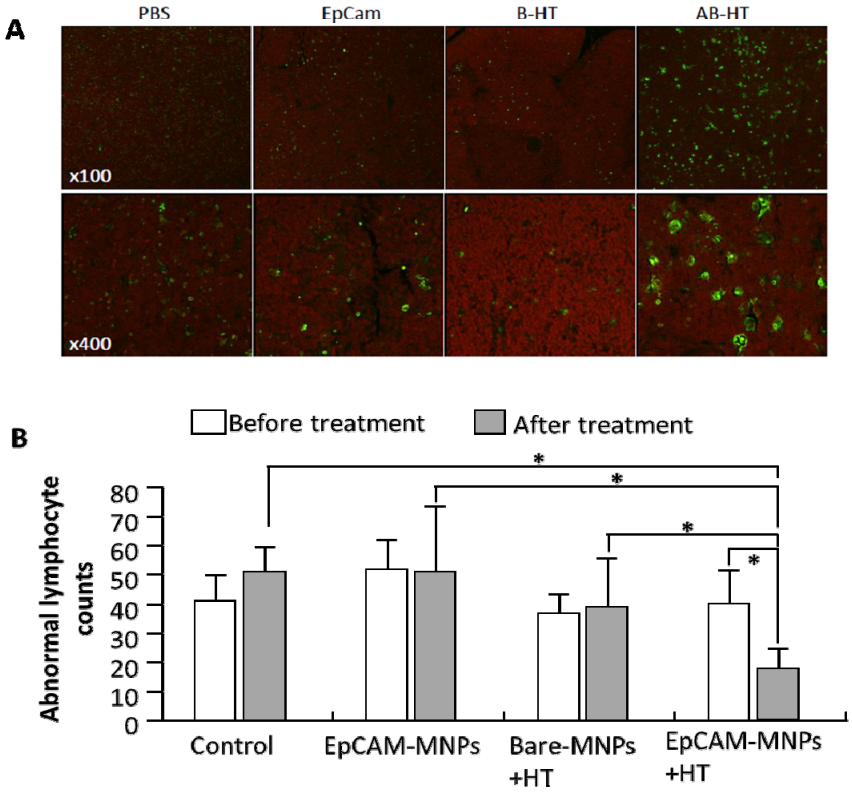

Fig. 1. Selective removal leukemia cells from (A) thymus and (B) blood of mice.

Multi-level anomalous Hall resistance changes due to DW motion in a single Hall cross for the application of a neuromorphic device

Yoonui Kim*, Jaesuk Kwon, Hee-Kyeong Hwang, and Chun-Yeol You
Department of Emerging Materials Science, DGIST, Daegu 42988, South Korea

A spintronic device carries out the digital information by using the magnetic domain walls in the 3D racetrack memory[1], and logic device application[2] for satisfying the modern computer needs.[3] While, a typical application for the memristive functionality[4] is introduced to the neuromorphic synaptic device[5]. Control of magnetization in spintronics device allows to be utilized in the non-volatile memory in the face of reliability and high performance with the low power consumption. The multi-steps in the Hall resistance switching in the DW device are tuned by modulation of intensity and duration in magnetic field pulses. We found that the multi-step Hall resistance (R_H) relied on the DW motion in the Hall cross according to the number of pulses. A film structure composed of Si/SiO2/Ta/Pt/$[Co/Pt]_4$/Pt was deposited by the sputtering system. We measured the anomalous Hall effect (AHE) and recorded the image from Kerr microscopy concurrently, as depicted in Fig. 1. The structural difference between the wire and the nucleation pad causes different shape anisotropy for a domain nucleation in the pad by external field. A domain nucleates in the nucleation pad placed at the ends of wire as field pulses are applied with ~303Oe. Besides, a domain expands towards a DW path in the wire, inducing a field-driven DW motion in the Hall cross by selected field pulse intensity. Then, we execute the appropriate intensity of pulses to drive the domain wall to the Hall cross via the DW path along wire. For the case of a DW motion, we have regulated a field pulse duration in the range of 0.4-0.9 sec. As well, the multi-steps of Hall resistance due to a DW motion at junction are also investigated with the field pulse intensities of +231 and +237Oe. The different ΔR_H values cause from the DW configuration change related to the pinning/ depinning at the structural defects (corners). A spintronics device based on the domain wall (DW) motion is applicable to obtain the multi-level Hall resistance for the application of synaptic device.

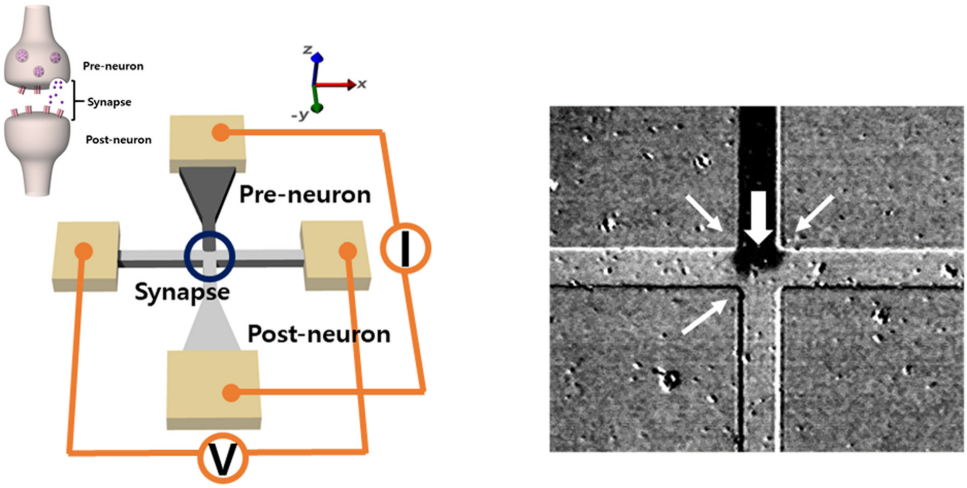

Fig. 1. Similitudes between the biological and the artificial synapse relevant to the DW motion

(Left) Schematic of experimental set-up for the measurement of anomalous Hall effect (AHE). The inset is an illustration of biological neuron system so that the synapse transmitted signals from pre-synaptic neuron to post-synaptic neuron and modulates its membrane potential. (Right) Kerr images for the field-driven DW motion at the junction of Hall cross. DW propagation through the synapse changing the Hall resistance (R_H). The pinning sites indicated white arrows at edge of corners in the Hall cross. The large white arrow in the wire indicates the direction of the propagation for the up-down DW.

Acknowledgement

This research was supported by the DGIST R&D Program and Basic Science Research Program through the National Research Foundation of Korea (NRF) funded by the Ministry of Education (18-BT-02, 2018R1A6A3 A11043437).

References

[1] Stuart S. P. Parkin, Masamitsu Hayashi, Luc Thomas, Science **320**, 190 (2008).

[2] D. A. Allwood, Gang Xiong, M. D. Cooke, C. C. Faulkner, D. Atkinson, N. Vernier, R. P. Cowburn, Science **296**, 14 (2002).

[3] E. Pekez, Technol. Soc. **12**, 65 (1990)

[4] Dmitri B. Strukov, Gregory S. Snider, Duncan R. Stewart, R. Stanley Williams, Nature **453**, 80 (2008).

[5] S. Lequeux, J. Sampaio, V. Cros, K. Yakushiji, A. Fukushima, R. Matsumoto, H. Kubota, S. Yuasa, and J. Grollier, Sci. Rep. **6**, 31510 (2016).

Controlling the configuration and creation of magnetic skyrmions by various manipulation techniques studied based on full-field soft X-ray microscopy

Mi-Young Im[1,2,3*], Soong-Geun Je[1,2], Weilun Chao[1], Ki-Suk Lee[3], Jung-Il Hong[2]
[1]Center for X-ray Optics, Lawrence Berkeley National Laboratory, Berkeley CA94720, USA
Email: mim@lbl.gov, web site: http://cxro.lbl.gov/staff/mim
[2]Department of Emerging Materials Science, DGIST, Daegu, Korea
[3]School of Materials Science and Engineering, KIST-UNIST Ulsan Center for Convergent Materials, Ulsan National Institute of Science and Technology, Ulsan, Korea

Magnetic skyrmion is a topologically protected spin structure stabilized by Dzyaloshinskii- Moriya interactions and/or dipolar interactions. Magnetic skyrmions have attracted enormous interests not only because of their fascinating topological characters to understand fundamental physics of nanospin behavior but also due to their potentials in a wealth of technological applications such as high efficient storage and memory devices. Recently, Magnetic skyrmions have also been considering as a promising candidate for neuromorphic computing with their particle-like behaviors and effective motions at low energy consumption. From the perspective for skyrmions to be practically used, one of the critical issues is whether the configuration of skyrmions including their sizes and densities and creating/deleting of skyrmions is manageable or not.

In our work, we experimentally addressed the issue by direct observation of skyrmions and skyrmion configurations in Pt/Co/Fe/Ir, Pt/Co/Pt, Fe/Gd, Pt/Co/Ta multilayered heterostructures utilizing a soft X-ray transmission microscope at Advanced Light Source (XM-1, BL6.1.2), enabling the direct observation of in-plane and out-of-plane magnetic components with a high spatial resolution down to 25 nm. We demonstrated that the properties of skyrmions such as size and density of skyrmions could be controlled by varying thickness of ferromagnetic layers and by changing the strength of magnetic field [1-3]. Additionally, it was found that skyrmions could be either created or annihilated by the injected current pulses depending on the strength of applied magnetic fields [4] where the Joule heating than spin-orbit torque effect plays a critical role in the formation and/or elimination of skyrmions. We also proposed a way to create and delete skyrmions in a certain selective area of systems based on using Oersted fields and Joule heating by optimizing design of sample geometries including electrodes [5].

This work was supported by Leading Foreign Research Institute Recruitment Program through the National Research Foundation (NRF) of Korea funded by the Ministry of Education, Science and Technology (MEST) (2012K1A4A3053565) and by the DGIST R&D programme of the Ministry of Science, ICT and future Planning (18-BT-02). Work at the ALS was supported by the U.S. Department of Energy (DE-AC02-05CH11231).

References

[1] A. Soumyanarayanan et al., Nature Materials 16, 898 (2017).
[2] Ivan Lemesh, Kai Litzius, Pedram Bassirian, Nico Kerber, Daniel Heinze, Felix Büttner, Lucas Caretta, Max Mann, Markus Weigand, Simone Finizio, Mi-Young Im, Mathias Kläui, and Geoffrey S. D. Beach,

10.1002/adma.201805461, Advanced Materials (2018).
[3] Sergio A. Montoya, Robert Tolley, Ian Gilbert, Soong-Gun Je, Mi-Young Im, Eric E. Fullerton, Phys. Rev. B 98, 104432 (2018).
[4] Soong-Geun Je, Min-Seung Jung, Mi-Young Im, Jung-Il Hong, Current Applied Physics, doi 10.1016 (2018).
[5] Soong-Geun Je et al., in preparation (2018).

Creation of valley magnetic domain and manipulation

J. D. Lee*
Department of Emerging Materials Science, DGIST, Daegu 42988, Korea

First-principles density functional theory provides significant insights into an interplay between an applied strain and the Berry curvature reconstruction in the uniaxially strained monolayer MoS_2, which leads to the unbalanced Berry curvatures centered at **K** and **-K** points and eventually the valley-polarized current under an external static electric field. This finding of the valley Edelstein effect (VEE) is shown to explain very well a recent experimental observation of the valley magnetoelectricity. In an opposite limit of VEE, the strain-induced homogeneous valley ferromagnetism, there is positioned the valley Hall effect (VHE), the inhomogeneous separation of valley pseudospins at zero strain. Here we propose to tune between VHE and VEE by controlling a strain strength (< 0.3%) or an external electric field and demonstrate to create the valley magnetic domain (VMD) and move the domain. The VMD manipulation should be a key ingredient of potential device applications of valleytronics, in parallel with spintronics.

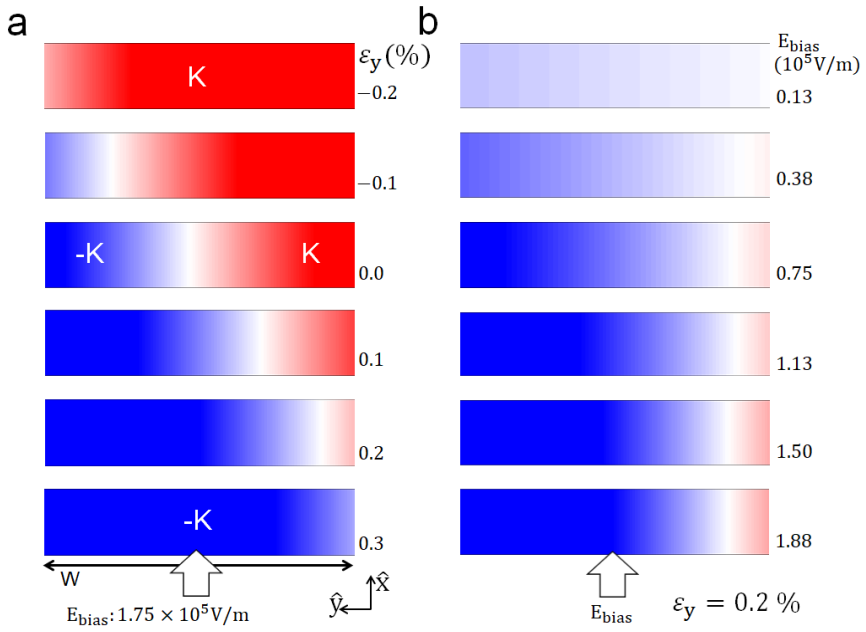

Fig. 1. Valley magnetic domain in monolayer MoS2

Longitudinal Monitoring of Cytokines in Mouse Tumor Models Using Magnetic Biosensors

Jung-Rok Lee*
Division of Mechanical and Biomedical Engineering, Ewha Womans University, Korea

Cancer development is a complicated biological process involved with interactions between the tumor cells and environment. The interactions between the host and tumor cells induce production of multiple cytokines and recruit immune cells. Upon therapeutic intervention, the proteomic signatures generated by these interactions become much more complicated. Thus, longitudinal monitoring on multiple cytokines related to systemic response to cancer development and therapy is greatly needed to understand the basic mechanism of cancer development and therapeutic intervention. However, most cancer studies utilize mouse models, which are unlikely to provide enough volumes of serum samples for multiple protein assays, because it is easier to manipulate the conditions for cancer development, inoculate tumor cells, and inject drugs in the mouse models, compared to humans. Thus, a new tool that can measure multiple proteins within a limited amount of serum sample is urgently needed, especially for mouse models. Here, we have developed drug-sensitive and -resistant mouse lymphoma models, and demonstrated that magnetic biosensors are capable of monitoring 6 different cytokines longitudinally in individual mice with different treatment and outcomes. We found that serum IL-6 and GCSF are differently expressed between drug-treated and untreated groups, and that IL-6 is secreted by the host in the presence of tumor cells upon the drug treatment. The multiplex magnetic biosensor assays enable longitudinal studies on proteomics of a single biological object. Combined with a mobile platform of magnetic biosensors, this technique can be utilized to monitor health conditions or diagnose diseases as point-of-care testing.

Fabrication of Large-area Plasmonic Substrate for Magneto-optical Sensing Platform

Cao Van Phuoc, S. Surabhi, Jaewoong Lee, Jong-Ryul Jeong*
Department of Materials Science and Engineering, Graduate School of Energy Science and Technology,
Chungnam Nationa University, Daejeon 34134, South Korea

In this study, we have fabricated large-area plasmonic substrate using self-assembled method for magneto-optical sensing platform. The plasmonic structures are prepared on the glass substrate by deposit noble metals such as Au and Ag. The plasmonic Au/Ag nanoparticles are formed by increasing the substrate temperature in a self-assembled way. We have found that the plasmon resonance wavelength can be tuned by controlling the Au/Ag deposition thickness and varying the film thickness. In this talk, we will present systematic investigations of fabrication and analysis of plasmonic nanostructures by using a three dimensional finite-difference time-domain (FDTD) calculation of extinction spectra with accurate modelling of the nanoparticle composition. Careful attention to the composition of the plasmonic nanostructures can help us understand the plasmon sensing sensitivity. It has far reaching implications related to the development of ultra-sensitive magneto-plasmonic sensing technology.

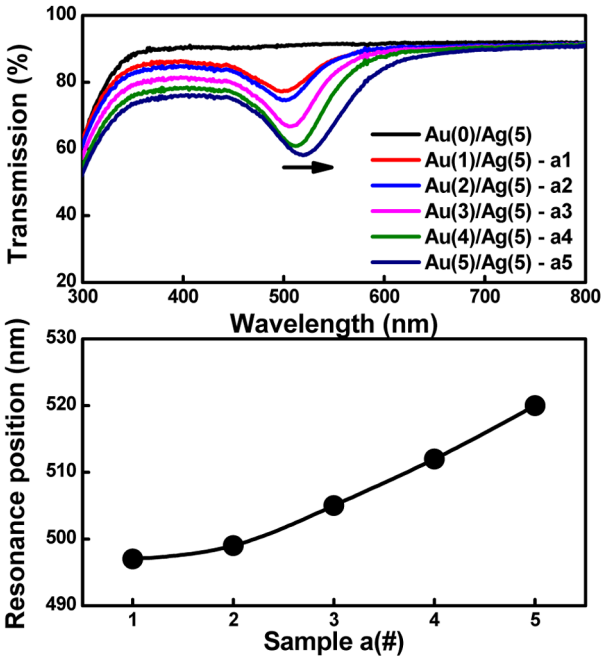

Fig. 1. (a) Experimental UV-vis spectrum of Au(x nm)/Ag(5 nm) samples (b) LSPR peak dependence on the thickness of deposited Au layer.

Control of Exchange Anisotropy in FM/AFM Bilayers by Piezoelectric Strains

Hyun-Joong Kim[1,2,3], Chun-Yeol You[1,2] and Jung-Il Hong[1,2,3*]
[1]Department of Emerging Materials Science, DGIST, Korea
[2]Global Center for Bio Convergence Spin Systems, DGIST, Korea
[3]DGIST-LBNL Research Center for Emerging Materials, DGIST, Korea

Controlled manipulation of magnetic anisotropy can find many applications in the devices based on magnetic films, thereby related research has been actively sought in recent years. As one of the control mechanisms, modulation of exchange anisotropy in FM/AFM structure by mechanical strains applied to the film through the piezoelectric substrate is considered in the present study with the fabrication of ferromagnetic (FM)/antiferromagnetic (AFM)/ferroelectric (FE) substrate. FM $Co_{60}Fe_{20}B_{20}$/AFM $Co_{0.7}Ni_{0.3}O$ bilayers were deposited by magnetron sputtering on the piezoelectric substrate of $Pb(Mg_{1/3}Nb_{2/3})O_3$-$PbZrO_3$-$PbTiO_3$ (PMN-PZT) with (011) plane. Subsequently, the samples were field-cooled from 390K to 300K under +5 T magnetic field applied along the [100] or $[0\bar{1}1]$ axis of PMN-PZT to set the pinned direction (P.D.) of AFM. A tensile stress along the $[0\bar{1}1]$ axis of PMN-PZT and a compressive stress along the [100] axis is induced as positive electric field is applied across the thickness of the PMN-PZT substrate. The piezoelectric strain was found to induce an appreciable change in the exchange bias field (H_E) and the coercivity (H_C) of exchange-biased bilayers, thus the exchange anisotropy can be controlled accordingly. Exchange bias field (H_E) and coercivity (H_C) at various azimuthal angles ranging from 0° to 180° with 10° step were obtained from the measurements of magnetic hysteresis loops employing vibrating sample magnetometer (VSM) at room temperature under various applied electric fields (-2,0,2,4,6 and 8 kV/cm), as shown in figure 1. The azimuthal dependence of H_E can be varied with the independent control of uniaxial anisotropy (K_U) and unidirectional anisotropy (K_E) in the magnetic films. Experimentally measured shift in the critical angle and altered asymmetry in the shape of H_E-ϕ curve are consistent with the simulation results based on the Meiklejohn-Bean model modified with an additional uniaxial anisotropy term for the strain.

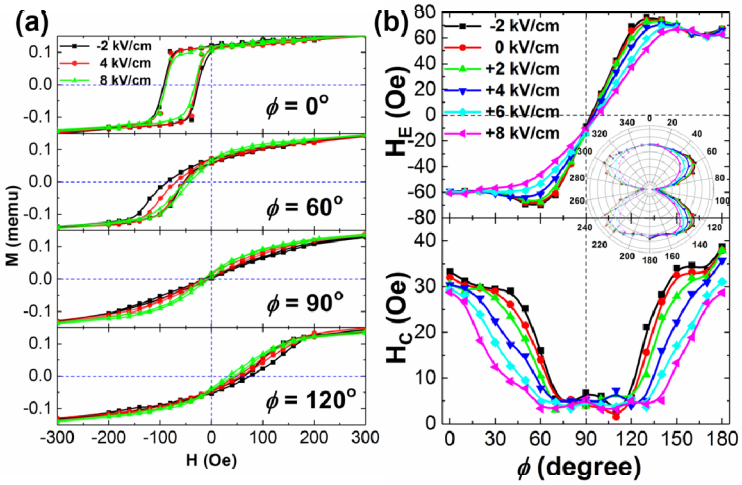

Fig. 1. (a) M-H loops at different angles (ϕ = 0°, 60°, 90° and 120°) (b) Angular dependence of H_E and H_C in FM/AFM/FE with pinned direction (P.D.) along the [100] direction at various electric fields

International Symposium on Magnetism and Magnetic Materials 2018

Special Session VII

'Spintronics with quantum materials'

Effective gauge field theory of spintronics

Gen Tatara*

RIKEN Center for Emergent Matter Science (CEMS), 2-1 Hirosawa, Wako, Saitama 351-0198, Japan

Spintronics phenomena are discussed based on the concept of effective gauge field. Effective gauge fields arise from structures of localized spin (magnetization) and couple to spin current of conduction electron.

The adiabatic component of the gauge field gives rise to spin Berry's phase, topological Hall effect and spin motive force, while nonadiabatic components are essential for spin-transfer torque, Dzyalosinski-Moriya interaction and spin pumping effects by inducing nonequilibrium spin accumulation.

Electromagnetic cross correlation effects and anomalous optical properties are discussed based on effective Lagrangian for conventional electromagnetic field and spin gauge field.

References

[1] Tatara, G.,Physica E: Low-dimensional Systems and Nanostructures (2018); https://doi.org/10.1016/j.physe.2018.05.011

[2] T. Kikuchi, T. Koretsune, R. Arita, G. Tatara, Phys. Rev. Lett. **116**, 247201 (2016).

[3] J. Shibata, A. Takeuchi, H. Kohno and G. Tatara, J. Phys. Soc. Japan, 85, 033701 (2016); J. Appl. Phys., 123, 063902 (2018); H. Kawaguchi and G. Tatara, Phys. Rev. B 94, 235148 (2016); H. Kawaguchi and G. Tatara, J. Phys. Soc. Japan, **87**, 064002 (2018).

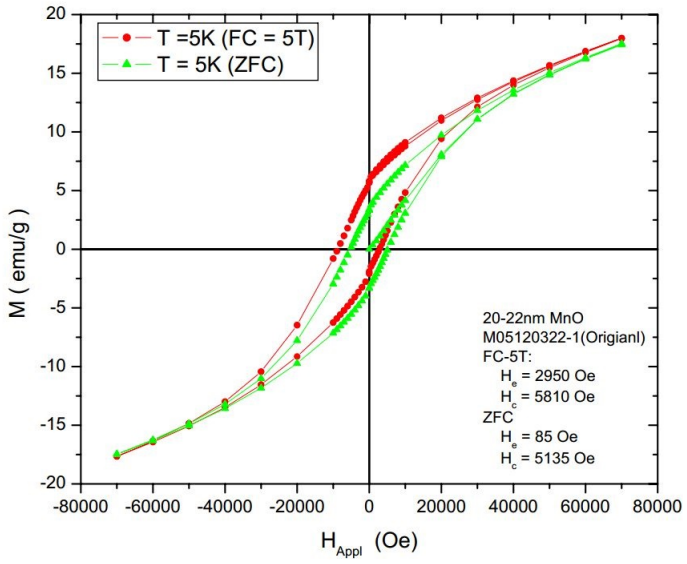

Fig. 1. A sample line graph (1line spacing / image size: 300 dpi)

Topological and ferromagnetic properties of iron-based van der Waals metals

Jun Sung Kim[1,2*]
[1]Center for Artificial Low Dimensional Electronic Systems, Institute of Basic Science, Pohang, Korea
[2]Department of Physics, POSTECH, Pohang, Korea

Topological semimetals, new states of matters whose low energy electronic structure possesses several band contact points or lines, are generally expected to exhibit intriguing topological responses. Up to now, most of the studies on topological semimetals are limited to non-magnetic materials with time-reversal symmetry. However, magnetic materials can also be endowed with topological band structures in which the interplay of magnetism and band topology can generate novel correlated topological phenomena. In this talk, I will introduce iron-based van der Waals (vdW) materials, where combination of magnetism, spin-orbit interaction, and topological band structures gives rise to unusual physical properties and magnetic tunability. This demonstrates that topological and ferromagnetic vdW materials have great potential for various spin-dependent electronic functionalities.

Theoretical Proposals for New Edelstein effects

Shuichi Murakami[1,2,3*], Taiki Yoda[1], Masato Hamada[1], Emi Minamitani[4], Motoaki Hirayama[5], Takehito Yokoyama[1]

[1]Department of Physics, Tokyo Institute of Technology
[2]TIES, Tokyo Institute of Technology, [3]CREST, JST
[4]Department of Materials Engineering, The University of Tokyo
[5]Center for Emergent Matter Science, RIKEN

In the Edelstein effect, a current in the crystal induces a spin polarization. It occurs in crystals without inversion symmetry, such as Rashba systems and surfaces of topological insulators. The spin polarization vanishes in equilibrium, but in the presence of the current, the electron distribution becomes off-equilibrium, giving rise to nonzero spin polarization, due to the spin-split band structure.

We propose an analogous effect for orbital angular momentum [1,2]. For example, in crystal with helical structure such as tellurium (Te) [3], we propose that a current along the helical axis induces an orbital magnetization [1,2] as well as spin magnetization. This effect is analogous to solenoids in classical electrodynamics (Fig. 1(a)). Within this analogy to solenoids, we quantify this effect by introducing a dimensionless parameter ξ, which represents a number of turns within the unit cell when regarded as a classical solenoid. Then we found that ξ is largely enhanced when the system is in the Weyl semimetal phase [1,2]. Here the Weyl semimetal phase [4] is allowed by broken inversion symmetry, and it is shown that Te becomes a Weyl semimetal at higher pressure [3]. There are other crystal structures that allow Edelstein effects, and we also demonstrate the orbital Edelstein effect for polar systems. Moreover, we propose a similar effect for phonons. In crystals, each phonon eigenmode has angular momentum due to rotational motions of the nuclei (Fig. 1(b)), but their sum is zero in equilibrium. Meanwhile a heat current in the Te crystal induces a nonzero total angular momentum [5]. We evaluate this effect for GaN and Te by ab initio calculation, and propose experiments to measure this effect (Fig. 1(c)).

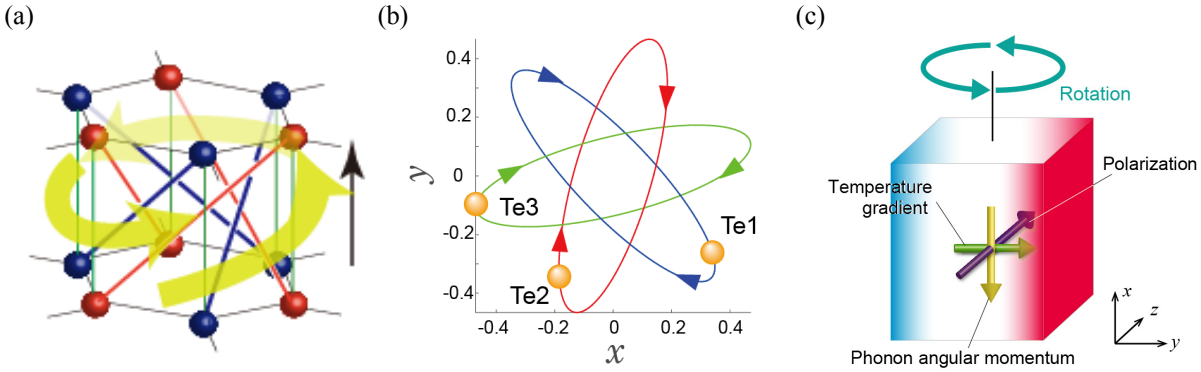

Fig. 1. (a) Schematic picture of the orbital Edelstein effect. (b) Rotational motion for a phonon mode in tellurium. (c) Proposed measurement for phonon Edelstein effect.

References

[1] T. Yoda, T. Yokoyama, and S. Murakami, Sci. Rep. 5, 12024 (2015).

[2] T. Yoda, T. Yokoyama, and S. Murakami, Nano Lett. 18, 916 (2018).

[3] M. Hirayama, R. Okugawa, S. Ishibashi, S. Murakami, and T. Miyake, Phys. Rev. Lett. 114, 206401 (2015).

[4] S. Murakami, New J. Phys. 9, 356 (2007).

[5] M. Hamada, E. Minamitani, M. Hirayama, S. Murakami, arXiv:1810.05359, to appear in Phys. Rev. Lett. (2018).

Chiral anomaly effect in electrical transport of $Bi_{0.96}Sb_{0.04}$

Heon-Jung Kim[1,2*]

[1]Department of Materials-Energy Science and Engineering, College of Engineering, Daegu University, Gyeongbuk 38453, Republic of Korea

[2]Department of Physics, College of Natural Science, Daegu University, Gyeongbuk 38453, Korea

As an exotic metallic state, the three-dimensional (3D) Weyl metal has pairs of Weyl nodes in the k space and shows topological surface state known as Fermi arcs and anomalous electrical transport originating from chiral anomaly. Ever since observed in $Bi_{0.96}Sb_{0.04}$, which becomes a 3D Weyl metal in parallel electric (E) and magnetic (B) fields, the negative longitudinal magnetoresistance had been the only transport signature of this exotic metallic state, also observable in TaAs, Na_3Bi, Cd_3As_2 and so on. As another indisputable fingerprint for existence of chiral anomaly, violation of Ohm's law was reported in $Bi_{0.96}Sb_{0.04}$ inthe longitudinal configuration (E//B). In this talk, I will discuss how violation of Ohm's law becomes direct evidence of chiral anomaly. Violation Ohm's law in Weyl metal is also expected to open a door to possible invention of a novel nonlinear electronic component at low frequencies.

International Symposium on Magnetism and
Magnetic Materials 2018

Special Session VIII

'Medical Science Research'

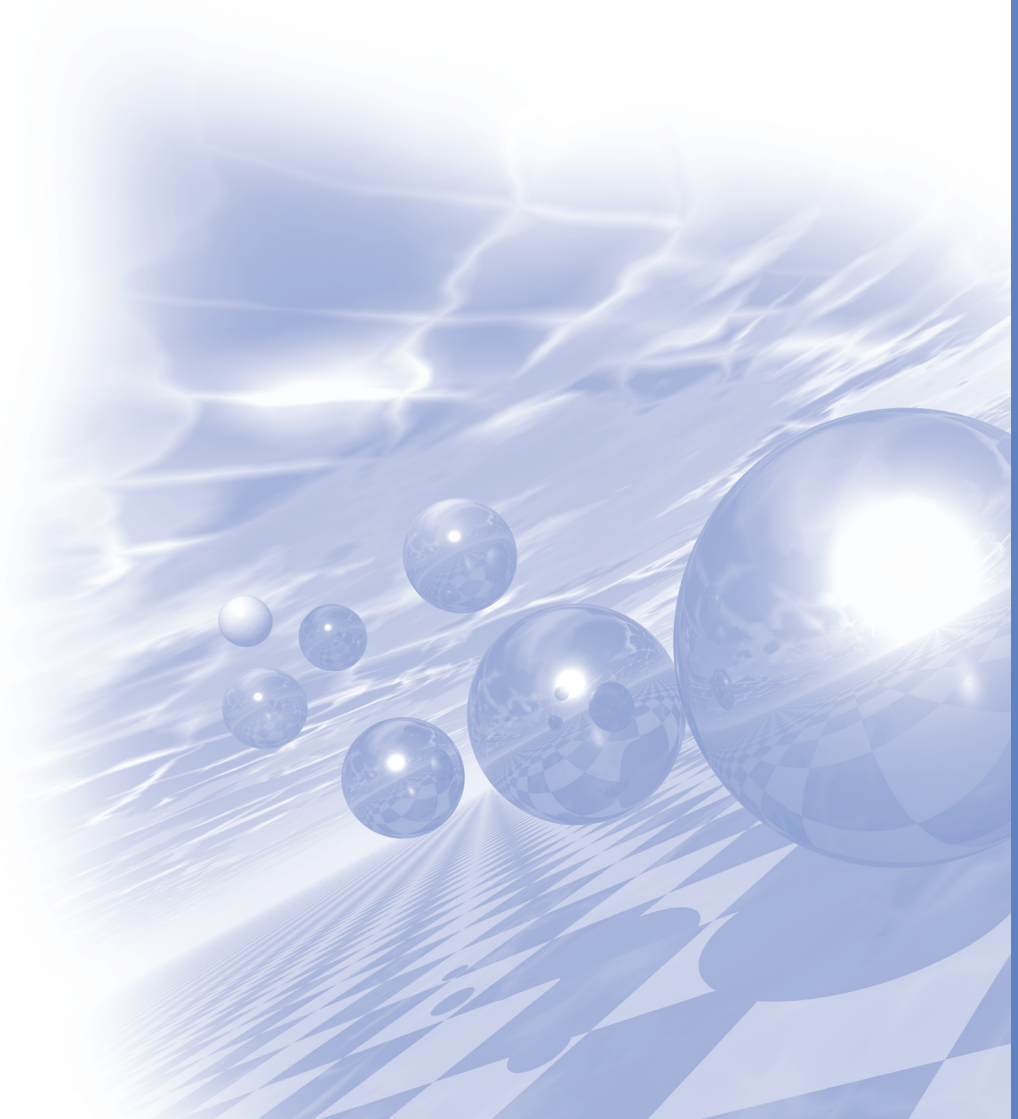

Development of phantom for IMRT delivery quality assurance in Tomotherapy

Jae-Uk Jang[1], Man-Seok Han[2*], Cheol-Soo Park[3], Gab-Jung Kim[4],
Se-Jong Yoo[5], Min-Cheol Jeon[5]

[1]Dept. of Radiation Oncology, Chungnam national university hospital, Daejeon, Korea
[2]Dept. of Radiological Science, Kangwon national university, Samcheok, Korea
[3]Dept. of Radiological Science, Hallym Polytechnic University, Chuncheon, Korea
[4]Dept. of Radiological Technology, Songho University, Hoengseong, Korea
[5]Dept. of Radiological Technology, Daejeon Health Institute of Technology, Daejeon, Korea

The primary goal of radiation therapy is to deliver a dose of radiation to cancer target while minimizing the dose that is given to adjacent normal tissue. Recently, radiation therapy is focused on precise radiation treatment like intensity modulated radiation therapy (IMRT). IMRT technique can deliver better optimal dose distribution compared to conventional radiation therapy. This technique can produce dose distributions that have improved conformity to the target with consequent avoidance of critical organ. Thus, an intensive dosimetry is necessary during the implementation of the technique and treatment verification processes before they can be applied to the patient

The purpose of this study was to evaluate the feasibility of the new phantom for verification of IMRT in Tomotherapy. This new QA phantom has the advantage over the conventional phantom. It was possible the dose distribution and absolute dose measurements were made simultaneously.

The results of this study demonstrate the good multipurpose capabilities of the new phantom for dose distribution and absolute dosimetry.

Keyword: Intensity modulated radiation therapy(IMRT), Deliver quality assurance(DQA), Tomotherapy, Phantom

References

[1] B. J. Jin, J. S. Kim, S. W. Ha and S. J. Ye, Radiation oncology, 6, 27 (2011)
[2] C-M Ma, S B Jiang, T Pawlicki, Y Chen, J S Li, J Deng and A L Boyer, Phys. Med. Biol, 48 (2003)
[3] H. S. Jeong, Y. Y. Han, O. Kum, C. H. Kim and J. H. Park, Nuclear engineering and technology, 43, 4 (2011)

Development of sensitivity enhancement detector using pixelization of block scintillator with 3D laser engraving

Seung-Jae Lee[1], Jong Hun Won[3*], Cheol-Ha Baek[2,3†]
[1]Department of Radiological Science, Dongseo University
[2]Department of Radiological Science, Kangwon National University
[3]Department of Medical Health Science, Kangwon National University

To improve the sensitivity, a detector using a block scintillator was developed. In the pixelated scintillator, a reflector is located between pixels to move the light generated from the scintillator to the photosensor as much as possible, and sensitivity loss occurs in the reflector portion. In order to improve the sensitivity and to have the characteristics of the pixelated scintillator, the block scintillator was processed into a scintillator in pixel form through three-dimensional laser engraving. The energy spectra and energy resolution of each pixel were measured, and sensitivity analysis of block and pixel scintillator was performed through GATE simulation. The measured global energy resolution was 20.7%, and the sensitivity was 4.7% higher than that of the pixel scintillator. When this detector is applied to imaging devices such as gamma camera and positron emission tomography, it will be possible to shorten the imaging time and reduce the dose of patient by using less radiation source.

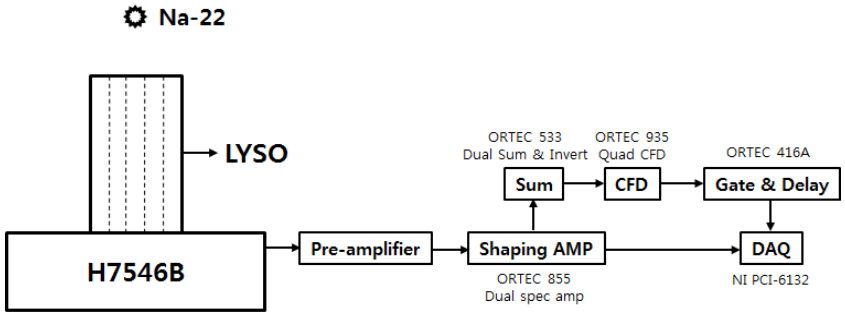

Fig. 1. Schematic of the experimental set-up

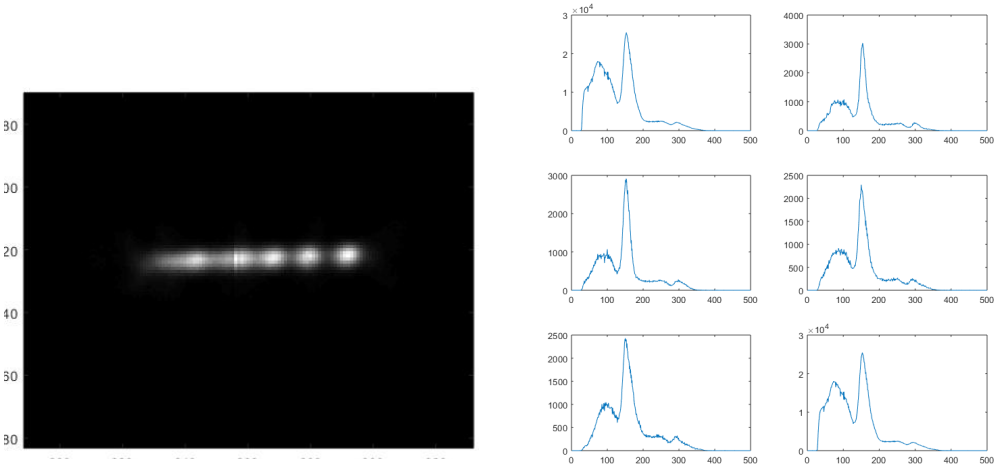

Fig. 2. The flood image and the profile of the block scintillator engraved with five pixels. (a) Flood imgae, (b) Energy spectrum

A Study on the Image Distortion and Signal Intensity Change due to the Correlation between Segment and GRAPPA in RESOLVE DWI when using Gd Contrast Agent

Yong Soo Han[1,2*], Cheol Soo Park[3]

[1]Department of Radiology, Dongguk University Ilsan Medical Center, Goyang 10326, Republic of Korea
[2]Department of Medical Device Industry, Dongguk University, Goyang 10326, Republic of Korea
[3]Department of Radiological Science, Hallym Polytechnic University, Chuncheon 24210, Republic of Korea

In this study, the correlation between GRAPPA acceleration factor (G.f) and readout interval (seg.) Of RESOLVE DWI based on T1 tirm dark-fluid after contrast enhancement was analyzed. The changes of signal intensity and image distortion according to contrast concentration were studied.

In order to characterize image distortion and signal intensity in RESOLVE DWI using Gd contrast agents, Primovist and physiological saline solution were diluted with a 1.4 cm diameter cylindrical syringe at a total concentration of 3 mL of 0.05 cm / mL to 250 mmol / mL, and 32 ghost samples were prepared and analyzed for image data. Statistical analysis was performed using correlation analysis (Pearson correlation coefficient, SPSS version 22.0 (IBM Co., Armonk, NY, USA).

RESOLVE DWI test after contrast, If increasing seg. as much as possible SNR increases, distortion degree decreases, signal intensity decreases but test time increases. Therefore, it is considered that the improvement effect is great if Gf is increased and the influence on the inspection time is minimized.

Study about Correction of Error in Patients Positioning System of Medical LINAC using Low-energy Electromagnetic Radiation

Jeong Ho Kim[1*], Se Jong Yoo[2†]
[1]Department of Radiation Oncology, KonYang University Hospital, Korea
[2]Department of Radiology, Daejeon Health Institute of Technology, Korea

Medical linear accelerators using high-energy electromagnetic radiation for cancer therapy have their own posture confirmation system to confirm the exact treatment setup of the patient. These patients positioning systems include EPID(Electronic Portal Image Device), ExacTrack, and the most commonly used OBI(On Board Imager). OBI is patients positioning system that evaluates three dimensions using two orthogonal images at 0 degree, 180 degree, 270 degree and 90 degree using low-energy electromagnetic radiation in kV unit. However, the actually obtained images are two-dimensional images, and the image does not change at the same magnification rate according to the movement of the orthogonal image. Therefore, it is aimed to decrease the irradiation of patient and efficiency of the treatment work by decrease the number of exposure by correcting the error at position movement. As shown in Fig. 1, images were acquired by changing the X-axis, Y-axis, Z-axis, and rotation angle using the evaluation phantom with the marker positioned in the center, X-axis, and diagonal directions. Then, we compared the actual moving distance and the moving distance in the OBI system by applying the acquired images and moving direction and distance. When without the rotation angle is applied, the maximum error is 16%. When with the rotation angle is applied, the maximum error is 52% at 15 degree rotation. As a result of applying the rate of error change according to the moving direction and the rotation angle, it can be confirmed that it is applied as shown in Eq. 1 to Eq. 4. In the future, it will be possible to dramatically reduce the number of exposure by applying the inverse conversion of formula at the patients positioning system using the low energy electromagnetic wave radiation attached to the medical linear accelerator.

$$\begin{aligned} &Visual\ distance\ at\ X\ axis \\ &\quad = [\cos(rotation\ angle) \\ &\quad \times \{distance\ of\ X\ axis - (0.04 \times interval\ to\ isocenter\ at\ X\ axis)\}] \\ &\quad + [\sin(rotation\ angle) \\ &\quad \times \{distance\ of\ Y\ axis - (0.04 \times interval\ to\ isocenter\ at\ Y\ axis)\}] \end{aligned} \quad \text{- Eq. 1.}$$

$$\begin{aligned} &Visual\ distance\ at\ \mathrm{Y}\ axis \\ &\quad = [\sin(rotation\ angle) \\ &\quad \times \{distance\ of\ X\ axis - (0.04 \times interval\ to\ isocenter\ at\ X\ axis)\}] \\ &\quad + [\cos(rotation\ angle) \\ &\quad \times \{distance\ of\ Y\ axis - (0.04 \times interval\ to\ isocenter\ at\ Y\ axis)\}] \end{aligned} \quad \text{- Eq. 2.}$$

$$\begin{aligned} &Visual\ distance\ at\ Z\ axis \\ &\quad = distance\ of\ Z\ axis - (0.04 \times interval\ to\ isocenter\ at\ Z\ axis) \end{aligned} \quad \text{- Eq. 3.}$$

$$\begin{aligned} &Visual\ distance\ at\ Y\ axis \\ &\quad = distance\ of\ Y\ axis \\ &\quad - \{interval\ to\ isocenter\ at\ Y\ axis \times \sin(rotation\ angle)\} \end{aligned} \quad \text{- Eq. 4}$$

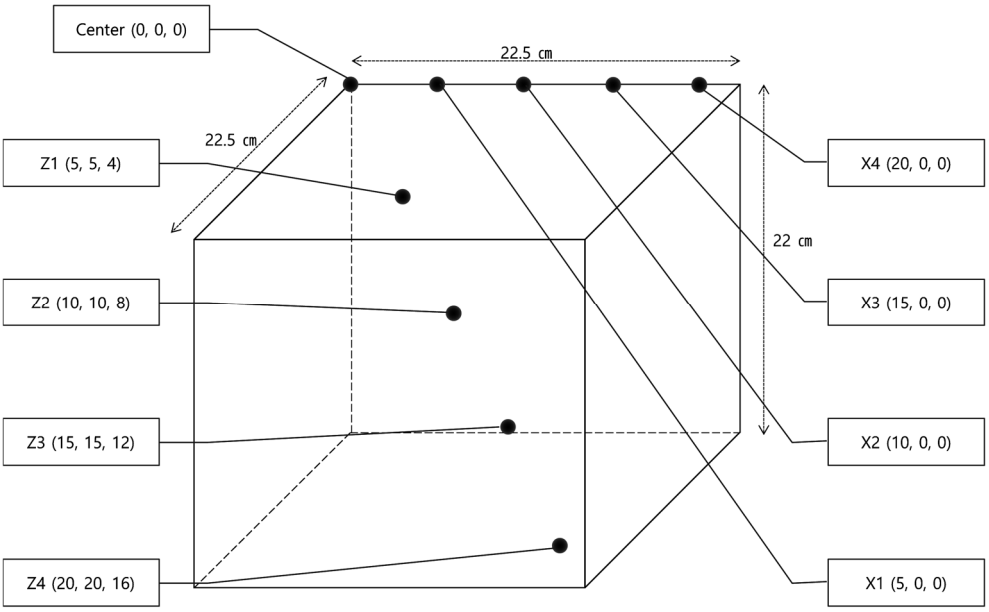

Fig. 1. A blueprint of evaluation phantom

Author Index

Digests of the International Symposium on Magnetism and Magnetic Materials 2018

The Korean Magnetics Society

International Symposium on Magnetism and Magnetic Materials 2018 Vol. 28, No. 2.

#905 KSTC, (Yeoksam-dong) 22, 7gil, Teheran-ro, Gangnam-gu, Seoul 06130, Korea

TEL. (02)3452-7363, **FAX.** (02)3452-7364

E-mail. komag@unitel.co.kr, **Home-page.** www.komag.org